Dietary grape in protection of ultraviolet radiation-mediated cutaneous damages and carcinogenesis

by

Charlotte Ann Mintie

A dissertation submitted in partial fulfillment of

the requirements for the degree of

Doctor of Philosophy

(Comparative Biomedical Sciences)

at the

UNIVERSITY OF WISCONSIN-MADISON

2019

Date of final oral examination: 04/23/2019

The dissertation is approved by the following members of the Final Oral Committee:

Nihal Ahmad, Professor, Department of Dermatology, Trainer of Comparative Biomedical Sciences
Vijayasaradhi Setaluri, Professor, Department of Dermatology
B. Jack Longley, Professor, Department of Dermatology
Mark Burkard, Associate Professor, Department of Oncology
Charles Czuprynski, Professor, Department of Pathobiological Sciences

Abstract

DIETARY GRAPE IN PROTECTION OF ULTRAVIOLET RADIATION-MEDIATED CUTANEOUS DAMAGES AND CARCINOGENESIS

Charlotte Ann Mintie

Under the supervision of Professor Nihal Ahmad

University of Wisconsin - Madison

As the outermost organ of the body, the skin serves as the first line of defense against external insults including solar ultraviolet (UV) radiation, which are classified as UVA (320-400 nm), UVB (290-320 nm), and UVC (200-290 nm). Cutaneous damage occurs via absorption of UV wavelengths UVA (90-99%) and UVB (1-10%) into the DNA of cells within the dermis and epidermis, respectively. UVC is absorbed by the stratospheric ozone with the majority of UVB. Unrepaired DNA lesions resultant from UVB-mediated pyrimidine dimers and UVA-induced oxidative products may lead to transversions resulting in initiated cells that potentially transform into the most common neoplasm, non-melanoma skin cancer (NMSC). Prevention of NMSC could be a plausible strategy due to the latency of the initiating mutation to the progression and development of cancer, which is incidentally continuing to rise with increasing life expectancy. Over the past few decades, the popularity of natural agents for prevention or treatment of diseases has increased. Diets containing phytonutrient-rich food, including fruits, vegetables, and whole grains, can balance oxidative damages to promote better health and prevent or reduce disease development or progression. In this thesis, the chemopreventive effects of a grape powder diet are investigated in separate cohorts of female and male SKH-1 hairless mice in relevant models of UVB-mediated carcinogenesis and short term cutaneous damage. Overall, the protective effects of dietary grape were observed against tumorigenesis in male and female mice treated with 180 mJ/cm^2 UVB for up to 28 weeks. Molecular analysis of skin and tumor tissues suggested that dietary grape enhances DNA damage repair and apoptosis, while

reducing proliferation, oxidative stress, and malignant conversion within tumors. Mechanistically, a large scale proteomics analysis utilizing LC-MS/MS uncovered the anti-inflammatory capacity of dietary grape possibly via an inhibition of inflammatory mediators MAPK and NF-κB. Protection of dietary grape consumption was also apparent in a short-term UVB study (180 mJ/cm^2; 7 doses), displaying reduced hyperplastic responses to UVB. Overall, this study suggests dietary grape affords protection against UV-mediated cutaneous damages including carcinogenesis. This study warrants attention to exploring the potential of dietary grape against UV-mediated damages in human trials.

Acknowledgements

My journey through graduate school has been challenging, yet flourishing. There have been many individuals who have helped me along this path. First and foremost I would like to thank my family for their continuous support. My husband, Brock, has been my rock throughout this entire experience. He has always kept things in perspective and has never faltered in this confidence and support of my work. My light on the darkest or hardest days throughout this journey has been my son, Rowan. His smile can break any sour mood. My parents, sisters, and in-laws have also encouraged me to follow this dream and have sacrificed their time to babysit while I needed to complete specific tasks.

I would also like to thank Liz Garcia-Peterson for being there and acting as a voice of reason. We began and ended this journey together, yet I don't know how I could've made it through without her. Thank you for being my best friend.

I would especially like to thank my PI and mentor, Professor Nihal Ahmad. Nihal is a prime example of what a mentor should be. He truly cares about his students and challenges them to further their success, yet is compassionate and provides guidance when things don't quite go right. None of this would have been possible without his confidence in hiring me to perform research in his lab. I could not have asked for someone better to serve as my mentor.

My thesis advisory committee, Professors Vijay Setaluri, Charles Czuprynski, Mark Burkard, and B. Jack Longley, have been critical in my development as a scientist. With different expertise, they challenged me to view things in a different scope, therefore I am grateful.

Finally, I would like to thank my fellow lab members, especially our scientist, Dr. Chandra Singh, and lab manager, Mary Ndiaye. Throughout my time in the lab, Chandra and I spent much time conversing about how to better execute our collaborative studies. I am grateful

for Mary's expertise, as she could easily assess an experimental problem and think of a way to prevent it from occurring in the future. Her vendor knowledge also made it easier to find the best products for out intended assays. Additionally, I would like to thank Dr. Gagan Chhabra, our post-doctoral fellow for aiding in experiments when needed. I would also like to thank previous lab members, Dr. Melissa Wilking-Busch and Rosie Gutteridge as their guidance and experiences made the first year easier. Lastly, I was very fortunate to train and mentor multiple undergraduate students throughout the last four years. I am very thankful for the experience they provided and believe I have become a better leader because of it.

Table of Contents

List of Figures

Chapter 1: Literature Review

Whole fruit and skin: phytonutrients combating cutaneous damage and carcinogenesis

Abstract

The skin is responsible for regulating temperature and hydration, while continuously subjected to intrinsic, extrinsic, and environmental damage. Skin is equipped with elaborate processes to maintain homeostasis, including antioxidant, anti-inflammatory capabilities. Unfortunately, in the presence of excessive oxidative stress, this system can be overwhelmed causing cutaneous damage including aging and/or carcinogenesis. Phytonutrients present in the foods we consume have demonstrated strong antioxidant properties that can protect the skin from damaging radicals produced external agents including chemicals and ultraviolet radiation. Although many chemoprotective phytonutrients are solely efficacious, when combined synergistic effects may be observed in the reduction of cutaneous damage. In this chapter, we discuss the benefits of select whole fruits, which are a natural amalgamation of phytonutrients, on cutaneous damage and carcinogenesis. All the outlined studies utilize representations of the whole fruit or an anatomical feature, such as seed or stem, in the form of extracts, oils, and freeze-dried powders, provided as a topical or oral supplement. Overall, this review aims to emphasize the importance of a diet rich in phytonutrients, namely through the consumption of healthful foods, to protect the integrity and health of the skin.

Introduction

The environment is full of many factors and entities that can impact the integrity of the skin. Therefore, as the first line of defense, the skin has mechanisms ensuring repair and replenishment to counteract the damages. Cumulative environmental or genetic insults may impair responsive elements of the skin leading to initiation of skin disorders and diseases. In 2013, over 27% of the population in the United States (nearly 85 million individuals) were seen by a physician for a skin disease [1]. Unfortunately, thousands of deaths were linked to these diagnoses with 60% being from skin cancers including melanoma, nonmelanoma skin cancer (NMSC), and cutaneous lymphoma [1]. There is potential to impact skin health through positive lifestyle enhancement including sun protection, not smoking or consuming alcohol, managing stress, and improving dietary habits. In the United States, the USDA dietary guidelines recommend consuming a variety of vegetables, fruits, grains, dairy, proteins, and oils [2]. Within this chapter, we provide insight into the health benefits imparted by whole fruits or extracts of critical anatomical components (i.e. stems and seeds) that contain phytonutrients, which promote skin health and disease reduction. We examine mechanisms of the protective response of whole fruits such as grapes, berries, pomegranate, apples, and tomatoes in wound healing, chemical-induced and ultraviolet radiation (UVR)-mediated cutaneous damage, and carcinogenesis. These phytonutrient-rich foods reduce DNA damage by enhancing repair or acting as a sunscreen, reducing oxidative stress and inflammation which play into each other to promote tumorigenesis [3, 4], and enhancing skin integrity. Overall suggesting that the consumption of whole fruits can promote skin health and healing, and aid in the reduction of disease.

Skin architecture

As the largest organ of the body, the skin itself is elaborately organized into three separate layers: hypodermis, dermis, and epidermis [5]. These layers are responsible for

protection, absorption, temperature regulation, and aesthetics. The hypodermis is mainly composed of adipocytes and connective tissue. The fibroblastic dermis contains blood vessels and nerve endings and is responsible for flexibility due to the presence of collagen-rich connective tissue and is separated from the outermost epidermis layer by the basal lamina [5, 6]. The epidermis is the mechanical, water-proof boundary between the body and the environment [5]. Approximately 80% of the cells composing the epidermis are keratinocytes that continuously proliferate and differentiate to renew the skin. These cells are organized into functional layers characterized by shape, size, nucleation, and keratin expression [7]. Epidermal cells include melanocytes responsible for pigment production [8], sensory Merkel cells [9], and immune Langerhans cells [10]. All cell types within the dermis and epidermis are responsible for the complex cross-talk that maintains homeostasis. This response counteracts endogenous and environmental insults including chemicals, UV radiation, temperature changes, mechanical trauma, and biological agents. When homeostasis is disrupted, the deregulation of normal cellular processes can lead to development of a multitude of skin disorders and diseases, including cancer and inflammatory disease [1, 11-14].

Effects of environmental factors on skin

Solar UV radiation is considered the most prevalent environmental carcinogen. Figure 1 outlines the three wavelengths of UV radiation, which are UVC (200-280 nm), UVB (280-320 nm), and UVA (320-400 nm). The majority of UV that reaches our skin is UVA (90-99%) and a smaller portion is UVB (1-10%) [13], much of UVB and UVC are absorbed by the stratospheric ozone, therefore not penetrating the skin. UVC is highly mutagenic, known to cause damaging effects to living cells and is used as a great disinfectant [15]. UVB that penetrates the epidermal layer interacts with cellular DNA leading to the creation of mutagenic pyrimidine dimers; cyclobutane pyrimidine dimers (CPDs) and (6–4) photoproducts (6-4 PPs) [16]. UVA reaches deep in the dermis where the absorbed photons generate reactive oxygen species (ROS) [17],

and promoting the production of a key marker of oxidative DNA damage, 8-oxo7,8-dihydroguanyl (8-oxodG), in purine bases of DNA [17-19]. Many studies have linked this detrimental UV-induced DNA damage, to mutations in key regulatory oncogenes and tumor suppressors, such as p53, that result in skin cancers [20-22].

Other environmental factors such as diesel fuel exhaust, chemicals, cigarette smoke, and ozone (O_3) can lead to oxidative stress caused by the excess generation of ROS. ROS include the superoxide anion (O_2^-), singlet oxygen ($^1O_2$), hydrogen peroxide, and the hydroxyl radical ($OH^\bullet$). The skin combats ROS by employing antioxidant enzymatic (glutathione peroxidase, superoxide dismutase, catalase) and non-enzymatic (glutathione, α-tocopherol, vitamin E, vitamin C) molecules to maintain a redox homeostasis [12]. However, when intrinsic and environmental factors overwhelm the skin's defenses, the detrimental effects of oxidative stress can lead to skin dysfunction. ROS can affect protein structure and function leading to changes in inflammation, cellular proliferation, and even cell death. ROS can also activate additional signaling pathways that are involved in the pathogenesis of many skin disorders including aging, inflammatory skin diseases, and NMSC [12, 23].

Responses to cutaneous damage and injury

Damaging agents, like UV, have many effects on the physiology of the skin, causing 10^4-10^5 DNA lesions per cell per day [24]. Upon injury, the upregulation of tumor suppressor p53, known also as the "guardian of the genome" [25], causes cell cycle arrest in keratinocytes that undergo damage response pathways, including nucleotide excision repair (NER), base excision repair (BER), double strand break repair, and crosslink repair [26]. NER is the cellular mechanism responsible for removing pyrimidine dimers caused by UVB, and chemically induced bulky adducts, drug-induced crosslinks, and oxidative cyclopurines [27]. Mutagenic 6-4 PPs are readily recognized by global genomic NER (GG-NER), which scans the whole genome for DNA damage. Because GG-NER poorly recognizes CPDs, transcription-coupled NER (TC-

NER) is activated when the RNA polymerase II stalls at the lesion during transcription [26-28]. After the complex is recruited, the lesion is excised from the DNA strand and the gap is filled to prevent irreversible DNA modifications [27]. Although most NER lesions arise from exogenous sources, BER utilizes glycosylases to remove each endogenous oxidative-induced base lesions [26, 29]. Hours after damage occurs, the signal subsides and keratinocytes again proliferate, leading to epidermal hyperplasia to better protect the skin against UV penetration [30]. If damage to the keratinocyte exceeds the capacity of repair mechanisms, apoptosis will be induced [31, 32]. Failure of the early repair mechanisms can lead to initiated keratinocytes which can eventually progress to tumor cells [33]. The fates of cells after DNA damage repair are outlined in Figure 2.

Upon injury, keratinocytes and fibroblasts secrete pro-inflammatory cytokines to recruit leukocytes to the site of injury. Inflammation ususally is a self-limiting process. However deregulation leads to persistence of cytokines and chemokines resulting in chronic inflammation and/or immunosuppression. These in turn lead to various pathologies, including cancer [34-36] and cancer-related inflammation has been suggested as a hallmark of cancer [37]. Transient levels of ROS can activate signaling pathways lead to an inflammatory response. The antioxidant nature of many phytonutrients reduce oxidative and suppress pro-inflammatory signal transduction pathways. In this chapter, we discuss the reported anti-inflammatory roles of selected whole fruits or products and the pathways believed to be involved.These include the mitogen-activated protein kinases family (MAPK) signaling, phosphoinositide 3-kinase/Akt8 virus oncogene cellular homolog (PI3K/Akt) signaling, and nuclear factor kappa B (NF-κB) and downstream AP-1 signaling.

The MAPK family includes ERK1/2, JNK1/2, and P38 kinases, which are downstream of RAS and activated in the presence of oxidative stress [38]. These are well documented for their link to tumor proliferation [39, 40]. The MAPK signal transduction pathway is responsible for

activation of many downstream targets including cyclooxygenase 2 (COX-2) and activator protein 1 (AP-1) [41, 42]. AP-1 is a transcription factor responsible for binding jun and fos dimers to control keratinocyte proliferation, differentiation, and apoptosis. An alteration of AP-1 response can lead to tumor development [43, 44]. Increased expression of Ras protein also plays into the activation of PI-3K and further AKT. Activation of this cascade and phosphorylation of downstream effectors such as, FOXO (forkhead box O transcription factor), MDM2 (mouse double minute 2 homolog), and BAD (Bcl-2-associated death promoter) have been linked to increased proliferation, survival and migration of cancer cells [45-47]. NF-κB is responsible for regulating many genes involved in the initiation of inflammation, including chemokines and cytokines (IL-1, IL-6, TNF), pro-inflammatory enzymes (COX-2, iNOS), and genes linked to cellular survival (Bcl-2, Survivin) and proliferation (cyclins, c-Myc) [48, 49]. Another family of proteins frequently activated in tumors are signal transducers and activators of transcription (STATs). These proteins regulate survival genes (Survivin, Bcl-xl), proliferation (c-fos, c-myc, cyclin D1), matrix metalloproteinases 2 (MMP-2), and cytokines (Il-6, Il-17, and Il-22) [50]. Increased inflammation and ROS can then feed into each other to enhance downstream biochemical effects leading to accumulation of oxidative damage of proteins, carbohydrates, and lipids within the epidermis and dermis after the skin's antioxidant response has been overpowered [3, 4].

Skin carcinogenesis

Many studies have demonstrated excessive exposure to UVR triggers many biological processes culminating into cumulative cutaneous damages. During an individual's lifetime, these cumulative damages, if not repaired, may lead to skin carcinogenesis [51, 52]. Carcinogenesis is a stepwise process with three distinct stages: initiation, promotion, and progression (Figure 2). Initiation can occur through exogenous (chemical, UV radiation) or endogenous (inflammation) factors when the cellular repair capacity is unable to fix DNA damage, being irreversible [53]. CPDs are responsible for the majority of UVB-induced

mutations, indicated by the presence of C to T or CC to TT transitions on regulatory genes, such as *p53*, in mice and humans [54, 55]. UVA-induced mutations occur through AT to CG transversions caused by 8-oxodG [55, 56]. Due to the mutation in *p53*, continued exposure to UVB can lead to clonal expansion (promotion) of initiated mutated cells [57], which appear to have a growth advantage over neighboring normal cells that will go through apoptosis [57-61]. In humans, primary precancerous skin lesions can include actinic keratosis (AK), which harbor a high mutational load when compared to normal skin [62].

NMSC are the most common form of cancer and their incidence rates are continuing to rise [63]. The most common forms of NMSC are basal cell carcinoma (BCC) and squamous cell carcinoma (SCC), also known as keratinocyte carcinomas, and are most prominent in Caucasians [11, 64]. Unfortunately, there are no registries to track NMSC incidence, therefore we rely on epidemiological studies to predict incidence and treatment rates. Most recently, Rogers et al. estimated 2,191,100 procedures in 1,336,800 individuals in 2012, but this has likely increased over the past years predicted by upward trends of the preceding years [63]. Because NMSC development has a long latency, many individuals develop lesions later in life (70-80 years) despite initiating UV-signature mutations generally occurring earlier in life [63]. Moreover, it is predicted that 1 in 5 non-Hispanics over 70 years of age had at least one case of NMSC [65]. NMSCs also affect more men than women [66] and is the fifth most costly malignancy to treat in the United States totaling billions of dollars spent in treatment and care costs on an annual basis [67, 68]. NMSC can also develop at a younger age, although not as common. A study by Christenson, et al. studied incidence in individuals under 40 in Olmsted County, Minnesota, United States showing an incidence of BCC in women at 25.9 and men at 20.9 per 100,000 persons and an incidence of SCC of 3.9 for both sexes per 100,000 persons [69]. Interestingly, many deaths of individuals diagnosed with NMSC are associated with the development of another cancer type such as lung, prostate, breast, colon, and melanoma [70].

Therefore, it is critical to determine prevention early on to protect all ages from disease development.

The majority of skin cancer cases are BCCs, affecting more than 3.3 million individuals in the United States on an annual basis [63, 71]. One study demonstrated that a North American child born in 1994 has a 30% lifetime risk of developing BCC [72]. While not life-threatening, BCCs are a slow growing neoplasm that rarely metastasizes, and have nearly 100% survival after diagnosis [73], although, if left untreated, BCC can invade locally [74]. Upregulation of the Hedgehog (HH) signaling, and further activation of pro-survival signal BCL-2, pathway has been linked to BCC development [75, 76]. To understand the pathogenesis of BCCs, we have limited models of carcinogenesis, but we can model BCCs in *Ptch*$^{+/-}$ mice exposed to UV or chemical inducers. This model has provided insight to the development of BCCs as the upregulation of HH signaling appears to be a consequence of p53 mutations [77]. Unfortunately, as no mouse models are perfect, as lower magnitude lesions in *Ptch*$^{+/-}$ mice do not resemble human BCCs to the same extent as more advanced lesions [78, 79].

Interestingly, epidemiological studies have revealed not only are men at a higher likelihood of developing NMSC, but the likelihood of SCC is 9% to 14% in men and 4% to 9% in women [51, 80-82], but this is hypothesized to be relative to lifestyle choices, as men seemingly have more occupational exposure [83, 84]. In the United States alone at least 200,000 to 400,000 cases of SCC are expected, accompanied by 3,000 disease related deaths, and a 25% higher mortality than those without SCC diagnosis [70, 85, 86]. The current mortality rate of SCCs is linked to the metastatic potential of the disease. Currently the risk of SCC metastasis is reported at 4% [87], yet this rate is 2 to 3 times higher in immunosuppressed individuals, such as organ transplant recipients [88]. Many studies have sought to determine the shift from normal skin to AK to SCC. Although AK and SCC appear to have similar profile of dysregulated pathways, it appears that AK could be responsible for counteracting additional deleterious

mutations leading to SCC, therefore leading to an extended latency of years prior to progression of the tumor [62, 89].

Although the diagnosis of NMSC can indicate increased susceptibility to subsequent lesions, the goal of current treatments are to completely eradicate the lesion while preserving structure and function, as well as aesthetics [90]. Current treatments for NMSC include surgical methods such as excision, Mohs micrographic surgery, curettage and electrodessication, laser ablation and cryosurgery and nonsurgical radiation and photodynamic therapies. Generally, surgical procedures are highly effective, with good cosmetic outcome for treating low risk lesions [91, 92], however unlike excision and Mohs microsurgery, there is a higher risk of reoccurrence after other procedures due to the lack of histological evaluation validating complete tumor excision [92, 93].

Mouse models of carcinogenesis

Although no model can fully replicate human tumorigenesis, multiple *in* vivo models have been generated to provide key mechanistic insight to carcinogenesis. In addition to the Ptch $^{+/+}$ BCC model mentioned briefly above, here we outline other mouse models relevant to studying current treatments and mechanisms of skin disease. Many strains of mice have varying susceptibility to chemical-induced carcinogenesis including CD-1, BALB/c, and C57BL/6 [94], whereas the SENsitive to CARcinogenesis (SENCAR) mouse strain is highly susceptible to carcinogenesis [61]. The genetic background of the mouse impacts the malignant conversion from papillomas to SCC. For example, the incidence of SCC in SENCAR and BALB/C is 1-10%, whereas up to 50% of papillomas may convert in FVB mice [95, 96]. However, in these mouse models, there is no human equivalent to the papillomas that develop, whereas malignant SCCS are histologically comparable to human, and can progress to spindle cell carcinomas, although very rare [97]. Unfortunately, the anatomy and physiology of mouse and human skin differ. Both undergo a defined cycle of hair growth, anagen (growth), catagen (regression), and telogen (rest) [98], yet mice have dense hair covering the whole body, whereas humans vary. In mice

the thick hair coat and frequent hair cycle can aid in enhancing tumorigenesis [99], therefore hairless models are, arguably, ideal. The two-stage skin carcinogenesis protocol is a good model for human skin cancer due to the long latency and the relevance that humans are exposed to multiple low doses of carcinogens and promoting agents throughout their lifetime [53, 61]. In the DMBA-TPA initiation-promotion skin carcinogenesis protocol, application of 7,12-dimethylbenzanthracene (DMBA) is sufficient to induce an initiating mutation, however cannot promote tumor growth. Therefore, pro-inflammatory, tumor promoter 12-*O*-tetradecanoylphorbol 13-acetate (TPA) is applied to initiated skin and visible tumors arise [94]. The DMBA-TPA skin carcinogenesis model has been exclusively used to study multi-stage carcinogenesis.

Due to a high accumulation of UVB signature mutations in skin cancers [13, 55] the best *in vivo* model for understanding UVB-induced carcinogenesis, arguably, is the SKH-1 hairless mouse. SKH-1 hairless mice are an outbred mouse strain that have an autosomal recessive mutation of the hairless (Hr^{hr}) allele causing 95% of the Hr transcript to be spliced, leading to absence of the thick fur coat seen in haired mice [100-102]. Interestingly, the first hair coat develops normally and then complete hair loss begins around 2 weeks of age leading to complete hair loss by 3 weeks of age [103-105]. The sudden disintegration of the hair follicle leaves behind two epithelial structures, dermal cysts and utriculus [105] and the mice are also susceptible to *Streptococcus* mediated spontaneous skin abscesses [106]. Yet, there are many benefits to using the hairless mouse in skin studies including: 1) the inflammation associated with hair-removal is avoided, 2) skin is permeable to measure drug penetration, 3) hair growth does not obscure wound healing, 4) tumors are visible, and 5) each mouse develops numerous independent skin tumors, that can be phenotypically variable modeling that of humans (reviewed in [104]).

Whole foods in chemoprevention

Chemoprevention is defined as the use of natural or synthetic agents to prevent, suppress, or reduce the progression of cancer and can be undertaken with a single or multiple agents that interfere with numerous pathways in the skin carcinogenesis process [107]. Many individual phytonutrients have demonstrated beneficial health effects. In our lab, previous studies have shown the protective effects of the stilbene, resveratrol, against UVB-mediated carcinogenesis [108]. However, as studies have continued to progress towards the utilization of natural products to benefit health, the natural matrix of polyphenols and antioxidants in whole foods are more and more attractive. This is partially because individuals can modify their dietary habits, rather than continuously ingest supplements or apply topical ointments. Fruits and vegetables are well known for their high nutrient content. The general recommendation for fruits in the American 2,000 calorie diet is a two cup equivalent [2]. Overall it is suggested to ingest whole fruits or 100% fruit juice, therefore preserving the nutrient-dense nature without the possibility of added fats, sugars, and sodium and whole fruits can be fresh, canned, frozen, or dried [2]. According to the USDA, the most consumed fruits in America are apples, bananas, watermelon, grapes, strawberries, oranges, peaches, cantaloupe, pears, blueberries, raisins, and pineapple [2]. These fruits are packed with phytonutrients that have antioxidant, anti-inflammatory, anti-mutagenic, or anti-carcinogenic effects. In the natural amalgamation within whole foods, phytonutrients can synergistically provide health benefits, and many studies have already implicated beneficial effects in many chronic pathological conditions, including cancers (reviewed in [109, 110]). Unfortunately three-fourths of the population does not consume the recommended serving of fruits, yet exceeds total grain, protein, and recommendations for added sugars, saturated fats, and sodium [2]. In this chapter, we discuss studies implicating the beneficial health effects of whole fruits on skin diseases and disorders. The discussion includes *in vitro* and *in vivo* research utilizing representation of whole fruit and fruit extracts of grapes, black raspberries, blackberries, pomegranate, apples, and tomatoes.

The chemoprotective effects of fruit

Grapes

Grapes have been cultivated for nearly 8,000 years, and wine has been deemed a highly valued commodity in many ancient cultures [111]. Moreover, traditional Ayurveda medicine, originating from the Indian subcontinent, utilized fermented grapes in many ways for beneficial affects against lethargy, weakness, and cardiac disease [112, 113]. Chromatographic evaluation of the tonic indicated a presence of many polyphenols, including resveratrol and pterostilbene [114]. Within the last century, the grape cure was propagated, with much criticism, by a South African dietician Johanna Brandt who promoted grapes as having anti-cancer effects [115], and the “French Paradox” gained popularity. This paradox describes the low heart disease rate of the French due to the consumption of wine, despite a high fat diet [116]. Since then, over 1600 compounds have been identified in grapes, including anthocyanins, catechins, resveratrol, lycopene, quercetin, and melatonin, among others [117]. Further, studies of the individual component, resveratrol, have demonstrated therapeutic efficacy in many skin conditions including atopic dermatitis, aging, cancer, and psoriasis [108, 118-120]. Although resveratrol works well as a topical agent, when ingested, resveratrol is believed to be rapidly metabolized [117]. However, combining resveratrol with other agents to act synergistically seems to increase oral efficacy (reviewed in [121]), therefore supporting a whole foods approach. Many researchers have moved to evaluating key features of the grape including the stem, skin, and the seed, while others have explored the benefits of the whole fruit.

To determine if grape skin could aid in wound healing, male Sprague Dawley rats were wounded, then topically received daily mupirocin, petroleum jelly, or grape-skin powder derived from the pomace of Cabernet Sauvignon variety in petroleum jelly until complete epithelialization. Rats receiving topical grape-skin powder exhibited significant increases in the rate of epithelialization, wound contraction, and hydroxypreline content, indicating increased collagen synthesis [122]. Further, Filip, *et al* sought to understand the protective effects of red

grape seed in UVB-induced damages using a prepared extract from the seed of *Vitis vinifera*. The extract was assessed for polyphenolic content and topically applied at 4 mg/ mouse/ cm^2 30 minutes prior to a single-dose of UVB (240 mJ/cm^2) on the female SKH-1 hairless mice. Results indicated that the extract attenuated UVB-induced oxidative stress by preventing damages by lipid peroxidation and nitric oxide, while reducing caspase-3 activity [123]. They further evaluated the protective capacity of the topical grape seed extract by extending the study to 10 consecutive days of UVB exposure at 240 mJ/cm^2. The extract effectively reduced CPDs, hyperplasia, cytokine release, and oxidative stress while increasing antioxidant response [124]. Utilizing a different portion of the grape, Che et al. sought to evaluate the efficacy of topical (50 mg/kg) grape stem extracts in UVB-induced damages. Using the C57BL strain, male mice were given the extract one week prior to dosing and throughout the study. The UVB dosage used was 120 mJ/cm^2 thrice weekly for three weeks. The treatment extract from this grape reduced lipid peroxidation, neutrophil and mast cell infiltrations, and COX-2 expression while retaining the integrity of the skin [125]. In a subsequent study, extract from the Muscat Bailey A grape was produced. Male Balb/c mice had the extract topically applied daily (1 mg), while receiving 120 mJ/cm^2 UVB thrice weekly for one month. The study proposed the extract reduced oxidative stress through recovered glutathione peroxidase and superoxide dismutase levels, while preserving the integrity of the skin and preventing DNA damage. Additionally, the extract reduced inflammatory response as indicated by reduced mast cell and neutrophil infiltration and pro-inflammatory cytokines [126]. In an *in vitro* study, spontaneously immortalized human keratinocyte cell line HaCaT were irradiated with UVB at ranges of 25-300 mJ/cm^2. A protective effect was observed from Burgund Mare variety red grape extract at concentrations of 10 and 20 μg/mL, increasing viability of the cells while reducing lipid peroxidation, apoptosis, and DNA photoproducts [127].

Kobayashi et al. sought to evaluate the protective effects of topical and dietary Y-grape juice and ethyl acetate extract from *Vitis coignetiae* Pulliat (Y-grape) on TPA-induced edema and DMBA-TPA carcinogenesis. Six-week old SENCAR mice were given a single dose of 1.7 nmol TPA upon the inner and outer surfaces of the ear. Both topical and oral treatments appeared to reduce edema in a dose-dependent manner. In a subsequent experiment, mice were subjected to DMBA-TPA induced carcinogenesis with topical Y-grape juice or oral extract water supplementation. All grape treatments imparted significant protection against tumor promotion in this model demonstrated through reduced tumor incidence, tumor number, and COX-2 activity [128]. Hanausek et al. performed a similar study utilizing the DMBA-TPA treated SENCAR mouse carcinogenesis model. Their model involved topical pretreatment with resveratrol, topical freeze-dried grape powder (GP, 1, 2, or 4 mg), or a continuous diet of 1% GP in AIN-93G starting 2 weeks prior to DMBA and up to 12 weeks. All treatments reduced tumor burden, COX-2, and DNA damage within the skin [129]. Unfortunately, chemically induced carcinogenesis does not model human carcinogenesis, as the majority (~90%) of human tumors, are linked to UVR as a causative factor [130, 131]. SKH-1 hairless mice are susceptible to UVR induced skin cancer and develop multiple, phenotypically different lesions resembling tumors in humans. Therefore, this is arguably the most suitable mouse model for UVR carcinogenesis to yield mechanistic data. In one photocarcinogenesis model, female SKH-1 mice were subjected to 180 mJ/cm^2 UVB three times weekly for 24 weeks to develop NMSC lesions while directly consuming a diet enriched with grape seed proanthocyanidins (0.2% or 0.5%). The authors suggested that the proanthocyanidins inhibit UVB-induced inflammatory mediators, including COX-2 and other cytokines in the skin and tumors [132]. In a study by Singh and Mintie *et al*. (Chapter 2) female SKH-1 mice were subjected to 180 mJ/cm^2 UVB two times weekly for 28 weeks while consuming diets enriched with GP at concentrations of 0%, 3%, or 5%, equivalent to 1.1 or 1.8 servings of grapes in humans. Dietary supplementation resulted in later onset of tumors and marked reduction of tumor multiplicity and volume. Further

mechanistic evaluation of the large tumors demonstrated that GP imparts chemoprotection through enhanced apoptosis and oxidative stress response while reducing proliferative marker and lipid peroxidation [133]. Additionally, evaluation of skin near the tumor suggested that GP enhanced NER repair capacity through the reduction of CPDs [133], DNA damages linked to C to T and CC to TT transitional mutations in skin cancers [130, 131]. In a subsequent study of male SKH-1 hairless mice, it was also noted the GP reduced the maliganant conversion of papillomas to microinvasive and fully invasice SCCs (Chapter 4). Collectively, grapes are one of the most studied whole fruits for protection of the skin and have proven beneficial in many models of cutaneous damage.

Plants of the genus *Rubus*

Fruits from plants of the genus *Rubus*, including raspberries and blackberries, have been associated with modulating many biological activities including antioxidant response and carcinogenesis [134]. The three main classes of polyphenols include anthocyanins, ellagitannins, and phenolic monomers, inducing phenolic acids and flavonoids [135]. Huang et al. sought to explore the health promoting effects of black raspberry, strawberry, and blueberry extracts on UV irradiated mouse epidermal C1 41 cells. Their methanol extract from black raspberries (BRE) (*Rubus occidentalis*) appeared to be the most potent inhibitor if UVB-induced NF-κB activation in the cells, as demonstrated by the suppression of IKK activation. Their results indicated that MAPKs, and consequently AP-1 activation, were not affected, therefore, the extract acted specifically on NF-κB [136]. A previous study using the similar extract demonstrated a differential inhibition of BaP diol-epoxide (BPDE) induced AP-1 and NF-κB in JB6 murine cells, suggesting an inhibition of carcinogen caused tumor development [137]. A subsequent follow-up to this study suggests that BRE reduced the expression of AP-1 and VEGF in BPDE treated epidermal C1 41 cells through inhibition of PI-3K/Akt pathway leading to anticarcinogenic effects of black raspberries [138]. Duncan et al. examined the *in vivo* effects of

BRE on two SKH-1 hairless mouse models. The first acute damage study subjected SKH-1 mice to one minimal erythemal dose of UVB (2,240 J/m^2), whereas in the second carcinogenesis model, mice were exposed to 2,240 J/m^2 dose of UVB thrice weekly for 25 weeks with each treatment followed by topical application of BRE. They found that topical application of 500 µg BRE reduces neutrophil activation, edema, and oxidative DNA damage suggesting the inhibition of many hallmarks of acute inflammatory response that have been suggested in skin cancer development [139]. In the carcinogenesis model, chemopreventive effects of BRE were observed though reduced tumor counts, tumor volume, and tumor-infiltrating CD4+ T cells [139]. Collectively, this indicates the antitumor properties of BRE are through alterations of inflammatory response.

Comparatively, another study used blackberry extract (BBE) to evaluate the beneficial effect on SKH-1 hairless mouse skin [140]. When topically applied (10% or 20%) the day before each UVB exposure (100 mJ/cm^2) alternating every other day for ten weeks, Divya et al. demonstrated that BBE acts on the MAPK signaling pathway to protect against the UVB induced damages. The reduction of phosphorylated ERK1/2, p38, and JNK1/2, were accompanied by inhibition of NF-κB nuclear localization and subsequent inflammatory mediators COX-2, iNOS, and prostaglandin E_2 [140]. Additionally, BBE suppressed CPD formation, as well as oxidative stress and subsequent 8-oxodG formation [140]. Calvo-Castro et al. utilized juice of the highland blackberry (*Rubus adenotrichos,* BBJ), rich in ellagitannins, to determine protective effects against UVB-exposed human epidermal keratinocytes and a human reconstituted skin equivalent (SE) model. Although BBJ was unable to protect the cells against UVB-induced loss of viability, protection against UVB-mediated base-line guanine oxidation and direct CPD DNA damage was observed in both cell cultures and a 3D skin model, as well as an increase in PARP cleavage [141]. Taken together, this study suggests BBJ may potentially act on the process of carcinogenesis by enhancing apoptosis of UVB-damaged cells.

Pomegranate

Pomegranate (*Punica granatum* L.) is 80% juice and 20% seed but rich in anthocyanins and hydrolysable tannins [142, 143]. Multiple studies have sought to evaluate the effects of pomegranate on skin damages and carcinogenesis. In one study, female CD-1 mice received 2 mg pomegranate fruit extract (PFE) in acetone, then received a treatment of TPA (3.2 nmole/mouse) 30 minutes later, followed by sacrifice at proceeding time points. Topical PFE inhibits the inflammatory response to TPA as shown through the reductions of skin edema, hyperplasia, dermal neutrophils, ODC, and COX-2. Subsequently, a reduction in the activation of the MAPK pathway was observed. The hypothesized anti-tumor effects of PFE were confirmed through DMBA-initiated and TPA-promoted (2x weekly application) tumorigenesis of CD-1 mice for 30 weeks. Not only had PFE extended tumor latency, but at the end of the study 20% of PFE-mice remained tumor free and tumor counts were equivalent to a 64% inhibition when compared to control counterparts [142]. This tumorigenesis study supported the chemoprotective effects of pomegranate against tumorigenesis as shown through a prior study, where CD-1 mice underwent the DMBA-TPA protocol and received topical 5% pomegranate seed oil [144].

Further exploration sought to determine the protective effects of ingested PFE in SKH-1 hairless mice exposed to UVB. Two studies provided PFE in the drinking water (0.2% wt/vol) for 14 days prior to a single dose of UVB [145], or seven alternate day doses of UVB (180 mJ/cm^2) [146]. Supporting the previous findings from topical PFE on CD-1 mice, oral feeding of PFE reduced cutaneous edema, hyperplasia, infiltration of leukocytes, and COX-2 expression. Additionally, apart from enhancing the repair of CPDs and 8-oxodG after a single dose of UVB, PFE enhanced p53 and p21 expression [145]. Demonstrating that PFE affords substantial protection against early biomarkers of photocarcinogenesis. As a hallmark of skin carcinogenesis, hyperproliferation of epidermal cells were evaluated by proliferative markers PCNA [145, 146], and Cyclin D1 [146], demonstrating a reduced proliferative index of PFE mice.

Further, PFE inhibited the UVB-mediated activation of NF-κB as shown through the increased accumulation of IκBα to keep NF-κB/p65 tethered to the cytoplasm, and subsequent inhibition of NF-κB and IKKα activation [145, 146]. Increased production of hydrogen peroxide can lead to the induction of MAPK signaling, and subsequent NF-κB activation. The multiple UVB dose study evaluated upstream regulators of NF-κB in the MAPK family. The reduction of activated ERK1/2, JNK1/2 and p38 demonstrate that PFE may act against the crosstalk of multiple pathways that lead to increased cell survival, inflammation, proliferation, and apoptosis, therefore leading to the photoprotection of skin cells [146]. The beneficial effects of pomegranate are also modeled in vitro. Utilizing pomegranate extract and oil, multiple studies validate the benefit against UVB-mediated damages to NHEK [147], immortalized HaCaT keratinocytes [148], and human reconstituted skin [149]. In addition to the observed reduction of activated MAPK molecules, proliferation, and DNA damage, pomegranate extract inhibits the phosphorylated activation of c-Jun and c-Fos, and MMP proteins which are linked to ECM and collagen breakdown [148, 149]. Taken together, all of these studies demonstrate the protective capacity of the pomegranate fruit against skin damages.

Apples

Within the United States, the second largest source of fruit phenolics in America is apples [150]. Apples have increased phenolic content in the skin as compared to the remainder of the fruit. Unfortunately, in the production of canned apples and applesauce, the peel is discarded [151]. The flesh contains catechins, procyanidins, and caffeic acid, whereas the peel contains these all including quercetin glycosides [151]. To determine the chemopreventive effects of fresh apples, Ding et al. utilized a 20 week DMBA initiation-TPA promotion protocol to mediated skin tumorigenesis in AP-1 luciferase reporter transgenic mice (C57BL/6 crossed with DBA2). The treated mice were provided apple peel extract (APE) in the drinking water *ad libitum* two days prior to the initiating dose of DMBA, then throughout the remainder of the studies bi-

weekly TPA treatments [152]. Although the authors observed a similar percentage of mice developing tumors, those ingesting the APE had greater than 50% inhibition in the number of papillomas present at the end of the study, accompanied by decreased tumor volume [152]. To determine if this reduction of tumorigenesis is relative to AP-1 activation, the authors performed a separate experiment utilizing the same transgenic mouse strain. Although the treated mice were still provided *ad libitum* access to APE in their water, mice also received six topical doses of APE over six days. Mice then received a single dose of TPA or UVB irradiation (10 kJ/m^2) on the fourth day and skin biopsy punches were collected 24 or 72 hours later. By 72 hours post treatment, APE significantly inhibited the activation of UVB induced and TPA-induced AP-1 activation [152]. *In vitro* validation in mouse epidermal JB6 cells treated with varying doses of APE and TPA (20 ng/mL) or UVB (4 kJ/m^2), demonstrated the same trend of reduced AP-1 activation in a dose dependent manner. The effect of inhibited AP-1 activation in JB6 cells was accompanied by the predicted reductions of activated MAPKs, ERK and JNK in the UVB treated cells, and ERK in TPA treated cells. Moreover, APE also appeared to be a potent scavenger for ROS and inhibited TPA-induced transformation of cells. Therefore this study demonstrates the mechanism of chemoprevention by apples occur through the reduction of ROS and subsequently interferes with MAPK signal transduction leading to AP-1 activation [152].

Tomato

The health effects of tomatoes have been linked to the presence of carotenoids, pigments which give the fruit color. Lycopene, the primary carotenoid of tomatoes, acts as a scavenger of singlet oxygen [153]. Stahl, et al. initially suggested that the lycopene in tomatoes, combined with other carotenoids and non-carotenoids, imparts a photoprotective affect against UV-dependent skin damage [154]. The Kopec et al. utilized the SKH-1 hairless mouse model to comparatively analyze the difference of males and females in photoprotection from UV when on a tomato diet [155]. After 10 weeks of dietary tomato consumption and one UVB exposure

(2240 J/m^2), female mice had higher levels of skin and blood carotenoids as compared to their male counterparts. Furthermore, the tomato containing diet reduced CPDs and p53 positive epidermal cells. However, the attenuation of UV-induced DNA damage in males was associated with reduced inflammation and CPD levels [155]. In a subsequent study by Cooperstone et al., a 10% tomato diet was given for a 35 week tumorigenesis study. In weeks 11 through 20, mice received UVB exposures (2240 J/m^2) three times weekly. This treatment induces papillomas in male mice at 6-10 weeks and in females at 10-12 weeks. Although there was no difference noted in the female cohort, male mice of the tomato-based diets developed significantly less tumors than those on the control diet [156], demonstrating the differential benefits that whole foods can provide for either gender.

Conclusion

The USDA recommended serving of fruits are 2 cups per day in a 2,000 calorie diet, however about three-fourths of the population in the United States are not meeting this quota on a daily basis [2]. Over the past decades, scientific evidence supporting healthy eating patterns being linked to reduced disease risk has grown monumentally. In this chapter, we evaluated studies of multiple fruits and their benefits to protect, prevent against or treat cutaneous damages or carcinogenesis, suggestively because fruits are packed with phytonutrients that possibly act synergistically to prevent oxidative and inflammatory stress (outlined in Table 1). Collectively these studies have demonstrated that beneficial effects of utilizing whole fruits in skin health as they are pro-apoptotic and reduce damaged cell survival, anti-proliferative, and anti-inflammatory while still reducing DNA damage through sunscreen effects or enhancing cellular machinery, and reducing oxidative stress (Figure 3). The idea of utilizing natural agents in food is continuously growing. There are currently over 200 clinical trials for each grape and apple products and trial numbers are continuing to increase with other fruits as well (Table 2). In a world where our average life expectancy is increasing, so is the likelihood of development

age-related disease, such as aging and cancer. Therefore, we must focus our efforts to understand the protective underlying mechanisms that whole foods can provide to extend our longevity.

References

1 Lim HW, Collins SAB, Resneck JS, Jr., Bolognia JL, Hodge JA, Rohrer TA, Van Beek MJ, Margolis DJ, Sober AJ, Weinstock MA, Nerenz DR, Smith Begolka W, Moyano JV: The burden of skin disease in the United States. J Am Acad Dermatol 2017;76:958-972.e952.

2 Agriculture USDoHaHSaUSDo: 2015 – 2020 Dietary Guidelines for Americans. 2015

3 Reuter S, Gupta SC, Chaturvedi MM, Aggarwal BB: Oxidative stress, inflammation, and cancer: how are they linked? Free radical biology & medicine 2010;49:1603-1616.

4 Pillai S, Oresajo C, Hayward J: Ultraviolet radiation and skin aging: roles of reactive oxygen species, inflammation and protease activation, and strategies for prevention of inflammation-induced matrix degradation – a review. International Journal of Cosmetic Science 2005;27:17-34.

5 Brohem CA, Cardeal LBD, Tiago M, Soengas MS, Barros SBD, Maria-Engler SS: Artificial skin in perspective: concepts and applications. Pigment Cell Melanoma Res 2011;24:35-50.

6 Kumari S, Pasparakis M: Epithelial Cell Death and Inflammation in Skin. Curr Top Microbiol Immunol 2017;403:77-93.

7 Fuchs E, Raghavan S: Getting under the skin of epidermal morphogenesis. Nat Rev Genet 2002;3:199-209.

8 Chhabra G, Ndiaye MA, Garcia-Peterson LM, Ahmad N: Melanoma Chemoprevention: Current Status and Future Prospects. Photochemistry and photobiology 2017;93:975-989.

9 Woo S-H, Lumpkin EA, Patapoutian A: Merkel cells and neurons keep in touch. Trends in cell biology 2015;25:74-81.

10 Deckers J, Hammad H, Hoste E: Langerhans Cells: Sensing the Environment in Health and Disease. Frontiers in Immunology 2018;9:93.

11 Apalla Z, Nashan D, Weller RB, Castellsague X: Skin Cancer: Epidemiology, Disease Burden, Pathophysiology, Diagnosis, and Therapeutic Approaches. Dermatol Ther (Heidelb) 2017;7:5-19.

12 Bickers DR, Athar M: Oxidative Stress in the Pathogenesis of Skin Disease. Journal of Investigative Dermatology 2006;126:2565-2575.

13 D'Orazio J, Jarrett S, Amaro-Ortiz A, Scott T: UV radiation and the skin. International journal of molecular sciences 2013;14:12222-12248.

14 Ryan JL: Ionizing Radiation: The Good, the Bad, and the Ugly. Journal of Investigative Dermatology 2012;132:985-993.

15 Urban L, Charles F, de Miranda MRA, Aarrouf J: Understanding the physiological effects of UV-C light and exploiting its agronomic potential before and after harvest. Plant Physiology and Biochemistry 2016;105:1-11.

16 Pfeifer GP: Formation and Processing of UV Photoproducts: Effects of DNA Sequence and Chromatin Environment. Photochemistry and Photobiology 1997;65:270-283.

17 Barnes JL, Zubair M, John K, Poirier MC, Martin FL: Carcinogens and DNA damage. Biochemical Society transactions 2018;46:1213-1224.

18 Arad S, Zattra E, Hebert J, Epstein EH, Jr., Goukassian DA, Gilchrest BA: Topical thymidine dinucleotide treatment reduces development of ultraviolet-induced basal cell carcinoma in Ptch-1+/- mice. Am J Pathol 2008;172:1248-1255.

19 Cooke MS, Loft S, Olinski R, Evans MD, Bialkowski K, Wagner JR, Dedon PC, Moller P, Greenberg MM, Cadet J: Recommendations for standardized description of and nomenclature concerning oxidatively damaged nucleobases in DNA. Chem Res Toxicol 2010;23:705-707.

20 Afaq F, Syed DN, Malik A, Hadi N, Sarfaraz S, Kweon MH, Khan N, Zaid MA, Mukhtar H: Delphinidin, an anthocyanidin in pigmented fruits and vegetables, protects human HaCaT keratinocytes and mouse skin against UVB-mediated oxidative stress and apoptosis. The Journal of investigative dermatology 2007;127:222-232.

21 de Gruijl FR, Rebel H: Early events in UV carcinogenesis--DNA damage, target cells and mutant p53 foci. Photochem Photobiol 2008;84:382-387.

22 Melnikova VO, Pacifico A, Chimenti S, Peris K, Ananthaswamy HN: Fate of UVB-induced p53 mutations in SKH-hr1 mouse skin after discontinuation of irradiation: relationship to skin cancer development. Oncogene 2005;24:7055-7063.

23 Valacchi G, Sticozzi C, Pecorelli A, Cervellati F, Cervellati C, Maioli E: Cutaneous responses to environmental stressors. Annals of the New York Academy of Sciences 2012;1271:75-81.

24 Swenberg JA, Lu K, Moeller BC, Gao L, Upton PB, Nakamura J, Starr TB: Endogenous versus exogenous DNA adducts: their role in carcinogenesis, epidemiology, and risk assessment. Toxicological sciences : an official journal of the Society of Toxicology 2011;120 Suppl 1:S130-145.

25 Botchkarev VA, Flores ER: p53/p63/p73 in the epidermis in health and disease. Cold Spring Harb Perspect Med 2014;4

26 Hoeijmakers JHJ: Genome maintenance mechanisms for preventing cancer. Nature 2001;411:366.

27 Marteijn JA, Lans H, Vermeulen W, Hoeijmakers JHJ: Understanding nucleotide excision repair and its roles in cancer and ageing. Nature Reviews Molecular Cell Biology 2014;15:465.

28 Jans J, Garinis GA, Schul W, van Oudenaren A, Moorhouse M, Smid M, Sert Y-G, van der Velde A, Rijksen Y, de Gruijl FR, van der Spek PJ, Yasui A, Hoeijmakers JHJ, Leenen PJM, van der Horst GTJ: Differential role of basal keratinocytes in UV-induced immunosuppression and skin cancer. Molecular and cellular biology 2006;26:8515-8526.

29 Hegde ML, Hazra TK, Mitra S: Early steps in the DNA base excision/single-strand interruption repair pathway in mammalian cells. Cell Research 2008;18:27.

30 Scott TL, Christian PA, Kesler MV, Donohue KM, Shelton B, Wakamatsu K, Ito S, D'Orazio J: Pigment-independent cAMP-mediated epidermal thickening protects against cutaneous UV injury by keratinocyte proliferation. Experimental dermatology 2012;21:771-777.

31 Pollet M, Shaik S, Mescher M, Frauenstein K, Tigges J, Braun SA, Sondenheimer K, Kaveh M, Bruhs A, Meller S, Homey B, Schwarz A, Esser C, Douki T, Vogel CFA, Krutmann J, Haarmann-Stemmann T: The AHR represses nucleotide excision repair and apoptosis and contributes to UV-induced skin carcinogenesis. Cell Death & Differentiation 2018;25:1823-1836.

32 Roos WP, Thomas AD, Kaina B: DNA damage and the balance between survival and death in cancer biology. Nature Reviews Cancer 2015;16:20.

33 Ratushny V, Gober MD, Hick R, Ridky TW, Seykora JT: From keratinocyte to cancer: the pathogenesis and modeling of cutaneous squamous cell carcinoma. The Journal of Clinical Investigation 2012;122:464-472.

34 Nichols JA, Katiyar SK: Skin photoprotection by natural polyphenols: anti-inflammatory, antioxidant and DNA repair mechanisms. Arch Dermatol Res 2010;302:71-83.

35 Schwarz T: 25 years of UV-induced immunosuppression mediated by T cells-from disregarded T suppressor cells to highly respected regulatory T cells. Photochem Photobiol 2008;84:10-18.

36 Halliday GM, Rana S: Waveband and dose dependency of sunlight-induced immunomodulation and cellular changes. Photochem Photobiol 2008;84:35-46.

37 Hanahan D, Weinberg RA: Hallmarks of cancer: the next generation. Cell 2011;144:646-674.

38 Katiyar SK, Afaq F, Azizuddin K, Mukhtar H: Inhibition of UVB-induced oxidative stress-mediated phosphorylation of mitogen-activated protein kinase signaling pathways in cultured human epidermal keratinocytes by green tea polyphenol (-)-epigallocatechin-3-gallate. Toxicol Appl Pharmacol 2001;176:110-117.

39 Chang L, Karin M: Mammalian MAP kinase signalling cascades. Nature 2001;410:37-40.

40 Kyriakis JM, Avruch J: Mammalian mitogen-activated protein kinase signal transduction pathways activated by stress and inflammation. Physiol Rev 2001;81:807-869.

41 Reuter S, Gupta SC, Chaturvedi MM, Aggarwal BB: Oxidative stress, inflammation, and cancer: how are they linked? Free radical biology & medicine 2010;49:1603-1616.

42 Kim AL, Labasi JM, Zhu Y, Tang X, McClure K, Gabel CA, Athar M, Bickers DR: Role of p38 MAPK in UVB-induced inflammatory responses in the skin of SKH-1 hairless mice. The Journal of investigative dermatology 2005;124:1318-1325.

43 Saez E, Rutberg SE, Mueller E, Oppenheim H, Smoluk J, Yuspa SH, Spiegelman BM: c-fos is required for malignant progression of skin tumors. Cell 1995;82:721-732.

44 Eckert RL, Adhikary G, Young CA, Jans R, Crish JF, Xu W, Rorke EA: AP1 transcription factors in epidermal differentiation and skin cancer. J Skin Cancer 2013;2013:537028.

45 Faes S, Dormond O: PI3K and AKT: Unfaithful Partners in Cancer. Int J Mol Sci 2015;16:21138-21152.

46 Manning BD, Cantley LC: AKT/PKB signaling: navigating downstream. Cell 2007;129:1261-1274.

47 Lake D, Correa SA, Muller J: Negative feedback regulation of the ERK1/2 MAPK pathway. Cell Mol Life Sci 2016;73:4397-4413.

48 Zhu J-W, Wu X-J, Lu Z-F, Luo D, Cai S-Q, Zheng M: Role of VEGF receptors in normal and psoriatic human keratinocytes: evidence from irradiation with different UV sources. PloS one 2013;8:e55463-e55463.

49 Bell S, Degitz K, Quirling M, Jilg N, Page S, Brand K: Involvement of NF-kappaB signalling in skin physiology and disease. Cell Signal 2003;15:1-7.

50 Aggarwal BB, Vijayalekshmi RV, Sung B: Targeting Inflammatory Pathways for Prevention and Therapy of Cancer: Short-Term Friend, Long-Term Foe. Clinical Cancer Research 2009;15:425-430.

51 Armstrong BK, Kricker A: The epidemiology of UV induced skin cancer. J Photochem Photobiol B 2001;63:8-18.

52 Matsumura Y, Ananthaswamy HN: Molecular mechanisms of photocarcinogenesis. Front Biosci 2002;7:d765-783.

53 Pitot HC, Dragan YP: Facts and Theories Concerning the Mechanisms of Carcinogenesis. Faseb J 1991;5:2280-2286.

54 You YH, Szabo PE, Pfeifer GP: Cyclobutane pyrimidine dimers form preferentially at the major p53 mutational hotspot in UVB-induced mouse skin tumors. Carcinogenesis 2000;21:2113-2117.

55 Benjamin CL, Ananthaswamy HN: p53 and the pathogenesis of skin cancer. Toxicology and applied pharmacology 2007;224:241-248.

56 Agar NS, Halliday GM, Barnetson RS, Ananthaswamy HN, Wheeler M, Jones AM: The basal layer in human squamous tumors harbors more UVA than UVB fingerprint mutations: A role for UVA in human skin carcinogenesis. Proceedings of the National Academy of Sciences of the United States of America 2004;101:4954-4959.

57 Rebel H, Mosnier LO, Berg RJ, Westerman-de Vries A, van Steeg H, van Kranen HJ, de Gruijl FR: Early p53-positive foci as indicators of tumor risk in ultraviolet-exposed hairless mice: kinetics of induction, effects of DNA repair deficiency, and p53 heterozygosity. Cancer research 2001;61:977-983.

58 Ziegler A, Jonason AS, Leffell DJ, Simon JA, Sharma HW, Kimmelman J, Remington L, Jacks T, Brash DE: Sunburn and p53 in the onset of skin cancer. Nature 1994;372:773-776.

59 Oda K, Arakawa H, Tanaka T, Matsuda K, Tanikawa C, Mori T, Nishimori H, Tamai K, Tokino T, Nakamura Y, Taya Y: p53AIP1, a potential mediator of p53-dependent apoptosis, and its regulation by Ser-46-phosphorylated p53. Cell 2000;102:849-862.

60 Mudgil AV, Segal N, Andriani F, Wang Y, Fusenig NE, Garlick JA: Ultraviolet B irradiation induces expansion of intraepithelial tumor cells in a tissue model of early cancer progression. The Journal of investigative dermatology 2003;121:191-197.

61 Abel EL, Angel JM, Kiguchi K, DiGiovanni J: Multi-stage chemical carcinogenesis in mouse skin: fundamentals and applications. Nat Protoc 2009;4:1350-1362.

62 Ra SH, Li X, Binder S: Molecular discrimination of cutaneous squamous cell carcinoma from actinic keratosis and normal skin. Mod Pathol 2011;24:963-973.

63 Rogers HW, Weinstock MA, Feldman SR, Coldiron BM: Incidence Estimate of Nonmelanoma Skin Cancer (Keratinocyte Carcinomas) in the U.S. Population, 2012. JAMA Dermatol 2015;151:1081-1086.

64 Bowden GT: Prevention of non-melanoma skin cancer by targeting ultraviolet-B-light signalling. Nat Rev Cancer 2004;4:23-35.

65 Stern RS: Prevalence of a history of skin cancer in 2007: results of an incidence-based model. Arch Dermatol 2010;146:279-282.

66 Wu S, Han J, Li WQ, Li T, Qureshi AA: Basal-cell carcinoma incidence and associated risk factors in U.S. women and men. Am J Epidemiol 2013;178:890-897.

67 Housman TS, Feldman SR, Williford PM, Fleischer AB, Jr., Goldman ND, Acostamadiedo JM, Chen GJ: Skin cancer is among the most costly of all cancers to treat for the Medicare population. J Am Acad Dermatol 2003;48:425-429.

68 Joseph AK, Mark TL, Mueller C: The period prevalence and costs of treating nonmelanoma skin cancers in patients over 65 years of age covered by medicare. Dermatologic surgery : official publication for American Society for Dermatologic Surgery [et al] 2001;27:955-959.

69 Christenson LJ, Borrowman TA, Vachon CM, Tollefson MM, Otley CC, Weaver AL, Roenigk RK: Incidence of basal cell and squamous cell carcinomas in a population younger than 40 years. Jama 2005;294:681-690.

70 Rees JR, Zens MS, Celaya MO, Riddle BL, Karagas MR, Peacock JL: Survival after squamous cell and basal cell carcinoma of the skin: A retrospective cohort analysis. Int J Cancer 2015;137:878-884.

71 Bichakjian C, Armstrong A, Baum C, Bordeaux JS, Brown M, Busam KJ, Eisen DB, Iyengar V, Lober C, Margolis DJ, Messina J, Miller A, Miller S, Mostow E, Mowad C, Nehal K, Schmitt-Burr K, Sekulic A, Storrs P, Teng J, Yu S, Huang C, Boyer K, Begolka WS, Alam M, Kim JYS, Kozlow JH, Mittal B, Moyer J, Olencki T, Rodgers P: Guidelines of care for the management of basal cell carcinoma. Journal of the American Academy of Dermatology 2018;78:540-559.

72 Hoban PR, Ramachandran S, Strange RC: Environment, phenotype and genetics: risk factors associated with BCC of the skin. Expert review of anticancer therapy 2002;2:570-579.

73 Jensen AO, Lamberg AL, Jacobsen JB, Olesen AB, Sorensen HT: Non-melanoma Skin Cancer and Ten-year All-cause Mortality: A Population-based Cohort Study. Acta Derm-Venereol 2010;90:362-367.

74 Epstein EH: Basal cell carcinomas: attack of the hedgehog. Nature Reviews Cancer 2008;8:743.

75 Epstein EH: Basal cell carcinomas: attack of the hedgehog. Nat Rev Cancer 2008;8:743-754.

76 Regl G, Kasper M, Schnidar H, Eichberger T, Neill GW, Philpott MP, Esterbauer H, Hauser-Kronberger C, Frischauf AM, Aberger F: Activation of the BCL2 promoter in response to Hedgehog/GLI signal transduction is predominantly mediated by GLI2. Cancer research 2004;64:7724-7731.

77 Wetmore C, Eberhart DE, Curran T: Loss of p53 but not ARF accelerates medulloblastoma in mice heterozygous for patched. Cancer research 2001;61:513-516.

78 Aszterbaum M, Epstein J, Oro A, Douglas V, LeBoit PE, Scott MP, Epstein EH, Jr.: Ultraviolet and ionizing radiation enhance the growth of BCCs and trichoblastomas in patched heterozygous knockout mice. Nature medicine 1999;5:1285-1291.

79 Grachtchouk V, Grachtchouk M, Lowe L, Johnson T, Wei L, Wang A, de Sauvage F, Dlugosz AA: The magnitude of hedgehog signaling activity defines skin tumor phenotype. The EMBO journal 2003;22:2741-2751.

80 Scrivener Y, Grosshans E, Cribier B: Variations of basal cell carcinomas according to gender, age, location and histopathological subtype. Br J Dermatol 2002;147:41-47.

81 Oberyszyn TM: Non-melanoma skin cancer: importance of gender, immunosuppressive status and vitamin D. Cancer Lett 2008;261:127-136.

82 Miller DL, Weinstock MA: Nonmelanoma skin cancer in the United States: incidence. J Am Acad Dermatol 1994;30:774-778.

83 Hall HI, May DS, Lew RA, Koh HK, Nadel M: Sun protection behaviors of the U.S. white population. Prev Med 1997;26:401-407.

84 Gawkrodger DJ: Occupational skin cancers. Occup Med (Lond) 2004;54:458-463.

85 Karia PS, Han J, Schmults CD: Cutaneous squamous cell carcinoma: estimated incidence of disease, nodal metastasis, and deaths from disease in the United States, 2012. J Am Acad Dermatol 2013;68:957-966.

86 Alam M, Armstrong A, Baum C, Bordeaux JS, Brown M, Busam KJ, Eisen DB, Iyengar V, Lober C, Margolis DJ, Messina J, Miller A, Miller S, Mostow E, Mowad C, Nehal K, Schmitt-Burr K, Sekulic A, Storrs P, Teng J, Yu S, Huang C, Boyer K, Begolka WS, Bichakjian C, Kim JYS, Kozlow JH, Mittal B, Moyer J, Olenecki T, Rodgers P: Guidelines of care for the management of cutaneous squamous cell carcinoma. Journal of the American Academy of Dermatology 2018;78:560-578.

87 Brantsch KD, Meisner C, Schonfisch B, Trilling B, Wehner-Caroli J, Rocken M, Breuninger H: Analysis of risk factors determining prognosis of cutaneous squamous-cell carcinoma: a prospective study. Lancet Oncol 2008;9:713-720.

88 Cooper JZ, Brown MD: Special concern about squamous cell carcinoma of the scalp in organ transplant recipients. Arch Dermatol 2006;142:755-758.

89 Rehman I, Takata M, Wu YY, Rees JL: Genetic change in actinic keratoses. Oncogene 1996;12:2483-2490.

90 Savoia P, Cremona O, Fava P: New Perspectives in the Pharmacological Treatment of Non-Melanoma Skin Cancer. Curr Drug Targets 2016;17:353-374.

91 Madan V, Lear JT, Szeimies RM: Non-melanoma skin cancer. Lancet 2010;375:673-685.

92 Fernandes AR, Santos AC, Sanchez-Lopez E, Kovačević AB, Espina M, Calpena AC, Veiga FJ, Garcia ML, Souto EB: Neoplastic Multifocal Skin Lesions: Biology, Etiology, and Targeted Therapies for Nonmelanoma Skin Cancers. Skin Pharmacology and Physiology 2018;31:59-73.

93 Werlinger KD, Upton G, Moore AY: Recurrence rates of primary nonmelanoma skin cancers treated by surgical excision compared to electrodesiccation-curettage in a private dermatological practice. Dermatologic surgery : official publication for American Society for Dermatologic Surgery [et al] 2002;28:1138-1142; discussion 1142.

94 Neagu M, Caruntu C, Constantin C, Boda D, Zurac S, Spandidos DA, Tsatsakis AM: Chemically induced skin carcinogenesis: Updates in experimental models (Review). Oncol Rep 2016;35:2516-2528.

95 Woodworth CD, Michael E, Smith L, Vijayachandra K, Glick A, Hennings H, Yuspa SH: Strain-dependent differences in malignant conversion of mouse skin tumors is an inherent property of the epidermal keratinocyte. Carcinogenesis 2004;25:1771-1778.

96 Stern MC, Benavides F, LaCava M, Conti CJ: Genetic analyses of mouse skin tumor progression susceptibility using SENCAR inbred derived strains. Mol Carcinogen 2002;35:13-20.

97 Lee KW, Kundu JK, Kim SO, Chun KS, Lee HJ, Surh YJ: Cocoa polyphenols inhibit phorbol ester-induced superoxide anion formation in cultured HL-60 cells and expression of cyclooxygenase-2 and activation of NF-kappaB and MAPKs in mouse skin in vivo. The Journal of nutrition 2006;136:1150-1155.

98 Wong VW, Sorkin M, Glotzbach JP, Longaker MT, Gurtner GC: Surgical approaches to create murine models of human wound healing. J Biomed Biotechnol 2011;2011:969618.

99 Miller SJ, Wei Z-G, Wilson C, Dzubow L, Sun T-T, Lavker RM: Mouse Skin Is Particularly Susceptible to Tumor Initiation During Early Anagen of the Hair Cycle: Possible Involvement of Hair Follicle Stem Cells. Journal of Investigative Dermatology 1993;101:591-594.

100 Cachon-Gonzalez MB, Fenner S, Coffin JM, Moran C, Best S, Stoye JP: Structure and expression of the hairless gene of mice. Proc Natl Acad Sci U S A 1994;91:7717-7721.

101 Cachon-Gonzalez MB, San-Jose I, Cano A, Vega JA, Garcia N, Freeman T, Schimmang T, Stoye JP: The hairless gene of the mouse: relationship of phenotypic effects with expression profile and genotype. Dev Dyn 1999;216:113-126.

102 Stoye JP, Fenner S, Greenoak GE, Moran C, Coffin JM: Role of endogenous retroviruses as mutagens: the hairless mutation of mice. Cell 1988;54:383-391.

103 Panteleyev AA, van der Veen C, Rosenbach T, Muller-Rover S, Sokolov VE, Paus R: Towards defining the pathogenesis of the hairless phenotype. The Journal of investigative dermatology 1998;110:902-907.

104 Benavides F, Oberyszyn TM, VanBuskirk AM, Reeve VE, Kusewitt DF: The hairless mouse in skin research. Journal of dermatological science 2009;53:10-18.

105 Montagna W, Chase HB, Melaragno HP: The skin of hairless mice. I. The formation of cysts and the distribution of lipids. The Journal of investigative dermatology 1952;19:83-94.

106 Rojas IG, Padgett DA, Sheridan JF, Marucha PT: Stress-induced susceptibility to bacterial infection during cutaneous wound healing. Brain Behav Immun 2002;16:74-84.

107 Tsao AS, Kim ES, Hong WK: Chemoprevention of cancer. CA: a cancer journal for clinicians 2004;54:150-180.

108 Aziz MH, Reagan-Shaw S, Wu J, Longley BJ, Ahmad N: Chemoprevention of skin cancer by grape constituent resveratrol: relevance to human disease? FASEB journal : official publication of the Federation of American Societies for Experimental Biology 2005;19:1193-1195.

109 Singh CK, Liu X, Ahmad N: Resveratrol, in its natural combination in whole grape, for health promotion and disease management. Ann N Y Acad Sci 2015;1348:150-160.

110 Block G, Patterson B, Subar A: Fruit, vegetables, and cancer prevention: A review of the epidemiological evidence. Nutrition and Cancer 1992;18:1-29.

111 McGovern PE: Ancient wine : the search for the origins of viniculture. Princeton, Princeton University Press, 2003.

112 Sekar S, Mariappan S: Traditionally fermented biomedicines, arishtas and asavas from Ayurveda. Indian J Tradit Knowl 2008;7:548-556.

113 Thakkur CG: Introduction to Ayurveda, the science of life. ASI Publishers, 1974.

114 Paul B, Masih I, Deopujari J, Charpentier C: Occurrence of resveratrol and pterostilbene in age-old darakchasava, an ayurvedic medicine from India. Journal of Ethnopharmacology 1999;68:71-76.

115 Brandt J: The grape cure. New York,, 1928.

116 Renaud S, de Lorgeril M: Wine, alcohol, platelets, and the French paradox for coronary heart disease. Lancet 1992;339:1523-1526.

117 Pezzuto JM: Grapes and human health: a perspective. J Agric Food Chem 2008;56:6777-6784.

118 Kjær TN, Thorsen K, Jessen N, Stenderup K, Pedersen SB: Resveratrol Ameliorates Imiquimod-Induced Psoriasis-Like Skin Inflammation in Mice. PLoS ONE 2015;10:e0126599.

119 Karuppagounder V, Arumugam S, Thandavarayan RA, Pitchaimani V, Sreedhar R, Afrin R, Harima M, Suzuki H, Nomoto M, Miyashita S, Suzuki K, Watanabe K: Resveratrol attenuates HMGB1 signaling and inflammation in house dust mite-induced atopic dermatitis in mice. International Immunopharmacology 2014;23:617-623.

120 Ndiaye M, Philippe C, Mukhtar H, Ahmad N: The Grape Antioxidant Resveratrol for Skin Disorders: Promise, Prospects, and Challenges. Archives of biochemistry and biophysics 2011;508:164-170.

121 Singh CK, George J, Ahmad N: Resveratrol-based combinatorial strategies for cancer management. Ann N Y Acad Sci 2013;1290:113-121.

122 Nayak BS, Ramdath DD, Marshall JR, Isitor GN, Eversley M, Xue S, Shi J: Wound-healing Activity of the Skin of the Common Grape (Vitis Vinifera) Variant, Cabernet Sauvignon. Phytother Res 2010;24:1151-1157.

123 Filip A, Daicoviciu D, Clichici S, Mocan T, Muresan A, Postescu ID: Photoprotective Effects of Two Natural Products on Ultraviolet B-Induced Oxidative Stress and Apoptosis in SKH-1 Mouse Skin. J Med Food 2011;14:761-766.

124 Filip A, Daicoviciu D, Clichici S, Bolfa P, Catoi C, Baldea I, Bolojan L, Olteanu D, Muresan A, Postescu ID: The effects of grape seeds polyphenols on SKH-1 mice skin irradiated with multiple doses of UV-B. Journal of Photochemistry and Photobiology B: Biology 2011;105:133-142.

125 Che DN, Xie GH, Cho BO, Shin JY, Kang HJ, Jang SI: Protective effects of grape stem extract against UVB-induced damage in C57BL mice skin. Journal of Photochemistry and Photobiology B: Biology 2017;173:551-559.

126 Cho BO, Che DN, Shin JY, Kang HJ, Jang SI: Ameliorative effects of fruit stem extract from Muscat Bailey A against chronic UV-induced skin damage in BALB/c mice. Biomed Pharmacother 2018;97:1680-1688.

127 Perde-Schrepler M, Chereches G, Brie I, Tatornir C, Postescu ID, Soran L, Filip A: Grape seed extract as photochemopreventive agent against UVB-induced skin cancer. J Photoch Photobio B 2013;118:16-21.

128 Arimoto-Kobayashi S, Zhang X, Yuhara Y, Kamiya T, Negishi T, Okamoto G: Chemopreventive effects of the juice of Vitis coignetiae Pulliat on two-stage mouse skin carcinogenesis. Nutr Cancer 2013;65:440-450.

129 Hanausek M, Spears E, Walaszek Z, Kowalczyk MC, Kowalczyk P, Wendel C, Slaga TJ: Inhibition of Murine Skin Carcinogenesis by Freeze-Dried Grape Powder and Other Grape-Derived Major Antioxidants. Nutr Cancer 2011;63:28-38.

130 de Gruijl FR: Skin cancer and solar UV radiation. Eur J Cancer 1999;35:2003-2009.

131 Mancebo SE, Wang SQ: Skin cancer: role of ultraviolet radiation in carcinogenesis. Reviews on environmental health 2014;29:265-273.

132 Sharma SD, Katiyar SK: Dietary grape seed proanthocyanidins inhibit UVB-induced cyclooxygenase-2 expression and other inflammatory mediators in UVB-exposed skin and skin tumors of SKH-1 hairless mice. Pharm Res 2010;27:1092-1102.

133 Singh CK, Mintie CA, Ndiaye MA, Chhabra G, Dakup PP, Ye T, Yu M, Ahmad N: Chemoprotective effects of dietary grape powder on ultraviolet B radiation-mediated skin carcinogenesis in SKH-1 hairless mice. The Journal of investigative dermatology 2018

134 Bobinaite R, Viskelis P, Venskutonis PR: Variation of total phenolics, anthocyanins, ellagic acid and radical scavenging capacity in various raspberry (Rubus spp.) cultivars. Food Chem 2012;132:1495-1501.

135 Gouveia-Figueira SC, Castilho PC: Phenolic screening by HPLC–DAD–ESI/MSn and antioxidant capacity of leaves, flowers and berries of Rubus grandifolius Lowe. Industrial Crops and Products 2015;73:28-40.

136 Huang C, Zhang D, Li J, Tong Q, Stoner GD: Differential inhibition of UV-induced activation of NF kappa B and AP-1 by extracts from black raspberries, strawberries, and blueberries. Nutr Cancer 2007;58:205-212.

137 Huang C, Huang Y, Li J, Hu W, Aziz R, Tang MS, Sun N, Cassady J, Stoner GD: Inhibition of benzo(a)pyrene diol-epoxide-induced transactivation of activated protein 1 and nuclear factor kappaB by black raspberry extracts. Cancer research 2002;62:6857-6863.

138 Huang C, Li J, Song L, Zhang D, Tong Q, Ding M, Bowman L, Aziz R, Stoner GD: Black raspberry extracts inhibit benzo(a)pyrene diol-epoxide-induced activator protein 1 activation and VEGF transcription by targeting the phosphotidylinositol 3-kinase/Akt pathway. Cancer research 2006;66:581-587.

139 Duncan FJ, Martin JR, Wulff BC, Stoner GD, Tober KL, Oberyszyn TM, Kusewitt DF, Van Buskirk AM: Topical treatment with black raspberry extract reduces cutaneous UVB-induced carcinogenesis and inflammation. Cancer Prev Res (Phila) 2009;2:665-672.

140 Divya SP, Wang X, Pratheeshkumar P, Son YO, Roy RV, Kim D, Dai J, Hitron JA, Wang L, Asha P, Shi X, Zhang Z: Blackberry extract inhibits UVB-induced oxidative damage and inflammation through MAP kinases and NF-kappaB signaling pathways in SKH-1 mice skin. Toxicol Appl Pharmacol 2015;284:92-99.

141 Calvo-Castro L, Syed DN, Chamcheu JC, Vilela FM, Perez AM, Vaillant F, Rojas M, Mukhtar H: Protective effect of tropical highland blackberry juice (Rubus adenotrichos Schltdl.) against UVB-mediated damage in human epidermal keratinocytes and in a reconstituted skin equivalent model. Photochem Photobiol 2013;89:1199-1207.

142 Afaq F, Saleem M, Krueger CG, Reed JD, Mukhtar H: Anthocyanin- and hydrolyzable tannin-rich pomegranate fruit extract modulates MAPK and NF-κB pathways and inhibits skin tumorigenesis in CD-1 mice. International journal of cancer 2005;113:423-433.

143 Gil MI, Tomas-Barberan FA, Hess-Pierce B, Holcroft DM, Kader AA: Antioxidant activity of pomegranate juice and its relationship with phenolic composition and processing. J Agric Food Chem 2000;48:4581-4589.

144 Hora JJ, Maydew ER, Lansky EP, Dwivedi C: Chemopreventive effects of pomegranate seed oil on skin tumor development in CD1 mice. J Med Food 2003;6:157-161.

145 Afaq F, Khan N, Syed DN, Mukhtar H: Oral feeding of pomegranate fruit extract inhibits early biomarkers of UVB radiation-induced carcinogenesis in SKH-1 hairless mouse epidermis. Photochem Photobiol 2010;86:1318-1326.

146 Khan N, Syed DN, Pal HC, Mukhtar H, Afaq F: Pomegranate fruit extract inhibits UVB-induced inflammation and proliferation by modulating NF-kappaB and MAPK signaling pathways in mouse skin. Photochem Photobiol 2012;88:1126-1134.

147 Afaq F, Malik A, Syed D, Maes D, Matsui MS, Mukhtar H: Pomegranate Fruit Extract Modulates UV-B–mediated Phosphorylation of Mitogen-activated Protein Kinases and Activation of Nuclear Factor Kappa B in Normal Human Epidermal Keratinocytes. Photochem Photobiol 2005;81:38-45.

148 Zaid MA, Afaq F, Syed DN, Dreher M, Mukhtar H: Inhibition of UVB-mediated oxidative stress and markers of photoaging in immortalized HaCaT keratinocytes by pomegranate polyphenol extract POMx. Photochem Photobiol 2007;83:882-888.

149 Afaq F, Zaid MA, Khan N, Dreher M, Mukhtar H: Protective effect of pomegranate-derived products on UVB-mediated damage in human reconstituted skin. Experimental dermatology 2009;18:553-561.

150 Vinson JA, Su X, Zubik L, Bose P: Phenol antioxidant quantity and quality in foods: fruits. J Agric Food Chem 2001;49:5315-5321.

151 Wolfe K, Wu X, Liu RH: Antioxidant activity of apple peels. J Agric Food Chem 2003;51:609-614.

152 Ding M, Lu Y, Bowman L, Huang C, Leonard S, Wang L, Vallyathan V, Castranova V, Shi X: Inhibition of AP-1 and neoplastic transformation by fresh apple peel extract. The Journal of biological chemistry 2004;279:10670-10676.

153 Di Mascio P, Kaiser S, Sies H: Lycopene as the most efficient biological carotenoid singlet oxygen quencher. Arch Biochem Biophys 1989;274:532-538.

154 Stahl W, Heinrich U, Aust O, Tronnier H, Sies H: Lycopene-rich products and dietary photoprotection. Photochemical & photobiological sciences : Official journal of the European Photochemistry Association and the European Society for Photobiology 2006;5:238-242.

155 Kopec RE, Schick J, Tober KL, Riedl KM, Francis DM, Young GS, Schwartz SJ, Oberyszyn TM: Sex differences in skin carotenoid deposition and acute UVB-induced skin damage in SKH-1 hairless mice after consumption of tangerine tomatoes. Molecular nutrition & food research 2015;59:2491-2501.

156 Cooperstone JL, Tober KL, Riedl KM, Teegarden MD, Cichon MJ, Francis DM, Schwartz SJ, Oberyszyn TM: Tomatoes protect against development of UV-induced keratinocyte carcinoma via metabolomic alterations. Scientific reports 2017;7:5106.

Figure Legends

Figure 1. Penetration of the ultraviolet radiation wavelengths into the skin.

Figure 2. The fates of the keratinocyte following UV-induced DNA damage and cellular repair mechanisms.

Figure 3. Summary of the beneficial effects of fruits in skin damage and carcinogenesis. Arrows and red text indicate upregulation and/or activation, lines with blunt end and green text indicated downregulation and/or inhibition.

Figures

Figure 1

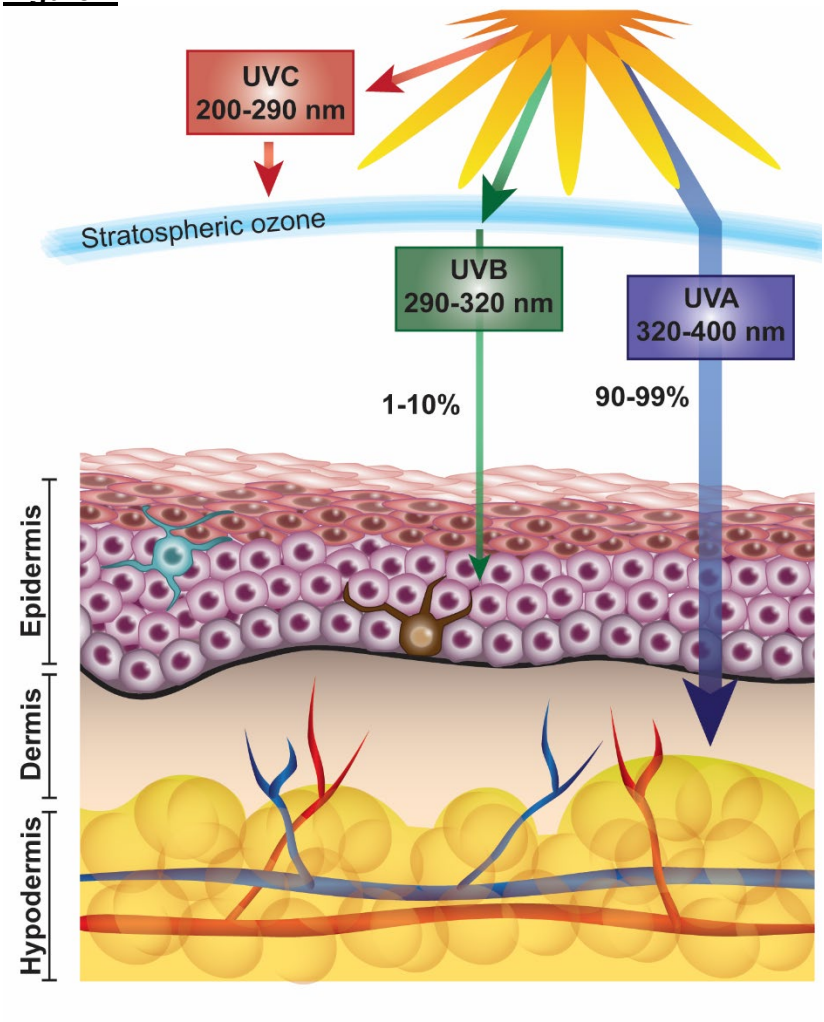

Figure 2

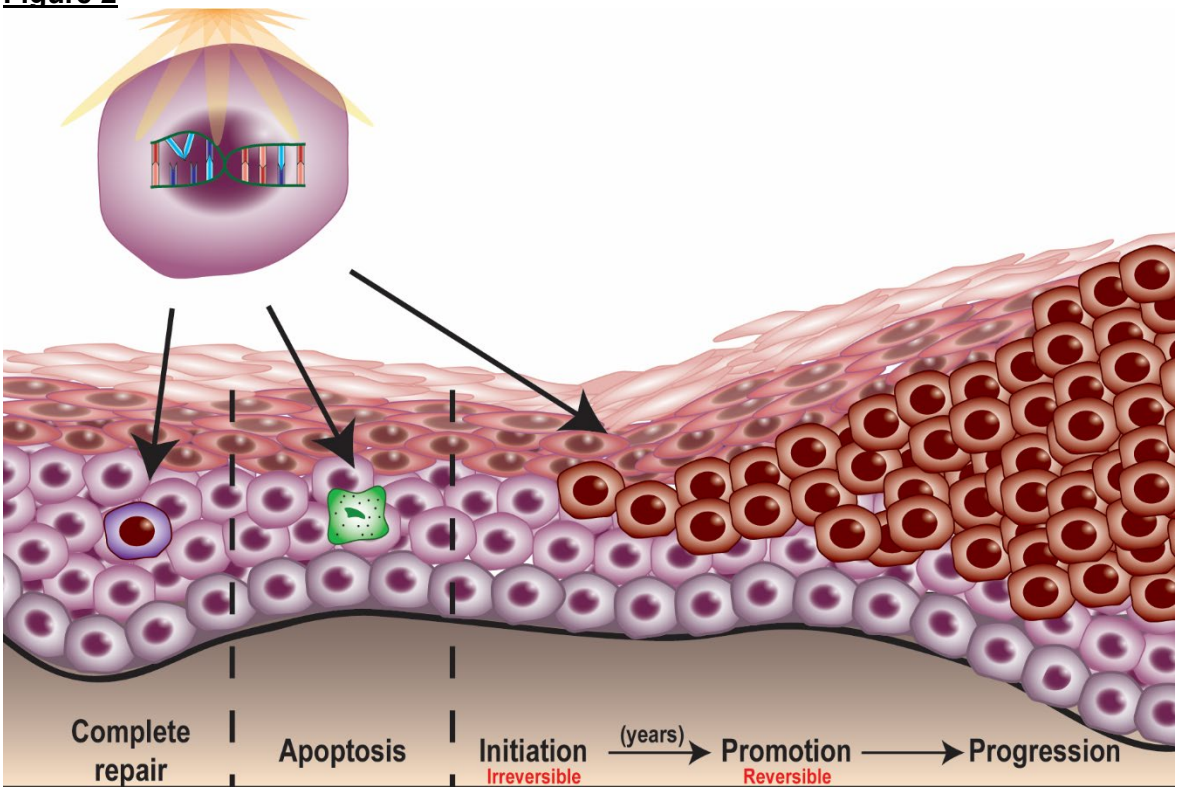
Complete repair
Apoptosis
Initiation
Irreversible
(years)
Promotion
Reversible
Progression

Figure 3

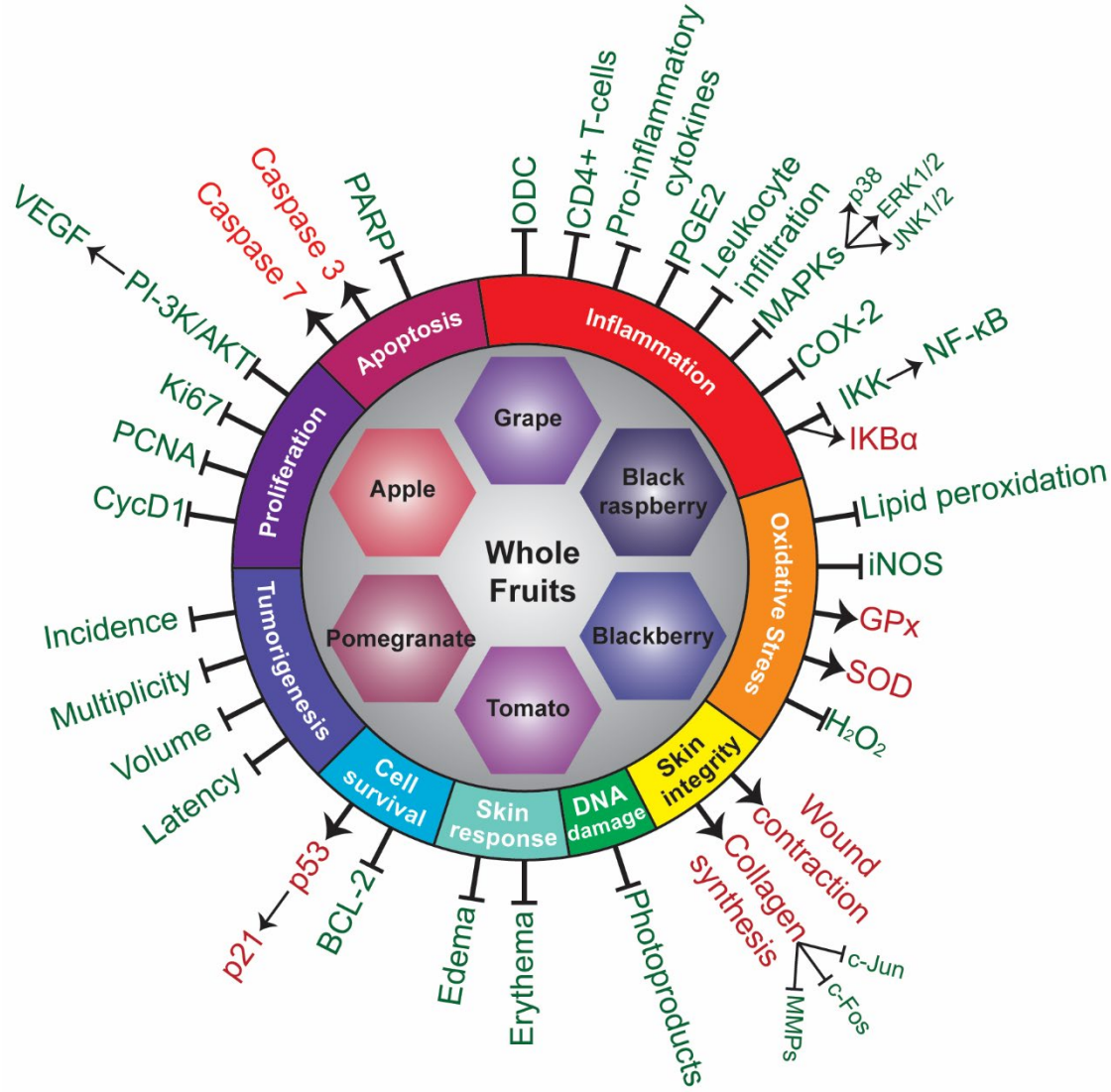
Whole Fruits
Grape
Apple
Black raspberry
Pomegranate
Blackberry
Tomato
Apoptosis
Inflammation
Oxidative Stress
Skin integrity
DNA damage
Skin response
Cell survival
Tumorigenesis
Proliferation
PARP
Caspase 3
Caspase 7
VEGF
PI-3K/AKT
Ki67
PCNA
CycD1
Incidence
Multiplicity
Volume
Latency
p21
p53
BCL-2
Edema
Erythema
Photoproducts
ODC
CD4+ T-cells
Pro-inflammatory cytokines
PGE2
Leukocyte infiltration
MAPKs
p38
ERK1/2
JNK1/2
COX-2
IKK
NF-κB
IKBα
Lipid peroxidation
iNOS
GPx
SOD
H2O2
Wound contraction
Collagen synthesis
c-Jun
c-Fos
MMPs

Table 1: *In vitro* and *in vivo* studies to assess the effects of fruits in skin and skin conditions

In Vitro Studies

Chemopreventive agent	Genus and variety	Cell Line	Chemopreventive agent dosing	Carcinogen dose	Ref.
Grape seed extract	*Vitis vinifera*, Burgund Mare	HaCaT	10 or 20 ug, single dose	UVB (100 or 200 mJ/cm^2), single dose	[127]
Black raspberry extract	*Rubus occidentalis*	JB6 C1 41, transected with AP-1-luciferase reporter	50 ug/mL, 30 min prior	UVB (2 KJ/m^2), single dose	[136, 137]
Black raspberry extract	*Rubus occidentalis*	JB6 C1 41, transfected with AP-1 luciferase reporter, NF-kB-luciferase reporter, or p53-luciferase reporter	25 ug/mL, 30 min prior	BPDE (2 uM), single dose	[137]
Black raspberry extract	*Rubus occidentalis*	JB6 C1 41, transfected with AP-1 luciferase reporter, VEGF-luciferase reporter, or dominant-negative PI-3K mutant	25 ug/mL, 30 min prior	B[a]PDE (2 uM), single dose	[138]
Blackberry juice	*Rubus adenotrichos*, tropical highland blackberry	NHEK	1:300 or 1:500, 2 h prior	UVB (25 mJ/cm^2), single dose	[141]
Blackberry juice	*Rubus adenotrichos*, tropical highland blackberry	NHEK	1:300 or 1:500, immediately post for 24 h	UVB (25 mJ/cm^2), single dose	[141]
Blackberry juice	*Rubus adenotrichos*, tropical highland blackberry	Human reconstituted skin equivalent	Topical (10 uL), 2 h prior	UVB (25 mJ/cm^2), single dose	[141]
Blackberry juice	*Rubus adenotrichos*, tropical highland blackberry	Human reconstituted skin equivalent	Topical (10 ul), immediately post for 24 h	UVB (25 mJ/cm^2), single dose	[141]
Pomegranate fruit extract	*Punica granatum*	NHEK	10-40 ug/mL, 24 h prior	UVB (40 mJ/cm^2), single dose	[147]

Pomegranate fruit extract (POMx)	*Punica granatum*	HaCaT	10-40 ug/mL, 24 h prior	UVB (15 or 30 mJ/cm^2), single dose	[148]
POMx extract	*Punica granatum*	Human reconstituted skin (Epiderm™ FT-200)	1-2 uL, 1 h prior	UVB (60 mJ/cm^2), single dose	[149]
POMx juice	*Punica granatum*	Human reconstituted skin (Epiderm™ FT-200)	5-10 ug, 1 h prior	UVB (60 mJ/cm^2), single dose	[149]
POMo (pomegranate seed)	*Punica granatum*	Human reconstituted skin (Epiderm™ FT-200)	1-2 uL, 1 h prior	UVB (60 mJ/cm^2), single dose	[149]
Apple peel extract	*Malus pumila*, Gala	JB6/AP/kB	1:10 to 1:640, 2 h prior	TPA (20 nmol) or UVB (4 KJ/m^2), single dose	[151]

In Vivo Studies

Chemopreventive agent	**Genus**	**Model**	**Chemopreventive agent dosing**	**Carcinogen dose**	**Ref**
Grape-skin powder	*Vitis vinifera*, Cabernet Sauvignon	Sprague Dawley rats	Topical (100 mg/kg), daily	N/A-inflicted wound	[122]
Fruit stem extract	*Vitis labrusca* x *Vitis vinifera*, Muscat Bailey A	Balb/c mice	Topical (1 mg), daily	UVB (120 mJ/cm^2), 3x weekly for 1 month	[126]
Grape stem extract	*Vitis labrusca*, Campbell Early	C57BL	Topical (50 mg/kg), daily dose, 1 week prior	UVB (120 mJ/cm^2), 3x weekly for 3 weeks	[125]
Y-grape juice	*Vitis coignetiae*, Yamabudo	SENCAR	Topical (20 uL), single dose	TPA (1.7 nmol), single dose	[128]
EtOAc-fr (extract)	*Vitis coignetiae*, Yamabudo	SENCAR	Topical (10 uL), single dose	TPA (1.7 nmol), single dose	[128]
Y-grape juice or EtOAc-fr (extract)	*Vitis coignetiae*, Yamabudo	SENCAR	Oral, *ad libitum* (in lieu of drinking water), single dose, 12 hr prior	TPA (1.7 nmol), single dose	[128]
Y-grape juice	*Vitis coignetiae*, Yamabudo	SENCAR	Topical (X2 or X10), 2X weekly, 30 min prior	DMBA-initiation (2.5 mg/animal), TPA promotion (1.7 nmol) for 20 weeks	[128]

Y-grape EtOAc-fr (extract)	*Vitis coignetiae*, Yamabudo	SENCAR	Oral, *ad libitum*, in lieu of drinking water (X2 or X10)	DMBA-initiation (2.5 mg/animal), TPA promotion (1.7 nmol), for 20 weeks	[128]
Grape seed proanthocyandins	N/A	SKH-1 hairless mice	Oral, *ad libitum* (0.2% or 0.5% in AIN-76A diet)	UVB (180 mJ/cm^2), 3X weekly for 24 weeks	[132]
Grape seed extract	*Vitis vinifera*, Burgund Mare	SKH-1 hairless mice	Topical, (4 mg/cm^2), single dose, 30 min prior	UVB (240 mJ/cm^2), single dose	[123]
Grape seed extract	*Vitis vinifera*, Burgund Mare	SKH-1 hairless mice	Topical (2.5 mg/cm^2 or 4 mg/cm^2), 30 min prior or 30 min post	UVB, (240 mJ/cm^2), daily for 10 days	[124]
Grape powder	*N/A*, Red, green, and black California grapes	SKH-1 hairless mice	Oral, *ad libitum* (3% or 5% in AIN-76A diet)	UVB (180 mJ/cm^2), 2X weekly for 28 weeks	[133]
Grape powder	*N/A*, Red, green, and black California grapes	SENCAR	Topical (1, 2, or 4 mg), 30 min post	DMBA (100 nmol), 2X weekly for 4 weeks	[129]
Powdered grape seed extract	*Vitis vinifera*	SENCAR	Topical (1, 2, or 4 mg), 30 min post	DMBA (100 nmol), 2X weekly for 4 weeks	[129]
Grape powder	*N/A*, Red, green, and black California grapes	SENCAR	Oral, *ad libitum* (1%, 2%, or 5% in AIN-93GA diet), 2 weeks prior	DMBA (100 nmol), 2X weekly for 12 weeks	[129]
Grape powder	*N/A*, Red, green, and black California grapes	SENCAR	Topical (2 mg), 30 min post	DMBA (100 nmol), 2X weekly for 24 weeks	[129]
Grape powder	*N/A*, Red, green, and black California grapes	SENCAR	Oral, *ad libitum* (1% in AIN-93GA diet), 2 weeks prior	DMBA (100 nmol), 2X weekly for 24 weeks	[129]
Black raspberry extract	*Rubus occidentalis*	SKH-1 hairless mice	Topical (500 ug), immediately post	UVB (2,240 KJ/m^2), 3X weekly for 25 weeks	[139]
Black raspberry extract	*Rubus occidentalis*	SKH-1 hairless mice	Topical (500 ug), immediately post	UVB (2,240 KJ/m^2), single dose	[139]
Blackberry extract	*N/A*	SKH-1 hairless mice	Topical (10% or 20%), one day prior	UVB (100 mJ/cm^2), 3X	[140]

				weekly for 10 weeks	
Pomegranate fruit extract	*Punica granatum*	CD-1	Topical (2 mg), 30 min prior	TPA (3.2 nmol), single dose	[142]
Pomegranate fruit extract	*Punica granatum*	CD-1	Topical (2 mg), prior to TPA	DMBA-initiation (50 nmol), TPA promotion (3.2 nmol) 2X weekly for 30 weeks	[142, 144]
Pomegranate seed oil	*Punica granatum*	CD-1	Topical (5%), 1 h prior	DMBA-initiation (200 nmol), TPA promotion (5 nmol) 2X weekly for 20 weeks	[144]
Pomegranate fruit extract	*Punica granatum*	SKH-1 hairless mice	Oral *ad libitum* (0.2% in drinking water), 14 days prior	UVB (180 mJ/cm^2), single dose	[145]
Pomegranate fruit extract	*Punica granatum*	SKH-1 hairless mice	Oral *ad libitum* (0.2% in drinking water), 14 days prior through termination	UVB (180 mJ/cm^2), 7 doses on alternating days	[146]
Apple peel extract	*Malus pumila*, Gala	AP-1-luciferase reporter transgenic mice (C57BL/6 x DBA2)	Oral, *ad libitum*, in lieu of drinking water and topical, 6X daily	TPA (5 ug) or UVB (10 KJ/m^2), single dose on fourth day of APE	[151]
Apple peel extract	*Malus pumila*, Gala	AP-1-luciferase reporter transgenic mice (C57BL/6 x DBA2)	Oral, *ad libitum*, in lieu of drinking water, 2 days prior	DMBA-initiation (400 nmol), TPA promotion (17 nmol), started 14 days post DMBA, 2X weekly for 20 weeks	[151]
Tangerine tomato powder	*Solanum lycopersicum*, Tangerine tomato	SKH-1 hairless mice	Oral, *ad libitum* (10% in AIN-93GA diet), 10 weeks prior	UVB (2,240 J/m^2), single dose at week 10	[154]
Tangerine tomato powder or Red tomato powder	*Solanum lycopersicum*, Tangerine tomato	SKH-1 hairless mice	Oral, *ad libitum* (10% in AIN-93GA diet), through 35 weeks	UVB (2,240 J/m^2), 3X weekly, weeks 11 through 20	[155]

Table 2: Clinical trials to assess the effects of whole fruit on varying diseases and health

Clinical trials					
	Grape	**Pomegranate**	**Apple**	**Berry**	**Tomato**
Active, not recruiting	16	4	8	8	6
Completed	123	62	132	48	49
Enrolling by invitation	1	1	3	0	0
Not yet recruiting	10	2	9	5	4
Recruiting	27	4	30	12	7
Unknown status	21	15	15	6	4
Withdrawn	1	2	5	2	3
Terminated	1	0	4	0	1
Total:	**200**	**90**	**206**	**81**	**74**

Chapter 2: Chemoprotective effects of dietary grape powder on ultraviolet B radiation-mediated skin carcinogenesis in SKH-1 hairless mice

Originally published in the *Journal of Investigative Dermatology*

J Invest Dermatol, 2019 Mar, Volume 139, Issue 3, 552 - 561

(Reprinted with permission from Elsevier)

Abstract

Skin cancer is the most frequently diagnosed cancer in the US, and solar ultraviolet (UV) radiation is an established causative factor for ~90% of these cases. Despite efforts aimed at UV protection, including use of sunscreen and clothing, annual cases of skin cancers continue to rise. Here, we report that dietary grape powder (GP) mitigates UVB-mediated skin carcinogenesis in SKH-1 hairless mouse model. Employing a UVB initiation-promotion protocol, where mice were exposed to 180 mJ/cm^2 UVB 2x/week for 28 weeks, we determined the effects of GP-fortified diet (3% or 5%) on skin carcinogenesis. GP consumption at both doses resulted in marked inhibition in tumor incidence, as well as a delay in onset of tumorigenesis. Molecular analyses of skin and tumor tissue demonstrated that GP-mediated protective response against UVB-induced skin cancer was accompanied by enhanced DNA damage repair, reduced proliferation, increased apoptosis and modulations in several oxidative stress markers specifically related to inhibition of oxidative stress and increased ROS metabolism. Interestingly, NRF2, an activator of cellular antioxidant response, was decreased by GP feeding, suggesting a supportive role in tumor cell survival. Overall, our study suggested that dietary grape, containing several antioxidants in natural amalgamation, may protect against UVB-mediated skin carcinogenesis.

Introduction

Nonmelanoma skin cancers (NMSCs) are the most commonly diagnosed malignancy, affecting more than 3.5 million Americans on an annual basis [1]. NMSCs are mostly comprised of basal cell carcinomas (BCCs) and squamous cell carcinomas (SCCs), which arise in the epidermis from keratinocytes that have undergone malignant transformation [2]. Solar ultraviolet (UV) radiation is believed to be the most prevalent natural carcinogen in our environment and has been identified as a causative factor for ~90% of NMSC cases [3]. Solar UV radiation that penetrates the atmosphere is mainly comprised of UVA (90–99%; 320–400 nm) and UVB (1–10%; 290–320 nm), whereas most of the higher energy UV radiation (UVC; 200-290 nm) is absorbed by stratospheric ozone and other atmospheric components [4]. Preventing skin damage from UV radiation is largely done through regular and ample application of sunscreen, seeking shade, and wearing clothing that covers the skin. However, continuously rising numbers of skin cancer cases suggest that implementation of these measures has not been fully effective. Interestingly, prior skin cancer history has been linked to an increased risk of developing other neoplasms [1, 5, 6]. Additionally, according to the most recent estimates, NMSC has a $4.8 billion annual burden on the US economy [7]. All these reasons provide a rationale to intensify our efforts towards the identification of additional approaches for skin cancer chemoprevention.

Using naturally occurring non-toxic antioxidants has practical implications in reducing cancer risk because unlike carcinogenic environmental factors that are difficult to control, individuals can make decisions to modify their choices of food and beverages they consume. The grape antioxidant resveratrol (3,5,4′-trihydroxystilbene) is one such agent that has been studied at length for its health-promoting and anticancer effects [8, 9]. However, the grape itself is a natural conglomeration of more than 1600 compounds that also includes quercetin, melatonin, lycopene and several other potent antioxidants [10, 11]. Recent studies indicate that these

compounds may help protect against certain cancers, heart disease, nerve and brain disorders, arthritis and an array of other conditions (reviewed in [12]). Because of the high antioxidant capacity of many of these constituents and their natural combination in grapes, we reasoned that dietary grapes, containing a number of useful food components, could be very useful against UVB-mediated skin carcinogenesis. We believe that the whole food concept, which relies on additive and synergistic response of multiple agents, is a better option for cancer chemoprevention. This study was undertaken to determine the protective effects and potential mechanisms of grape powder-fortified diet on UVB-induced skin cancer in SKH-1 hairless mice, a relevant model for skin carcinogenesis [13].

Materials and Methods

Dietary grape feed

Freeze-dried grape powder (GP), composed of fresh red, green, and black grapes (*Vitis vinifera*) of both seeded and seedless varieties was obtained from the CTGC. This mixture is a representative of the mix of grapes available to consumers in the U.S. during the 9-month long California grape season, typically between July and October. For GP production, grapes were frozen, ground on dry ice, freeze-dried, then re-ground to preserve the integrity of the biologically active compounds. For our studies, we used GP from a single batch made in 2011, which was incorporated into AIN-76A diet by Envigo (Madison, WI) at concentrations of 0, 3, or 5% GP. All diets were matched to the natural sugar content of the 5% GP diet.

UVB-mediated skin carcinogenesis model of SKH-1 hairless mice.

The animal experiments were approved by the University of Wisconsin (UW) Institutional Animal Care and Use Committee. SKH-1 hairless mice (female, 5 weeks old, n=12 per group) were obtained from Charles River Laboratories (Wilmington, MA) and allowed to acclimatize for

one week prior to study initiation. Animals had access to water and feed *ad libitum*. The experimental diets (containing 0, 3, or 5% GP) were started beginning on day one of UV exposure and continued until the termination of the experiment. Throughout the experiment, animals were closely monitored for general health, body weight, and food consumption. Measured doses of UVB irradiation were administered using a calibrated Research Irradiator (Daavlin Company, Bryan, OH). All animals received UVB exposures twice weekly at 180 mJ/cm^2 starting at 6 weeks of age and continuing for 28 weeks. “Dosing holidays,” where one UV dose was purposefully skipped, happened during weeks 8, 10, and 18, due to noticeably high amounts of erythema. Mice were examined for tumors before each UVB exposure. Distinguishable tumors (initially arising as papules) were counted weekly up to 27 weeks, as well as at time of euthanasia, and tumor measurements using a digital caliper were started upon reaching at least 2 mm in diameter. Tumor volume was calculated using the formula length x width x height x (π / 6). At the termination of the experiment, mice were euthanized 3-5 days after their last UV exposure and skin and tumor tissue were collected for further analysis.

Tissue embedding, epidermal thickness evaluation and immunohistology

Harvested tumors, adjacent (involved) skin, and non-UV treated (un-involved) stomach skin were formalin fixed, paraffin embedded, sectioned, and mounted on serial slides at the UW Carbone Cancer Center Experimental Pathology Core Laboratory. One serial slide from each mouse was stained with hematoxylin and eosin (H&E) and analyzed for epidermal thickness as described in Supplementary Information online. Epidermal thicknesses were evaluated by analyzing 5 fields of view from each mouse section using an EVOS XL Core Cell Imaging System (Thermo Fisher Scientific) and measured using ImageJ software (NIH, Rockville, MD). Sections of measurement were obtained if the following criteria were present, 1) the hair follicle was in the correct orientation and 2) a basal layer was present. Sample measurements were averaged together, graphed and subjected to statistical analysis.

Immunohistochemistry

For immunostaining, slides were deparaffinized using xylenes and rehydrated via graded ethanol (100-70%). Using heat-induced epitope retrieval, slides were steamed for 45 minutes in IHC-Tek Epitope Retrieval Solution (#IW-1100, IHC World, LLC, Ellicott City, MD), followed by a 20 minute RT incubation. Slides were immunostained using the Vectastain ABC Kit (#AK-5001, Vector Labs, Burlingame, CA) per manufacturer's protocol, with an overnight incubation at 4°C with primary antibody (see Supplementary Table S3) in a humidifying chamber. After a final wash, slides were exposed to Vector Red Alkaline Phosphatase Substrate Kit (#SK-5100, Vector Labs) until desired staining intensity was observed (approximately 5 minutes) then washed and counterstained with Harris modified hematoxylin (#SH30-500D, Fisher Scientific), dehydrated with graded ethanol (70-100%) and xylenes, then mounted with Permount mounting medium (Fisher Scientific) diluted in xylene (1:2). Images for Ki-67 and NRF2 were obtained at 20x using a Nuance Multispectral Tissue Imaging System (Perkin Elmer, Waltham, MA) and 4-HNE imaging was captured at 20x using an EVOS® XL Core Cell Imaging System (Thermo Fisher Scientific).

Preparation of epidermal gDNA and immuno-slot blot analysis

Epidermal gDNA was isolated from involved and un-involved skin from 5 randomly selected animals in the control and 5% GP groups. Skin from 5 randomly selected animals in the control and 5% GP groups were heated for 15 seconds at 60°C followed immediately by incubation for 30 seconds in ice water. Excess water was removed by placing tissue between two paper towels and the epidermis was gently separated from the remaining tissue, treated with Proteinase K and RNase A, and then genomic DNA (gDNA) was isolated using the QIAamp DNA Mini Kit (Qiagen) according to manufacturer's protocol. The quality and quantity of the gDNA were assessed using a NanoDrop 2000 spectrophotometer (Thermo Fisher Scientific)

before measurement of photoproducts by immuno-slot blot analysis as previously reported (Gaddameedhi et al., 2010). Briefly, 200 ng and 300 ng of gDNA was used per slot for CPDs and (6-4) PPs detection, respectively. gDNA was denatured by heating for 10 minutes at 100°C, and neutralized immediately by placing on ice and adding cold ammonium acetate to a final 1 M concentration. Prepared gDNA samples were bound to a nitrocellulose membrane (pre-wet with 6x saline-sodium citrate (SSC) buffer) using a Bio-Dot SF slot-blot apparatus (BioRad Laboratories, Hercules, CA) and crosslinked by baking for 2 hours at 80°C in a vacuum oven (Shel Lab, Cornelius, OR). Blots were subsequently blocked in PBS-T and 5% nonfat dry milk for 1 hour at room temperature (RT). The membrane was incubated with anti-CPD or anti-(6-4) PP antibodies (see Supplementary Table S3) in ice-cold PBS-T for 12-16 hours at 4°C with gentle shaking. A secondary antibody (anti-mouse conjugated with HRP) was detected using Clarity Western ECL chemiluminescent substrate (#170-5061, Bio-Rad Laboratories) or SuperSignal West Femto (#34096, Thermo Fisher) reagents using Bio-Rad Imager. Afterward, the membrane was stained with SYBR gold (#S11494, 1:5000 dilution, Thermo Fisher) as an internal control, by incubating for 1 hour at RT under light protection. Signals were quantified using Adobe Photoshop CS6.

Tissue lysate preparation, immunoblot analysis, and RT-qPCR

Liquid nitrogen flash-frozen tumors were ground into powder using a mortar and pestle in liquid nitrogen before being divided for protein and RNA analysis. Equal amounts of protein or RNA from 3 mice from each experimental group were pooled for subsequent studies, with 3 separate groupings made to represent averages of the entire cohort. For protein analysis, the powdered tissue was lysed in 1X RIPA lysis buffer (Millipore, Billerica, MA) with freshly added PMSF (Amresco, Solon, OH) and protease inhibitor cocktail (Thermo Scientific, Waltham, MA). Protein concentration was determined by BCA Protein Assay (Thermo Scientific), and used for immunoblot analysis. Equal amounts of protein from 3 mice from each experimental group were

pooled for subsequent studies, with 3 separate groupings made to represent averages of the entire cohort. These pooled protein samples were subjected to SDS-PAGE, transferred to a 0.2 μm nitrocellulose membrane (Bio-Rad, Hercules, CA), and blocked with 5% non-fat dry milk in TBS-T. Membranes were probed with primary antibody (see Supplementary Table S3) and appropriate secondary antibody conjugated with horseradish peroxidase (HRP) (Cell Signaling Technology, Danvers, MA) before chemiluminescence detection using the Kodak ImageStation 4000MM (Carestream Health, Inc, Rochester, NY).

RNA was isolated from the tumor tissue powder (described above) was subjected to RNA isolation using the RNeasy Plus Mini Kit (Qiagen, Germantown, MD) according to manufacturer's protocol, followed by RNA quantification. Equal amounts of RNA from 3 mice from each experimental group were pooled for subsequent studies, with 3 separate groupings made to represent averages of the entire cohort. RNA was transcribed using random primers and M-MLV reverse transcriptase (Promega, Madison, WI). RT-qPCR was then performed with SYBR Premix Ex Taq II (TaKaRa, Mountain View, CA) and the appropriate primer set (see Supplementary Table S4). Relative target mRNA levels were calculated using the ΔΔCT comparative method using *Gapdh* and *Actb* as endogenous controls.

Oxidative stress PCR array and Ingenuity Pathway Analysis (IPA)

The effects of GP feeding on oxidative stress and antioxidant response genes were assessed using the Qiagen Mouse Oxidative Stress RT2 Profiler™ PCR Array (#PAMM-065Z) per manufacturer's instructions. Resultant Ct values were uploaded to the Qiagen GeneGlobe Data Analysis Center and analyzed using *Gapdh* and *Actb* reference genes. The data analysis web portal calculated fold-change using ΔΔCT method (Supplementary Table S1 and S2), and also presented data as heat map (Supplementary Figure S2). Selected genes from the PCR array results were validated using RT-qPCR analysis. Primer pairs detailed in Supplementary

Table S4 were retrieved from Primer Bank (Wang et al., 2012). Further, to understand the pathways affected by GP supplementation, differentially expressed genes from the PCR array were analyzed by Qiagen's IPA software. The predicted gene-gene interaction and functional networks were generated and analyzed using the inputs of gene identifiers and fold-change regulation (≥1.75-fold change in 5% GP with statistical significance as well as with minimum 1.4-fold change in 3% GP).

Caspase-Glo 3/7 Assay

Protein lysates were prepared as described above. Caspase-Glo 3/7 Assay (Promega) was used according to the manufacturer's protocol. Protein lysates from 5 tumors from each group (control and 5% GP) were prepared by grinding with mortar and pestle on liquid nitrogen, then resuspended in PBS + 1% NP40 with protease (Thermo Fisher) and phosphatase (CalBioChem, Millipore Sigma) inhibitors and sonicated on ice. Protein was quantified using a BCA Assay (Thermo Fisher), normalized to 100 µg/mL, and loaded with an equal volume of Caspase-Glo reagent. Luminescence was read using a Biotek Synergy H1 plate reader (Biotek, Winooski, VT).

Statistical analysis

Statistical support for tumor data was provided by the collaborating statistics core facility statisticians (TY and MY). One mouse from the control group developed lymphoma at week 21 and therefore euthanized early and excluded from analysis. Weekly tumor incidence and mean tumor volume measurements were analyzed by a mixed effect model $Y_{ij} = \mu_0 + \mu_1 I(G_i = 2) + \mu_2 I(G_i = 3) + \beta t_j + b_{i,0} + b_{i,1} t_j + \varepsilon_{ij}$, where G_i is the group indicator, which equals 1, 2, and 3 for the control, 3% GP, and 5% GP feed groups, respectively. The 'fixed' effect parameters $\mu_0, \mu_1, \mu_2, \beta$ represent the underlying population average effect, $b_{i,0}, b_{i,1}$ are subject-specific

random effects, and ε_{ij} is the error or noise term. Intuitively, the time effect is modeled linearly for every subject, but the intercept and slope of the linear time trend can deviate from the population average. Due to the skew in tumor counts, a small number was added to every tumor to ensure a positive value. The data was log transformed and treated as the response variable. Tumor-free survival was defined as the time (in weeks) until tumor development. Because all mice developed tumors, no censoring was needed; therefore, Dunn's Kruskal-Wallis multiple comparisons test was performed to examine the treatment effects, with the p-value adjusted using the Benjamini-Hochberg method. Note that Dunn's test is non-parametric, leaving no assumption on the distribution. At the time of euthanasia, the treatment effects with respect to the final counts (multiplicity) of discernable papules (<2 mm) and large tumors (>2 mm) are estimated by fitting linear regression model $Y_i = \mu_0 + \mu_1 I(G_i = 2) + \mu_2 I(G_i = 3) + \varepsilon_i$, respectively, where Y_i is the log tumor count. All other statistical analyses were performed using GraphPad PRISM 5.0 software (GraphPad Software, La Jolla, CA).

Results & Discussion

Dietary grape powder (GP) decreases skin tumor incidence and delays onset of tumorigenesis in SKH-1 hairless mouse model of skin carcinogenesis

Since UV exposure, especially the UVB spectrum is a major risk factor for skin cancer, this study was designed to access the effects of dietary GP feeding on UVB exposure mediated skin tumorigenesis in mice. The details of the major compounds of GP (obtained from the California Table Grape Commission (CTGC)) are presented in Figure 1a. As laid out in Figure 1b, we determined the effects of dietary GP in a long-term, chronic UVB-mediated skin carcinogenesis model in SKH-1 hairless mice that closely mimics human skin photocarcinogenesis [14, 15]. We found that GP supplementation was well tolerated by the mice, and average diet consumption/mouse/day corresponded to 102 and 180 mg of GP consumption by 3% and 5%

GP supplemented groups, respectively. These correspond to human equivalent doses of 24.77 and 43.61 g/day, using the dose translation model proposed in [16], or 1.07 and 1.85 servings of grapes, respectively.

During the study, mice developed different sized tumors, as shown in Figure 1c. Details about the tumor multiplicity data of weeks 24-27 showing the significant differences in tumor incidence, especially in 5% GP, are presented in Figure 1d. Small papules started appearing at 10, 14, and 13 weeks of treatment in control, 3%, and 5% GP mice, respectively (Figure 2a). Our statistical model of the observed reduction in tumor incidence indicated that the overall group effects of the fitted results are not significant; however, the time effect is borderline significant with a p-value of 0.0506 (Figure 2a), indicating the weekly tumor incidence is increasing over time. Survival analysis indicated no significant difference in the onset of tumors, with median survival without appearance of papules at 15 weeks (control and 5% GP) and 17 weeks (3% GP) (Figure 2b). Both GP groups demonstrated reduced tumor volume by week 26 (Figure 2c). By week 28, average tumor volume was markedly reduced in 3% GP (23.35±6.34 mm^3) and 5% GP (15.36±2.90 mm^3) from control (92.1±50.89 mm^3); however, the fitted results indicate that the group and time effects from 3% and 5% GP feeds are not significant. At the time of euthanasia, final counts (multiplicity) of discernable papules (<2 mm) were taken as an independent measure and, along with large tumors (>2 mm), were recorded and analyzed. Our data suggested a marked reduction of both small and large tumors, and 5% GP was found to cause a significant decrease (p-value 0.021) in smaller tumors (Figure 2d). Interestingly for several of the tumor parameters analyzed (Figures 1c-d and 2a-d), the effects of 3% and 5% GP treatments did not considerably differ, leading us to conclude that the chemoprotective response of GP is similar at both the tested doses.

Dietary GP reduces UVB-mediated DNA damages and decreases epidermal thickening

UVB causes direct DNA damage via formation of mutagenic/carcinogenic cyclobutane pyrimidine dimers (CPDs) and 6-4 photoproducts (6-4 PPs) [2]. Under normal conditions, nucleotide excision repair (NER) removes 6-4 PP and CPDs after probing the genome for helix distortions. However, CPDs are poorly recognized and repair can be ineffective. These dimers result in the transcription of C→T or CC→TT UVB signature mutations [3, 17, 18] found in multiple tumor-related genes, including tumor suppressor *p53*, a gene mutated in ~90% of human SCCs [19] and up to 100% in SKH-1 mouse [20]. Moreover, it has been shown that CPDs may cause NMSC tumorigenesis [21]. To determine the effect of GP on the repair of UVB photoproducts, epidermal DNA was isolated from the harvested skin and photoproduct damage was measured by slot blot.

As demonstrated in Figures 3a-b, we found a significant reduction in CPD levels in the involved (adjacent to tumors, with UV exposure) skin of the 5% GP group, and a trend of reduced CPDs in the un-involved (stomach skin, no UV exposure) skin. Collectively, the reduction of CPDs remaining in the skin 3-5 days after UVB exposure suggests that there is likely enhanced NER capacity in mouse skin epidermis with GP consumption since NER is the sole mechanism for the repair of CPDs and (6-4) PPs in mice and humans [22, 23]. Our assay was not able to detect (6-4) PPs, potentially due to their shorter half-life (data not shown). No CPDs were detected in normal skin samples from a separate cohort of untreated mice that had no UV exposure (Supplementary Figure S1).

Due to the fact that epidermal keratinocytes are at a high risk of UVB-induced damages, the epidermal thickness was determined as a measure of keratinocyte proliferation [24]. Representative images of H&E stained skin are shown in Figure 3c. Measurement of the epidermal thickness using ImageJ showed a trend towards reduced thickness with GP supplementation, although statistical significance was not attained (Figure 3d). This could also

be due to chronic UV exposure protocol used in our experiments, especially since epidermal hyperplasia is mostly seen as a result of acute UV exposure.

Chemoprotective response of dietary GP was associated with decreased proliferation and increased apoptosis in UVB-induced tumors

We next determined the effect of GP feeding on the expression of the proliferation marker proliferating cell nuclear antigen (PCNA), a protein that is not only involved in many cellular functions, including DNA replication and repair [25], but also can serve as an indirect indicator of UVB-induced damage [26]. We found reduced expression of PCNA at mRNA and protein levels in both the 3% and 5% GP groups (Figures 4a-b). Additionally, analysis of Ki-67, a classic marker for proliferating cells that is often regarded as having prognostic significance in many neoplasms [27, 28], demonstrated the similar trend (Figures 4c-d), indicating decreased cellular proliferation in the tumor tissue of the GP-supplemented mice.

One of the key hallmarks of cancer is the ability of cells to escape apoptosis. Therefore, we evaluated the effects of GP on the apoptosis markers. Utilizing the Caspase-Glo 3/7 assay, which measures executioner caspase-3 and -7 activities, we observed a trend towards increased mean relative intensity in 5% GP tumors as compared to control tumors (Figure 4e). To explore this further, we determined the effect of GP feeding on caspases-3 and -7 proteins using immunoblot analyses. Although we found no significant change in caspase-3 (data not shown), we found a marked increase in the levels of cleaved caspase-7 (Figure 4f) in both 3% and 5% GP groups, though the increase appeared higher in the 3% GP group. Further, caspase-7 has been shown to cleave poly (ADP-ribose) polymerase (PARP), a protein whose cleavage facilitates cellular disassembly and indicates that cells are undergoing apoptosis [29]. Immunoblot analysis revealed an increase in the levels of cleaved PARP in tumor tissues of GP-supplemented mice, suggesting an enhanced apoptosis by GP feeding (Figure 4g). Further, evaluation of the pro-survival protein BCL-2, which is known to be differentially expressed in

various malignancies and considered as a useful prognostic biomarker [30], demonstrated downregulation in the GP supplemented groups (Figure 4h). Collectively, these observations suggest that GP decreases proliferation and increases apoptosis of tumor cells, contributing to reduced tumor incidence and volume.

Chemoprotective effects of dietary GP were associated with modulation of oxidative stress marker 4-hydroxynonenal (4-HNE), independent of nuclear factor erythroid 2–related factor 2 (NRF2)

UV radiation has been shown to induce reactive oxygen species (ROS) in skin [31]. Although the skin contains elaborated antioxidant defense mechanisms, excessive ROS can lead to oxidative stress in skin. To evaluate the effect of GP on epidermal oxidative stress, we assessed the lipid peroxidation biomarker 4-HNE and oxidative stress response marker NRF2. 4-HNE accumulates during oxidative stress due to ROS attack on the polyunsaturated fatty acid chain of the lipid membrane, leading to severe cell damage [32]. As shown in Figures 5a-b, a marked decrease in the accumulation of 4-HNE was found in the tumors of both groups of GP-supplemented mice. Interestingly, NRF2, an activator of the cellular antioxidant response, was also found to be decreased in the tumor samples of GP-supplemented mice (Figures 5c-d). Traditionally, it is thought that NRF2 signaling quenches ROS, leading to repair of oxidative damage. However, NRF2 has been found to be dysregulated in many cancers, and in many cases has constitutive activation resulting in higher proliferation rates and tumorigenicity [33], suggesting that increased NRF2 expression is contributing to a pro-survival environment in the tumor.

Dietary GP significantly alters multiple oxidative stress genes and pathways

In an attempt to uncover other genes or pathways associated with oxidative stress and antioxidants that may be modulated by GP supplementation, we used a commercially available oxidative stress PCR array profiling the expression of 84 key genes related to oxidative stress.

Details of the expression analyses are presented in Supplementary Table S1-S2 and Supplementary Figure S2. We found that out of 84 genes tested, 13 were upregulated and 3 were downregulated significantly by ≥1.75-fold change in 5% GP, and ≥1.4-fold change in 3% GP (Figure 6a). The expression of these 16 genes was validated using RT-qPCR assay (Figure 6b). Upregulated genes included antioxidant gene *Srxn1*, glutathione peroxidase *Gpx7*, peroxiredoxins *Prdx2, 4, 5* and *6*, peroxidase *Ptgs2*, genes involved in superoxide metabolism *Cyba* and *Nox4*, oxidative stress-responsive genes *Ccl5, Gss and Hmox*, and the oxygen transporter *Vim*. Downregulated genes included *Ucp2*, a gene known to be involved in superoxide metabolism, and the oxidative stress-responsive genes (*Ercc2* and *Gclc*). However, only 5 genes were found to be significantly modulated during validation (*Ccl5, Cyba, Gpx7, Nox4,* and *Pxdx5*). All others were found with similar trends to the array but were not statistically significant. All the validated genes, except *Prdx5*, are known to be involved in ROS metabolism. *Ccl5* and *Gpx7* are known to act as oxidative stress response genes, while *Cyba* and *Nox4* are involved in superoxide metabolism. *Cyba* encodes p22(phox) protein, which is known to be involved in superoxide production and phagocytosis [34]. Interestingly, p22(phox) partners with NADPH oxidases (Noxs), including *Nox4*, to generate superoxide intracellularly [34]. *Gpx7* is the only member of the glutathione peroxidase (GPx) family without any GPx activity, although it is an important oxidative stress sensor and has been found to suppress ROS and protect against oxidative DNA damage [35]. *Prdx5* is an antioxidant gene that codes for a mitochondrial peroxiredoxin, which is known to play an important role in cell protection against oxidative stress by detoxifying peroxides and as a sensor of hydrogen peroxide-mediated signaling events [36].

To further analyze the gene-gene interactions, the 16 significantly modulated genes obtained from PCR array were uploaded into IPA software to identify networks of interacting genes. IPA suggested links to other genes with potential involvement in antioxidant functions, resulting in a network. Interestingly, all of the identified network genes were found to have links

to cancer (shown with a pink boundary in Figure 6c). Additionally, the potential involvement of other important genes such as *Erk1/2, P38 Mapk, Tgfβ, Ap1* and *Hsp27* were identified by IPA, as they were not part of the PCR array. Analysis of cumulative gene functions predicted that GP supplementation inhibits oxidative stress and the quantity of ROS, while increasing the metabolism of ROS (Figure 6d).

Collectively, our data suggested that GP-supplementation imparts a marked chemoprotective response against UVB exposure-mediated skin carcinogenesis in SKH-1 mice via multiple molecular mechanisms, as it affects DNA damage repair, cell proliferation, apoptosis and oxidative stress pathways (Figure 6e). Moreover, the observed effects appear to occur by modulating genes involved in antioxidant function, metabolism of ROS, superoxide metabolism and/or oxidative stress-response. The chemoprotective effects of dietary GP observed in this study are in accordance with our earlier investigation, where we showed that the topical application of the grape antioxidant resveratrol resulted in a significant inhibition in tumor incidence and delay in the onset of tumorigenesis [9]. Additionally, in another study, though not related to UVB-induced skin cancer, GP was shown to inhibit chemically-induced skin carcinogenesis in SENCAR mice [37]. This study also evaluated the effects of other grape constituents and found that similar to GP, resveratrol, quercetin and grape seed extract containing proanthocyanidin B-2-gallate, inhibited the 7,12-dimethylbenz[a]anthracene (DMBA)-induced epidermal hyperplasia, proliferation, and inflammation.

A limited number of studies have suggested reasonable pharmacokinetics profile of grape polyphenol following consumption of grape constituents. One such study looked at oral supplementation of a standardized grape polyphenol mixture (consisting of grape seed extract, concord grape juice and resveratrol) to Zucker diabetic fatty rats. The authors found definite bioavailability of polyphenol metabolites, with C_{max} between 1-3 hours, which then declined by 8 hours [38]. Additionally, because of the promising health effects of grape and grape

constituents, few human clinical trials have been performed in the recent past (reviewed in [12]). One study evaluating postprandial hydrophilic plasma antioxidant capacity (AOC) after GP intake in 6 women found significantly increased AOC suggesting that GP consumption can maintain a redox balance from the free radicals that occur during carbohydrate metabolism [39]. These studies suggest that the oral grape consumption can provide a systemic distribution of its various constituents, capable of imparting health-promoting effects.

As the cases of NMSC continue to rise, it is imperative to find chemoprotective measures to prevent damages caused by UV radiation. Natural dietary agents, including grapes, offer us beneficial antioxidants and other phytonutrients, which can enrich our diets and lead to better health. In this *in vivo* study, we demonstrated that dietary grape powder afforded protection against UVB-induced damages that lead to skin carcinogenesis, as evidenced by increased DNA damage repair, reduced cell proliferation and oxidative stress, and enhanced apoptotic response and ROS metabolism. These findings suggest that ingestion of antioxidant-rich GP may lead to decreased tumorigenesis of NMSC in humans and that inclusion of 1-2 daily servings of grapes may be beneficial for a healthy lifestyle. However, further investigation is required to validate our findings and to develop strategies for skin cancer management using grapes.

Acknowledgments

This work was partially supported by funding from the California Table Grape Commission (CTGC), as well as the NIH (grant numbers R01AR059130 and R01CA176748 to NA), and the Department of Veterans Affairs (VA Merit Review Award I01CX001441; and a Research Career Scientist Award IK6BX003780 to NA). We also acknowledge the core facilities supported by the Skin Diseases Research Center (SDRC) Core Grant P30AR066524 from NIH/NIAMS. Use of the Experimental Pathology Laboratory and Biostatistics Shared Resource are supported through the UW Carbone Cancer Center Support Grant P30 CA014520.

References

1 Rogers HW, Weinstock MA, Feldman SR, Coldiron BM: Incidence Estimate of Nonmelanoma Skin Cancer (Keratinocyte Carcinomas) in the U.S. Population, 2012. JAMA Dermatol 2015;151:1081-1086.

2 Bowden GT: Prevention of non-melanoma skin cancer by targeting ultraviolet-B-light signalling. Nat Rev Cancer 2004;4:23-35.

3 Mancebo SE, Wang SQ: Skin cancer: role of ultraviolet radiation in carcinogenesis. Reviews on environmental health 2014;29:265-273.

4 Chhabra G, Ndiaye MA, Garcia-Peterson LM, Ahmad N: Melanoma Chemoprevention: Current Status and Future Prospects. Photochem Photobiol 2017;93:975-989.

5 Kahn HS, Tatham LM, Patel AV, Thun MJ, Heath CW, Jr.: Increased cancer mortality following a history of nonmelanoma skin cancer. JAMA 1998;280:910-912.

6 Levi F, La Vecchia C, Te VC, Randimbison L, Erler G: Incidence of invasive cancers following basal cell skin cancer. Am J Epidemiol 1998;147:722-726.

7 Guy Jr GP, Machlin SR, Ekwueme DU, Yabroff KR: Prevalence and Costs of Skin Cancer Treatment in the U.S., 2002−2006 and 2007−2011. Am J Prev Med 2015;48:183-187.

8 Singh CK, Ndiaye MA, Ahmad N: Resveratrol and cancer: Challenges for clinical translation. Biochimica et biophysica acta 2015;1852:1178-1185.

9 Aziz MH, Reagan-Shaw S, Wu J, Longley BJ, Ahmad N: Chemoprevention of skin cancer by grape constituent resveratrol: relevance to human disease? FASEB journal : official publication of the Federation of American Societies for Experimental Biology 2005;19:1193-1195.

10 Pezzuto JM: Grapes and human health: a perspective. Journal of agricultural and food chemistry 2008;56:6777-6784.

11 Singh CK, Siddiqui IA, El-Abd S, Mukhtar H, Ahmad N: Combination chemoprevention with grape antioxidants. Mol Nutr Food Res 2016;60:1406-1415.

12 Singh CK, Liu X, Ahmad N: Resveratrol, in its natural combination in whole grape, for health promotion and disease management. Annals of the New York Academy of Sciences 2015;1348:150-160.

13 Benavides F, Oberyszyn TM, VanBuskirk AM, Reeve VE, Kusewitt DF: The hairless mouse in skin research. J Dermatol Sci 2009;53:10-18.

14 de Gruijl FR, Forbes PD: UV-induced skin cancer in a hairless mouse model. BioEssays 1995;17:651-660.

15 Kligman LH, Kligman AM: Histogenesis and progression in ultraviolet light-induced tumors in hairless mice. J Natl Cancer Inst 1981;67:1289-1293.

16 Reagan-Shaw S, Nihal M, Ahmad N: Dose translation from animal to human studies revisited. FASEB journal : official publication of the Federation of American Societies for Experimental Biology 2008;22:659-661.

17 Ichihashi M, Ueda M, Budiyanto A, Bito T, Oka M, Fukunaga M, Tsuru K, Horikawa T: UV-induced skin damage. Toxicology 2003;189:21-39.

18 de Gruijl FR: Skin cancer and solar UV radiation. Eur J Cancer 1999;35:2003-2009.

19 Agar NS, Halliday GM, Barnetson RS, Ananthaswamy HN, Wheeler M, Jones AM: The basal layer in human squamous tumors harbors more UVA than UVB fingerprint mutations: A role for UVA in human skin carcinogenesis. Proceedings of the National Academy of Sciences of the United States of America 2004;101:4954-4959.

20 Melnikova VO, Pacifico A, Chimenti S, Peris K, Ananthaswamy HN: Fate of UVB-induced p53 mutations in SKH-hr1 mouse skin after discontinuation of irradiation: relationship to skin cancer development. Oncogene 2005;24:7055-7063.

21 Jans J, Schul W, Sert Y-G, Rijksen Y, Rebel H, Eker APM, Nakajima S, van Steeg H, de Gruijl FR, Yasui A, Hoeijmakers JHJ, van der Horst GTJ: Powerful Skin Cancer Protection by a CPD-Photolyase Transgene. Curr Biol 2005;15:105-115.

22 Gaddameedhi S, Selby CP, Kaufmann WK, Smart RC, Sancar A: Control of skin cancer by the circadian rhythm. Proc Natl Acad Sci U S A 2011;108:18790-18795.

23 Dakup P, Gaddameedhi S: Impact of the Circadian Clock on UV-Induced DNA Damage Response and Photocarcinogenesis. Photochem Photobiol 2017;93:296-303.

24 Hassan SMA, Hussein AJ, Saeed AK: Role of green tea in reducing epidermal thickness upon ultraviolet light-B injury in BALB/C mice. Adv Biol 2015;890632:1-6

25 Moldovan G-L, Pfander B, Jentsch S: PCNA, the Maestro of the Replication Fork. Cell 2007;129:665-679.

26 Moore JO, Palep SR, Saladi RN, Gao D, Wang Y, Phelps RG, Lebwohl MG, Wei H: Effects of ultraviolet B exposure on the expression of proliferating cell nuclear antigen in murine skin. Photochem Photobiol 2004;80:587-595.

27 Koseoglu RD, Sezer E, Eyibilen A, Aladag İ, Etikan İ: Expressions of p53, cyclinD1 and histopathological features in basal cell carcinomas. J Cutan Pathol 2009;36:958-965.

28 Scholzen T, Gerdes J: The Ki-67 protein: From the known and the unknown. J Cell Physiol 2000;182:311-322.

29 Boucher D, Blais V, Denault JB: Caspase-7 uses an exosite to promote poly(ADP ribose) polymerase 1 proteolysis. Proc Natl Acad Sci U S A 2012;109:5669-5674.

30 Thomadaki H, Scorilas A: BCL2 family of apoptosis-related genes: functions and clinical implications in cancer. Crit Rev Clin Lab Sci 2006;43:1-67.

31 Heck DE, Vetrano AM, Mariano TM, Laskin JD: UVB light stimulates production of reactive oxygen species: unexpected role for catalase. J Biol Chem 2003;278:22432-22436.

32 Mylonas C, Kouretas D: Lipid peroxidation and tissue damage. In vivo (Athens, Greece) 1999;13:295-309.

33 Rojo de la Vega M, Chapman E, Zhang DD: NRF2 and the Hallmarks of Cancer. Cancer Cell 2018;34:21-43.

34 Stasia MJ: CYBA encoding p22(phox), the cytochrome b558 alpha polypeptide: gene structure, expression, role and physiopathology. Gene 2016;586:27-35.

35 Chen YI, Wei PC, Hsu JL, Su FY, Lee WH: NPGPx (GPx7): a novel oxidative stress sensor/transmitter with multiple roles in redox homeostasis. Am J Transl Res 2016;8:1626-1640.

36 Knoops B, Goemaere J, Van der Eecken V, Declercq JP: Peroxiredoxin 5: structure, mechanism, and function of the mammalian atypical 2-Cys peroxiredoxin. Antioxid Redox Signal 2011;15:817-829.

37 Hanausek M, Spears E, Walaszek Z, Kowalczyk MC, Kowalczyk P, Wendel C, Slaga TJ: Inhibition of Murine Skin Carcinogenesis by Freeze-Dried Grape Powder and Other Grape-Derived Major Antioxidants. Nutr Cancer 2011;63:28-38.

38 Chen TY, Ferruzzi MG, Wu QL, Simon JE, Talcott ST, Wang J, Ho L, Todd G, Cooper B, Pasinetti GM, Janle EM: Influence of diabetes on plasma pharmacokinetics and brain bioavailability of grape polyphenols and their phase II metabolites in the Zucker diabetic fatty rat. Mol Nutr Food Res 2017;61

39 Prior RL, Gu L, Wu X, Jacob RA, Sotoudeh G, Kader AA, Cook RA: Plasma antioxidant capacity changes following a meal as a measure of the ability of a food to alter in vivo antioxidant status. J Am Coll Nutr 2007;26:170-181.

40 Gaddameedhi S, Kemp MG, Reardon JT, Shields JM, Smith-Roe SL, Kaufmann WK, Sancar A: Similar nucleotide excision repair capacity in melanocytes and melanoma cells. Cancer Res 2010;70:4922-4930.

41 Wang X, Spandidos A, Wang H, Seed B: PrimerBank: a PCR primer database for quantitative gene expression analysis, 2012 update. Nucleic Acids Res 2012;40:D1144-1149.

Figure Legends

Figure 1. Study design and tumor analysis of GP supplementation in SKH-1 hairless mice.

(**a**) Analysis report for major GP phytochemical constituents (analyzed by Covance Laboratories, Madison, WI; report provided by CTGC). (**b**) Experimental timeline. (**c**) Representative SKH-1 hairless mice from each group at the end of the study. Location of large tumors is indicated by circles. (**d**) Analysis of tumor multiplicity and numbers for the last 4 weeks. Linear regression is fitted separately for each week, where the model is $Y_i = \mu_0 + \mu_1 I(G_i = 2) + \mu_2 I(G_i = 3) + \varepsilon_i$, where G_i is the group indicator, which equals 1, 2, and 3 for the control, 3% GP, and 5% GP feed groups, respectively, Y_i is the tumor incidence counted at that particular week.

Figure 2. Effect of dietary GP on UVB-mediated skin carcinogenesis in SKH-1 hairless mice.

(**a**) Average tumor incidence per group. Statistical model is described in materials and methods, p-value 0.306 and 0.174 for 3% GP and 5% GP, respectively. (**b**) Kaplan-Meier plot of tumor-free mice, p-values 0.157 and 0.940 for 3% GP and 5% GP, respectively. (**c**) Average tumor volume per group for weeks 16 to 28, p-value 0.352 and 0.455 for 3% GP and 5% GP, respectively. (**d**) Tumor multiplicity at the time of euthanasia. For <2 mm tumors p-value 0.132 and 0.021 for 3% GP and 5% GP, and for >2 mm tumors p-value 0.331 and 0.505 for 3% GP and 5% GP, respectively. All data are presented as mean ± SEM.

Figure 3. Effect of dietary GP on UVB-induced DNA damages and epidermal thickness.

(a) Detection of CPDs in SKH-1 mouse involved (stomach) and uninvolved (adjacent) skin by slot blot following chronic UVB exposure. Each row represents an individual mouse. SYBR gold,

which stains total nucleic acid, was used as an internal control. (**b**) Relative quantification of CPD signal from slot blot. AU = arbitrary units, as designated by the imaging software. Statistical analysis was performed using two-way ANOVA with Tukey's multiple comparison. Statistical significance is denoted as *p<0.05, ns = no significance. (**c**) Representative images, and (**d**) Quantification of epidermal thickness in skin adjacent to tumors from formalin-fixed, paraffin-embedded tissue sections stained with hematoxylin and eosin. Images captured at 20x (scale bar = 200 μm). Statistical analysis was performed using one-way ANOVA with Tukey's multiple comparison. p-value 0.072 and 0.111 for 3% GP and 5% GP, respectively All data presented as mean ± SEM.

Figure 4. Effect of dietary GP on cell proliferation and apoptosis in UVB-induced tumors.

(**a**) Expression of PCNA protein (by immunoblot), and (**b**) mRNA (by RT-qPCR). (**c**) Expression of Ki-67 protein (by immunohistochemical staining; 20x magnification; scale bar = 200 μm), and (**d**) mRNA (by RT-qPCR). Data is presented as mean ± SEM, with statistical analysis performed using one-way ANOVA with Tukey's multiple comparison. Statistical significance denoted as *p<0.05 and **p<0.01. Effect on (**e**) caspase-3/7 activity, p=0.061, and (**f**) immunoblot analysis of total and cleaved caspase-7; (**g**) immunoblot analysis of total and cleaved PARP; (**h**) immunoblot analysis of BCL-2 protein. β-actin was used as loading control. RLU = relative intensity unit. Each immunoblot lane represents a pool of three animals as described in materials and methods.

Figure 5. Effect of dietary GP on oxidative stress biomarker 4-HNE and oxidative stress response marker NRF2.

(**a**) Expression of lipid peroxidation marker 4-hydroxynonenal (4-HNE) by immunoblot, and (**b**) immunohistochemical staining. (**c**) Expression of activator of antioxidant response element, NRF2, by immunoblot, and (**d**) immunohistochemical staining. Each immunoblot lane represents

a pool of three animals as described in materials and methods. A representative image (20x magnification; scale bar = 200 μm) from each group is presented.

Figure 6. Mechanistic analysis of GP-mediated chemoprotective effects against UVB-induced skin carcinogenesis.

(**a**) Differentially expressed genes in 3 and 5% GP group from the oxidative stress PCR array. Genes with ≥1.75-fold change and $p<0.05$ in response to 5% GP and ≥1.4-fold change in response to 3% GP are included. P-values are calculated based on Student's t-test of the replicate 2^(-ΔCT) values for each gene. (**b**) RT-qPCR validation of key altered genes in response to 3 and 5% GP. The data presented here are from RNA pooled evenly from 9 mouse tumor samples per group as described in materials and methods. Statistical analysis performed using two-way ANOVA with Tukey's multiple comparison. Data are represented as mean ± SEM (*$p<0.05$, **$p<0.01$, ***$p<0.001$). (**c**) A gene network pathway was generated with key altered genes (≥1.75-fold change in response to 5% GP) using IPA software. Red= upregulated genes; Green= downregulated genes; Pink outline= Cancer-associated genes; Uncolored nodes= genes not included in the PCR array but found during IPA analysis. Gene-gene interactions are indicated by arrows, the solid lines denote a robust correlation with partner genes, and dashed lines indicate statistically significant but less frequent correlations. (**d**) Using IPA, the functional annotations of 5% GP-modulated genes were generated showing inhibition of oxidative stress and quantity of ROS, as well as increased metabolism of ROS. Blue lines= inhibition; Orange= activation; Yellow= findings inconsistent with the state of downstream molecules. (**e**) Schematic representation of the effects of dietary GP on skin tumorigenesis are presented. Green= downregulated/decreased, Red= upregulated/increased measurements.

Figures

Figure 1

a

Major Compounds in Grape Powder	Concentration (mg/kg GP) ±SD
Catechins	
Catechin	19.59 ± 1.06
Epicatechin	8.77 ± 0.71
Anthocyanins	
Peonidin	148.75 ± 8.19
Cyanidin	20.1 ± 1.33
Malvidin	127.77 ± 8.33
Flavonols	
Kaempferol	1.03 ± 0.16
Isorhamnetin	1.06 ± 0.11
Quercetin	14.44 ± 1.20
Taxifolin	1.87 ± 0.10
Stilbenes	
Resveratrol	0.85 ± 0.16
Total Polyphenols (in gallic acid equivalents)	3260

b

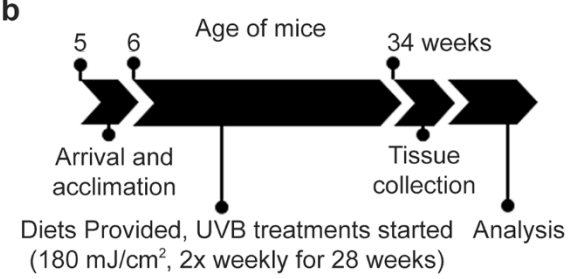

c

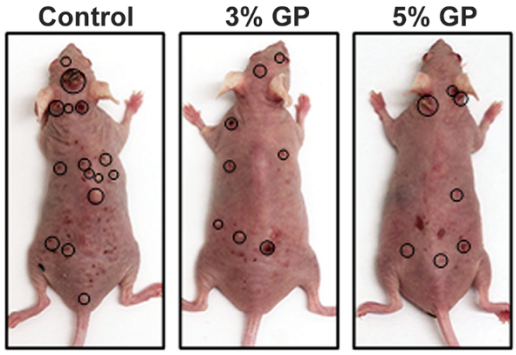

d

	Control			3% GP				5% GP			
	n=11			n=12				n=12			
Tumor multiplicity at:	Total tumors /group	Tumor mean	SEM	Total tumors /group	Tumor mean	SEM	p-value	Total tumors /group	Tumor mean	SEM	p-value
Week 24	215	19.5	2.1	175	14.6	1.7	0.0408	166	13.8	1.0	0.0198
Week 25	221	20.1	2.2	183	15.3	1.9	0.0595	171	14.3	1.1	0.0247
Week 26	306	27.8	3.9	271	22.6	1.8	0.1744	240	20.0	2.0	0.0462
Week 27	335	30.5	3.9	291	24.3	1.8	0.1067	261	21.8	1.9	0.0263

Figure 2

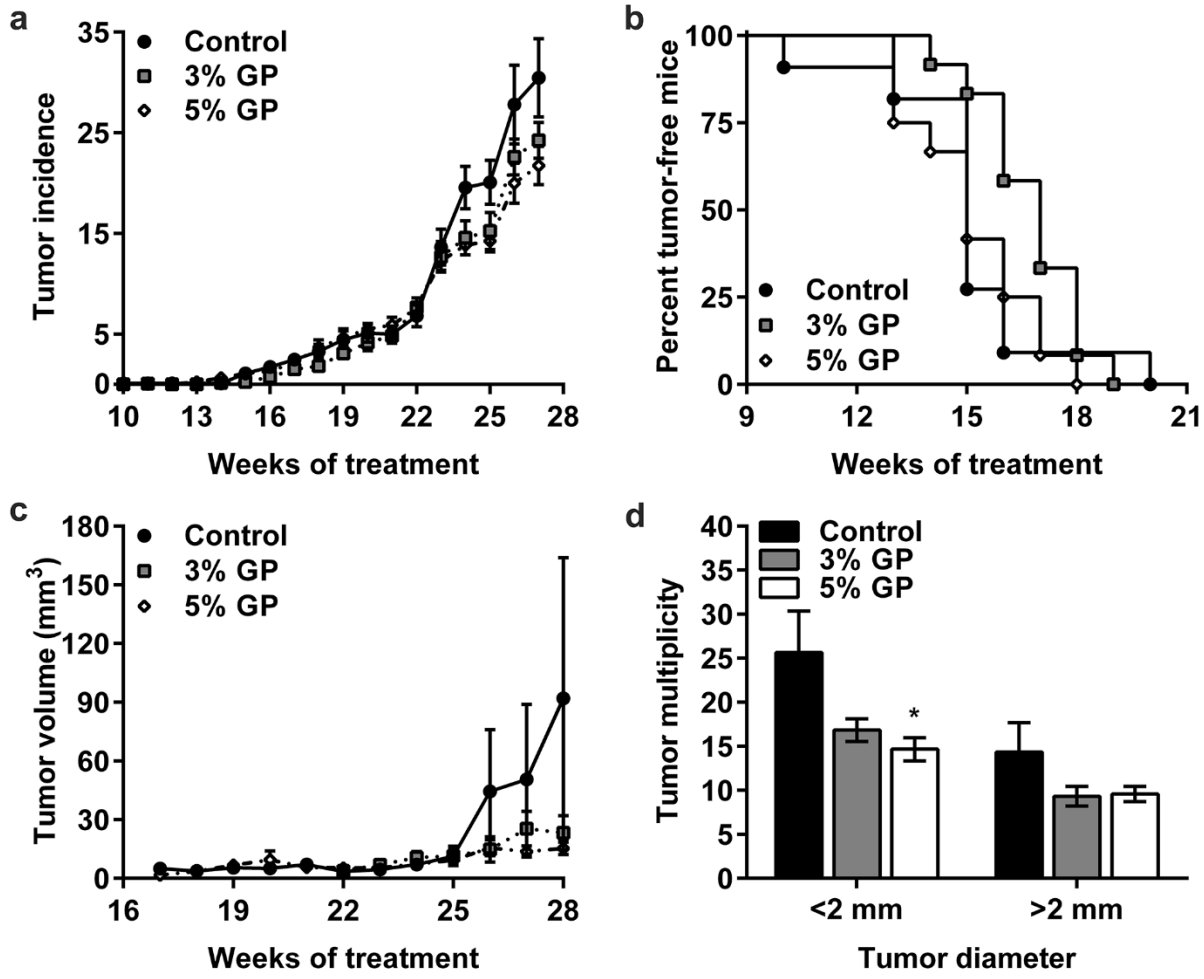
a
Tumor incidence
Control
3% GP
5% GP
Weeks of treatment
b
Percent tumor-free mice
Control
3% GP
5% GP
Weeks of treatment
c
Tumor volume (mm3)
Control
3% GP
5% GP
Weeks of treatment
d
Tumor multiplicity
Control
3% GP
5% GP
*
<2 mm
>2 mm
Tumor diameter

Figure 3

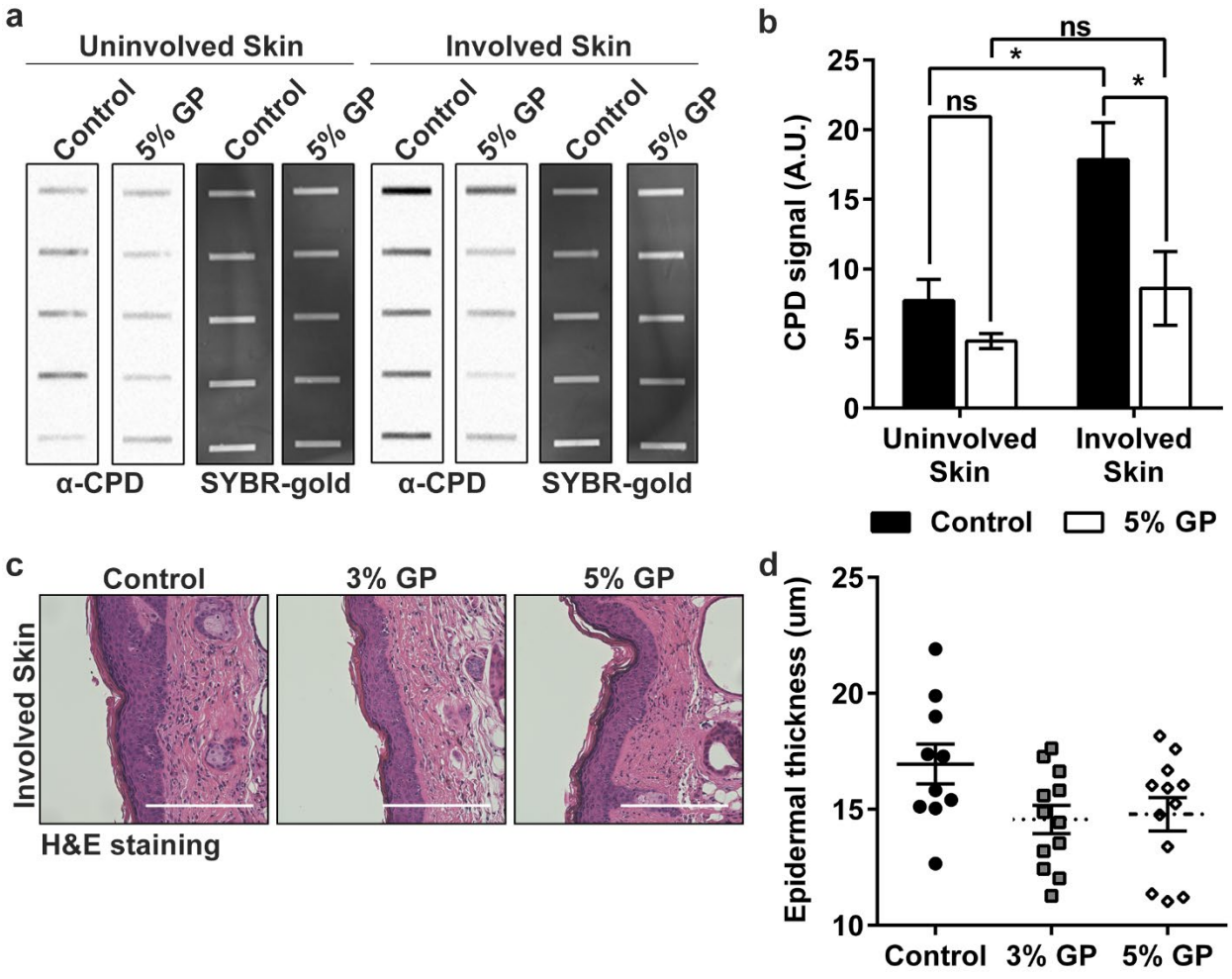
a
Uninvolved Skin
Involved Skin
Control
5% GP
Control
5% GP
Control
5% GP
Control
5% GP
α-CPD
SYBR-gold
α-CPD
SYBR-gold
b
ns
*
ns
*
CPD signal (A.U.)
25
20
15
10
5
0
Uninvolved Skin
Involved Skin
Control
5% GP
c
Control
3% GP
5% GP
Involved Skin
H&E staining
d
Epidermal thickness (um)
25
20
15
10
Control
3% GP
5% GP

Figure 4

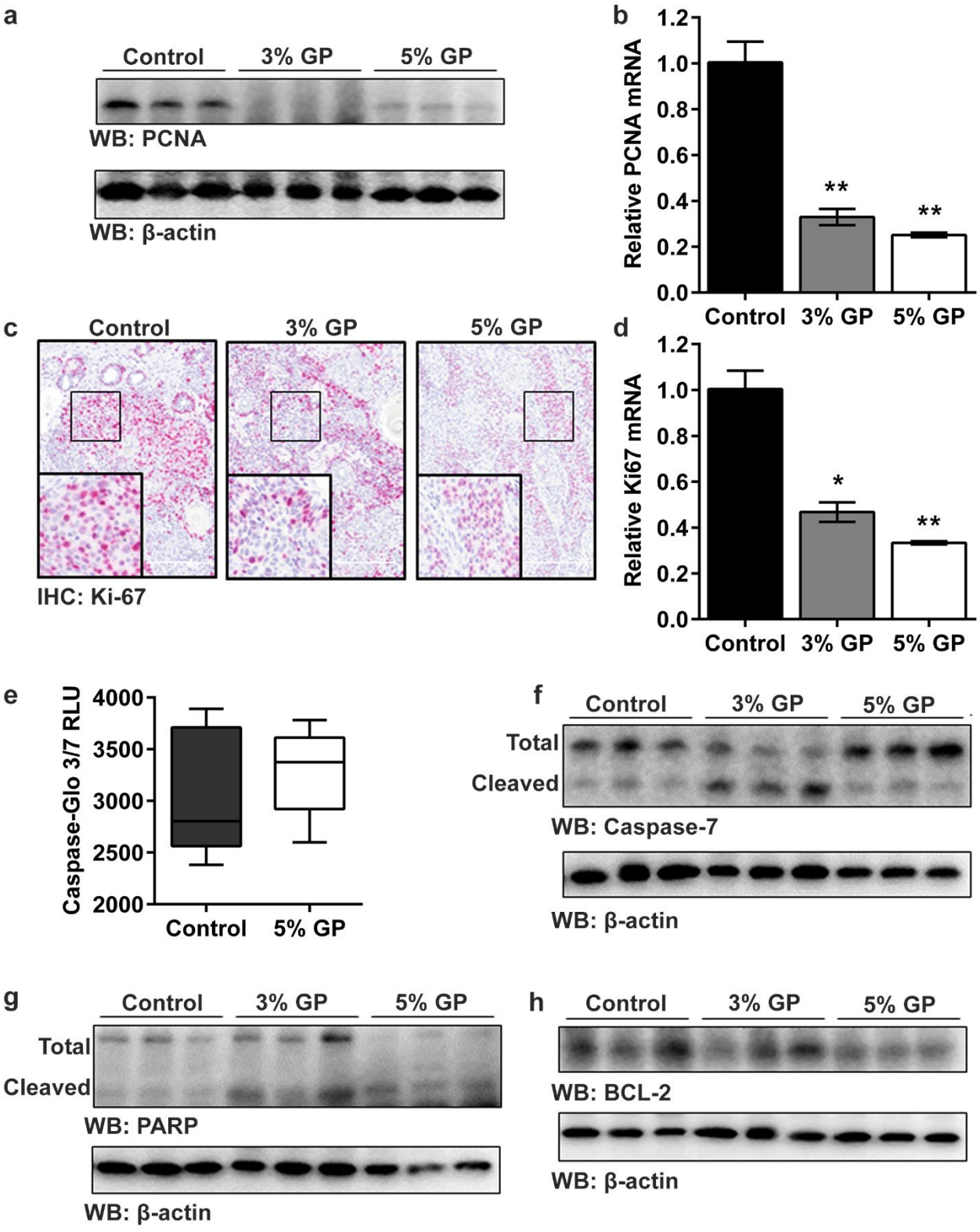
a
Control
3% GP
5% GP
WB: PCNA
WB: β-actin
b
Relative PCNA mRNA
1.2
1.0
0.8
0.6
0.4
0.2
0.0
**
**
Control
3% GP
5% GP
c
Control
3% GP
5% GP
IHC: Ki-67
d
Relative Ki67 mRNA
1.2
1.0
0.8
0.6
0.4
0.2
0.0
*
**
Control
3% GP
5% GP
e
Caspase-Glo 3/7 RLU
4000
3500
3000
2500
2000
Control
5% GP
f
Control
3% GP
5% GP
Total
Cleaved
WB: Caspase-7
WB: β-actin
g
Control
3% GP
5% GP
Total
Cleaved
WB: PARP
WB: β-actin
h
Control
3% GP
5% GP
WB: BCL-2
WB: β-actin

Figure 5

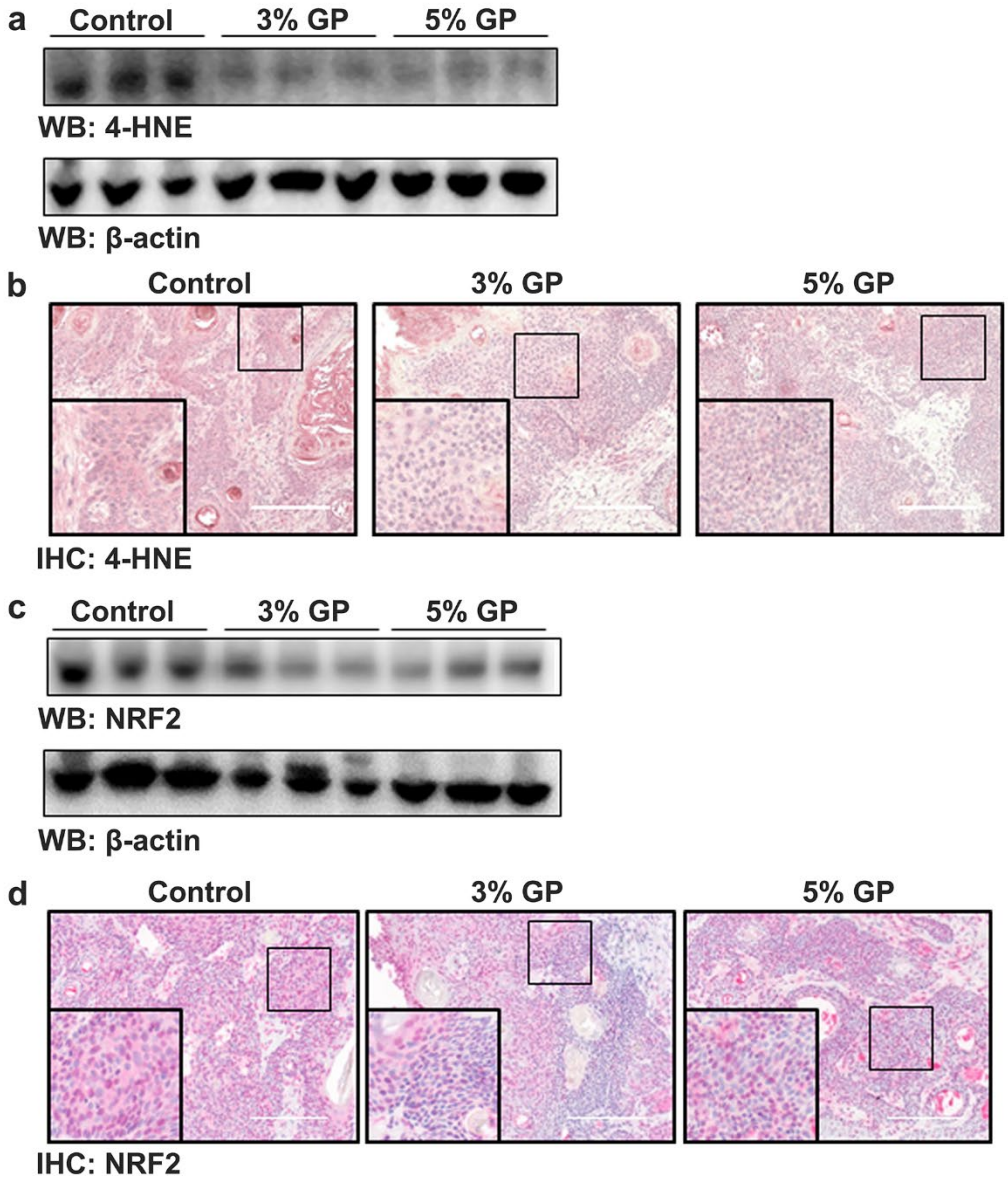
a
Control
3% GP
5% GP
WB: 4-HNE
WB: β-actin
b
Control
3% GP
5% GP
IHC: 4-HNE
c
Control
3% GP
5% GP
WB: NRF2
WB: β-actin
d
Control
3% GP
5% GP
IHC: NRF2

Figure 6

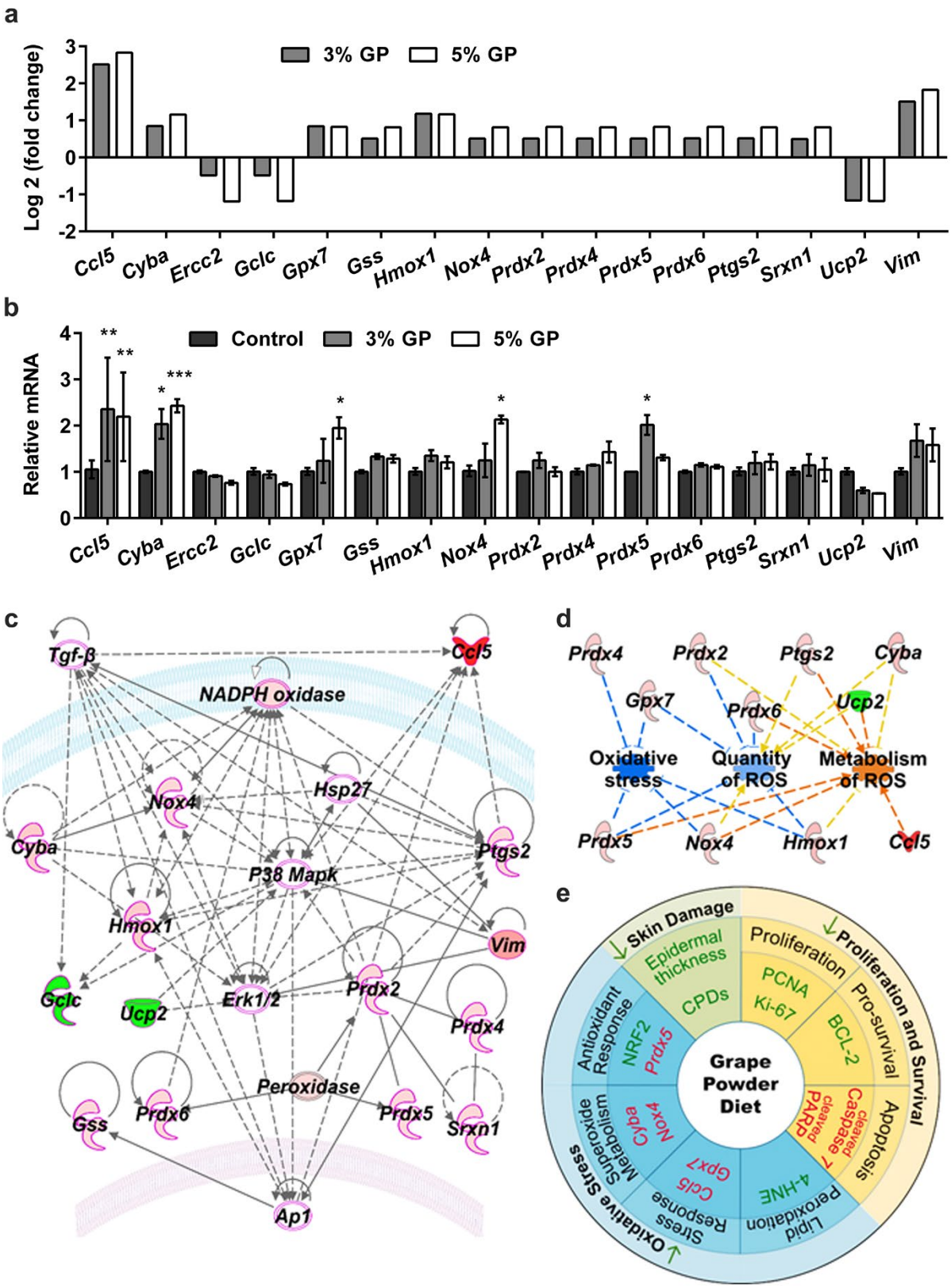
a
Log 2 (fold change)
3% GP
5% GP
Ccl5 Cyba Ercc2 Gclc Gpx7 Gss Hmox1 Nox4 Prdx2 Prdx4 Prdx5 Prdx6 Ptgs2 Srxn1 Ucp2 Vim
b
Relative mRNA
Control
3% GP
5% GP
c
Tgf-β
Ccl5
NADPH oxidase
Nox4
Hsp27
Cyba
Ptgs2
P38 Mapk
Hmox1
Vim
Gclc
Ucp2
Erk1/2
Prdx2
Prdx4
Peroxidase
Gss
Prdx6
Prdx5
Srxn1
Ap1
d
Prdx4
Prdx2
Ptgs2
Cyba
Gpx7
Prdx6
Ucp2
Oxidative stress
Quantity of ROS
Metabolism of ROS
Prdx5
Nox4
Hmox1
Ccl5
e
Grape Powder Diet
Skin Damage
Epidermal thickness
CPDs
Proliferation
PCNA
Ki-67
Proliferation and Survival
Pro-survival
BCL-2
Apoptosis
Cleaved Caspase 7
Cleaved PARP
Lipid Peroxidation
4-HNE
Stress Response
Ccl5
Gpx7
Oxidative Stress
Metabolism
Cyba
Nox4
Antioxidant Response
NRF2
Prdx5

Chapter 3a: Identification of molecular targets of dietary grape-mediated chemoprevention of ultraviolet B skin carcinogenesis: *A comparative quantitative proteomics analysis*

This chapter has been submitted as a prepared manuscript to the *Journal of Proteomics*

Abstract

We recently showed that dietary grape powder (GP) imparts considerable protection against ultraviolet B (UVB)-mediated skin carcinogenesis in SKH-1 mice. To determine molecular mechanisms of this response, we employed tandem mass tag (TMT) quantitative global proteomics approach on skin tumors from mice exposed to 180 mJ/cm^2 UVB twice per week and fed control or 5% GP diet. We found 2,629 proteins modulated by GP feeding, with 34 identified using stringent cutoffs (false discovery rate (FDR) q-value ≤0.1, fold change ≥1.2, p-value ≤0.05, ≥3 unique peptides). Ingenuity Pathway Analysis helped identify seven proteins involved in protein ubiquitination, including the deubiquitinase UCHL5 and 6 subunits of the 20S proteasome (PSMA1,3,4,6 and PSMB4,7). A second data set without the FDR q-value identified 239 modulated proteins, seven of which are involved in protein ubiquitination. Further, 14 proteins involved in acute phase response signaling were modulated >1.5-fold, including acute phase proteins (APPs) APCS, FGA, FGB, HP, HPX, RBP1. Evaluation of upstream regulators found inhibition of ERK1/2 phosphorylation and NF-κB p65, and an increase in IκBα in GP-treated tumors. Overall, our data suggested that GP consumption may mitigate tumorigenesis by enhancing protein ubiquitination and degradation caused by oxidative stress, and manipulates an otherwise tumor-promoting anti-inflammatory environment.

Introduction

Ultraviolet (UV) radiation is the most prevalent carcinogen in our environment, and can be divided into three categories: UVA, UVB, and UVC (reviewed in [1]). Of these, UVB is commonly thought to cause the most damage to the skin, although UVA and UVC can be harmful as well. While UVB light is required to stimulate the skin to produce vitamin D that is essential for calcium homeostasis and metabolism [2, 3], excessive UVB can lead to oxidative stress within the skin via disproportionate generation of reactive oxygen species (ROS), if not balanced by antioxidant defenses to maintain redox homeostasis [4]. UVB radiation also directly causes DNA damage by formation of cyclobutane pyrimidine dimers (CPDs) and pyrimidine (6-4)-pyrimidone photoproduct lesions, which have been shown to be carcinogenic [1, 5]. Collectively, oxidative stress, DNA damage, and inflammation, as well as mutation(s) in regulatory genes by UV radiation have been linked to cellular dysfunction and the development of greater than 90% of skin cancer cases [1]. As the most common neoplasm in the United States, non-melanoma skin cancers (NMSC) are morbid, but can often be treated by surgery, chemotherapy, photodynamic therapy, and/or radiation therapy unless left untreated for too long or present in hard-to-treat areas [6]. However, after a primary diagnosis of NMSC, most commonly basal cell carcinoma (BCC) or squamous cell carcinoma (SCC) of the skin, patients are at an increased risk of developing subsequent NMSCs and other cancers [7, 8]. Further, the existing approaches have not been sufficient in curtailing the increasing incidence of NMSCs, emphasizing the need for newer preventative and/or therapeutic strategies for the management of these cancers.

Recently, the use of nutritional supplements and/or antioxidants for the management of diseases, including cancer, has increased dramatically. Emerging research strongly supports the beneficial effects of strategically combining two or more natural agents or consuming whole

foods, as these combinations may provide synergistic response over the individual constituents [9-11]. We recently demonstrated that a grape powder (GP)-supplemented diet reduces UVB-mediated skin tumorigenesis in SKH-1 hairless mice, which was accompanied by reduced oxidative stress, increased repair of DNA damage, reduced cell proliferation, and enhanced apoptotic response and ROS metabolism (Chapter 2, [12]). The study rationale for the use of GP was based on the fact that grapes contain hundreds of polyphenols, and their combination may provide synergistic chemopreventive response via enhancing their cumulative bioavailability and actions against multiple oncogenic signaling pathways. As an extension of this study, here we seek to identify the molecular mechanisms of the observed skin cancer chemopreventive effect of GP by employing a comparative quantitative proteomics approach. Employing TMT LC-MS/MS for peptide quantification and analysis, we identified multiple pathways linked to the observed biological response of GP. These pathways included acute phase response signaling, response to inflammation, and protein ubiquitination, which regulate proteins in many ways including degradation via the proteasome. Our study provides insights to the molecular targets of GP-mediated skin cancer chemoprevention of UVB-mediated skin carcinogenesis.

Materials and Methods

Materials

TMT-10plex Isobaric Label Reagent Sets were purchased from Thermo Scientific. GP was received from the California Table Grape Commission (CTGC). Resveratrol, catechin, epicatechin, peonidin, cyanidin, malvidin, kaempferol, isorhamnetin, taxifolin and quercetin were the top 10 polyphenols present in the GP used in this study (detailed in Chapter 2 [12]).

Mice, treatments, tissue collection, and protein isolation

For this study, we used tissue samples collected during our recently published study where we determined the chemopreventive efficacy of dietary grape against UVB-mediated skin carcinogenesis in SKH-1 hairless mice (Chapter 2 [12]). Briefly, we employed a UVB initiation-promotion protocol, where mice were exposed to 180 mJ/cm^2 UVB twice weekly for 28 weeks. The mice were given GP-fortified diet at a dose of 3% or 5%. All diets were matched to the natural sugar content of the 5% GP diet. Details of mice and treatment protocol are provided in our previous publication (Chapter 2 [12]). At the termination of the experiment, mice were euthanized and skin and tumor tissue were collected and flash frozen in liquid nitrogen and stored at -80°C until further use. For protein isolation, skin tissues were pulverized into a powder using a mortar and pestle on liquid nitrogen. Powdered tissue was lysed in 1X RIPA lysis buffer (MilliporeSigma) with freshly added PMSF (Amresco) and protease inhibitor cocktail (Thermo Scientific). Total protein concentration was determined using Pierce BCA Protein Assay (Thermo Scientific) per manufacturer's protocol.

Tandem Mass Tagging (TMT) and LC-MS/MS analysis

For this study, we used the tumor lysates obtained from five randomly selected mice, each from control diet and 5% GP diet. Methods for mass spectrometry analysis are outlined in [13]. Briefly, protein were precipitated and digested prior to labeling with the TMT-10plex Isobaric Label Reagent Set (Thermo Scientific). TMT-labeled pooled samples were subjected to reverse-phase fractionation and LC-MS/MS was performed on an Orbitrap Elite (Thermo Scientific) fitted with the Easy-Spray source and coupled to Agilent 1100 Nanopump and temperature-controlled autosampler. Chromatography was performed using an Easy-Spray column with integrated emitter and heater, 15 cm x 75 µm, packed with Pepmap RSLC C18, 3 µm, 100 Å stationary phase (Thermo Scientific). Raw mass spectral data were assigned to peptides and proteins using MaxQuant [14] and searching with a mouse protein database from Uniprot. Post-search analysis was performed by importing the MaxQuant files into Perseus [15].

After normalization and assignment of the reporter ion abundances, the data was analyzed using a two-tailed Student's T-test. The Permutation-FDR approach was utilized to convert p-values to q-values for correct multiple hypothesis testing. Finally, fold-change heat maps were created for protein expression by dividing each TMT channel abundance by the mean of all channels for that protein and subjecting the result to log2 transformation. Hierarchical clustering was performed on the total protein matrix, with increasing TMT abundance assigned to red and decreasing TMT abundance assigned to green.

Protein cut-offs and analysis by IPA

After post-search analysis, the 2,629 proteins were subjected to additional cut-off criteria of i) peptides with a permutation-FDR calculated q-value of ≤0.1, and ii) a fold change ≥1.2, iii) 3 or more unique peptide hits, and iv) significant change in expression (T-test p-value of ≤0.05) between 5% GP and control diets. A secondary data set was created excluding the FDR-calculated q-value. The molecular function and biological process of the remaining proteins were assessed using PANTHER (Protein ANalysis THrough Evolutionary Relationships) software [16]. Additionally, the remaining protein aliases and fold change were uploaded into Qiagen's Ingenuity Pathway Analysis (IPA) software [17]. The predicated canonical pathways were generated and evaluated.

Immunoblot analysis

Immunoblot analyses were performed using standard protocols, described previously (Chapter 2 [12]) using lysates from control, 3% GP, and 5% GP treatment groups. Details of antibodies used are provided in Supplementary Table S1. Densitometry analysis was performed using Adobe photoshop CC 2018. Band intensity was transformed against the loading control, then normalized to the band intensity in lane one. The mean ± standard error of the three normalized lanes are represented graphically using GraphPad Prism version 7 for Windows

(GraphPad Software). Statistical analysis was performed using two way ANOVA followed by Tukey's multiple comparisons test.

20S Proteasome activity assay

For determining the 20S proteasome activity, tumor lysates in RIPA buffer from control, 3% GP, and 5% GP tumors were pooled for 2 mice per sample for a final concentration of 20 µg protein per well in technical duplicate. The 20S Proteasome Activity Assay (MilliporeSigma) was performed per manufacturer's protocol and incubated at 37°C for 2 h. The 20S proteasome activity was quantified using fluorescence intensity (λ_{ex} = 380/λ_{em} = 460) on the BioTek Synergy H1 Hybrid Multi-Mode Microplate reader. The assay was repeated twice with 3-6 biological replicates that were averaged. To account for assay variability within each set, all values were transformed Y/K, where Y = sample readout and K = lowest sample readout within the control group. Sets were then combined, represented graphically, and one way ANOVA followed by Tukey's multiple comparisons test was performed using GraphPad Prism version 7 for Windows (GraphPad Software).

Results & Discussion

Identification of GP-modulated proteins using TMT-10plex LC-MS/MS

We have previously demonstrated the chemopreventive effects of dietary GP (3% and 5% GP in diet) feeding against UVB-mediated skin tumorigenesis in SKH-1 hairless mice. In both treatment groups of 3% and 5% GP diet, we demonstrated reductions in tumorigenesis through decrease in proliferative markers, oxidative stress, and skin damages, and increase in apoptosis (Chapter 2 [12]). In an effort to determine downstream molecular mechanisms of the reduction of tumorigenesis from GP supplementation, we used the tumor lysates obtained from five randomly selected mice, each from control diet and 5% GP diet, and subjected them to tandem mass tagged (TMT-10plex) LC-MS/MS (Figure 1a). A total of 2,629 differentially

modulated proteins were quantified across all tumor replicates (Supplementary table S1 in [13]). Fold-change heat maps were created using Perseus and hierarchical clustering was performed with increasing TMT abundance assigned to red and decreasing TMT abundance assigned to green (Figure 1b). Distribution of unique peptides recognized and distribution of the reporter ion intensity ratios (5% GP/control) in the identified 2,629 proteins are outlined in Figures 1c and 1d. Interestingly, Ctl3 and Ctl4 clustered with 5GP samples possibly due to the similarity of the tumor biology. We speculate this is due to the tumor heterogeneity of the SKH-1 hairless mouse. This is an ideal model for UVB-mediated skin carcinogenesis due to the following: 1) the loss of hair cycle reduces variability of tumorigenesis based on the modifying effects of hair cycle, 2) tumors are independent, displaying significant differences in the rate of development and aggressiveness, and 3) the developed tumors model UVR-induced tumors in man [18]. Therefore, tumors can range from pre-malignant papilloma growths to malignant SCCs and spindle cell carcinomas [18].

To identify proteins of interest, our initial cut-off parameters included i) peptides with a permutation-FDR calculated q-value of ≤0.1, ii) a fold change ≥1.2, iii) 3 or more unique peptide hits, and iv) significant change in expression (T-test p-value of ≤0.05) between 5% GP and control diets, resulting in 34 upregulated proteins (shown as circle with black outline in Figure 1e). A second data set was generated to help us elucidate modified targets of GP consumption, which had the same cut-off parameters, except we excluded the permutation FDR cut-off. As shown in the volcano plot (Figure 1e), this resulted in 239 total proteins (32 down-regulated (green) and 207 up-regulated (red)). A list of the modified proteins can be found in Supplementary Table S2. Due to the nature of isobaric mass tagging, ratio compression is a bias in the quantitative output leading to an underestimation or compression of the actual protein amount when co-eluting peptides [19]. To compensate for this, we have lowered our

fold-change threshold to 1.2-fold to allow us to identify the most modified proteins of interest and generate further hypotheses on downstream targets of GP consumption.

Gene ontology and pathway analysis

We utilized PANTHER software to assess cellular processes affected by GP feeding. Within the secondary data set of 239 proteins, 48% of the proteins are involved in catalytic activity (Figure 2a). Interestingly 15% of these catalytically involved proteins, including peroxiredoxins 5 (PRDX5) and 6 (PRDX6), are associated with oxidoreductase activity, supporting our previous claim that GP feeding modulates oxidative stress in skin. Furthermore, using PANTHER to identify biological processes, a large number of the affected proteins appear to be involved in metabolic or cellular processes (Figure 2b). A small fraction of the proteins (~7%) were found to be related to response to stimulus, involving responses to stress, external stimulus, and immune response. Next, we attempted to identify the molecular pathways that are affected by GP consumption in tumorigenesis by employing IPA, a knowledge base that uses algorithms to predict upstream regulators, canonical pathways, and regulator effects of data sets such as proteomics or gene expressions [17]. The secondary data set was uploaded to IPA with the calculated q-value, the p-value, the number of peptides identified, and the corresponding ratio (5% GP/control). Interestingly, disease and function prediction analysis in IPA found that the modulation of 204 of the 239 proteins were correlated to slightly decrease cancer (Supplementary Figure S1), which supported our previous findings (Chapter 2 [12]). Moreover, we also found the involvement of GP-modulated proteins in enhancing the metabolism of ROS and inhibiting hydrogen peroxide (Figure 2c). This supports previous evidence suggesting resveratrol (a major antioxidant constituent of GP) to act as an anti-inflammatory agent [20] and the notion that GP modulates oxidative stress. Upon further evaluation of the data sets, we found that several other canonical pathways were affected by GP (Figure 2d), with the top two hits being protein ubiquitination pathway (in the first data set)

and APR signaling (in the second data set). The identification of APR signaling by IPA, as a top affected pathway matches with the identification of response to stimulus by PANTHER, which includes stress response. These findings led us to explore this pathway further along with the effects of GP on protein ubiquitination and the 20S proteasome.

Dietary GP modulates multiple 20S proteasomal subunits

Our analysis revealed that GP consumption results in the modulation of proteins involved in the Protein Ubiquitination Pathway (grey bar in Figure 2d). Due to the increased cut-off stringency, this was the only pathway identified by IPA to be significantly modulated in this data set. The 26S proteasome (Figure 3a) is a proteolytic complex, which plays an integral role in cellular homeostasis and is responsible for the degradation of poly-ubiquitinated proteins [21, 22]. This complex consists of 19S regulatory cap structures surrounding the catalytic 20S core particle. The 19S cap recognizes the poly-ubiquitinated chain, then unfolds and translocates the protein to the 20S catalytic core for degradation. The 20S core is composed of four stacked rings containing 7 α (PSMA1-7) or β (PSMB1-7) proteins each with a α7β7β7α7 configuration. The β proteins PSMB6, PSMB7, and PSMB5 (β1, β2, and β5, respectively) are responsible for caspase-like, trypsin-like, and chymotrypsin-like protein cleavage, whereas α subunits act as a docking site for the 19S cap and prevent proteins from random degradation [23, 24].

Within the primary data set created using stringent cutoffs, we identified 6 of the 39 proteins to be subunits of the 20S proteasome, and 1 involved enzyme (UCHL5) (red, Figure 3b). When compared to the tumors of mice on a control diet, the tumors from the 5% GP treated mice indicated a 1.23-1.58 fold change in α subunits 6,7,3, and 1 (PSMA1, 3, 4, 6), and β subunits 7 and 2 (PSMB4, 7). Additional analysis using the secondary data set found that the protein ubiquitination pathway was scored at #11 in terms of significance in the secondary data set, and revealed 7 additional proteins involved in this pathway (grey bars, Figure 3b). Because these data suggest that GP affects many of the subunits within the 20S proteasome, we sought

to assess if the observed protein modulations affect proteasome cleavage, we quantified 20S proteasome activity in the tumors of all treatment groups (control, 3% GP, and 5% GP). Our data suggested that the 3% GP enhanced proteasome activity, whereas 5% GP diet had no effect, although the proteomics data set showed protein expression differences between the 5% GP and control diets (Figure 3b). We also performed immunoblot analysis of all treatment groups evaluating two of the α subunits, PSMA3 and 6, the trypsin-like, catalytically active β2 subunit, PSMB7, and UCHL5, an enzyme responsible for deubiquitination prior to proteasomal degradation of proteins [25, 26] (Figure 3d). By performing density analysis, we observed significant increases in UCHL5 expression within the 3% GP group, but not the 5% GP group consistent with the proteasome assay. This increase was accompanied by slight increases in the 3% GP group of PSMA3 and PSMA6, yet no change in PSMB7 (Figure 3e).

Although proteasomes play a pivotal role in regulating the redox balance of cells by degrading oxidized proteins and is susceptible to oxidative modifications, their regulation is poorly understood. Proteasome dysfunction can lead to the accumulation of oxidized proteins, which in turn can feedback to further inhibition of the proteasome and lead to cytotoxicity. Unfortunately, dysregulation can also contribute to pathologies and oxidative stress-associated disorders including neurodegenerative disorders and various cancers [27]. In our previous study, we demonstrated that GP reduced the lipid peroxidation product 4-hydroxynoneal (HNE) (Chapter 2 [12]). A number of studies have suggested that proteins cross-linked by HNE can inhibit proteasome function, thereby altering the balance of ubiquitination and degradation of oxidized proteins [28-30]. This disturbance can then lead to accumulation of cellular damages which contribute to skin aging. Furthermore, the antioxidant capacity of natural compounds should enhance the proteasome activity against these damage by balancing homeostasis. Consumption of the Mediterranean diet (a balanced diet of non-starchy vegetables, fruits, legumes, etc) in elderly populations has demonstrated the efficacy of natural compounds

against aging [31]. Therefore, we reason that the natural components within GP may enhance proteasome activity, leading to the proper removal of damaged proteins.

Dietary GP reduces chronic acute phase response

Within the secondary canonical pathway analysis (Figure 2d), APR signaling was the top predicted pathway, with 14 proteins identified. This pathway is linked with UV radiation, as UV induces inflammation in the skin, leading to the influx of cytokines by surrounding cells. This response prompts the liver to produce acute phase proteins (APPs), a set of early responses by the body to acute damage or trauma (Figure 4a) [32, 33]. APR results in the changes of many proteins grouped as either positive or negative acute phase proteins. Positive acute phase proteins, such as fibrinogen (FG) and haptoglobin (HP), appear to be increased during inflammation, whereas negative APPs, including albumin, retinol-binding protein, and transferrin, are decreased. Although APR response aids in initial inflammatory mediation, prolonged expression of acute phase proteins can support a constitutively active inflammatory environment [34-36]. Within our comparative proteomics analysis, we found that GP altered 14 proteins involved in the APR signaling pathway (Figure 2b). Following our analysis, we identified five positive APPs (APCS, FGA, FGB, HP, and HPX; green bars in Figure 4b) as being more than 1.5-fold downregulated and one negative APP (RBP1; red bar in Figure 4b) as 2.14-fold upregulated. The other seven identified proteins included AMBP, C1RA, C1S1, IL-36γ, ITIH3, RALB, and RAP1B. Because these data suggest a change of positive APP between the 5% GP and the control diet tumors, we performed an immunoblot and densitometry analysis to determine if the changes applied to 3% GP treated mice as well. We confirmed significant decreases in positive APPs- HP, fibrinogen α (FGA), and fibrinogen β (FGB) as well as slight decreases in serum amyloid P-component (APCS), and bikunin (AMBP) in both treatment groups (Figure 3c-d). This data suggests an anti-inflammatory response for GP in the skin.

Upon inflammatory response modulating the expression of APPs, C-reactive protein upregulation can lead to the activation of the complement system (C1S and C1R, modulated -1.43 and -1.38, respectively), which further recruit inflammatory cells [37]. Because the feedback loop of chronic inflammation in tumor environments, many of these positive APPs, including SAA and HP, have been proposed as potential biomarkers in patients with colorectal [38-40], lung [41, 42], hepatocellular [43], breast [44], and endometrial [45] cancers. In addition to involvement in coagulation, FG appears to have a direct role in the inflammatory response. In a wound-healing model, FG-deficient mice exhibited a deficiency in wound repair through the inability of cells to efficiently organize, although wound closure times were similar [46]. Elevated FG levels have been associated with various malignancies [47-50] and can indicate the metastatic potential of circulating tumor cells in models of lung carcinoma and melanoma [51]. Our proteomics data also suggests that GP preserves the functions of negative APPs, such as RBP1, which is responsible for the binding and transport of retinol (vitamin A), from the liver to cells [52]. Therefore, GP may not only reduce inflammation, but prevent the suppression of proteins involved in cell heath. Due to the increased levels of APPs within our data set, we sought to evaluate the expression of upstream regulators that are linked to chronic inflammation.

Dietary GP reduces chronic inflammatory response

Although neither of our proteomics data sets picked up these proteins, we were interested in assessing if the increased positive APP expression in control tumors was due to upstream regulators including nuclear factor kappa B (NF-κB) and mitogen-activated protein kinase (MAPK) signaling pathways. UV-induced photodamage activates multiple protective signaling cascades involved in inflammation and ROS, which are known to enhance each other [53]. To maintain the redox balance within the cell, antioxidant response systems scavenge the ROS produced by the photodamage. With time, the overabundance of ROS caused by UV

radiation can deplete antioxidants and decrease the efficiency of the response systems, leading to cumulative DNA damages and stress [54]. Oxidative stress caused by UV radiation has been shown to induce many cascades leading to the activation of MAPKs, which regulate multiple transcriptional factors, such as NF-κB [55]. ERKs 1 and 2, members of the MAPK family, can be activated by UV radiation and oxidative stress to mediate multiple cellular functions, including proliferation. Activation of ERK is dysregulated in many cancers, including skin cancer [56-59]. Upon assessment of ERK1/2 activation in our tumor lysates, we observed a significant inhibition in the activation of ERK2 (p42) in the 3% GP group, with marked reduction in the ERK2 (p42) 5% GP and ERK1 (p44) in the 3% GP group upon immunoblot and densitometry analysis (Figure 4e-f).

Next, we sought to explore changes in the NF-κB signaling pathway tas MAPK proteins (ERK1/2, p38 kinase, and JNK) are known to be mediators of NF-κB signaling [60, 61]. UV light activates p38 and inhibitory kappa kinase (IKK) to activate NF-κB, which serves as a key regulator in the pro-inflammatory response upon activation and localization to the nucleus [62]. NF-κB is a key transcription factor required for the induction of pro inflammatory genes including Il-6 and TNF-α [63]. STAT3, another protein that has been shown to be constitutively active in cancers, activation occurs upon an accumulation of Il-6. Additionally, activated STAT3 and NF-κB can interact within the nucleus leading to further inflammatory response [64]. Upon their upregulation, both STAT3 and NF-κB p65 have been linked to upregulation of HP [65] and SAA [66]. Therefore, we evaluated the expression of NF-κB to determine if upstream activation is leading to constitutively active positive acute phase proteins within UVB-mediated tumors. As demonstrated in Figure 4g-h, the 3% GP had significant reduction in expression of NF-κB p65 and significant increase in IκBα, a protein known to tether non-phosphorylated subunits of the NF-κB complex (p65 and p50) to the cytosol. Although the slight increase in IκBα was confounding in the 5% GP group, it was accompanied by a marked reduction in NF-κB p65

expression. Interestingly, we have previously demonstrated that the grape antioxidant resveratrol can inhibit the inflammatory and oncogenic effector NF-κB in the skin [67]. Therefore, we believe that the combined polyphenol effects of the GP diet inhibit the phosphorylation of ERK signaling by oxidative stress, therefore inhibiting activation of downstream NF-κB signaling.

Conclusion

As the most common malignancy in the United States, NMSC cases are at an all-time high and continuing to rise [6]. Therefore, we need additional measures for the management of these cancers. In recent years, the beneficial effects of commonly consumed, naturally occurring dietary agents and supplements are being widely investigated for prevention of cancer. Moreover, the consumption of these compounds in their natural matrix, as whole foods, in a polyphenol-rich diet has been repeatedly linked to additive/synergistic responses against a variety of diseases, including cancer [10, 68-70]. Therefore, whole foods as part of a manageable diet are gaining considerable attention for better heath and disease prevention. However, the molecular mechanisms of action of dietary supplements need to be carefully evaluated. Our study has sought to evaluate the mechanisms of the beneficial effects of dietary grape against skin tumorigenesis. Our data suggests that grape powder acts as an anti-inflammatory agent and enhances activity of the 20S proteasome for the disposal of ubiquitinated proteins. Based on our findings, we have proposed a mechanism of GP-meditated action against skin cancer in Figure 5. Further studies are needed to determine upstream regulators and detailed studies aimed at identifying the interactions among different pathways and proteins, providing an overall skin cancer chemopreventive response.

Acknowledgements

This work was partially supported by funding from the California Table Grape Commission, as well as the National Institutes for Health (grant numbers R01AR059130 and

R01CA176748 to NA), and the Department of Veterans Affairs (VA Merit Review Awards I01CX001441 and I01BX004221; and a Research Career Scientist Award IK6BX003780 to NA). We also acknowledge the core facilities supported by the Skin Diseases Research Center (SDRC) Core Grant P30AR066524 from NIH/NIAMS. The mass spectrometry work reported here was performed in the Mass Spectrometry/Proteomics Facility in the Biotechnology Center, UW-Madison.

References

1 Mancebo SE, Wang SQ. Skin cancer: role of ultraviolet radiation in carcinogenesis. Rev Environ Health 2014;29:265-73.

2 Wacker M, Holick MF. Sunlight and Vitamin D: A global perspective for health. Dermatoendocrinol 2013;5:51-108.

3 MacLaughlin JA, Anderson RR, Holick MF. Spectral character of sunlight modulates photosynthesis of previtamin D3 and its photoisomers in human skin. Science 1982;216:1001-3.

4 Heck DE, Vetrano AM, Mariano TM, Laskin JD. UVB light stimulates production of reactive oxygen species: unexpected role for catalase. J Biol Chem 2003;278:22432-6.

5 Ichihashi M, Ueda M, Budiyanto A, Bito T, Oka M, Fukunaga M, Tsuru K, Horikawa T. UV-induced skin damage. Toxicology 2003;189:21-39.

6 Rogers HW, Weinstock MA, Feldman SR, Coldiron BM. Incidence Estimate of Nonmelanoma Skin Cancer (Keratinocyte Carcinomas) in the U.S. Population, 2012. JAMA Dermatol 2015;151:1081-6.

7 Nugent Z, Demers AA, Wiseman MC, Mihalcioiu C, Kliewer EV. Risk of second primary cancer and death following a diagnosis of nonmelanoma skin cancer. Cancer Epidemiol Biomarkers Prev 2005;14:2584-90.

8 Kahn HS, Tatham LM, Patel AV, Thun MJ, Heath CW, Jr. Increased cancer mortality following a history of nonmelanoma skin cancer. JAMA 1998;280:910-2.

9 Singh P, Arora D, Shukla Y. Enhanced chemoprevention by the combined treatment of pterostilbene and lupeol in BaP-induced mouse skin tumorigenesis. Food Chem Toxicol 2017;99:182-9.

10 Singh CK, Liu X, Ahmad N. Resveratrol, in its natural combination in whole grape, for health promotion and disease management. Ann N Y Acad Sci 2015;1348:150-60.

11 Singh CK, Siddiqui IA, El-Abd S, Mukhtar H, Ahmad N. Combination chemoprevention with grape antioxidants. Mol Nutr Food Res 2016;60:1406-15.

12 Singh CK, Mintie CA, Ndiaye MA, Chhabra G, Dakup PP, Ye T, Yu M, Ahmad N. Chemoprotective Effects of Dietary Grape Powder on UVB Radiation-Mediated Skin Carcinogenesis in SKH-1 Hairless Mice. J Invest Dermatol 2019;139:552-61.

13 Mintie CA, Singh, CK, Ndiaye, MA, Barrett-Wilt, GA, Ahmad, N. A Tandem Mass Tag (TMT) proteomics analysis of the chemoprevention of dietary grape against UVB-mediated carcinogenesis in SKH-1 hairless mice Data Brief 2019; Submitted.

14 Cox J, Mann M. MaxQuant enables high peptide identification rates, individualized p.p.b.-range mass accuracies and proteome-wide protein quantification. Nat Biotechnol 2008;26:1367-72.

15 Tyanova S, Temu T, Sinitcyn P, Carlson A, Hein MY, Geiger T, Mann M, Cox J. The Perseus computational platform for comprehensive analysis of (prote)omics data. Nat Methods 2016;13:731-40.

16 Thomas PD, Campbell MJ, Kejariwal A, Mi H, Karlak B, Daverman R, Diemer K, Muruganujan A, Narechania A. PANTHER: a library of protein families and subfamilies indexed by function. Genome Res 2003;13:2129-41.

17 Kramer A, Green J, Pollard J, Jr., Tugendreich S. Causal analysis approaches in Ingenuity Pathway Analysis. Bioinformatics 2014;30:523-30.

18 Benavides F, Oberyszyn TM, VanBuskirk AM, Reeve VE, Kusewitt DF. The hairless mouse in skin research. J Dermatol Sci 2009;53:10-8.

19 Rauniyar N, Yates JR. Isobaric Labeling-Based Relative Quantification in Shotgun Proteomics. J Proteome Res 2014;13:5293-309.

20 Das S, Das DK. Anti-inflammatory responses of resveratrol. Inflamm Allergy Drug Targets 2007;6:168-73.

21 Shen M, Schmitt S, Buac D, Dou QP. Targeting the ubiquitin-proteasome system for cancer therapy. Expert Opin Ther Targets 2013;17:1091-108.

22 Hayter JR, Doherty MK, Whitehead C, McCormack H, Gaskell SJ, Beynon RJ. The subunit structure and dynamics of the 20S proteasome in chicken skeletal muscle. Mol Cell Proteomics 2005;4:1370-81.

23 Sahara K, Kogleck L, Yashiroda H, Murata S. The mechanism for molecular assembly of the proteasome. Adv Biol Regul 2014;54:51-8.

24 Voutsadakis IA. Proteasome expression and activity in cancer and cancer stem cells. Tumour Biol 2017;39:1010428317692248.

25 Arpalahti L, Hagstrom J, Mustonen H, Lundin M, Haglund C, Holmberg CI. UCHL5 expression associates with improved survival in lymph-node-positive rectal cancer. Tumour Biol 2017;39:1010428317716078.

26 Tanaka K. The proteasome: overview of structure and functions. Proc Jpn Acad Ser B Phys Biol Sci 2009;85:12-36.

27 Aiken CT, Kaake RM, Wang X, Huang L. Oxidative stress-mediated regulation of proteasome complexes. Mol Cell Proteomics 2011;10:R110 006924.

28 Bulteau AL, Lundberg KC, Humphries KM, Sadek HA, Szweda PA, Friguet B, Szweda LI. Oxidative modification and inactivation of the proteasome during coronary occlusion/reperfusion. J Biol Chem 2001;276:30057-63.

29 Keller JN, Huang FF, Zhu H, Yu J, Ho YS, Kindy TS. Oxidative stress-associated impairment of proteasome activity during ischemia-reperfusion injury. J Cereb Blood Flow Metab 2000;20:1467-73.

30 Friguet B, Szweda LI. Inhibition of the multicatalytic proteinase (proteasome) by 4-hydroxy-2-nonenal cross-linked protein. FEBS Lett 1997;405:21-5.

31 Athanasopoulou S, Chondrogianni N, Santoro A, Asimaki K, Delitsikou V, Voutetakis K, Fabbri C, Pietruszka B, Kaluza J, Franceschi C, Gonos ES. Beneficial Effects of Elderly Tailored Mediterranean Diet on the Proteasomal Proteolysis. Front Physiol 2018;9:457-.

32 Cray C, Zaias J, Altman NH. Acute Phase Response in Animals: A Review. Comp Med 2009;59:517-26.

33 D'Orazio J, Jarrett S, Amaro-Ortiz A, Scott T. UV Radiation and the Skin. Int J Mol Sci 2013;14:12222-48.

34 Gabay C, Kushner I. Acute-phase proteins and other systemic responses to inflammation. N Engl J Med 1999;340:448-54.

35 Jain S, Gautam V, Naseem S. Acute-phase proteins: As diagnostic tool. J Pharm Bioallied Sci 2011;3:118-27.

36 Krzystek-Korpacka M, Matusiewicz M, Diakowska D, Grabowski K, Blachut K, Kustrzeba-Wojcicka I, Terlecki G, Gamian A. Acute-phase response proteins are related to cachexia and accelerated angiogenesis in gastroesophageal cancers. Clin Chem Lab Med 2008;46:359-64.

37 Korkmaz HI, Krijnen PAJ, Ulrich MMW, de Jong E, van Zuijlen PPM, Niessen HWM. The role of complement in the acute phase response after burns. Burns 2017;43:1390-9.

38 Holm M, Saraswat M, Joenväärä S, Ristimäki A, Haglund C, Renkonen R. Colorectal cancer patients with different C-reactive protein levels and 5-year survival times can be differentiated with quantitative serum proteomics. PLoS One 2018;13:e0195354.

39 Glojnaric I, Casl MT, Simic D, Lukac J. Serum amyloid A protein (SAA) in colorectal carcinoma. Clin Chem Lab Med 2001;39:129-33.

40 Sun L, Hu S, Yu L, Guo C, Sun L, Yang Z, Qi J, Ran Y. Serum haptoglobin as a novel molecular biomarker predicting colorectal cancer hepatic metastasis. Int J Cancer 2016;138:2724-31.

41 Cho WC, Yip TT, Cheng WW, Au JS. Serum amyloid A is elevated in the serum of lung cancer patients with poor prognosis. Br J Cancer 2010;102:1731-5.

42 Chang Y-K, Lai Y-H, Chu Y, Lee M-C, Huang C-Y, Wu S. Haptoglobin is a serological biomarker for adenocarcinoma lung cancer by using the ProteomeLab PF2D combined with mass spectrometry. Am J Cancer Res 2016;6:1828-36.

43 Tai C-S, Lin Y-R, Teng T-H, Lin P-Y, Tu S-J, Chou C-H, Huang Y-R, Huang W-C, Weng S-L, Huang H-D, Chen Y-L, Chen WL. Haptoglobin expression correlates with tumor differentiation and five-year overall survival rate in hepatocellular carcinoma. PLoS One 2017;12:e0171269-e.

44 Tabassum U, Reddy O, Mukherjee G. Elevated serum haptoglobin is associated with clinical outcome in triple-negative breast cancer patients. Asian Pac J Cancer Prev 2012;13:4541-4.

45 Cocco E, Bellone S, El-Sahwi K, Cargnelutti M, Buza N, Tavassoli FA, Schwartz PE, Rutherford TJ, Pecorelli S, Santin AD. Serum amyloid A: a novel biomarker for endometrial cancer. Cancer 2010;116:843-51.

46 Drew AF, Liu H, Davidson JM, Daugherty CC, Degen JL. Wound-healing defects in mice lacking fibrinogen. Blood 2001;97:3691-8.

47 Pichler M, Hutterer GC, Stojakovic T, Mannweiler S, Pummer K, Zigeuner R. High plasma fibrinogen level represents an independent negative prognostic factor regarding cancer-specific, metastasis-free, as well as overall survival in a European cohort of non-metastatic renal cell carcinoma patients. Br J Cancer 2013;109:1123-9.

48 Takeuchi H, Ikeuchi S, Kitagawa Y, Shimada A, Oishi T, Isobe Y, Kubochi K, Kitajima M, Matsumoto S. Pretreatment plasma fibrinogen level correlates with tumor progression and metastasis in patients with squamous cell carcinoma of the esophagus. J Gastroenterol Hepatol 2007;22:2222-7.

49 Fan S, Guan Y, Zhao G, An G. Association between plasma fibrinogen and survival in patients with small-cell lung carcinoma. Thorac Cancer 2018;9:146-51.

50 Seebacher V, Aust S, D'Andrea D, Grimm C, Reiser E, Tiringer D, Von Mersi H, Polterauer S, Reinthaller A, Helmy-Bader S. Development of a tool for prediction of ovarian cancer in patients with adnexal masses: Value of plasma fibrinogen. PLoS One 2017;12:e0182383.

51 Palumbo JS, Kombrinck KW, Drew AF, Grimes TS, Kiser JH, Degen JL, Bugge TH. Fibrinogen is an important determinant of the metastatic potential of circulating tumor cells. Blood 2000;96:3302-9.

52 Quadro L, Hamberger L, Colantuoni V, Gottesman ME, Blaner WS. Understanding the physiological role of retinol-binding protein in vitamin A metabolism using transgenic and knockout mouse models. Mol Aspects Med 2003;24:421-30.

53 Pillai S, Oresajo C, Hayward J. Ultraviolet radiation and skin aging: roles of reactive oxygen species, inflammation and protease activation, and strategies for prevention of inflammation-induced matrix degradation - a review. Int J Cosmet Sci 2005;27:17-34.

54 Takashima A, Bergstresser PR. Impact of UVB radiation on the epidermal cytokine network. Photochem Photobiol 1996;63:397-400.

55 Kyriakis JM, Avruch J. Mammalian Mitogen-Activated Protein Kinase Signal Transduction Pathways Activated by Stress and Inflammation. Physiol Rev 2001;81:807-69.

56 Yang G, Fu Y, Malakhova M, Kurinov I, Zhu F, Yao K, Li H, Chen H, Li W, Lim DY, Sheng Y, Bode AM, Dong Z, Dong Z. Caffeic acid directly targets ERK1/2 to attenuate solar UV-induced skin carcinogenesis. Cancer Prev Res (Phila) 2014;7:1056-66.

57 Russo AE, Torrisi E, Bevelacqua Y, Perrotta R, Libra M, McCubrey JA, Spandidos DA, Stivala F, Malaponte G. Melanoma: molecular pathogenesis and emerging target therapies (Review). Int J Oncol 2009;34:1481-9.

58 Einspahr JG, Calvert V, Alberts DS, Curiel-Lewandrowski C, Warneke J, Krouse R, Stratton SP, Liotta L, Longo C, Pellacani G, Prasad A, Sagerman P, Bermudez Y, Deng J, Bowden GT, Petricoin EF, 3rd. Functional protein pathway activation mapping of the progression of normal skin to squamous cell carcinoma. Cancer Prev Res (Phila) 2012;5:403-13.

59 Moriyama M, Moriyama H, Uda J, Kubo H, Nakajima Y, Goto A, Morita T, Hayakawa T. BNIP3 upregulation via stimulation of ERK and JNK activity is required for the protection of keratinocytes from UVB-induced apoptosis. Cell Death Dis 2017;8:e2576-e.

60 Somensi N, Brum PO, de Miranda Ramos V, Gasparotto J, Zanotto-Filho A, Rostirolla DC, da Silva Morrone M, Moreira JCF, Pens Gelain D. Extracellular HSP70 Activates ERK1/2, NF-kB and Pro-Inflammatory Gene Transcription Through Binding with RAGE in A549 Human Lung Cancer Cells. Cell Physiol Biochem 2017;42:2507-22.

61 Bonvin C, Guillon A, van Bemmelen MX, Gerwins P, Johnson GL, Widmann C. Role of the amino-terminal domains of MEKKs in the activation of NFκB and MAPK pathways and in the regulation of cell proliferation and apoptosis. Cell Signal 2002;14:123-31.

62 Bickers DR, Athar M. Oxidative stress in the pathogenesis of skin disease. J Invest Dermatol 2006;126:2565-75.

63 Liu T, Zhang L, Joo D, Sun S-C. NF-κB signaling in inflammation. Signal Transduct Target Ther 2017;2:17023.

64 Chung SS, Vadgama JV. Curcumin and epigallocatechin gallate inhibit the cancer stem cell phenotype via down-regulation of STAT3-NFkappaB signaling. Anticancer Res 2015;35:39-46.

65 Uskokovic A, Dinic S, Mihailovic M, Grdovic N, Arambasic J, Vidakovic M, Bogojevic D, Ivanovic-Matic S, Martinovic V, Petrovic M, Poznanovic G, Grigorov I. STAT3/NF-kappaB interactions determine the level of haptoglobin expression in male rats exposed to dietary restriction and/or acute phase stimuli. Mol Biol Rep 2012;39:167-76.

66 Hagihara K, Nishikawa T, Sugamata Y, Song J, Isobe T, Taga T, Yoshizaki K. Essential role of STAT3 in cytokine-driven NF-kappaB-mediated serum amyloid A gene expression. Genes Cells 2005;10:1051-63.

67 Adhami VM, Afaq F, Ahmad N. Suppression of Ultraviolet B Exposure-Mediated Activation of NF-κB in Normal Human Keratinocytes by Resveratrol. Neoplasia 2003;5:74-82.

68 Shah R. The Role of Nutrition and Diet in Alzheimer Disease: A Systematic Review. J Am Med Dir Assoc 2013;14:398-402.

69 Godic A, Poljšak B, Adamic M, Dahmane R. The role of antioxidants in skin cancer prevention and treatment. Oxid Med Cell Longev 2014;2014:860479-.

70 Scalbert A, Manach C, Morand C, Remesy C, Jimenez L. Dietary polyphenols and the prevention of diseases. Crit Rev Food Sci Nutr 2005;45:287-306.

Figure Legends

Figure 1. Summary of quantitative proteomics approach in protocol and analysis.

(**a**) Overview of TMT 10-plex mass tagging experimental design from large tumor protein lysates isolated from control mice (n=5) and 5% GP mice (n=5). (**b**) Heat map of log 2 transformed fold change of reporter ion intensity mean of all channels, including hierarchical clustering using MaxQuant software based upon the tumor sample ID (Ctl or 5GP). (**c**) Histogram of unique peptide sequences and (**d**) distribution of the reporter ion intensity ratios (5% GP / Ctl) in the identified 2,629 proteins. (**e**) Volcano plot of log 2 transformed reporter ion intensity ratios (x-axis) against log 10 transformed p-values calculated by a student's t-test (y-axis). Significant, differentially expressed proteins were determined by two sets of cut-off parameters. Primary analysis involved proteins with a FDR q-value ≤0.1, fold change ≥1.2, p-value ≤0.05, and ≥3 unique peptides, whereas secondary analysis excluded the FDR q-value cut-off. Proteins with the primary cut-offs are indicated by black circles. Colored dots indicate decreased (green) and increased (red) protein levels within the secondary cut-off parameters. Ctl, control diet. 5GP, 5% GP diet. TMT, tandem mass tag. FDR, false discovery rate.

Figure 2. Functional analysis of the significant, differentially expressed proteins.

Proteins of interest were classified by PANTHER reporting (**a**) molecular function (**b**) and biological processes. (**c**) Functional analysis of the secondary cut-off analysis utilizing IPA shows interactions of proteins suppressing oxidative stress through increased metabolism of ROS and reduced quantity of hydrogen peroxide. Indirect interactions are denoted by dashed lines. Blue lines suggest inhibition; orange suggest activation; yellow suggest inconsistent findings; grey indicates that an effect is not predicted. (**d**) Pathway analysis was conducted using IPA. Primary FDR analysis (gray bar) and secondary cut-off analysis (black bars). Bars represent the –log transformed p-value calculated using a right-tailed Fisher Exact test of the

number of focus genes in the dataset and the total number of genes known to be associated with the process. (n) indicates the number of proteins within our dataset that are involved in the corresponding pathway. IPA, Ingenuity Pathway Analysis. FDR, false discovery rate. ROS, reactive oxygen species.

Figure 3. Proteomics analysis showing proteins associated with the Protein Ubiquitination Pathway.

(**a**) Basic structure of the 26S proteasome, a complex composed of two 19S regulatory particles capping the barrel-shaped 20S catalytic core. The 20S core consists of four stacked rings with a α7β7β7α7 configuration. The α subunits are predominantly structural while the β subunits are primarily catalytic. (**b**) Proteins identified in our dataset that are involved in the Protein Ubiquitination Pathway identified by IPA. Red bars represent modulated proteins that are within primary cut-off criteria, while grey bars are within secondary cut-off. (**c**) 20S proteasome activity assay (**** $p < 0.0001$), with statistical significance determined using one way ANOVA with Tukey's multiple comparison. (**d**) Immunoblot analysis of modulated 20S subunits PSMA3, PSMA6, and PSMB7 and deubiquitinating enzyme, UCHL5. β-tubulin and vinculin are loading controls for the respective immunoblots. (**e**) Densitometry analysis for quantification of the ratios of the proteasome proteins to the loading control. After normalization to the loading control, all densitometry bars are normalized to the first lane of the control group. Data is represented as the mean ± standard error of the mean of the normalized three bands. Two-way ANOVA with Tukey's multiple comparison was performed to determine significance (** $p < 0.01$). RFU, relative fluorescent units. GP, grape powder diet.

Figure 4. Proteomics analysis showing proteins associated with the Acute Phase Response.

(**a**) Overview of APR, which is induced upon cellular damage from UV. After UV damage, the surrounding cells will secrete cytokines, such as Il-6 and TNFα, which signal the liver to increase the production of APPs to aid in regeneration and repair of the tissue. Upon repair, the signal is abated. However, a chronic tumor inflammatory response can lead to the constitutive activation on upstream inflammatory regulators, and therefore APPs. (**b**) Proteins identified in the dataset involved in APR, including positive (green) and negative (red) APPs. (**c**) Immunoblot evaluation of APPs. (**d**) Densitometry analysis for quantification of the ratios of the APPs to the loading control. (**e**) Immunoblot analysis of the activated (pERK) and total ERK1/2 (p44/42). (**f**)) Densitometry analysis for quantification of the ratios of activated to total ERK units p44 and p42. Bands were normalized to loading control prior to calculating ratio. (**g**) Immunoblot evaluation of NF-κB and IκBα. (**h**) Densitometry analysis for quantification of the ratios of NF-κB and IκBα to the loading control. After normalization to the loading control, all densitometry bars are normalized to the first lane of the control group. Data is represented as the mean ± standard error of the mean of the normalized three bands. Two-way ANOVA with Tukey's multiple comparison was performed to determine significance in all densitometry graphs (* $p < 0.05$, ** $p < 0.01$, *** $p < 0.001$). β-tubulin, β-actin and vinculin are loading controls for the respective immunoblots. APR, acute phase response. APP, acute phase protein. GP, grape powder diet.

Figure 5. Proposed mechanisms of the cutaneous biological response to UV damage with GP consumption.

Summary of the mechanisms explored in our previous study (Chapter 2 [12]) and based on data obtained in this study. Previously we reported that the chemoprotective effects of GP consumption were associated with reductions in oxidative stress, survival, and proliferation. The current study demonstrated the anti-inflammatory response of GP was associated with the modulation of APPs and therefore, upstream regulators (NF-κB and MAPK). GP consumption also modulated the proteasome activity, which activity is suggestively decreased upon oxidative

stress. Red arrows indicate an upregulation of the protein or process. Green arrows indicate downregulation of protein or process. APP, acute phase protein.

Figures

Figure 1

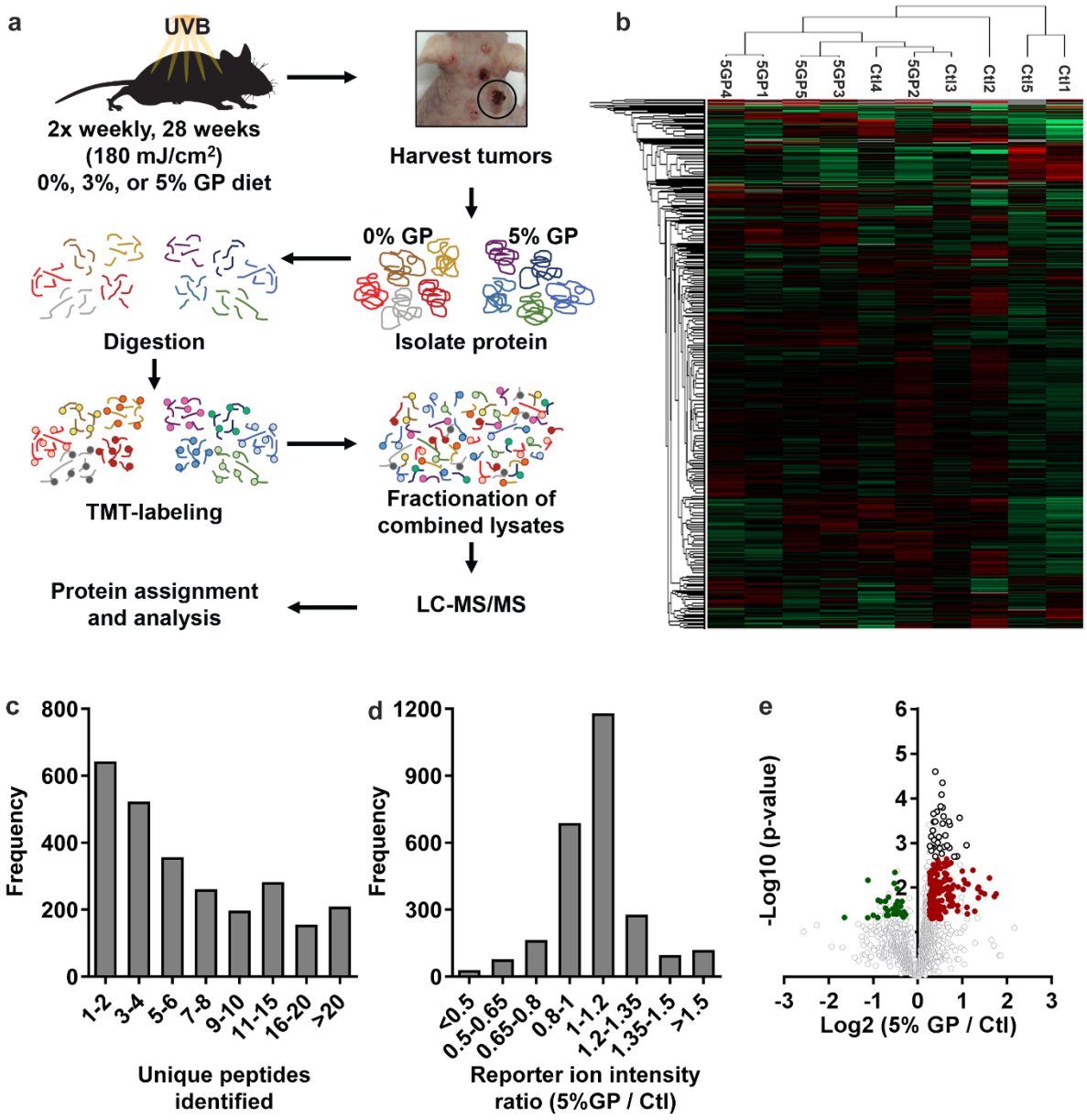

Figure 2

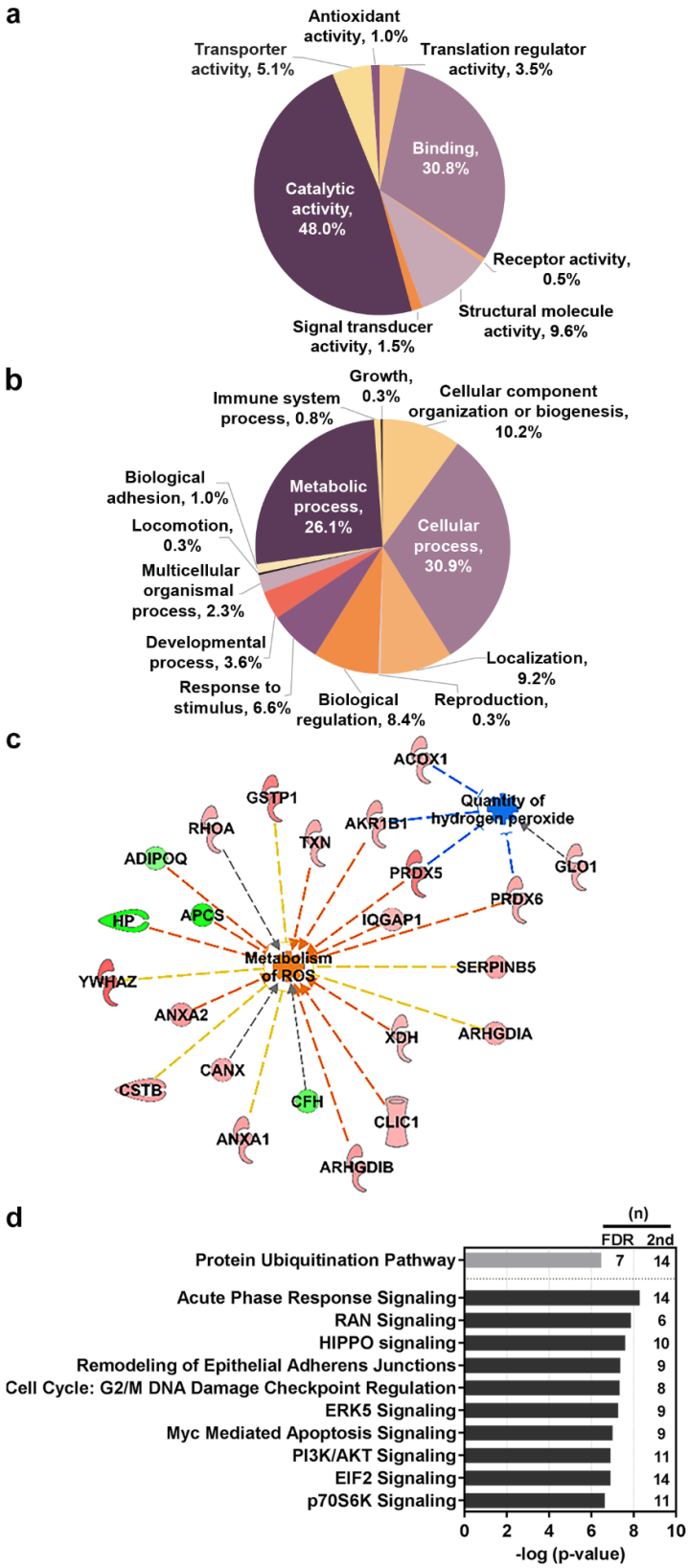
a
Antioxidant activity, 1.0%
Translation regulator activity, 3.5%
Transporter activity, 5.1%
Binding, 30.8%
Catalytic activity, 48.0%
Receptor activity, 0.5%
Structural molecule activity, 9.6%
Signal transducer activity, 1.5%
b
Growth, 0.3%
Immune system process, 0.8%
Cellular component organization or biogenesis, 10.2%
Biological adhesion, 1.0%
Metabolic process, 26.1%
Cellular process, 30.9%
Locomotion, 0.3%
Multicellular organismal process, 2.3%
Developmental process, 3.6%
Localization, 9.2%
Response to stimulus, 6.6%
Biological regulation, 8.4%
Reproduction, 0.3%
c
ACOX1
GSTP1
Quantity of hydrogen peroxide
RHOA
AKR1B1
TXN
ADIPOQ
PRDX5
GLO1
PRDX6
HP
APCS
IQGAP1
Metabolism of ROS
SERPINB5
YWHAZ
ANXA2
XDH
ARHGDIA
CANX
CSTB
CFH
CLIC1
ANXA1
ARHGDIB
d
(n)
FDR 2nd
Protein Ubiquitination Pathway 7 14
Acute Phase Response Signaling 14
RAN Signaling 6
HIPPO signaling 10
Remodeling of Epithelial Adherens Junctions 9
Cell Cycle: G2/M DNA Damage Checkpoint Regulation 8
ERK5 Signaling 9
Myc Mediated Apoptosis Signaling 9
PI3K/AKT Signaling 11
EIF2 Signaling 14
p70S6K Signaling 11
0 2 4 6 8 10
-log (p-value)

Figure 3

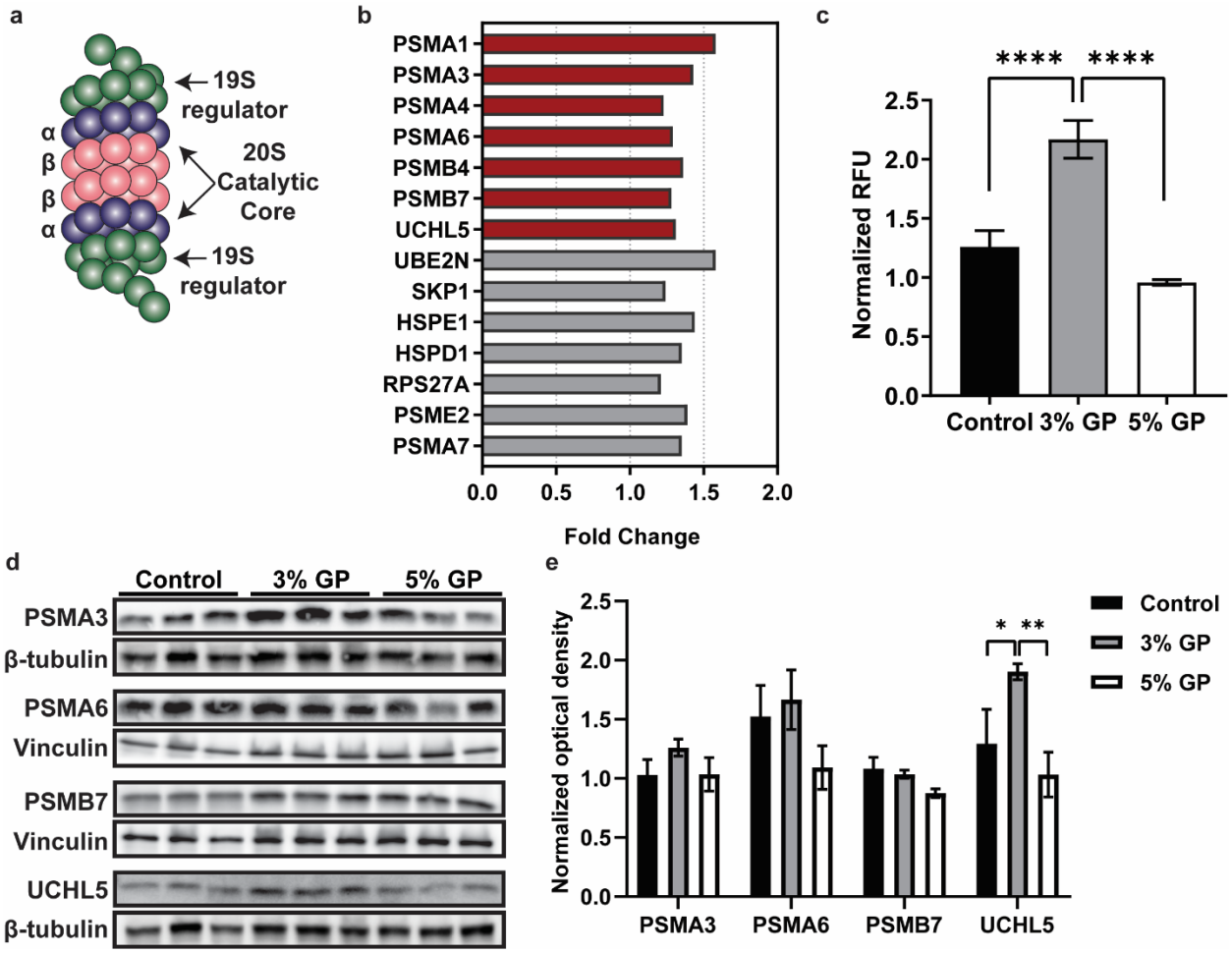
a
19S regulator
α
β
β
α
20S Catalytic Core
19S regulator
b
PSMA1
PSMA3
PSMA4
PSMA6
PSMB4
PSMB7
UCHL5
UBE2N
SKP1
HSPE1
HSPD1
RPS27A
PSME2
PSMA7
0.0
0.5
1.0
1.5
2.0
Fold Change
c
****
****
Normalized RFU
2.5
2.0
1.5
1.0
0.5
0.0
Control
3% GP
5% GP
d
Control
3% GP
5% GP
PSMA3
β-tubulin
PSMA6
Vinculin
PSMB7
Vinculin
UCHL5
β-tubulin
e
Normalized optical density
2.5
2.0
1.5
1.0
0.5
0.0
* **
Control
3% GP
5% GP
PSMA3
PSMA6
PSMB7
UCHL5

Figure 4

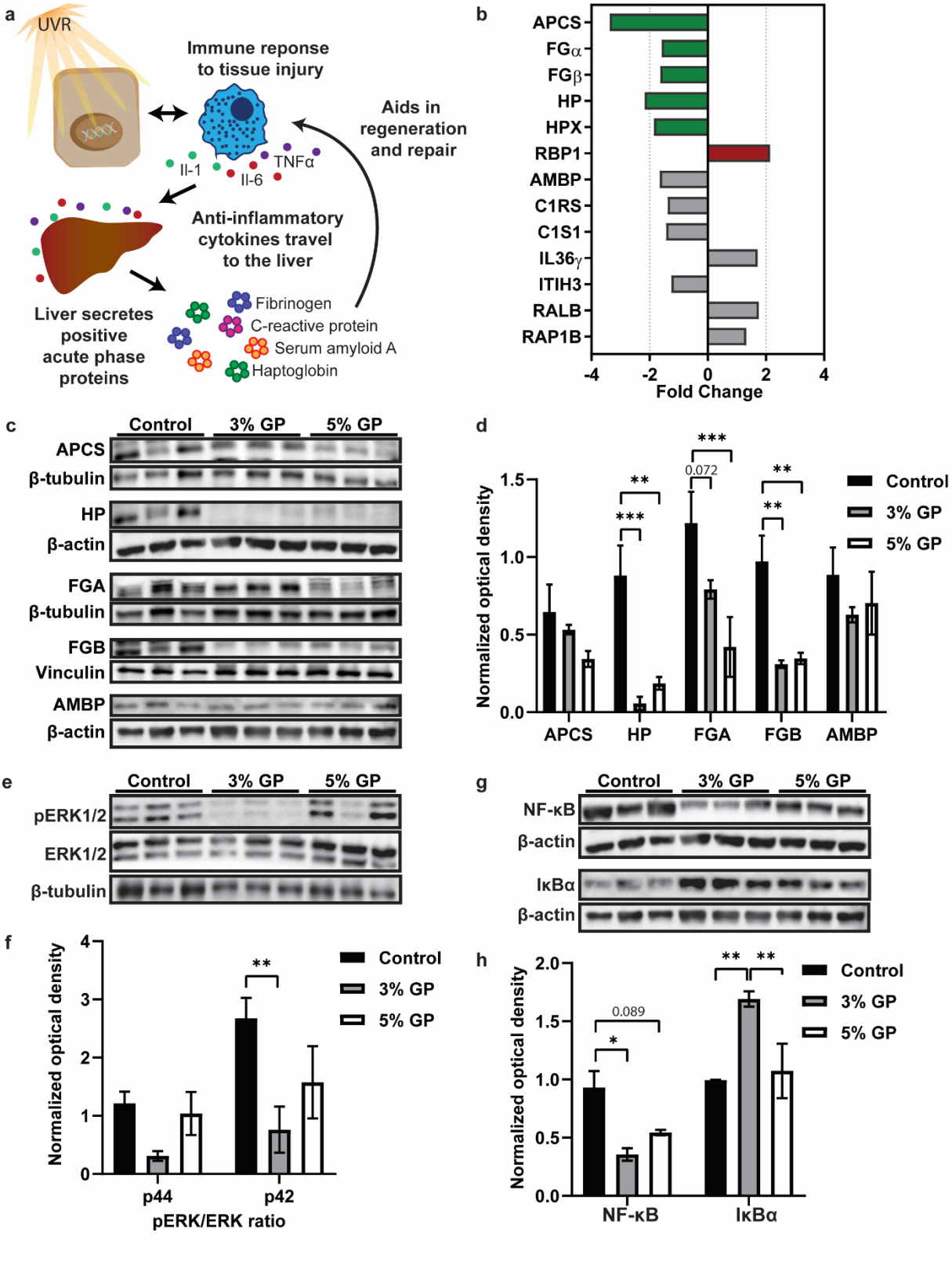
a
UVR
Immune reponse to tissue injury
Aids in regeneration and repair
Il-1
Il-6
TNFα
Anti-inflammatory cytokines travel to the liver
Liver secretes positive acute phase proteins
Fibrinogen
C-reactive protein
Serum amyloid A
Haptoglobin
b
APCS
FGα
FGβ
HP
HPX
RBP1
AMBP
C1RS
C1S1
IL36γ
ITIH3
RALB
RAP1B
-4
-2
0
2
4
Fold Change
c
Control
3% GP
5% GP
APCS
β-tubulin
HP
β-actin
FGA
β-tubulin
FGB
Vinculin
AMBP
β-actin
d
Normalized optical density
1.5
1.0
0.5
0.0
***
**
***
0.072
**
**
Control
3% GP
5% GP
APCS
HP
FGA
FGB
AMBP
e
Control
3% GP
5% GP
pERK1/2
ERK1/2
β-tubulin
f
Normalized optical density
4
3
2
1
0
**
Control
3% GP
5% GP
p44
p42
pERK/ERK ratio
g
Control
3% GP
5% GP
NF-κB
β-actin
IκBα
β-actin
h
Normalized optical density
2.0
1.5
1.0
0.5
0.0
0.089
*
**
**
Control
3% GP
5% GP
NF-κB
IκBα

Figure 5

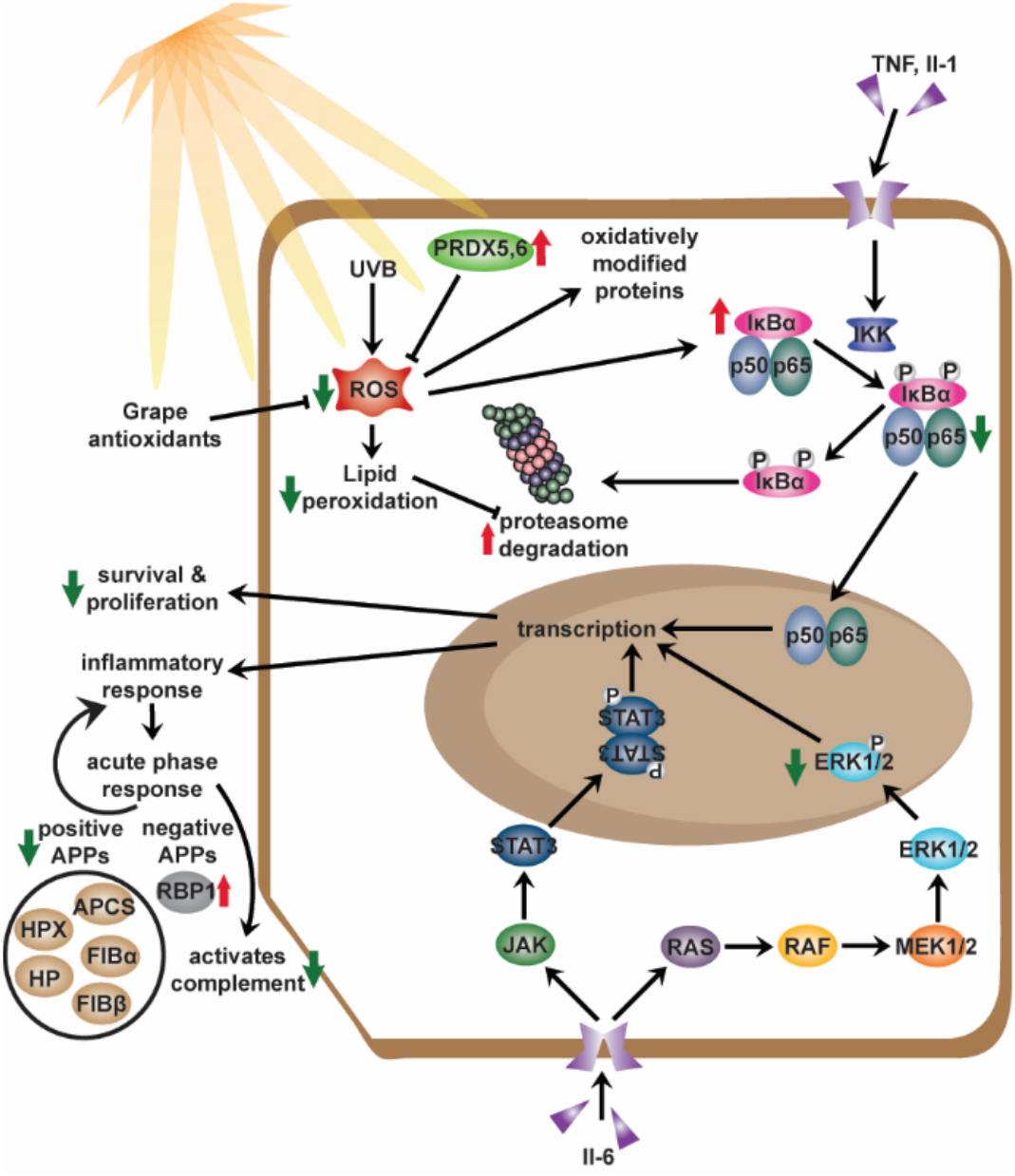
TNF, Il-1
UVB
PRDX5,6
oxidatively modified proteins
IκBα
p50 p65
IKK
ROS
Grape antioxidants
Lipid peroxidation
proteasome degradation
P
IκBα
p50 p65
survival & proliferation
transcription
inflammatory response
STAT3
ERK1/2
acute phase response
positive APPs
negative APPs
RBP1
APCS
HPX
FIBα
HP
FIBβ
activates complement
JAK
RAS
RAF
MEK1/2
Il-6

Chapter 3b: A Tandem Mass Tag (TMT) proteomics analysis of the chemoprevention of dietary grape against UVB-mediated carcinogenesis in SKH-1 hairless mice

This chapter has been submitted as a prepared manuscript to *Data in Brief*

Abstract

The comparative proteomic data presented in this article support the findings within "Identification of molecular targets of dietary grape-mediated chemoprevention of ultraviolet B skin carcinogenesis: A comparative quantitative proteomics analysis" (Chapter 3a). Here we provide the datasets of the proteomics analysis utilizing TMT 10plex mass tagging in UVB-mediated tumors of SKH-1 hairless mice to determine the chemopreventive effects of a grape powder diet. The analyzed proteomic data resulted in 2,629 modulated proteins.

Data

Total protein was extracted from skin tumors of female SKH-1 hairless mice. These tumors developed from a 28 week initiation-promotion protocol described in Chapter 2. This study served to determine the chemopreventive effects of dietary grape and the downstream modulation of proteins. A Tandem Mass Tag (TMT) approach was utilized to obtain the modulated protein expression between two groups of mice treated with UVB, where one group had access to a grape-supplemented diet.

Experimental Design, Materials and Methods

Protein precipitation and digestion

For this study, we used the tumor lysates obtained from five randomly selected mice, each from control diet and 5% GP diet. Proteins were isolated as described in Chapter 2. Equal amounts of protein were aliquoted into tubes, and sample volumes were adjusted with water to 20 µL. Proteins were precipitated by adding 180 µL 8:1 acetone:trichloroacetic acid (TCA) for final concentrations of 80% acetone and 10% TCA and incubated at -20°C for 1 hour (h). Precipitated proteins were washed twice with cold neat acetone followed by cold 80% methanol in water. Proteins were resolubilized in 25 µL 8 M urea dissolved in 50 mM ammonium bicarbonate (ABC, pH 8) in water containing 5 mM Tris. Proteins were held overnight at 4°C to resolubilize. To each sample was added 125 µL ABC to dilute urea to 1.33 M. Protein disulfides were reduced using dithiothreitol (DTT) at a solution concentration of 2 mM by incubating at 55°C 30 minutes (min). Free sulfhydryls were then alkylated by reaction with iodoacetamide (IAA) at 5 mM final concentration with incubation at room temperature in the dark for 45 min. A second addition of DTT to final concentration of 2 mM was made to quench the alkylation reaction. Proteins were simultaneously digested with lys-C (Wako) and trypsin (Promega) proteases at an enzyme to substrate ratio of 1:25 and 1:20, respectively. Digestion was done for 16 h at 37°C with gentle shaking and the digests were acidified with heptafluorobutyric acid to

pH 2, then cleaned up by solid-phase extraction using 100 µL Omix tips (Agilent Technologies, Inc.) and eluting with 75% acetonitrile, 0.1% formic acid in water.

Tandem mass tag (TMT) labeling

Samples were labeled using the TMT-10plex Isobaric Label Reagent Set (Thermo Scientific) generally according to manufacturer's instructions with some minor changes as follows. Samples were dried by vacuum centrifugation and resolubilized in 40 µL 100 mM triethyl ammonium bicarbonate (TEAB) pH 8 (Thermo Scientific). To each 8 mg vial of TMT labeling reagent was added 100 µL dry acetonitrile. Then, 41 µL dissolved TMT reagent was added to each sample (131-fold excess) and the reaction was carried out for 1 h at room temperature. The reaction was quenched by addition of hydroxylamine to 0.44%.

A trial pool of digested samples individually labeled with the 10 different TMT reagents was created by pooling 2 µL from each reaction. This trial pool was acidified and subjected to solid-phase extraction, followed by analysis of 1.1 µg total labeled digest by Orbitrap LC-MS/MS. Reporter ion abundances for all identified peptides were summed to determine an approximate protein abundance ratio among all the samples in a 10-plex experiment. Inputs for each TMT-labeled sample were then adjusted to compensate for lower- and higher-abundance samples as shown in Table 1.

High pH fractionation

TMT-labeled pooled samples were subjected to reverse-phase fractionation at pH 10. Solvent A consisted of 10 mM ammonium formate in water (pH adjusted to 10 with ammonium hydroxide) and solvent B consisted of 10 mM ammonium formate (pH 10), 80% acetonitrile in water. The column used was a Gemini C18 column (Phenomenex), 4.6 mm x 250 mm packed with 5 µm particles. The gradient is shown in Table 2a.

The flow rate was 1 mL/min. Absorbance was monitored by a photodiode array detector at 214 nm and 280 nm. Labeled, pooled samples (described above) were dried by vacuum centrifugation and resolubilized in 200 µL solvent A. The entire sample was loaded into a 500 µL sample loop and fractions were collected every 1 min from the start of the gradient program. Fractions were pooled together so as to reduce LC-MS/MS analyses while preserving chromatographic distribution. Every sixth fraction starting from fraction 6 and ending at fraction 31 were pooled together, yielding 5 overall fractions (e.g. fractions 6, 11, 16, 21, 26, and 31 are combined to make fraction 1, while fractions 7, 12, 17, 22, and 27 are combined to make fraction 2, etc.). This results in reduction in complexity of the individual fractions compared to the unfractionated material while preserving a broad distribution of peptide hydrophobicities within a fraction. Pooled fractions were dried and resolubilized in 0.2% formic acid in water at a concentration of 1 µg/µL.

LC-MS/MS

LC-MS/MS was performed on an Orbitrap Elite (Thermo Scientific) fitted with the Easy-Spray source and coupled to Agilent 1100 Nanopump and temperature-controlled autosampler. Chromatography was performed using an Easy-Spray column with integrated emitter and heater, 15 cm x 75 µm, packed with Pepmap RSLC C18, 3 µm, 100 Å stationary phase (Thermo Scientific). The HPLC method used 0.1% formic acid in water as solvent A and 0.1% formic acid in acetonitrile as solvent B. The gradient is shown in Table 2b.

The autosampler was held at 6°C. The Orbitrap Elite mass spectrometer was operated in data-dependent mode using higher-energy collisional dissociation (HCD) activation for MS/MS. The Orbitrap acquisition parameters are as follows: 230 min acquisition time with 1 MS scan collected in profile mode at 60,000 resolving power over the m/z range 350-1800 followed by 10 HCD MS/MS scans collected in centroid mode at 30,000 resolving power. MS/MS spectra used a 2.0 m/z isolation window, 38% normalize collision energy, 0.1 millisec activation time,

and a fixed start m/z of 100. Dynamic exclusion was enabled with exclusion duration of 30 s and exclusion window of -0.51 Da to +1.1 Da. Charge state exclusion was also enabled with unassigned and singly-charged ions excluded from precursor selection. Nano-electrospray ionization was performed at 1.8kV, capillary temperature of 205°C, and S-lens RF level at 45%. Roughly, 38,000 spectra were collected across 230 min of acquisition time for each of the five high pH fractions per TMT experiment.

Data analysis

Raw mass spectral data were assigned to peptides and proteins using MaxQuant [1] and searching with a mouse protein database from Uniprot containing 50,961 sequences. All five high pH fractions from a single TMT experiment were searched together. Parameters for MaxQuant searching included trypsin specificity with up to two missed cleavages, fixed carbamidomethylation of cysteines and peptide N-termini and lysines with the TMT-10plex reagent, variable oxidation of methionine, variable acetylation of protein N-termini, variable deamidation of asparagine and glutamine residues, and variable carbamylation of peptide N-termini. TMT quantitation acceptance required a precursor intensity fraction of 0.75 to limit co-isolation interference. First search precursor tolerance was 20 ppm with main search precursor tolerance of 4.5 ppm. Fragment ion tolerance was 20 ppm. Identifications were controlled to 1% false discovery rate at the peptide spectrum match (PSM) and protein levels. Proteins with only 1 unique or razor peptide were permitted. Post-search analysis was performed using Perseus [2]. Quantitative analysis was performed at the protein group level by importing the MaxQuant results file. Reverse-decoy and contaminant proteins were removed and protein groups were eliminated that did not have at least one unique peptide. Entries were required to have at least 3 reporter ion abundances (of 10 possible) greater than zero. Reporter ion abundances were normalized within a TMT channel across all proteins by dividing by the mean abundance for that TMT channel. TMT channels were then assigned to groups based on the sample type and

analyzed by two-tailed Student's T-test. Resultant p-values were converted to q-values to correct for multiple hypothesis testing using the Permutation-FDR approach. Finally, fold-change heat maps were created for protein expression by dividing each TMT channel abundance by the mean of all channels for that protein and subjecting the result to log2 transformation. Hierarchical clustering was performed on the total protein matrix. A total of 2,629 proteins were identified after post search analysis outlined in supplementary table 1.

References

1 Cox J, Mann M, MaxQuant enables high peptide identification rates, individualized p.p.b.-range mass accuracies and proteome-wide protein quantification, Nat. Biotechnol. 26(12) (2008) 1367-72.

2 Tyanova S, Temu T, Sinitcyn P, Carlson A, Hein MY, Geiger T, Mann M, Cox J, The Perseus computational platform for comprehensive analysis of (prote)omics data, Nat. Methods 13(9) (2016) 731-40.

Tables

Table 1: Adjustment of TMT-labeled samples

Test Pool 1

TMT reagent	Normalization to minimum reporter ion	Volume to add	Digest mass added
126	1	87	24.4
127N	0.81	70.4	19.8
127C	0.58	50.1	14.1
128N	0.74	64.4	18.1
128C	0.84	73.6	20.7
129N	0.73	63.2	17.8
129C	0.9	78.6	22.1
130N	0.59	51.7	14.5
130C	0.93	81.1	22.8
131	0.98	84.8	23.8
		Total mass:	198.0 µg

Test Pool 2 semi-normalization

TMT reagent	Normalization to maximum reporter ion	Volume to add (87 µL maximum)	Digest mass added
126	0.48	87	24.4
127N	1.11	78.4	22
127C	1.65	52.7	14.8
128N	1.22	71.4	20.1
128C	0.88	87	24.4
129N	0.98	87	24.4
129C	0.93	87	24.4
130N	1	87	24.4
130C	0.9	87	24.4
131	0.65	87	24.4
		Total mass:	228.1 µg

Table 2: HPLC gradients for a) offline fractionation and b) LC/MS/MS

a.

Time	%B
0	0
2	0
3	5
23	60
25	100
26	100
27	0
36	0

b.

Time (min)	%B	Flow (uL/min)
0	0	0.5
29	0	0.5
30	0	0.3
31	3	0.3
185	30	0.3
195	50	0.3
202	95	0.3
203	95	0.3
207	0	0.3
208	0	0.3
210	0	0.5
230	0	0.5

Chapter 4: Sex differences in the chemoprotective effects of dietary grape powder on ultraviolet B radiation-mediated cutaneous damage and carcinogenesis in SKH-1 hairless mice

Contents of this chapter to be communicated for publication

Abstract

Among all cancers, non-melanoma skin cancers have the highest rate of diagnosis annually within the United States, and are diagnosed more frequently in males than females. As incidences rise, it is evident that additional preventive measures are needed to reduce development and/or reoccurrence of this neoplasm. Natural agents found in foods have gained considerable attention as supplemental preventative measures in skin protection. Whole grapes contain a natural amalgamation of phytonutrients with antioxidant and anti-inflammatory properties. We previously demonstrated the chemoprotective effects of dietary grape powder (GP) in an initiation-promotion protocol of UVB-mediation tumorigenesis in female SKH-1 hairless mice, a relevant model of non-melanoma skin cancer. To build on this evidence, the studies here aimed to uncover the effects of GP in a short term UVB damage setting as well as to determine any sex-related similarities and/or differences in UVB-mediated carcinogenesis in the SKH-1 mice. The short-term UVB-mediated cutaneous damage study suggested that GP protects against early stage epithelial hyperplasia and inflammation in both sexes. The male long term UVB-mediated tumorigenesis study found reduced tumor burden and volume, and allowed us to establish tumor diagnostic classifications in which a reduction in malignant conversion of tumors was seen in our GP-fed mice. Further, we found that a significant anti-inflammatory response was imparted by GP, as shown by the inhibition of p38 activation and subsequent reductions in proliferative markers. Moreover, we observed modulation of genes involved in regulating telomeres, hypoxia, and DNA damage and repair. Overall, this study has suggested that GP may protect against short and long-term UVB-mediated skin damage and carcinogenesis in both male and female SKH-1 mice.

Introduction

Non-melanoma skin cancers (NMSCs) are the most frequently diagnosed cancer, affecting more than 3.5 million Americans annually [1]. The most prevalent NMSCs are basal cell carcinoma (BCC) and squamous cell carcinoma (SCC), with lifetime development risks 18-20 times higher than melanoma [2]. These forms of NMSC have low mortality rates (0.12 in 100,000 for BCC and 0.3 in 100,000 for SCC [2]), yet current treatments, including resections and chemotherapies, are falling short, as recurrence rate after surgical excision may be as high as 4.2% after 6.6 years [3]. Additionally, epidemiological studies have shown significantly higher incidence of NMSC in men over women, thought to be due to sex-related differences in occupations, lifestyle, and skin barrier functions [4, 5]. In the US alone, the national annual expenditures for NMSC, including direct medical costs as well as indirect costs, such as decreases in productivity and loss of potential life-years, are estimated at $4.8 billion [6].

Ultraviolet Radiation (UVR) is thought to be the primary cause of NMSC development in 90% of cases, via direct or indirect DNA damage. UVR can be classified into three subsections: UVA (320-400 nm), UVB (280-320 nm), and UVC (200-280 nm), although the vast majority of UVC is absorbed by the atmosphere. UVA radiation accounts for 90-99% of the UVR that penetrates the atmosphere, and affects DNA indirectly by creating reactive oxygen species (ROS) [7]. An accumulation of ROS causes an imbalance of redox homeostasis, leading to inflammation and edema, as well as modulations of biochemical markers and signal transduction pathways [8], such as the Nox and inflammatory pathways [9]. The 1-10% of UVB radiation that penetrates the epidermis, however, is directly absorbed by DNA and is deemed a complete carcinogen due its potential to influence all three stages of skin carcinogenesis [8]. UVB damage is characterized by formation of cyclobutane pyrimidine dimers (CPDs) and (6,4) photoproducts, which can then overload the nucleotide-excision repair (NER) mechanisms and lead to sequence transformations of C→T and CC→TT [10]. These mutations have been

detected as initiating events in tumorigenesis via the *TP53* tumor suppressor gene [10], as seen in 30-60% of cases of actinic keratosis (AK), a precancerous skin lesion [10, 11]. Up to 100% of SKH-1 mouse [12] and 90% of human [13] SCC tumors harbor *TP53* mutant alleles. Several other key cancer-related pathways have previously been shown to be affected by UVB, including epidermal growth factor (EGF) [14], mitogen-activated protein kinase (MAPKs) [15], and phosphatidylinositol 3-kinase (PI3K) pathways [14, 16]. Additionally, DNA damages caused by UVR can deregulate cytokine levels, including interleukin-1 (IL-1) and tumor necrosis factor-alpha (TNF-α), leading to chronic inflammation, characterized by increased duration, marked tissue destruction, and fibrosis [17]. This deregulation can then lead to the development of cancer via apoptotic resistance and enhanced cancer cell proliferation, survival, response to chemotherapy and hormones, metastasis, and vascularization and repair of tissues [17].

At this time, the principle methods to prevent DNA damage from UVR are the proper use of sunscreen and limiting unnecessary skin exposure via shade and clothing that covers the skin [18]. However, the rising rates of skin cancer diagnoses suggest that either taking these actions are not sufficient alone, or that these recommendations are too difficult or unwieldy for people to follow. Therefore, we must find other approaches to decrease carcinogenesis. One such approach is the consumption of naturally occurring antioxidants, such as resveratrol, which has been studied for its health and chemopreventive benefits. Resveratrol is found in multiple foods, including red grapes, though grapes contain many more antioxidants, including quercetin, melatonin, and lycopene [19]. Research has found that these antioxidants may prevent or mitigate many health conditions, such as cancer, heart disease, and arthritis [19]. The multitude of health benefits related to the biochemistry of grapes has led us to believe that grapes could effectively prevent UVB-mediated skin carcinogenesis, especially when used in its whole food form due to the possibility of synergistic activity between the many antioxidants and other bioactive compounds they contain.

Materials and Methods

Materials

Freeze-dried grape powder (GP) was kindly provided by the California Table Grape Commission. This proprietary mix is composed of fresh red, green, and black grapes cultivated in California. The diet was formulated in the AIN-76A base diet by Envigo (Madison, WI) as described in [19]. The control diet contained no GP, whereas the 3% and 5% GP diets contained the indicated amount GP. All diets were sugar matched to the natural content of the 5% diet. For our calculations, 23 g of GP is equivalent to one ¾ cup servings of whole grapes.

Animal care

All animal experiments were approved by the University of Wisconsin (UW) Institutional Animal Care and Use Committee. SKH-1 Elite mice (Crl:SKH1-*Hr*^{hr}, Strain 477) were purchased from Charles River Laboratories (Wilmington, MA) at 5 weeks of age and allowed to acclimate for one week prior to study initiation. Animals had access to water and feed *ad libitum*. Throughout the experiments, all animals were monitored for general health, body weight, and food consumption. A calibrated Research Irradiator (Daavlin Company, Bryan, OH) was used to administer measured doses of UVB for all studies

Short-term UVB-mediated cutaneous damage study

Male and female SKH-1 hairless mice (n=5 per sex, per group) were separated into the following groups: 1) control diet with no UVB, 2) control diet with UVB, and 3) 5% GP diet with UVB. The respective diets were provided to mice 2 weeks prior to the first dose of UVB. A dose of 180 mJ/cm^2 was given every other day for a total of 2 weeks. All mice were euthanized 24 hours after the seventh dose of UVB and skin samples were formalin fixed and submitted for histology. Additional skin samples were snap frozen in liquid nitrogen then stored at -80°C until further processing.

Histology

Formalin-fixed tissues were paraffin embedded, sectioned, and mounted on serial slides at the UW Translational Research Initiatives in Pathology (TRIP) laboratory. One serial slide from each mouse was stained with hematoxylin and eosin (H&E) for histological determination.

Epidermal thickness measurement

Epidermal thickness was evaluated by analyzing five fields of view from H&E-stained dorsal skin sections of each mouse using an EVOS XL Core Cell Imaging System (Thermo Fisher Scientific) and measured using ImageJ software (NIH, Rockville, MD). Five measurements from the basement membrane to the base of the stratum corneum were obtained from five dorsal views and averaged per animal. Statistical analysis was performed in GraphPad software using a two-way ANOVA with Tukey's multiple comparisons test.

Toluidine blue staining

Tissue slides from both studies were deparaffinized in xylenes, then rehydrated in an ethanol concentration gradient of 100% to 70% followed by running water. The slides were then stained 3 minutes in fresh toluidine blue working solution. The solution was prepared as follows: 5 mL of 1% toluidine blue O (Millipore Sigma, Burlington, MA) in 70% ethanol was mixed with 45 mL 1% sodium chloride (pH 2.0-2.5). Slides were washed in distilled water, dehydrated in 95% and 100% ethanol, cleared in xylenes and coverslipped for imaging in xylene:permount (1:1). Mast cells were quantified by obtaining five images of the dorsal skin sections and counting the violet cells at 10-20x magnification. Representative images were obtained using Nikon Plan Apo lenses at 10x and 40x on a Nikon Eclipse Ci microscope equipped with a Nikon DsRi2 digital color camera (Nikon, Tokyo, Japan). Statistical analysis was performed in GraphPad software using a one-way ANOVA with Tukey's multiple comparisons test.

UVB-mediated photocarcinogenesis study

Male SKH-1 hairless mice (n=12 per group) were separated into the following groups: 1) control diet with no UVB, 2) control diet with UVB, 3) 3% GP diet with UVB, and 4) 5% GP diet with UVB. Respective diets were provided on the first day of UVB exposure at six weeks of age. Mice in groups 2-4 were irradiated with 180 mJ/cm^2 UVB twice weekly for 27 weeks. Distinguishable tumors were counted and location noted weekly and at the time of euthanasia. If a tumor did not persist for more than two weeks, it was determined to be a papule and eliminated from the dataset. When the diameter of tumors exceeded 2 mm, a digital caliper was used to measure length (l), width (w), and height (h), and tumor volume was calculated by l x w x h x ($\pi/6$). Mice were euthanized 3-5 days after their last UVB exposure. Immediately after euthanasia, blood was collected via cardiac puncture and allowed to clot for 30 minutes before centrifugation at 1,500 x g for 15 minutes at RT for the collection of serum. Dorsal skin adjacent to the tumors and cross sections of a subset of both large tumors and papules with intact adjacent skin were formalin fixed and submitted for histology. Other tumors and adjacent skin samples were snap frozen in liquid nitrogen then stored at -80°C until further processing. Statistical analysis of tumor weekly tumor counts and tumor volume was done using a mixed model linear regression using R software.

Lesion scoring

Tumors were collected with flanking dorsal skin to ensure lesions were well oriented in cross section and through full-thickness skin. One H&E stained slide of skin samples from each male mouse in the UVB-mediated tumorigenesis study was examined and neoplastic lesions were scored in a blinded manner by a board-certified veterinary pathologist (R.S.). Some groups of lesions were scored independently twice to verify diagnosis. Grading guidelines were similar to those outlined in [20, 21] with the following additions. Exophytic papillomas encompassed flat epithelial lesions lacking a pronounced papillary pattern and lacking atypical cells (grade 1) through exophytic papillary masses with some atypical cells (grade 3) as described in

Benavides et al. We also observed hyperplastic epidermal lesions with dysplasia and cellular atypia that tended towards sessile (flat) or inward (endophytic) growth. We scored these as flat and endophytic papillomas respectively with increasing dysplasia and atypia reflected as grades 2 and 3. Although the flat and some endophytic lesions could have histologic features that could resemble a lesion class termed "pseudoepitheliomatous hyperplasia" by Voigt et al. and described as associated with cutaneous ulceration [22], in the absence of histologic evidence of association of the lesions observed in our study with skin ulcers, we utilized the designation "papilloma" for clarity. The exophytic, endophytic, and flat papilloma lesions were considered pre-malignant. An additional group of lesions that were scored as high-grade pre-neoplastic lesions in one blinded review of the slides and as "presumed transitional" (see below) lesions on a second blinded review were categorized as "intermediate" and were included among the pre-malignant lesions. The lesions categorized as "presumed transitional" exhibited increasingly malignant features that surpassed features of pre-malignant lesions and breaching of the basement membrane and/or angular extension into the surrounding connective tissue (invasion) that was either minimal or equivocal. These were interpreted to be lesions transitioning from the pre-malignant group into the microinvasive squamous cell carcinoma (MiSCC) class. We observed MiSCC as described in Benavides et al. and characterized these both by their depth of penetration into the superficial dermis (SD, superficial ~50% of the dermis superficial to the dermal cysts observed in the hairless model), deep dermis (DD, deep ~50% of the dermis at and deep to the level of the dermal cysts observed in the hairless model), or subcutis (SQ, into the panniculus adiposus), and also by their extent of invasion into the surrounding connective tissue (degree 2=mild, degree 3=moderate). In instances when the panniculus adiposus was minimal or not evident, tumors that extended beneath the deep dermis were classified as SQ. As described by previous authors [21], we observed SCCs, spindle cell carcinomas (SpCC), and one anaplastic tumor. SpCC tumors were Vimentin positive (data not shown). We categorized these as described by Benavides et al. Tumors were only scored as SCC if they

invaded into the panniculus carnosus muscle as described while SpCCs and anaplastic tumors were scored based on morphology regardless of depth of penetration. miSCC, SCC, SpCC, and anaplastic lesions were categorized as malignant lesions.

Immunohistochemistry

The slides were deparaffinized in xylenes and rehydrated in a gradient of ethanol concentration from 100% to 60%. The slides were then washed in distilled water, steamed for 40 minutes while in 1x IHC Epitope retrieval solution (IHC World, LLC, Ellicott City, MD), and cooled for 20 minutes at room temperature. The slides were washed with tris-buffered saline with 0.1% Tween-20 (TBS-T). Non-specific binding was blocked using 5% normal goat serum (Vector Labs, Burlingame, CA) in TBS-T. Slides were incubated in primary antibody in TBS-T overnight at 4°C in a humidified chamber. A list of antibodies used can be found in Supplemental Table S1. On a subsequent day, the slides were washed, then incubated in secondary antibody and ABC-AP per manufacturer's instructions of the Vectastain ABC Kit (Vector Labs). After a final wash slides were exposed to Vector Red Alkaline Phosphatase Substrate Kit (Vector Labs) until desired staining intensity was observed (7-15 minutes) and counterstained using Hematoxylin QS (Vector labs) for 8 seconds. The slides were rinsed in running tap water, dehydrated via ethanol concentration gradient from 60% to 100%, and cleared by two 5 minute rounds of xylenes and coverslipped for imaging in xylene:permount (1:1).

Tumor tissue protein and RNA isolation

Tumor tissues from the UVB-mediated carcinogenesis study were removed from -80°C storage and ground to a powder in liquid nitrogen before being divided for protein and RNA analysis. For protein analysis, the powdered tissue was lysed in 1X RIPA lysis buffer (Millipore, Billerica, MA) with freshly added PMSF (Amresco, Solon, OH), and both phosphatase and

protease inhibitor cocktails (ThermoFisher Scientific, Waltham, MA). Samples were then placed on ice and homogenized using a Kinematica Polytron PT 2500 E (ThermoFisher Scientific) for 5 seconds intervals until fully disrupted. Tissues were allowed to lyse with intermittent vortexing prior to centrifugation at 15,000 x g for 30 minutes at 4°C. Supernatants were isolated and protein concentration was determined by BCA Protein Assay (ThermoFisher Scientific) per manufacturer's protocol. For RNA analysis, powdered tumor tissue was placed into buffer RLT and processed using the RNeasy Fibrous Tissue Mini Kit (Qiagen) according to manufacturer's protocol, followed by RNA quantification.

IgE ELISA

IgE levels were examined using the Mouse IgE ELISA (Abcam, Cambridge, MA) per manufacturer's instructions. Three biological replicates per group, serum pooled from three mice each, were examined in technical triplicate. Serum pools were diluted 1 to 50 in the diluent buffer provided prior to application on the plate. The plate was read at λ=450 nm on a Biotek Synergy H1 plate reader (Biotek, Winooski, VT).

Cytokine array

The expression of various cytokines was performed using the Invitrogen Cytokine & Chemokine 36-Plex Mouse ProcartaPlex™ Panel 1A (ThermoFisher Scientific) per manufacturer's instructions. Three biological replicates per group, serum pooled from three mice each, were examined in technical duplicate. The plate was analyzed using a Luminex MagPix (Luminex Corporation, Austin, TX). The raw data, with bead lot information, was then imported into the ProcartaPlex Analyst Software (ThermoFisher Scientific) for data analysis.

Immunoblotting

Immunoblotting was performed as described previously [19]. Densitometry was performed to determine band intensity using Adobe Photoshop CC 2015. Background intensity

was subtracted from the band intensity prior to normalization to the loading control (target/loading control). Lanes were normalized against the average intensity of the control lanes (lane/(average of lanes1,2,3)). Values for each group were analyzed in GraphPad software using a one-way ANOVA with Tukey's multiple comparisons test. All antibodies used for immunoblotting are shown in Supplementary Table S1.

Cancer PathwayFinder Profiler PCR array and Ingenuity Pathway Analysis (IPA)

Pooled tumor RNA from three mice in three separate groupings were reverse transcribed to cDNA using the RT2 First Strand Kit (Qiagen) per manufacturer's instructions. The Cancer PathwayFinder RT2 Profiler PCR Array (Qiagen) was used per manufacturer's instructions with 1 µg of cDNA dispersed per plate. Ct values for the genes were uploaded to the Qiagen GeneGlobe Data Analysis Center and analyzed using the reference genes. The genes with a p-value ≥0.05 in the 3% or 5% GP-treated tumors were validated as described below. The differentially expressed genes were also uploaded into Qiagen's Ingenuity Pathway Analysis (IPA) software for related pathway analysis.

Reverse transcription and quantitative real-time PCR (RT-qPCR) analysis

For reverse transcription of papules from the UVB-mediated photocarcinogenesis study, RNA from three mice were pooled per sample in three separate groupings to represent the biological averages across the cohort. RNA for assay validations was transcribed using random primers and M-MLV reverse transcriptase (Promega, Madison, WI). RT-qPCR was then performed with SYBR Premix Ex Taq II (TaKaRa, Mountain View, CA) and the appropriate primer set. Indicated primer pairs were retrieved from Primer Bank [23] and are outlined in Supplementary Table S2. Relative target mRNA levels were calculated using the ΔΔCT comparative method using *Gapdh* as endogenous controls.

Results and Discussion

Dietary GP decreases epidermal thickening and mast cell counts in a short-term UVB damage study

The exposure of the skin to UVB leads to a cascade of events that may result in carcinogenesis. Previously, we demonstrated the long-term benefits of GP consumption in SKH-1 mice, a well-established model of UVB-mediated skin damage and NMSC [19]. Here, we sought to evaluate the short-term benefits of GP consumption using the same model. In this study using both male and female mice, animals were divided into three groups: 1) No UVB, control diet and no UVB; 2) UVB, control diet with UVB; 3) 5% GP, 5% GP diet with UVB). After two weeks of GP consumption, a dose of 180 mJ/cm^2 UVB was given every other day for a total of 2 weeks, mimicking a vacation in a sunny destination. Skin tissue was collected 24 hours after the last dose, as described in the Materials and Methods section. As previously observed [19], GP supplementation was well tolerated in all mice. The average daily GP consumption in the 5% GP group corresponded to 239.8 ± 11.3 mg and 197.5 ± 4.1 mg for males and females, respectively. These correspond to human equivalent doses of 58.3 and 48.0 g/day, based on a dose translation model [7], or 2.4 and 2.07 servings of grapes.

Previous research has shown that after UVB exposure on the skin, the upregulation of tumor suppressor TP53 forces G1 cell cycle arrest allowing the keratinocytes time to repair and recover from DNA damages or undergo apoptosis [24, 25]. Subsequently, cells enter a hyperproliferative state to thicken the epidermis, protecting against further damages. To determine if this effect was found in our model, we measured the epidermal thickness after seven UVB exposures using H&E stained dorsal skin in all groups. We found a significant decrease in the epidermal thickening of the 5% GP treated group as compared to UVB alone in both sexes, whereas all UVB treated mice had significantly higher thickness than naïve no UVB counterparts (Figure 2A). Following onset of hyperplasia, UVB can induce an inflammatory

response [25]; more specifically, the infiltration of inflammatory mast cells. Mast cells release soluble mediators (i.e. IL-10, TNF-α and VEGF) and are known to participate in tissue remodeling, repair, and wound healing [26, 27]. Although there are endogenous mast cell populations, increases in infiltration have been shown in multiple murine models upon UV radiation [26]. In our model, we observed significant increases in mast cell infiltration in all groups treated with UVB, with trending reductions in the 5% GP group in both sexes from UVB control mice (Figure 2B). Reductions in mast cell infiltration have also been observed after the topical application of grape stem extract in UVB-exposed C57BL mice [28]. Interestingly, the mast cell infiltration in the UVB alone treated group, were significantly higher in the females versus the males, and this effect was not seen in the 5% GP group. This observation supports a previous finding that female SKH-1 mice exhibit higher levels of inflammation compared to males [20]. The proliferative markers PCNA and Ki67 were evaluated by immunohistochemical staining. Upon visual examination, the qualitative pattern of expression in both groups treated with UVB with and without GP appeared to be expanded in basal regions of skin, consistent with the enhanced proliferation observed in UVB treated skin. Treatment with GP did not result in overt changes in the histologic pattern of PCNA and Ki67 expression response to UVB treatment in this study (Figure 2C-D). Yet, as expected, the expanded expression of both markers is consistent with the observed epidermal thickening in these mice. Although major changes were not observable in this analysis, the trends towards reductions in epidermal thickening and mast cells infiltrations provides insight to the short term benefits of GP consumption in protecting against UVB damages.

GP reduced tumorigenesis in long term UVB-treated male SKH-1 mice

Although no registries are available to document the current incidence of NMSC cases in the United States, epidemiological studies have reported that cases of NMSC are significantly higher in men than women [4, 5]. Previously, we demonstrated the long term effects of GP

consumption against UVB-mediated carcinogenesis in female SKH-1 hairless mice [19]. In this study, we sought to determine if GP would also impart chemoprotection on male SKH-1 hairless mice utilizing the same initiation-promotion protocol (180 mJ/cm^2 UVB twice weekly for 28 weeks). We conducted a separate study for male and female SKH-1 mice because of the tendency of males to produce larger tumors and for those tumors to develop earlier in studies compared to females [20]. The study design information for this new study is outlined in Figure 3. Although we provided the same percent GP diet *ad libitum* to the mice, males consume more food per day than females, resulting in a higher equivalent dose of GP per day (160 ± 2.7 mg and 268 ± 6.3 mg for the 3% GP and 5% GP groups, respectively). This would be equivalent to 1.70 or 2.84 servings of grapes per day in humans, as compared to the female study where mice consumed human equivalents of 1.07 and 1.85 servings of grapes, respectively [19].

Over the course of the study, all mice treated with UVB developed tumors. The first small discernable papule (small tumor less than 2 mm in diameter) arose in the UVB control group at week 7, whereas the first papules were observed at weeks 10 and 14 for the 3% GP and 5% GP groups, respectively. Our statistical model of the observed reduction in average tumor burden per mouse, including papules and large tumors, was not significant at 27 weeks, as the average tumor count per mouse was 13.46 ± 1.85 for UVB, 9.58 ± 1.99 for 3% GP, and 12.50 ± 1.9 for 5% GP (Figure 4A). When taking into account the total tumor count at termination, we observed marked reductions of 22% and 16% for the 3% and 5% GP treatments groups, respectively, when compared to UVB-exposed control counterparts (Figure 4B). When papule growth exceeded 2 mm in diameter, a digital caliper was used to measure and track the weekly growth of the tumors. The first large tumor was observed at weeks 8, 11, and 15 for the UVB control, 3% GP, and 5% GP groups, respectively, and by week 24, the large tumor incidence rates were 82%, 50%, and 40% for the groups (Figure 4C). Interestingly, by the end of the study three mice in the 3% GP group did not have measureable large tumors. By week

26, the average tumor volume was reduced in the 3% GP (p=0.001) and 5% GP (p=0.95) and significant in both groups by week 27 (3% GP, 14.26 ± 3.74, p=3.31E-12; 5% GP, 45.51 ± 26.1, p=1.74E-5) versus UVB (104.52 ± 88.2). Utilizing this mixed model of linear regression, we also observed that the 3% GP group tumor volume was significantly lower than the 5% GP group at 27 weeks (Figure 4D, p=0.014), and was not significantly variable from the no UVB group in which no tumors arose (Figure 4D, p=0.484). As we observed many unique tumors, we sought to determine whether GP reduces the capacity of the tumor to convert into a malignant phenotype.

GP reduces the malignant conversion of UVB-mediated tumors in SKH-1 hairless mice

To determine the comparative effects on tumor growth in all mice exposed to chronic UVB, representative lesions of each size were processed for histologic evaluation to classify the lesions. The lesions were scored based on criteria previously described by Benavides et al. [21] with additional criteria added as described in the materials and methods. Papillomas were determined to be premalignant lesions, whereas MiSCCs, fully invasive SCC, SpCCs, and anaplastic tumors were deemed malignant. In addition, we included a class of "Presumed transitional" lesions that exhibited increasingly malignant features that surpassed features of pre-malignant lesions, but failed to unequivocally display the clear invasive growth that defines MiSCC. For maximum stringency, "presumed transitional" lesions were also categorized as malignant MiSCC, because our study is a prevention study, and under-reporting malignancy would bias our results towards observing a favorable effect of our intervention. Images of exemplar lesions in each of the diagnostic categories are shown in Supplementary figure S1. Of the tumors graded, 81% and 74% of the tumors in the 3% and 5% GP diet groups, respectively, were diagnosed as premalignant compared to the 60% of tumors in the UVB control group (Figure 5A), and all mice developed premalignant diagnosable lesions (Table 1). The most prevalent premalignant lesions were G2 papillomas across all groups with an incidence rate of

29.7%, 43.9%, and 28.82% for UVB, 3% GP, and 5% GP, respectively (Figure 5B). In each group, premalignant intermediate tumors, which were lesions classified as premalignant in one blinded assessment and as early malignant in a second independent blind evaluation and ultimately classified as pre-malignant, were observed with similar incidence (Figure 5B). Although all mice developed premalignant lesions, we observed a reduction in the malignant conversion in both GP treatment groups. In total, only 50% and 60% of mice in the 3% GP and 5% GP groups developed malignant lesions versus the 73% of the UVB animals (Table 1). The majority of malignant lesions in both GP treatment groups were MiSCC, 93.3% and 84.6% for 3% GP and 5% GP, respectively, as compared to 73.3% of the UVB counterparts (Figure 5C). However, 17% of the tumors diagnosed in the UVB control group were fully invasive SCC or SpCC, as compared to no SCCs present in either treatment group, although one anaplastic tumor was diagnosed in the 3% GP group and SpCCs were present in the 5% GP group (7.0%) (Figure 5D). These findings suggest that GP consumption slows tumor progression and malignant conversion when compared to UVB control counterparts, consistent with the findings of reduced tumor volume and burden. The increased tumor volume in the UVB control group is consistent with the trend for malignant tumors.

GP consumption did not alter premalignant growth patterns

Although the consumption of GP did not fully inhibit tumor growth, we observed a reduction in the conversion to malignant tumors. To further characterize these lesions, we performed immunostaining for epithelial marker TP63 and proliferation marker Ki67. The SKH-1 hairless mouse model is known for developing SCC lesions that resemble human tumors [21] and in humans, TP63, a transcription factor in the TP53 family, is expressed in the basal proliferative layer within the skin and overexpressed in SCCs [29, 30]. To fully understand the protection imparted by dietary grape it is critical to determine mechanisms effected in early stage tumorigenesis. Although staining was performed on the majority of tumor types, staining

shown in Figure 6 are from representative grade 2 exophytic papillomas diagnosed from H&E staining, selected based on the highest frequency of diagnosis across the majority of groups, with the exception of the 3% GP group having the highest incidence of grade 2 flat papillomas. Our evaluation of low grade tumor served to reduce bias of expression in all groups, as higher grade tumors are not as prevalent in both GP treatment groups. Upon evaluation of TP63 in the tumor tissue of each group, we did not observe qualitative differences in patterns of TP63 protein expression among the groups. Patterns of Ki67 expression, a marker indicative of cell proliferation, were also qualitatively similar among the groups. These observations suggest that GP is not affecting the growth of low-grade tumors as these lesions are still proliferative and morphologically squamous, therefore we must elucidate early stage mechanisms of response evaluating other markers and pathways relevant to tumorigenesis.

GP imparts anti-inflammatory effects in the serum, skin, and low grade tumors of long-term UVB-treated SKH-1 male mice

Tumor-promoting inflammation in NMSC has been implicated as playing a major role in promotion and progression, and later in further angiogenesis and metastasis within the tumor [17, 31]. In a previous study, we employed tandem mass tagging LC-MS/MS to determine downstream targets of GP chemoprevention in a female model of UVB-induced carcinogenesis (Chapter 3a). Our findings suggested GP attenuates the chronic pro-inflammatory tumor environment linked to skin tumor development. However, in a study using the SKH-1 hairless model, Thomas-Ahner et al. demonstrated that not only do male mice develop more histological advanced tumors when compared to females, but the two genders have variable amounts of DNA damage and inflammation [20]. Some studies have demonstrated that UV irradiation increases the mast cell density and, further, mast cells are required for UV-induced immune suppression leading to skin cancer susceptibility [32]. Toluidine blue was used to stain mast cells within the dermis of all mice. Toluidine blue could also stain basophils present in the skin,

but basophils are generally a low abundance leukocyte in the circulatory system, whereas mast cells mature in tissue [33]. Upon quantifying mast cell number in the UVB-exposed dermis, we observed a marked decrease in mast cell infiltration in both GP treatment groups (Figure 7A, p=0.002 and 0.0654, for 3% GP and 5% GP, respectively). As mast cell accumulation in the dermis has been linked to UV radiation, there are currently conflicting opinions on mast cells and skin cancer [27], yet in this data it appears that reduced accumulation is due to an anti-inflammatory effect of GP. As an activator of mast cells, Immunoglobulin E (IgE), known to be upregulated in allergy responses [34], was evaluated based on the observation that all mice treated with UVB appeared to have pruritus, or extensive itching, resulting in scratch and bite wounds throughout the study (data not shown). Interestingly, research has suggested that elevated human IgE levels may be indicative of increased susceptibility to subsequent SCC lesions [35]. Although we cannot predict the extent to which serum IgE might activate mast cell infiltration, we observed significant decreases of IgE in both GP treatment groups (Figure 7B, p=0.0001 and 0.0017, for 3% GP and 5% GP, respectively). Additionally, we utilized the serum to profile cytokines potentially linked to the chemopreventive response using the Cytokine & Chemokine 36-Plex Mouse ProcartaPlex™ Panel 1A using magnetic beads on a Luminex platform. Although it can be difficult to detect minute changes in cytokine response using this platform, we detected slight changes in Eotaxin (CCL-11) expression with the serum, and therefore sought to evaluate expression within small papules using RT-qPCR analysis (Figure 7C). Overall, the observable reduction of *Eotaxin* in the papule tissue and the reduction in mast cells as seen through toluidine blue staining suggests that an anti-inflammatory response could occur through reduced expression of pro-inflammatory IL-4 and therefore reduced *Eotaxin* [36], although further validation would need to occur.

Taken together with the observation of modulated mast cell, IgE, and cytokines responses, we sought to determine if GP acts on inflammatory mediators in male mice that

otherwise are linked to advancing tumorigenesis. To elucidate early targets, protein lysates of papules were subjected using immunoblot analysis. Many studies assessing the chemopreventive nature of individual compounds found in grapes (such as resveratrol) or whole food agent (grapes, pomegranate, etc.) have revealed their regulatory effects over molecules in the MAPK signaling pathway, which can be responsible for transcription and control of cellular proliferation, differentiation, and apoptosis [37-40]. Additionally, in our previous proteomics study evaluating the anti-tumorigenic effect of dietary grape in female SKH-1 tumors, we found that acute phase response (APR) signaling was abated with the consumption of grape. Upon evaluation of upstream regulators of APR in the female mice, including ERK1/2 and NF-κB, we determined the anti-inflammatory effects of GP were associated with the modulation in these pathways leading to inhibition of tumor growth (Chapter 3a). Here, we performed immunoblotting on phosphorylated and total ERK1/2, p38, and STAT3 to elucidate if GP reduced inflammatory signaling within the MAPK signaling pathway in male SKH-1 hairless mouse UVB-mediated tumorigenesis. Our data show that UVB-mediated phosphorylation of p38, but not ERK1/2, was prevented by GP consumption in low grade papules (Figure 8). It had been noted that p38 plays a role in controlling cell proliferation in head and neck SCC and activation is more prominent in less differentiated tumors associated with poor prognosis, whereas the accumulation of activated ERK1/2 was not as prominent [41]. Therefore, we suspect dietary GP acts upon p38 signaling to reduce proliferation and growth of the tumor. Another inflammatory molecule is STAT3, which is a direct upstream regulator of APR response, and whose expression can be upregulated in the presence of cytokines, such as IL-6, IFN-γ, TNF-α, and G-CSF [42]. Upon immunoblot analysis, we observed similar activation of STAT3 across all samples, with a significant increase in the 5% GP group ($p < 0.0001$), Although significant, this increase was not as pronounced as p38. As accumulated p38 expression is linked to increased cellular proliferation, we also evaluated gene expression of proliferative markers *Pcna* and *Ki67* via RT-qPCR using cDNA from papules. In both markers,

we observed marked reduction in both GP treatments groups (Figure 8C-D). We also observed a marked reduction of pro-survival marker *Bcl-2* in the papules (Figure 8E). Collectively, we believe that anti-inflammatory capacity of dietary GP on early stage, low-grade papules inhibits p38 MAPK, and therefore acts as an upstream regulator to prevent proliferation and induce apoptosis of tumor cells.

Dietary grape significantly altered multiple cancer pathways and gene-gene interactions

To obtain further insight into the early stage anti-tumor action of GP, a PCR array profiling the expression of 84 key genes related to transformation and tumorigenesis was performed utilizing cDNA from papules in each group. A heat map was generated showing that GP modulates several important genes related to angiogenesis, apoptosis, cell cycle, cellular senescence, DNA damage repair, epithelial-to-mesenchymal transition (EMT), hypoxia signaling, metabolism and telomere maintenance (Figure 9A). Our results demonstrated the modulation of several key genes from all these pathways. Interestingly, most of the genes in 3% and 5% GP show the fold change in the same direction albeit at different levels for cellular senescence, DNA damage repair, and telomere maintenance. However, the genes involved in other pathways show dose-dependent differential expression for 3% GP and 5% GP. Data for validation were selected if a statistically significant change ($p < 0.05$) was noticed in 3% and/or 5% GP, with the same trend in both the GP treatment groups (13 genes). Additionally, *Adm* was selected to be validated due to a greater than 2 fold change regulation being observed in both 3% and 5% GP groups compared to control group, although it was not statistically significant. Overall, 14 key genes appeared to be modulated. Therefore, expression was validated using RT-qPCR analysis of cDNA created from papules (Figure 9B). Validated genes with significant expression changes are described below.

Of the 14 genes validated, we observed significant modulation in six genes involved in Hypoxia signaling (*Hmox1* and *Ldha*), DNA damage and repair (*Ercc3*), and telomeres and

telemerase (*Terf2ip*, *Tinf*, *and Tnks2*). The transcription of Heme oxygenase (decycling) 1 (*Hmox1*, also known as HO-1) occurs through the activation of the NRF2 antioxidant response pathway. *Hmox1* is therefore responsible for protection against oxidative stress and upregulates anti-inflammatory cytokines Il-10 and IL-1Ra [43, 44]. We believe that dietary grape may act to conserve the transcription of *Hmox1* as shown by upregulation, because mutations in this gene have become apparent in age-related diseases including cancer [45]. Lactate dehydrogenase A (*Ldha*) is activated via phosphorylation by kinases HER2 and SRC. Upregulation contributes to an increased resistance of anoikis, or cellular death from detachment to the surrounding extracellular matrix, and further promotes the invasion of metastatic cancer cells [46]. The significant decrease in 5% GP and a marked decrease in 3% GP groups could relate to the reduction of malignant conversion in the observed tumors as described above.

In our previous study, we demonstrated that dietary GP reduced the presence of CPDs, therefore suggesting an enhanced capacity of the NER pathway to effectively repair these DNA damages [19]. Excision repair cross-complementing rodent repair deficiency, complementation group 3 and 5 (*Ercc3* and *Ercc5*) are molecules required for nucleotide excision repair (NER) to effectively repair DNA damages. Although we observed no change in *Ercc5* upon validation, the downregulation in *Ercc3* suggest that dietary GP protects the skin from the accumulation of DNA damage in the male SKH-1 male mouse skin. Another possibility is that mutations of *Ercc3* would render the 3’-5’ helicase subunit of TFIIH, a transcription factor, ineffective, so NER and gene transcription would not be able to occur. Observing mutations of this gene would indicate that the cells in question would either be unable to replicate, which would stop any proliferation, but also unable to repair other mutations, potentially leading to NMSC tumorigenesis [25, 47, 48].

Although there appears to be heterogeneity in NMSC and telomere length, there have been links to telomere length being positively correlated to nevus number and melanoma risk

[49]. We were interested to see that three genes involved in telomere management were significantly downregulated in our data: telomeric repeat binding factor 2, interacting protein (*Terf2ip*), Terf1 (TRF1)-interacting nuclear factor 2 (*Tinf2*), and Tankyrase, TRF1-interacting ankyrin-related ADP-ribose polymerase 2 (*Tnks2*). TINF2 and TNKS2 are both part of the shelterin complex which is necessary for telomere function, including protection from degradation, abnormal recombination, inappropriate processing by DNA repair mechanisms, and chromosome capping to regulate telomerase activity [50]. Interestingly, increased expression of TNKS2 is observed in multiple different types of cancers, such as breast, ovarian, gastric, fibrosarcoma, and pancreatic adenocarcinoma [51] and observing mutations of TERF2IP would indicate higher risks of cancer [52]. Telomere length has also been correlated to positive expression of TERF2 in inflamed tissues, and tissues susceptible to dysregulation [50], and TERF2 has been suggested as a target for cancer therapy [53]. Overall, these reductions in telomere proteins suggest that dietary GP suppresses the protection of the telomere ends leading to genomic instability, therefore allowing damaged cells to undergo cell death and/or senescence. Contrary to expectations, we observed a greater than 2 fold increase in adrenomedullin (*Adm*) in both GP treatments, though not statistically significant. ADM is known to regulate proliferation, differentiation, migration, growth, apoptosis, angiogenesis, and its expression has shown to be associated with the development of several tumor types, such as colorectal, nasopharyngeal, hepatocellular, and renal [54]. Therefore, the possibility of ADM also being related to the development of NMSCs still needs to be explored. During cancer development and progression, gene mutations or expression deregulation related to these key pathways can allow cells to grow and divide unchecked. In our study, GP supplementation appears to regain control of these pathways, specifically relative to telomere regulation, hypoxia, and DNA damage repair.

Next, we uploaded the GP-altered genes identified in the cancer PCR array into Ingenuity Pathway Analysis software (IPA) and identified cumulative actions of GP-altered genes to understand the GP-mediated chemoprotective response against UVB-mediated skin carcinogenesis. This analysis identified links to increased cellular homeostasis and apoptosis, as well as decreased cell migration, viability, and proliferation in tumors, which all support the chemoprotective response of GP (Figure 10A-B). Additionally, IPA was used to understand the upstream regulators of GP-altered genes, which indicate possible inhibition of hydrogen peroxide, PI3K, STAT3, IGF1, IL1A&B, RELA, and activation of tumor suppressor TP53 (Figure 10C). A network pathway of interacting genes was also generated, which further shows suggestive links to other genes (NF-κB, PI3K, P38 MAPK, ERK1/2, AMPK, CD3, and histone H3 and H4) (Figure 10D), supporting the anti-tumor properties of dietary grape.

Conclusion

As the leading diagnosed neoplasm in the United States, NMSC are a burden and have increased likelihood of multiple diagnoses. It is crucial to find additional preventative measures to avoid damages caused by UVR, the leading cause of NMSC. As the chemoprevention field expands, more studies are describe the beneficial effects of modifying dietary habits to prevent disease. In this set of *in vivo* studies, we demonstrated that consumption of dietary grape powder aids in the reduction of UVB-mediated cutaneous damage and skin carcinogenesis in SKH-1 hairless mice. We believe that antioxidant-rich dietary grape powder impairs early oxidative injury, therefore leading to downstream anti-inflammatory effects and modulations to other pathways dysregulated in NMSC, resulting in a reduction in tumor growth and malignant conversion. As many differences are noted between males and females in the development of NMSC, this study complements our previous work demonstrating reduced tumorigenesis in female SKH-1 mice [19]. Although further investigation is required to validate these findings, this

study suggests that dietary grape powder may serve as a suitable supplement in preventing NMSC in high risk patients.

Acknowledgements

This work was partially supported by funding from the California Table Grape Commission, as well as the National Institutes for Health (grant numbers R01AR059130 and R01CA176748 to NA), and the Department of Veterans Affairs (VA Merit Review Awards I01CX001441 and I01BX004221; and a Research Career Scientist Award IK6BX003780 to NA). We also acknowledge the core facilities supported by the Skin Diseases Research Center (SDRC) Core Grant P30AR066524 from NIH/NIAMS. The author(s) thank the University of Wisconsin Translational Research Initiatives in Pathology (TRIP) laboratory and the Biostatistics Shared Resource, supported by the UW Department of Pathology and Laboratory Medicine, UWCCC (P30 CA014520) and the Office of The Director- NIH (S10OD023526) for use of its facilities and services.

References

1 Rogers HW, Weinstock MA, Feldman SR, Coldiron BM: Incidence Estimate of Nonmelanoma Skin Cancer (Keratinocyte Carcinomas) in the U.S. Population, 2012. JAMA Dermatol 2015;151:1081-1086.

2 Apalla Z, Lallas A, Sotiriou E, Lazaridou E, Ioannides D: Epidemiological trends in skin cancer. Dermatol Pract Concept 2017;7:1-6.

3 Chren MM, Torres JS, Stuart SE, Bertenthal D, Labrador RJ, Boscardin WJ: Recurrence after treatment of nonmelanoma skin cancer: a prospective cohort study. Arch Dermatol 2011;147:540-546.

4 Armstrong BK, Kricker A: The epidemiology of UV induced skin cancer. J Photochem Photobiol B 2001;63:8-18.

5 Foote JA, Harris RB, Giuliano AR, Roe DJ, Moon TE, Cartmel B, Alberts DS: Predictors for cutaneous basal- and squamous-cell carcinoma among actinically damaged adults. International journal of cancer 2001;95:7-11.

6 Guy GP, Jr., Machlin SR, Ekwueme DU, Yabroff KR: Prevalence and costs of skin cancer treatment in the U.S., 2002-2006 and 2007-2011. Am J Prev Med 2015;48:183-187.

7 Reagan-Shaw S, Nihal M, Ahmad N: Dose translation from animal to human studies revisited. FASEB Journal 2008;22:659-661.

8 Afaq F, Adhami VM, Ahmad N: Prevention of short-term ultraviolet B radiation-mediated damages by resveratrol in SKH-1 hairless mice. Toxicology and applied pharmacology 2003;186:28-37.

9 Finkel T: Signal transduction by reactive oxygen species. J Cell Biol 2011;194:7-15.

10 Ichihashi M, Ueda M, Budiyanto A, Bito T, Oka M, Fukunaga M, Tsuru K, Horikawa T: UV-induced skin damage. Toxicology 2003;189:21-39.

11 Taguchi M, Watanabe S, Yashima K, Murakami Y, Sekiya T, Ikedat S: Aberrations of the Tumor Suppressor p53 Gene and p53 Protein in Solar Keratosis in Human Skin. Journal of Investigative Dermatology 1994;103:500-503.

12 Melnikova VO, Pacifico A, Chimenti S, Peris K, Ananthaswamy HN: Fate of UVB-induced p53 mutations in SKH-hr1 mouse skin after discontinuation of irradiation: relationship to skin cancer development. Oncogene 2005;24:7055-7063.

13 Agar NS, Halliday GM, Barnetson RS, Ananthaswamy HN, Wheeler M, Jones AM: The basal layer in human squamous tumors harbors more UVA than UVB fingerprint mutations: A role for UVA in human skin carcinogenesis. Proceedings of the National Academy of Sciences of the United States of America 2004;101:4954-4959.

14 Wan YS, Wang ZQ, Shao Y, Voorhees JJ, Fisher GJ: Ultraviolet irradiation activates PI 3-kinase/AKT survival pathway via EGF receptors in human skin in vivo. International Journal of Oncology 2001;18:461-466.

15 Chen W, Tang Q, Gonzales MS, Bowden GT: Role of p38 MAP kinases and ERK in mediating ultraviolet-B induced cyclooxygenase-2 gene expression in human keratinocytes. Oncogene 2001;20:3921.

16 Kabuyama Y, Hamaya M, Homma Y: Wavelength specific activation of PI 3-kinase by UVB irradiation. FEBS Letters 1998;441:297-301.

17 Maru GB, Gandhi K, Ramchandani A, Kumar G: The role of inflammation in skin cancer. Advances in experimental medicine and biology 2014;816:437-469.

18 Ulrich C, Jurgensen JS, Degen A, Hackethal M, Ulrich M, Patel MJ, Eberle J, Terhorst D, Sterry W, Stockfleth E: Prevention of non-melanoma skin cancer in organ transplant patients by regular use of a sunscreen: a 24 months, prospective, case-control study. Br J Dermatol 2009;161 Suppl 3:78-84.

19 Singh CK, Mintie CA, Ndiaye MA, Chhabra G, Dakup PP, Ye T, Yu M, Ahmad N: Chemoprotective Effects of Dietary Grape Powder on UVB Radiation-Mediated Skin Carcinogenesis in SKH-1 Hairless Mice. J Invest Dermatol 2019;139:552-561.

20 Thomas-Ahner JM, Wulff BC, Tober KL, Kusewitt DF, Riggenbach JA, Oberyszyn TM: Gender differences in UVB-induced skin carcinogenesis, inflammation, and DNA damage. Cancer Res 2007;67:3468-3474.

21 Benavides F, Oberyszyn TM, VanBuskirk AM, Reeve VE, Kusewitt DF: The hairless mouse in skin research. Journal of dermatological science 2009;53:10-18.

22 Voigt AY, Michaud M, Tsai KY, Oh J, Sundberg JP: Differential hairless mouse strain-specific susceptibility to skin cancer and sunburn. J Invest Dermatol 2019

23 Wang X, Seed B: A PCR primer bank for quantitative gene expression analysis. Nucleic Acids Res 2003;31:e154.

24 Benjamin CL, Ullrich SE, Kripke ML, Ananthaswamy HN: p53 tumor suppressor gene: a critical molecular target for UV induction and prevention of skin cancer. Photochem Photobiol 2008;84:55-62.

25 D'Orazio J, Jarrett S, Amaro-Ortiz A, Scott T: UV radiation and the skin. International journal of molecular sciences 2013;14:12222-12248.

26 Siiskonen H, Smorodchenko A, Krause K, Maurer M: Ultraviolet radiation and skin mast cells: Effects, mechanisms and relevance for skin diseases. Exp Dermatol 2018;27:3-8.

27 Varricchi G, Galdiero MR, Marone G, Granata F, Borriello F, Marone G: Controversial role of mast cells in skin cancers. Exp Dermatol 2017;26:11-17.

28 Che DN, Xie GH, Cho BO, Shin JY, Kang HJ, Jang SI: Protective effects of grape stem extract against UVB-induced damage in C57BL mice skin. Journal of Photochemistry and Photobiology B: Biology 2017;173:551-559.

29 Missero C, Antonini D: p63 in Squamous Cell Carcinoma of the Skin: More Than a Stem Cell/Progenitor Marker. Journal of Investigative Dermatology 2017;137:280-281.

30 Keyes WM, Pecoraro M, Aranda V, Vernersson-Lindahl E, Li W, Vogel H, Guo X, Garcia EL, Michurina TV, Enikolopov G, Muthuswamy SK, Mills AA: ΔNp63α Is an Oncogene that Targets Chromatin Remodeler Lsh to Drive Skin Stem Cell Proliferation and Tumorigenesis. Cell Stem Cell 2011;8:164-176.

31 Hanahan D, Weinberg RA: Hallmarks of cancer: the next generation. Cell 2011;144:646-674.

32 Sarchio SNE, Kok L-F, O'Sullivan C, Halliday GM, Byrne SN: Dermal mast cells affect the development of sunlight-induced skin tumours. Experimental Dermatology 2012;21:241-248.

33 Falcone FH, Haas H, Gibbs BF: The human basophil: a new appreciation of its role in immune responses. Blood 2000;96:4028-4038.

34 Stone KD, Prussin C, Metcalfe DD: IgE, mast cells, basophils, and eosinophils. The Journal of allergy and clinical immunology 2010;125:S73-S80.

35 Wiemels JL, Wiencke JK, Li Z, Ramos C, Nelson HH, Karagas MR: Risk of squamous cell carcinoma of the skin in relation to IgE: a nested case-control study. Cancer epidemiology, biomarkers & prevention : a publication of the American Association for Cancer Research, cosponsored by the American Society of Preventive Oncology 2011;20:2377-2383.

36 Otsuka A, Nonomura Y, Kabashima K: Roles of basophils and mast cells in cutaneous inflammation. Semin Immunopathol 2016;38:563-570.

37 Singh CK, Siddiqui IA, El-Abd S, Mukhtar H, Ahmad N: Combination chemoprevention with grape antioxidants. Mol Nutr Food Res 2016;60:1406-1415.

38 Afaq F, Saleem M, Krueger CG, Reed JD, Mukhtar H: Anthocyanin- and hydrolyzable tannin-rich pomegranate fruit extract modulates MAPK and NF-κB pathways and inhibits skin tumorigenesis in CD-1 mice. International journal of cancer 2005;113:423-433.

39 Divya SP, Wang X, Pratheeshkumar P, Son YO, Roy RV, Kim D, Dai J, Hitron JA, Wang L, Asha P, Shi X, Zhang Z: Blackberry extract inhibits UVB-induced oxidative damage and inflammation through MAP kinases and NF-kappaB signaling pathways in SKH-1 mice skin. Toxicol Appl Pharmacol 2015;284:92-99.

40 Khan N, Syed DN, Pal HC, Mukhtar H, Afaq F: Pomegranate fruit extract inhibits UVB-induced inflammation and proliferation by modulating NF-kappaB and MAPK signaling pathways in mouse skin. Photochem Photobiol 2012;88:1126-1134.

41 Leelahavanichkul K, Amornphimoltham P, Molinolo AA, Basile JR, Koontongkaew S, Gutkind JS: A role for p38 MAPK in head and neck cancer cell growth and tumor-induced angiogenesis and lymphangiogenesis. Molecular oncology 2014;8:105-118.

42 Siveen KS, Sikka S, Surana R, Dai X, Zhang J, Kumar AP, Tan BKH, Sethi G, Bishayee A: Targeting the STAT3 signaling pathway in cancer: Role of synthetic and natural inhibitors. Biochimica et Biophysica Acta (BBA) - Reviews on Cancer 2014;1845:136-154.

43 Piantadosi CA, Withers CM, Bartz RR, MacGarvey NC, Fu P, Sweeney TE, Welty-Wolf KE, Suliman HB: Heme oxygenase-1 couples activation of mitochondrial biogenesis to anti-inflammatory cytokine expression. The Journal of biological chemistry 2011;286:16374-16385.

44 Zhao P, Alam MB, Lee SH: Protection of UVB-Induced Photoaging by Fuzhuan-Brick Tea Aqueous Extract via MAPKs/Nrf2-Mediated Down-Regulation of MMP-1. Nutrients 2018;11

45 Loboda A, Damulewicz M, Pyza E, Jozkowicz A, Dulak J: Role of Nrf2/HO-1 system in development, oxidative stress response and diseases: an evolutionarily conserved mechanism. Cellular and molecular life sciences : CMLS 2016;73:3221-3247.

46 Jin L, Chun J, Pan C, Alesi GN, Li D, Magliocca KR, Kang Y, Chen ZG, Shin DM, Khuri FR, Fan J, Kang S: Phosphorylation-mediated activation of LDHA promotes cancer cell invasion and tumour metastasis. Oncogene 2017;36:3797-3806.

47 Ruczinski I, Jorgensen TJ, Shugart YY, Schaad YB, Kessing B, Hoffman-Bolton J, Helzlsouer KJ, Kao WH, Wheless L, Francis L, Alani RM, Strickland PT, Smith MW, Alberg AJ: A population-based study of DNA repair gene variants in relation to non-melanoma skin cancer as a marker of a cancer-prone phenotype. Carcinogenesis 2012;33:1692-1698.

48 Song J, Kemp MG, Choi JH: Detection of the Excised, Damage-containing Oligonucleotide Products of Nucleotide Excision Repair in Human Cells. Photochem Photobiol 2017;93:192-198.

49 Caini S, Raimondi S, Johansson H, De Giorgi V, Zanna I, Palli D, Gandini S: Telomere length and the risk of cutaneous melanoma and non-melanoma skin cancer: a review of the literature and meta-analysis. Journal of dermatological science 2015;80:168-174.

50 Poojary SS, Mishra G, Singh TD, Gupta S, Shrivastav BR, Tiwari PK: Telomere length variation and expression analysis of shelterin complex genes during gallbladder carcinogenesis. J Cancer Res Ther 2017;13:235-239.

51 Xu W, Lau YH, Fischer G, Tan YS, Chattopadhyay A, de la Roche M, Hyvonen M, Verma C, Spring DR, Itzhaki LS: Macrocyclized Extended Peptides: Inhibiting the Substrate-Recognition Domain of Tankyrase. Journal of the American Chemical Society 2017;139:2245-2256.

52 Aoude LG, Pritchard AL, Robles-Espinoza CD, Wadt K, Harland M, Choi J, Gartside M, Quesada V, Johansson P, Palmer JM, Ramsay AJ, Zhang X, Jones K, Symmons J, Holland EA, Schmid H, Bonazzi V, Woods S, Dutton-Regester K, Stark MS, Snowden H, van Doorn R, Montgomery GW, Martin NG, Keane TM, Lopez-Otin C, Gerdes AM, Olsson H, Ingvar C, Borg A, Gruis NA, Trent JM, Jonsson G, Bishop DT, Mann GJ, Newton-Bishop JA, Brown KM, Adams DJ, Hayward NK: Nonsense mutations in the shelterin complex genes ACD and TERF2IP in familial melanoma. Journal of the National Cancer Institute 2015;107

53 Fadri-Moskwik M, Zhou Q, Chai W: Beyond Telomerase: Telomere Instability as a Novel Target for Cancer Therapy. J Mol Genet Med 2013;7

54 Maia LL, Peterle GT, Dos Santos M, Trivilin LO, Mendes SO, de Oliveira MM, Dos Santos JG, Stur E, Agostini LP, Couto C, Dalbo J, de Assis A, Archanjo AB, Mercante A, Lopez RVM, Nunes FD, de Carvalho MB, Tajara EH, Louro ID, Alvares-da-Silva AM: JMJD1A, H3K9me1, H3K9me2 and ADM expression as prognostic markers in oral and oropharyngeal squamous cell carcinoma. PloS one 2018;13:e0194884.

Figure Legends

Figure 1. Timeline of short term UVB-mediated cutaneous damage study.

Mice were acclimated for seven days prior to receiving respective diets. UVB treatments (180 mJ/cm^2) were started two weeks after initial administration of the diet and performed every other day totaling seven doses, as indicated by short arrows.

Figure 2. The inhibitory effect of GP consumption on UVB-mediated cutaneous hyperplasia and mast cell infiltrations in SKH-1 hairless mice.

Male and female SKH-1 mice were divided into groups of 5 each as follows: 1) No UVB with control diet, 2) UVB with control diet, 3) UVB with 5% GP diet. Diet was provided for 14 days prior to the first dose of UVB. Mice treated with UVB received a dose of 180 mJ/cm^2 every other day up to a total of seven treatments. Twenty-four hours after the seventh dose of UVB, animals were sacrificed and skin sections processed for histology. (**A**) GP consumption significantly reduced epidermal thickness as determined by measuring epidermal thickness from the base of the stratum basale to the base of the stratum corneum on H&E stained tissue sections. (**B**) Mast cell infiltration shown by toluidine blue staining. At least five images were taken at 10x magnification across five different skin sections of each mouse. Mast cells (violet metachromatic cytoplasmic granules) were counted using ImageJ, then averaged per mouse. Expression of proliferative markers PCNA (**C**), and Ki67 (**D**) were assessed using immunohistochemical staining techniques. Representative sections are shown. All images are represented at 10x magnification with a 40x inset. The data represents the mean ± SEM of all five animals per groups. A two-way ANOVA with Tukey's multiple comparison test was performed (*$p < 0.05$, **$p < 0.01$, ****$p < 0.0001$).

Figure 3. Timeline of chronic UVB-mediated carcinogenesis study.

After a 1-week acclimation period, male SKH-1 mice were administered the appropriate diet for their group, and treated 2 times per week with 180 mJ/cm^2 UVB. After 28 weeks, mice were euthanized and tissues were collected.

Figure 4. Effect of GP consumption on UVB-mediated carcinogenesis in male mice.

(**A**) Average number of total tumors per mouse per group. (**B**) Additive large (> 2mm diameter, grey) and small (< 2 mm diameter, black) tumor count at termination of the experiment. (**C**) Large tumor latency shown as the percentage of mice without measureable tumors greater than 2 mm in diameter. (**D**) Average tumor volume of measurable tumor per group. All data are presented as mean ± SEM.

Figure 5. Histological evaluation of tumors in male mice.

After 27 weeks of UVB exposure, representative tumors from each UVB-exposed mouse were prepared for histology as described in the materials and methods. Representative H&E stained tumors from each group were graded in a blinded manner by a board-certified veterinary pathologist. All data columns are represented as the percentage of total tumors diagnosed per group. (**A**) Tumor diagnoses fell into two categories of premalignant (black) or malignant (grey) tumors. (**B**) Premalignant tumors were papillomas diagnosed based on grade and growth pattern. Grading was assigned based on the pattern of growth and degree of atypia (G1 to G3, minimal-moderate-marked). Papillary growth patterns relative to the dermis were as follows, outward (exophytic), flat, and inward (endophytic). Premalignant intermediate lesions were also observed. (**C**) Malignant microinvasive squamous cell carcinomas (MiSCC) identified based on the presence of stromal invasion and categorized based their depth of extension into the dermis and subcutis. Invasion extent was also scored based on the amount of invasive extension into surrounding stroma (I2 to I3, mild-moderate). Presumed transitional lesions exhibited increasingly malignant features that surpassed features of pre-malignant lesions but failed to

unequivocally display the clear invasive growth that defines microinvasive squamous cell carcinomas (miSCC) and were included among the malignant lesions for stringency of analysis. (**D**) Fully invasive tumor diagnosis. Squamous cell carcinomas (SCC) diagnosed upon invasion into the panniculus carnosus. Spindle cell carcinomas (SpCC) and one anaplastic tumor diagnosed based on their morphology, rather than the depth of invasion.

Figure 6. Histological analysis of exophytic papillomas with a G2 atypia score from the UVB treated groups.

Staining includes hematoxylin and Eosin (H&E), epithelial marker TP63, and proliferative marker Ki67. Images were obtained at 4x and inset are 20x.

Figure 7. Effect of chronic UVB exposure on dermal mast cell presence, and serum IgE and *Eotaxin* expression after GP consumption.

After 27 weeks of twice weekly UVB exposures, the skin and serum of male SKH-1 hairless mice were collected as described in the materials and methods section. (**A**) Mast cells were identified by toluidine blue staining in the dermal region of the dorsal skin of the No UVB groups and the involved skin directly adjacent to tumors of all groups treated with UVB. Images are 10x with a 40x inset to show mast cell appearance. Mast cell number was quantified from five 20x images per animal using ImageJ and averaged. The data represents the mean ± SEM of all animals per group. A one-way ANOVA with Tukey's multiple comparison test was used (**$p < 0.01$, ****$p < 0.0001$). (**B**) Total serum IgE concentration was determined by ELISA. (**C**) RT-qPCR validation of *Eotaxin* expression in papules. Data is presented by the mean ± SEM of three biological pools of three animals per group (n=9) in technical triplicate. A one-way ANOVA with Tukey's multiple comparison test was performed (**$p < 0.01$, *** $p < 0.001$, ****$p < 0.0001$).

Figure 8. Evaluation of inflammatory, proliferative, and survival markers linked to NMSC progression.

Immunoblot analysis of (**A**) MAPK proteins p38 and ERK1/2, and (**B**) downstream STAT3. VINCULIN was used as a loading control. (**C-E**) RT-qPCR analysis of proliferative markers (**C**) *Pcna* and (**D**) *Ki67*, Pro-survival marker (**E**) *Bcl-2*. Statistical analysis was performed on the p/t ratio using a one-way AVOVA with Tukey's multiple comparisons. p/t indicates the ratio of phosphorylated/total protein.

Figure 9. GP modulates the expression of multiple genes involved in various pathways of cancer.

After termination, a subset of representative tumors were flash frozen, stored, then RNA isolation and reverse transcription was performed as stated in the materials and methods. The expression profiles of 84 genes involved in nine different cancer pathways were evaluated in the Cancer PathwayFinder PCR array in UVB, 3% GP, and 5% GP tumors. (**A**) Heat maps of the variations in the expression of the genes are represented as the fold change (GP treatment/UVB). cDNA was prepared as a pool of three mice and the assay was performed using biological triplicate within each group. Upregulated genes appear red in color and downregulated genes are green. (*) indicates a p-value < 0.05. (**B**) Validation of gene expression was confirmed by quantitative real-time reverse transcriptase–PCR across the control, 3% GP, and 5% GP groups. P-value less than 0.05 calculated based on a Student's t-test of the replicate 2^(- Delta CT) values for each gene in the control group and treatment groups.

Figure 10. Functional analysis of the GP-mediated chemoprotective response against UVB-mediated skin carcinogenesis.

Differentially expressed genes from the Cancer PathwayFinder PCR array with $p < 0.05$ were placed in Ingenuity Pathway Analysis (IPA) software. Functional analysis were generated showing (**A**) increases in cellular homeostasis, apoptosis, and cell death of tumor cell lines, as

well as (**B**) decreasing migration, cell viability, and cell proliferation in tumor cell lines. (**C-D**) IPA gene upstream regulator analysis is used to identify the genes responsible for expression changes in the analysis. Genes from the profiler array are in red (upregulated) and green (downregulated), while predicted functions and upstream regulator genes and interaction lines are in orange (activation) and blue (inhibition). Gene is white and lines in yellow indicate findings inconsistent with the state of downstream molecules. Solid lines indicate robust interactions, whereas dashed lines are significant but less frequent.

Figures

Figure 1

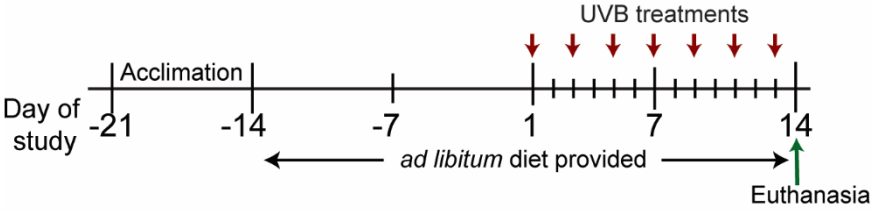

Group	AIN-76A diet	Human equivalent	No. mice
No UVB	No grape powder	0 servings	5M 5F
UVB	No grape powder	0 servings	5M 5F
5% GP	5% grape powder	2.1-2.4 servings	5M 5F

Figure 2

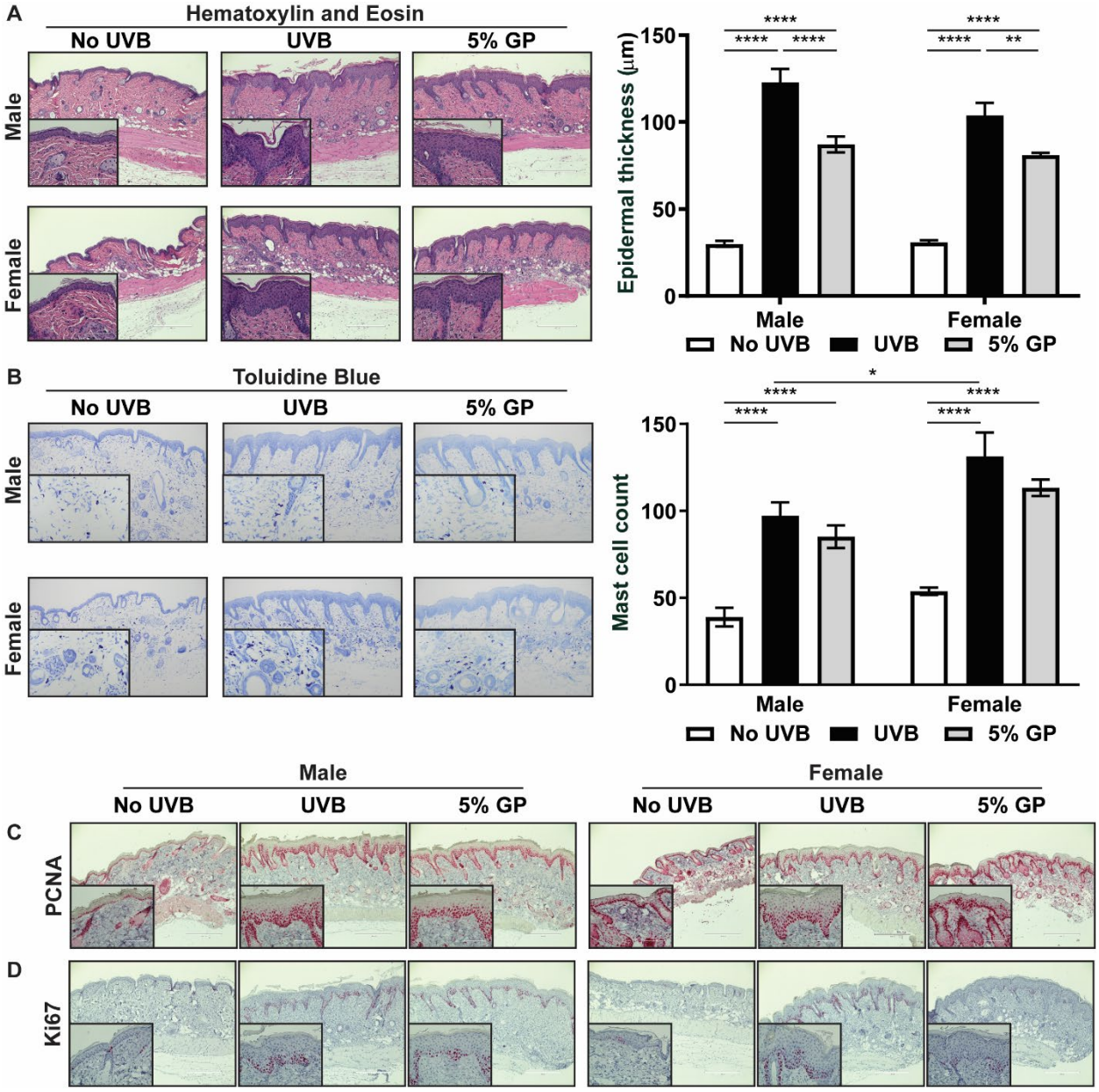
A
Hematoxylin and Eosin
No UVB
UVB
5% GP
Male
Female
Epidermal thickness (μm)
150
100
50
0
****
****
****
****
****
**
Male
Female
No UVB
UVB
5% GP
B
Toluidine Blue
No UVB
UVB
5% GP
Male
Female
Mast cell count
150
100
50
0
*
****
****
****
****
Male
Female
No UVB
UVB
5% GP
C
PCNA
D
Ki67
Male
Female
No UVB
UVB
5% GP

Figure 3

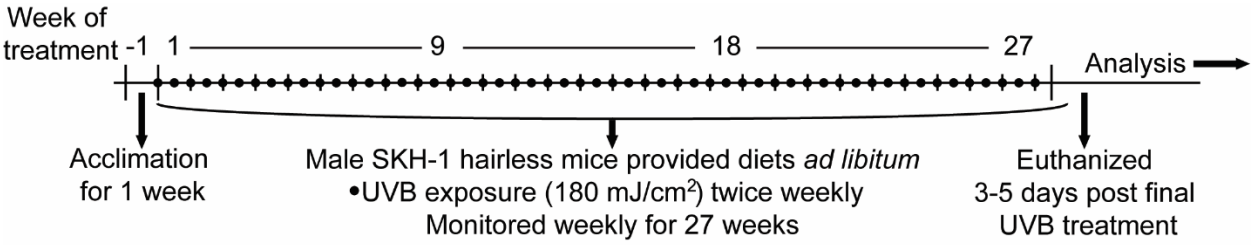

Group	AIN-76A diet	Human equivalent	No. mice
No UVB	No grape powder	0 servings	12
UVB	No grape powder	0 servings	12
3% GP	3% grape powder	1.7 servings	12
5% GP	5% grape powder	2.8 servings	12

All diets matched to the natural sugar content of 5% feed

Figure 4

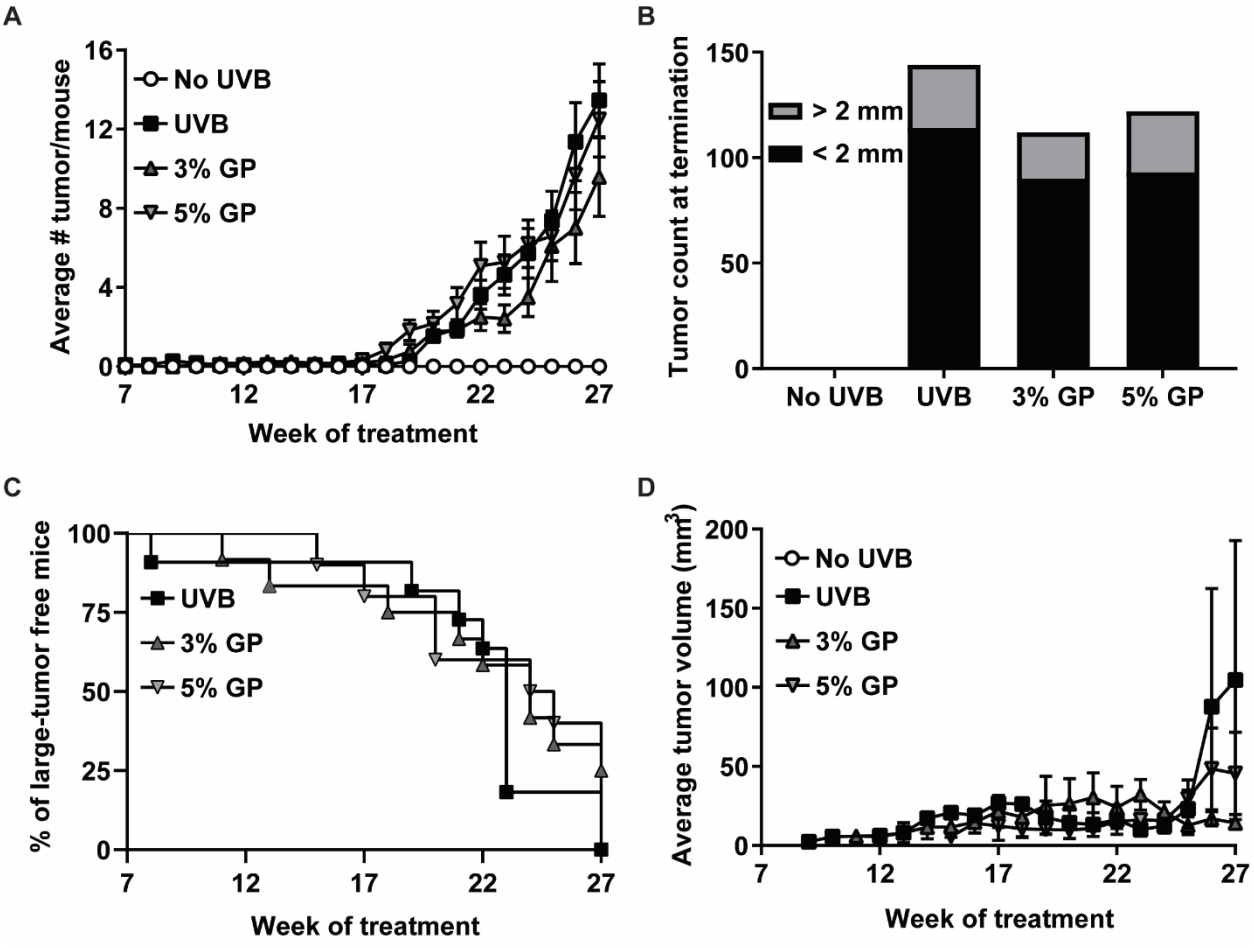
A
Average # tumor/mouse
No UVB
UVB
3% GP
5% GP
Week of treatment
B
Tumor count at termination
> 2 mm
< 2 mm
No UVB
UVB
3% GP
5% GP
C
% of large-tumor free mice
UVB
3% GP
5% GP
Week of treatment
D
Average tumor volume (mm3)
No UVB
UVB
3% GP
5% GP
Week of treatment

Figure 5

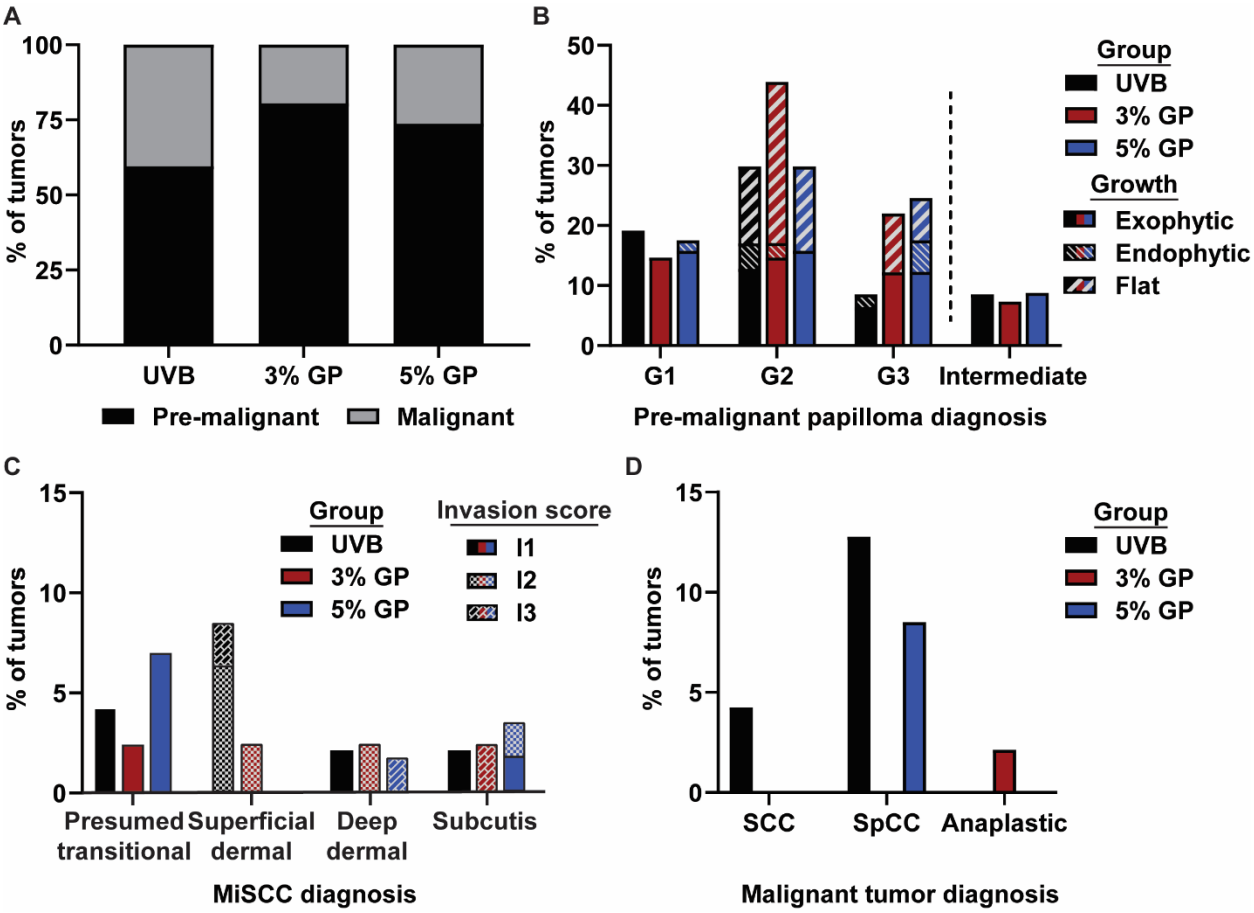
A
100
75
50
25
0
% of tumors
UVB
3% GP
5% GP
Pre-malignant
Malignant
B
50
40
30
20
10
0
% of tumors
G1
G2
G3
Intermediate
Pre-malignant papilloma diagnosis
Group
UVB
3% GP
5% GP
Growth
Exophytic
Endophytic
Flat
C
15
10
5
0
% of tumors
Group
UVB
3% GP
5% GP
Invasion score
I1
I2
I3
Presumed transitional
Superficial dermal
Deep dermal
Subcutis
MiSCC diagnosis
D
15
10
5
0
% of tumors
Group
UVB
3% GP
5% GP
SCC
SpCC
Anaplastic
Malignant tumor diagnosis

Figure 6

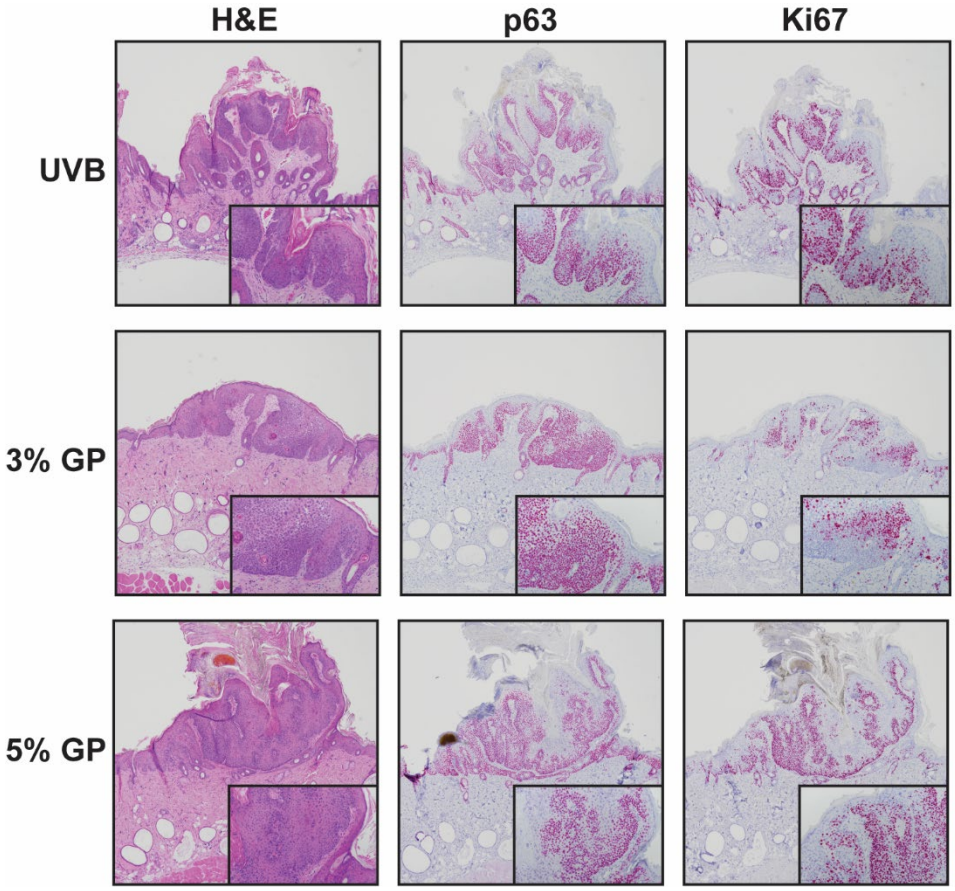

Figure 7

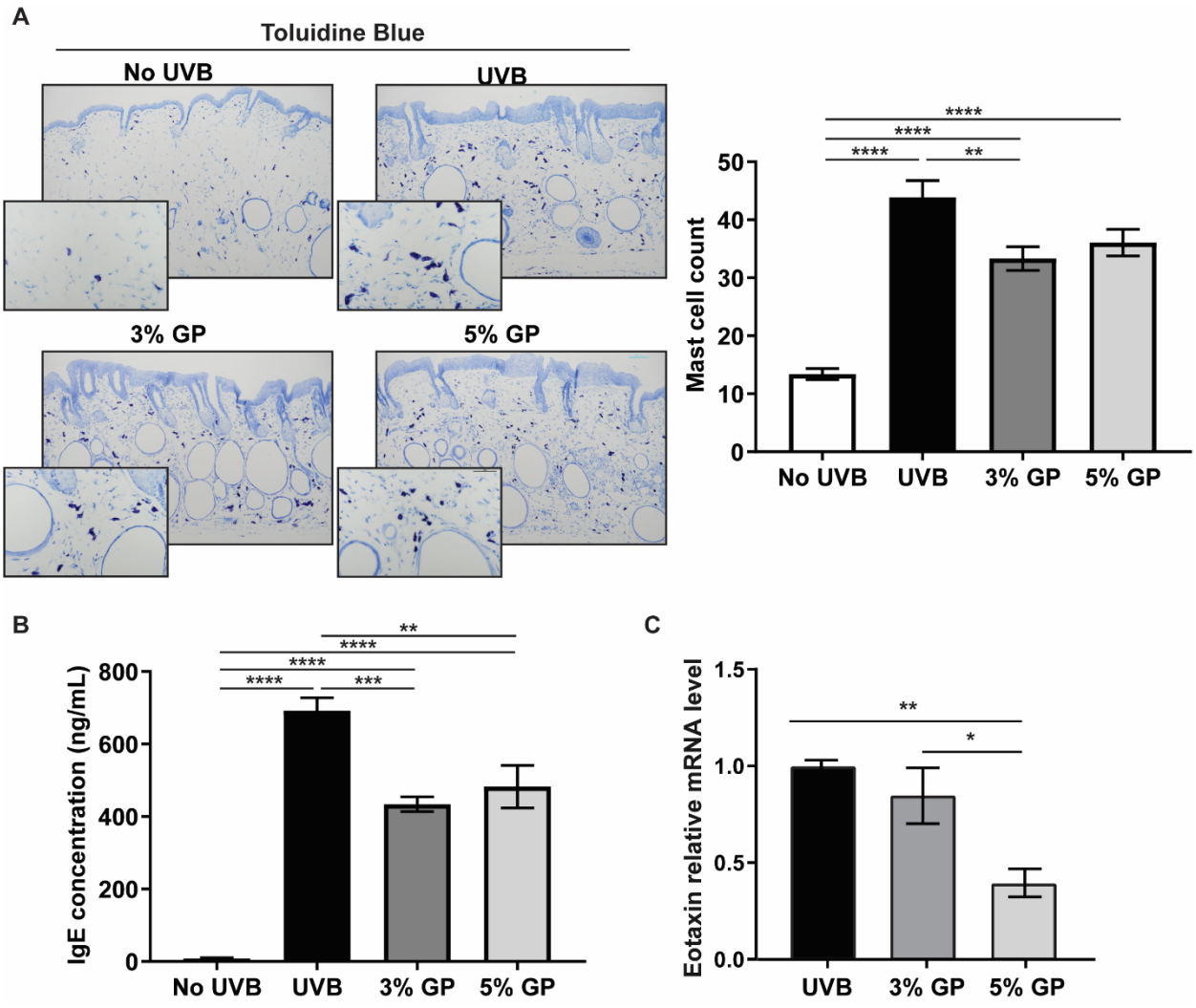
A
Toluidine Blue
No UVB
UVB
3% GP
5% GP
Mast cell count
No UVB
UVB
3% GP
5% GP
B
IgE concentration (ng/mL)
C
Eotaxin relative mRNA level

Figure 8

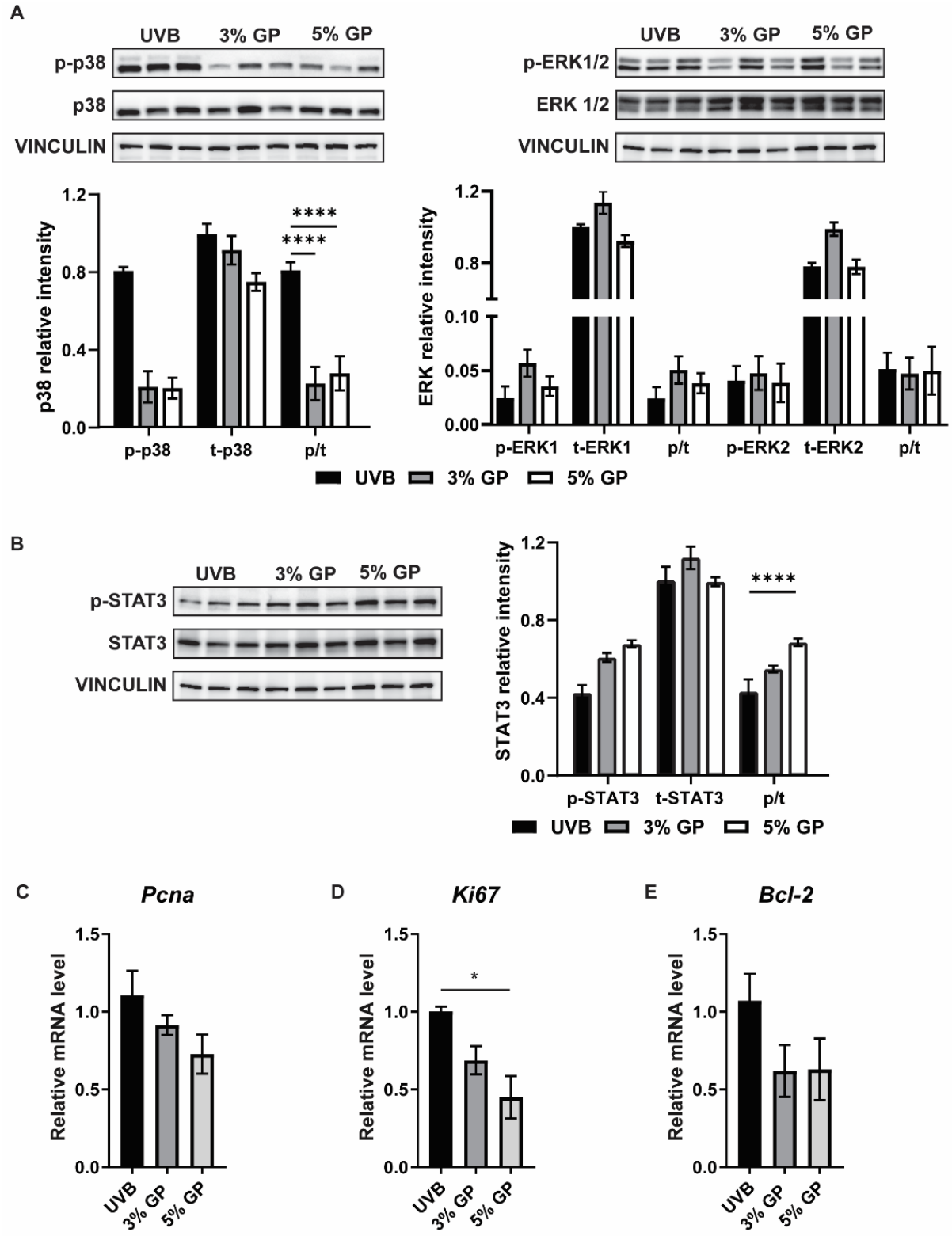
A
UVB
3% GP
5% GP
p-p38
p38
VINCULIN
p-ERK1/2
ERK 1/2
VINCULIN
p38 relative intensity
ERK relative intensity
****
****
p-p38
t-p38
p/t
p-ERK1
t-ERK1
p/t
p-ERK2
t-ERK2
p/t
UVB
3% GP
5% GP
B
p-STAT3
STAT3
VINCULIN
STAT3 relative intensity
****
p-STAT3
t-STAT3
p/t
C
Pcna
D
Ki67
*
E
Bcl-2
Relative mRNA level

Figure 9

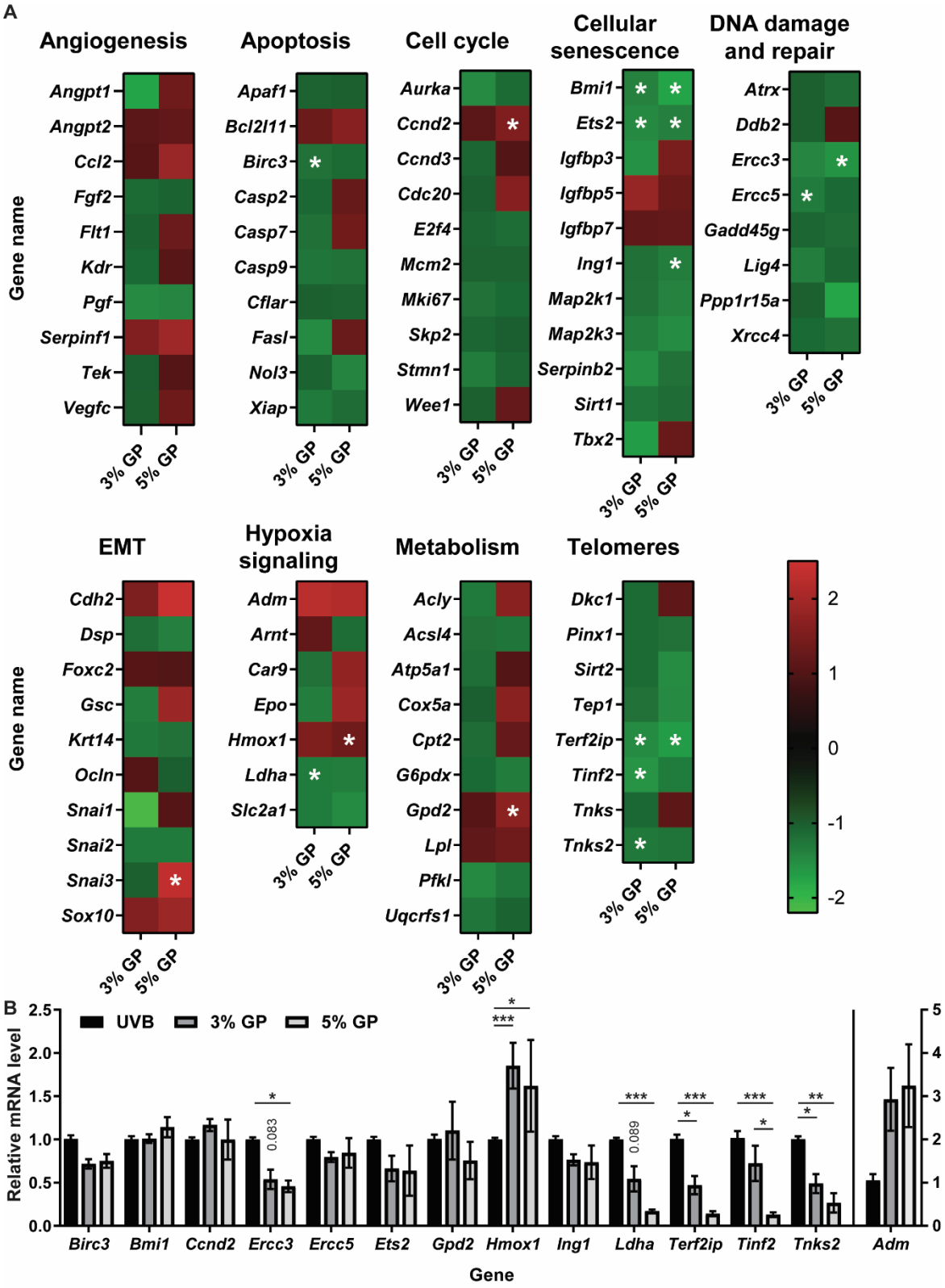
A
Angiogenesis
Angpt1
Angpt2
Ccl2
Fgf2
Flt1
Kdr
Pgf
Serpinf1
Tek
Vegfc
Apoptosis
Apaf1
Bcl2l11
Birc3
Casp2
Casp7
Casp9
Cflar
Fasl
Nol3
Xiap
Cell cycle
Aurka
Ccnd2
Ccnd3
Cdc20
E2f4
Mcm2
Mki67
Skp2
Stmn1
Wee1
Cellular senescence
Bmi1
Ets2
Igfbp3
Igfbp5
Igfbp7
Ing1
Map2k1
Map2k3
Serpinb2
Sirt1
Tbx2
DNA damage and repair
Atrx
Ddb2
Ercc3
Ercc5
Gadd45g
Lig4
Ppp1r15a
Xrcc4
Gene name
3% GP
5% GP
EMT
Cdh2
Dsp
Foxc2
Gsc
Krt14
Ocln
Snai1
Snai2
Snai3
Sox10
Hypoxia signaling
Adm
Arnt
Car9
Epo
Hmox1
Ldha
Slc2a1
Metabolism
Acly
Acsl4
Atp5a1
Cox5a
Cpt2
G6pdx
Gpd2
Lpl
Pfkl
Uqcrfs1
Telomeres
Dkc1
Pinx1
Sirt2
Tep1
Terf2ip
Tinf2
Tnks
Tnks2
2
1
0
-1
-2
B
UVB
3% GP
5% GP
Relative mRNA level
0.083
0.089
Birc3
Bmi1
Ccnd2
Ercc3
Ercc5
Ets2
Gpd2
Hmox1
Ing1
Ldha
Terf2ip
Tinf2
Tnks2
Adm
Gene

Figure 10

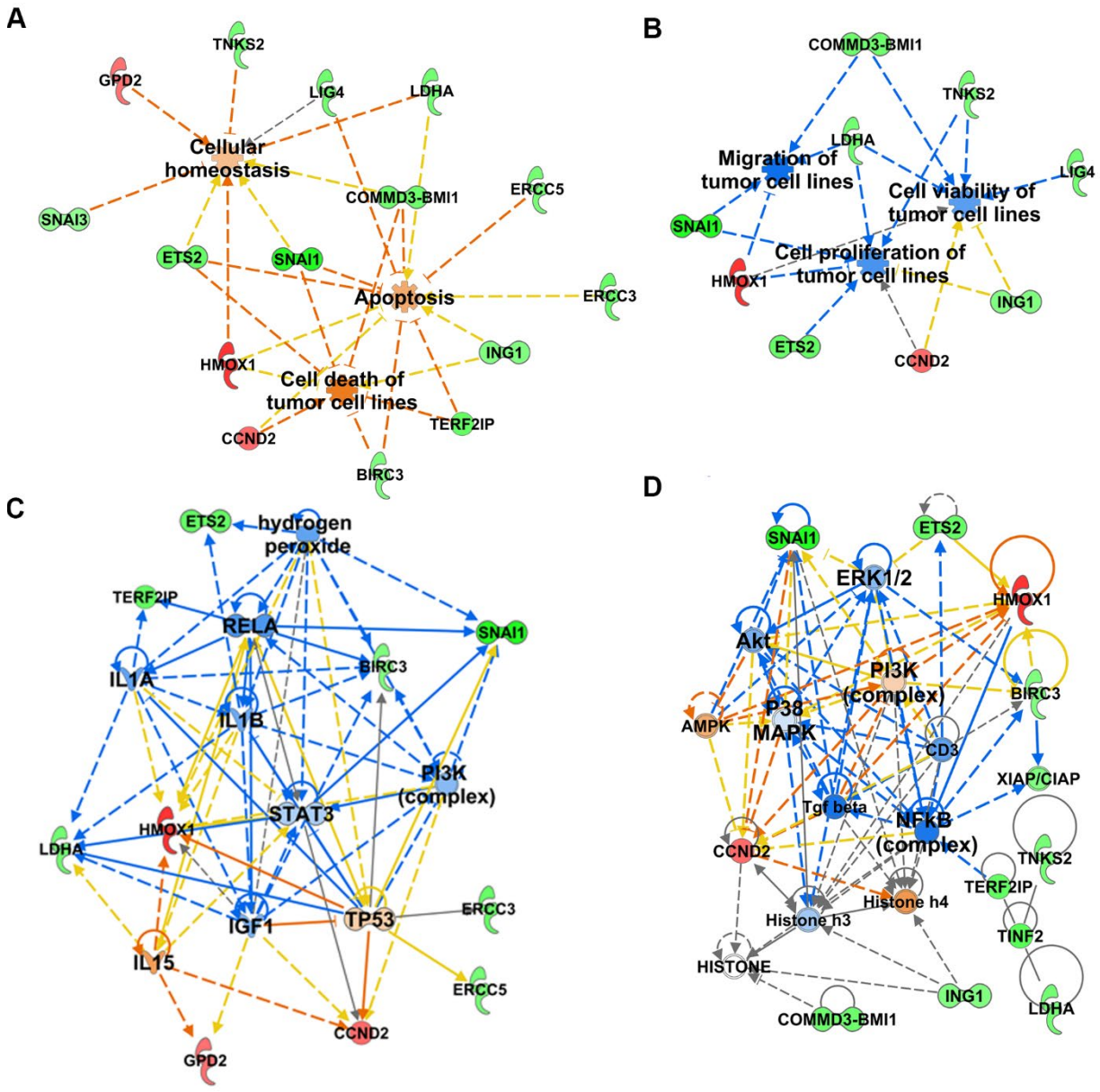
A
TNKS2
GPD2
LIG4
LDHA
Cellular homeostasis
SNAI3
COMMD3-BMI1
ERCC5
ETS2
SNAI1
Apoptosis
ERCC3
HMOX1
ING1
Cell death of tumor cell lines
TERF2IP
CCND2
BIRC3
B
COMMD3-BMI1
TNKS2
LDHA
Migration of tumor cell lines
LIG4
Cell viability of tumor cell lines
SNAI1
Cell proliferation of tumor cell lines
HMOX1
ING1
ETS2
CCND2
C
ETS2
hydrogen peroxide
TERF2IP
RELA
SNAI1
IL1A
BIRC3
IL1B
PI3K (complex)
STAT3
HMOX1
LDHA
TP53
ERCC3
IGF1
IL15
ERCC5
CCND2
GPD2
D
SNAI1
ETS2
ERK1/2
HMOX1
Akt
PI3K (complex)
BIRC3
P38 MAPK
AMPK
CD3
XIAP/CIAP
Tgf beta
NFkB (complex)
CCND2
TNKS2
TERF2IP
Histone h4
Histone h3
TINF2
HISTONE
ING1
LDHA
COMMD3-BMI1

Table 1. Percentages of mice within each treatment group exhibiting lesions in the histologic-based classes

Treatment Group	Premalignant Papilloma Grade (%)			Intermediate (%)
	1	2	3	
UVB (n=11)	5 (45%)	8 (73%)	5 (45%)	3 (27%)
3% GP (n=12)	3 (25%)	11 (92%)	7 (58%)	2 (17%)
5% GP (n=10)	7 (70%)	8 (80%)	6 (60%)	4 (40%)

Treatment Group	Presumed Transitional (%)	Malignant Microinvasive SCC Grade (%)			Fully Invasive Tumors (%)			Mice with Malignant Diagnosis (%)
		SD	DD	SQ	SCC	SpCC	Ana	
UVB (n=11)	2 (18%)	4 (36%)	2 (18%)	1 (9%)	2 (18%)	4 (36%)	0 (0%)	8 (73%)
3% GP (n=12)	1 (8%)	1 (8%)	1 (8%)	1 (8%)	0 (0%)	0 (0%)	1 (8%)	6 (50%)
5% GP (n=10)	3 (30%)	0 (0%)	1 (10%)	2 (20%)	0 (0%)	3 (30%)	0 (0%)	6 (60%)

Chapter 5: Future Directions

This thesis work provides insight into our understanding of chemoprevention of UVB-mediated carcinogenesis by whole foods, namely grapes. This work was a continuation of an ongoing investigation within our lab and department to determine the efficacy of chemopreventive agents, whether alone or in combination, to prevent and/or treat the onset of skin diseases and disorders. Here, we have only scratched the surface, as these studies lay the groundwork for further investigations with grape powder. Not only did we expose dietary grape as an agent that reduces tumorigenesis in mice, but we aimed to determine mechanisms of chemoprevention, in doing so, we utilized proteomics analysis to uncover the anti-inflammatory effect of grape on carcinogenesis. These data warrant further investigation into the chemoprotective nature of dietary grape.

The intent of this chapter is to present new avenues of investigation. There is plenty of work to be done, particularly in determining the whether dietary grape affords protection in other relevant models of skin carcinogenesis and skin disease. Therefore, we propose to evaluate dietary grape on pre-clinical models and clinical trials of NMSC. Additionally, as mentioned in Chapter 1, immunocompromised individuals and solid organ transplant recipients (OTRs) are at a 2-3 fold higher risk of developing metastatic NMSC, therefore a targeted focus on chemoprevention will be suggested for this population. Last, we will discuss the reasoning to expand to pre-clinical evaluation of dietary in other forms of skin disease, namely Atopic Dermatitis. Our suggestions for future directions are described below.

Dietary grape as a chemopreventive agent in an in vivo model of BCC

As stated in chapter one, a limitation of the SKH-1 hairless mouse model is the restriction to the development of malignant squamous cell carcinomas (SCC), which only account for a small portion of skin cancer diagnoses and deaths in humans. Whereas basal cell carcinomas (BCC) account for over 3.3 million annual cases yet minimal mortality [1]. To expand our current understanding of the chemoprotective nature of dietary grape, we will

replicate our diet experiments utilizing a strain of mice susceptible to BCC. As the Patched (PTCH) protein is a receptor responsible for repressing the hedgehog (HH) signaling pathway, the dysregulation can lead to the upregulated expression of HH in BCCs [2]. *PTCH*$^{+/-}$ are a conventional mouse model created on the C57BL/6 background, generally crossed with another strain of interest, that develop BCCs, SCCs, and trichoblastomas after months of chronic UV exposure thrice weekly, serving as a reasonable model for chemoprevention studies of BCC [3]. Therefore the exploration of the chemoprotective effects of dietary should be further explored in other relevant models of skin carcinogenesis for BCC.

PTCH$^{+/-}$ mice will be provided 0, 3, or 5% GP-fortified AIN76A diets over the course of 12 months of UV exposure, to assure tumor develop within the 0% GP diet. Selectively, over the course of the study, cohorts of mice will be euthanized and skin biopsies evaluated for dysplasia, and microscopic BCC incidence by hematoxylin and eosin staining, DNA damage (CPDs), oxidative stress (4-HNE and NRF2), and proliferation (Ki67 and PCNA). Over the course of the study, tumors measuring greater than 2 mm in diameter will be measured weekly to track growth. At the final termination (12 months), skin sections and cross sections of tumors will be collected for tumor diagnosis of SCCs and BCCs and staining of markers mentioned above will be assessed. After 12 months of UV exposure, one cohort of mice within each treatment group will end UV treatments and continue *ad libitum* access to their respective diets. At 18 months, or until tumor burden in one group reaches 1000 mm^3, these mice will be euthanized and the skin and lymph nodes will be collected and evaluated for metastatic growth potential. Epithelial (cytokeratin, p63, E-cadherin) and mesenchymal (N-cadherin, Vimentin) markers will be evaluated in skin, tumors, and lymph nodes to determine the potential of dietary grape to reduce malignant conversion of tumor cells.

Dietary grape as a chemopreventive agent against NMSC in clinical trials

Our exploration of dietary grape chemoprevention is a step towards finding new therapeutics methods to reduce the risk and prognosis of NMSC. Although this study accompanies many others with compelling evidence that dietary grape had beneficial effect on health in general and reduction of disease, studies addressing its efficacious effects in humans are limited. Currently, one clinical trial from the University of Alabama has been completed evaluating the effect of grape powder consumption in the sunburn reaction of humans (ID: NCT02760160), yet no evaluations of the beneficial effects in patients with a high-risk for NMSC diagnosis.

To assess if dietary grape can aid in protecting against the development of NMSC lesions, a multiple cohort study will be employed. In the first cohort, individuals will be at high risk for NMSC development, including those with actinic keratosis. The second cohort will be individuals with that undergone excision of an NMSC lesion within the previous three months. Freeze-dried grape powder (30 grams) will be provided as a daily drinking water supplement for consumption over the course of the study. If patients develop a lesion during this time will undergo surgical excisions and continue treatment. Baseline measurements recording serum antioxidant and cytokine levels will be measured, and a blood draw conducted every 6 months for 5 years. Biopsies will also be obtained every 6 months to evaluate MAPK family proteins (shown to be modulated in chapters 3a and 4).

Pre-clinical and clinical studies in organ transplant models/ patients who are at a greater risk for BCC/SCC and other cancers

Not only does a diagnosis of NMSC dictate an increased likelihood of subsequent diagnosis, immunosuppressed individuals, such as those on immunosuppressive drugs and organ transplant patients, are at an even higher risk of developing SCCs and BCCs [4-6]. Consequently, the likelihood of metastasis of these NMSCs are also elevated in these patients

[4]. Therefore, therapeutic methods to reduce the risk of NMSC development in this class of patients is a necessity, as current methods are not fully effective. Within this thesis, we outlined that dietary grape in the form of whole grape powder affords protection by acting as an anti-inflammatory agents, reduced oxidative stress, and increased apoptosis in tumor cells. A critical portion of this study also demonstrated that the consumption of dietary grape also reduced the malignant conversion of tumors in male SKH-1 hairless mice (Chapter 2). Therefore, based on the diagnostic rationale of these studies, we believe dietary grape is a promising agent in the immunosuppressed individuals with highly likelihood of NMSC incidence, metastasis and mortality. This study will be broken into two portion, pre-clinical and clinical as the efficacy of dietary grape must be evaluated in immunosuppressed mouse models.

Due to the finding that immunosuppressed individuals have a higher likelihood of NMSC [4, 5], we will employ an immunosuppressed UVR-mediated NMSC mouse model to determine the efficacy of dietary grape. Therefore the *Ptch+/-* mouse will be irradiated as described above with a 0%, 3% or 5% GP fortified diet. Intraperitoneal injections of Cyclosporin A, an immunosuppressive drug widely used for OTR patients, will occur multiple times weekly to suppress the immune system. As this immune impairment has previously demonstrated increased BCC tumor burden [7], tumor growth and incidence will be monitored as stated previously. We expect to see the anti-inflammatory effects of dietary grape in the prevention of tumor progression. If the results are positive, we would seek to provide a grape powder supplement to patients who have had at least one NMSC lesion and a solid organ transplant. Trial will include evaluating the number of NMSC lesions in OTR patients, including evaluation of epidermal dysplasia and actinic keratosis damage every three months over the course of years every 3 months. Additionally, key biomarkers will be assessed including Wnt signaling, HH signaling and oxidative stress.

Treatment and prevention of atopic dermatitis utilizing dietary grape

Many studies have unveiled the anti-inflammatory actions of phytonutrients, such as resveratrol, in inflammatory skin diseases including cancer [8], atopic dermatitis (AD) [9], and psoriasis [10]. In particular, AD is a chronic inflammatory skin disease characterized by abnormal immune function, environmental causes, and skin barrier dysfunction that generally onsets in early childhood [11]. Unfortunately, current treatment options are falling short for the management and prevention of AD. Therefore, after advocating that dietary grape protects against UVB-mediated cutaneous damage and carcinogenesis by targeting multiple genes/pathways, we believe dietary grape could act to improve a therapeutic outcome in AD. The NC/Nga Tnd mouse, are known to develop spontaneous AD lesions resembling AD in humans when in exposed to conventional air [12]. Many studies retain mice in clean air conditions and induce AD by an irritant (such as DNFB) to evaluate the therapeutic effects of agents in a controlled setting [13, 14]. The hypothesis to be tested is that dietary grape will impart a protective response shown through the inhibition of the development and progression of AD.

To determine the effects of dietary grape against AD in NC/Nga Tnd mice, we will use two distinct protocols; prevention and intervention. A subset of mice will be left in ventilated housing with no irritant application, whereas all other will have weekly application of DNFB upon a shaved back. In the prevention protocol, mice will be provided a 3 or 5% GP fortified diet at the beginning of the study to determine if the diet can reduce onset and severity of disease. In the intervention protocol, mice will be provided a 0% diet until the onset of disease in the majority of the mice, then provided a 3 or 5% GP fortified diet to determine the therapeutic effect of dietary grape. Throughout the study, clinical severity scores based on edema, erythema/haemorrhage, excoriation/erosion, and dryness/scaling will be evaluated as gross observations. After study termination, histopathological analysis of the skin will include the

evaluation of epidermal hyperplasia, mast cells and inflammatory cell infiltration, and pathological markers of AD, such as IL-4 and Filaggrin. As AD is an inflammatory disorder, spleens and lymph nodes will also be collected and evaluated for B cell and T cells populations by flow cytometry.

References

1. Bichakjian, C., et al., *Guidelines of care for the management of basal cell carcinoma.* Journal of the American Academy of Dermatology, 2018. **78**(3): p. 540-559.
2. Ingham, P.W., *The patched gene in development and cancer.* Curr Opin Genet Dev, 1998. **8**(1): p. 88-94.
3. So, P.L., et al., *Topical tazarotene chemoprevention reduces Basal cell carcinoma number and size in Ptch1+/- mice exposed to ultraviolet or ionizing radiation.* Cancer Res, 2004. **64**(13): p. 4385-9.
4. Berg, D. and C.C. Otley, *Skin cancer in organ transplant recipients: Epidemiology, pathogenesis, and management.* J Am Acad Dermatol, 2002. **47**(1): p. 1-17; quiz 18-20.
5. O'Reilly Zwald, F. and M. Brown, *Skin cancer in solid organ transplant recipients: advances in therapy and management: part II. Management of skin cancer in solid organ transplant recipients.* J Am Acad Dermatol, 2011. **65**(2): p. 263-279.
6. Euvrard, S., J. Kanitakis, and A. Claudy, *Skin cancers after organ transplantation.* N Engl J Med, 2003. **348**(17): p. 1681-91.
7. Vogt, A., et al., *Anti-Rejection Drug Treatment Increases Basal Cell Carcinoma Burden in Ptch1+/- Mice.* Journal of Investigative Dermatology, 2005. **124**(1): p. 263-267.
8. Montes de Oca, M.K., et al., *Phytochemicals for the Prevention of Photocarcinogenesis.* Photochemistry and photobiology, 2017. **93**(4): p. 956-974.
9. Caglayan Sozmen, S., et al., *Resveratrol ameliorates 2,4-dinitrofluorobenzene-induced atopic dermatitis-like lesions through effects on the epithelium.* PeerJ, 2016. **4**: p. e1889-e1889.
10. Kjær, T.N., et al., *Resveratrol ameliorates imiquimod-induced psoriasis-like skin inflammation in mice.* PloS one, 2015. **10**(5): p. e0126599-e0126599.
11. Arkwright, P.D., et al., *Management of difficult-to-treat atopic dermatitis.* J Allergy Clin Immunol Pract, 2013. **1**(2): p. 142-51.
12. Suto, H., et al., *NC/Nga mice: a mouse model for atopic dermatitis.* Int Arch Allergy Immunol, 1999. **120 Suppl 1**: p. 70-5.
13. Kim, T.H., et al., *The inhibitory effect of naringenin on atopic dermatitis induced by DNFB in NC/Nga mice.* Life Sci, 2013. **93**(15): p. 516-24.
14. Takahashi, N., et al., *Scratching behavior in spontaneous- or allergic contact-induced dermatitis in NC/Nga mice.* Exp Dermatol, 2005. **14**(11): p. 830-7.

Appendix 1: Supplementary tables and figures

Chapter 2: Supplementary Figure S1

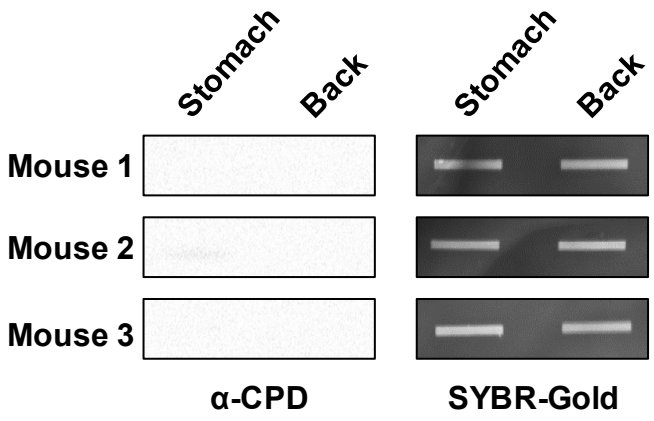

Immuno-slot blot analysis for CPDs in normal skin samples from a separate cohort of untreated mice that had no UV exposure. A separate cohort of 12 female retired breeder mice were aged to 36 weeks while on the control diet. At the termination of the experiment, mice were euthanized and tissues were collected for further analysis of DNA damage. Stomach and back skin from 3 representative animals is displayed above. SYBR gold, which stains total nucleic acid was used as an internal control. No CPDs were detected in normal skin samples.

Chapter 2: Supplementary Figure S2

a. Heat map of control vs. 3% GP

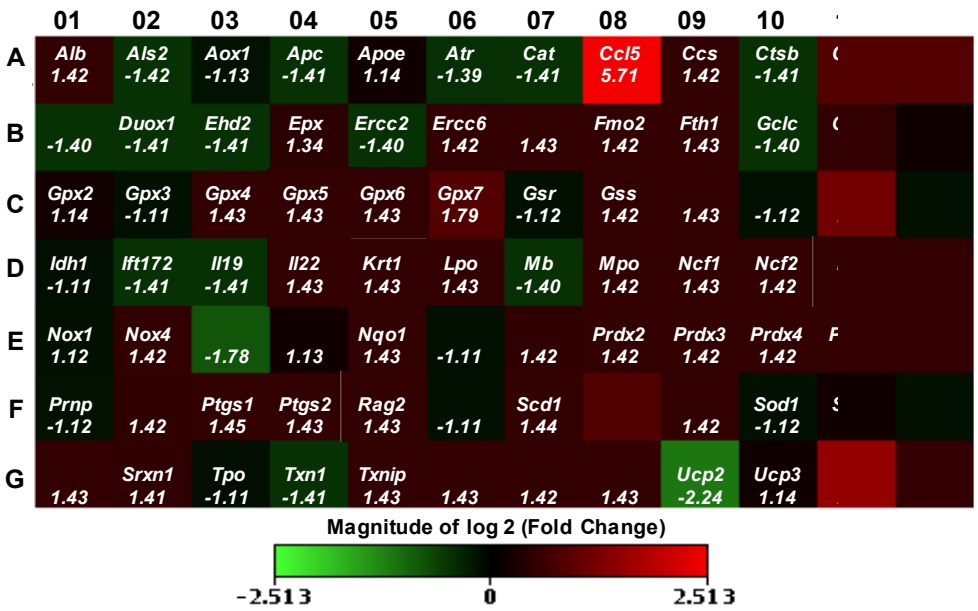

b. Heat map of control vs. 5% GP

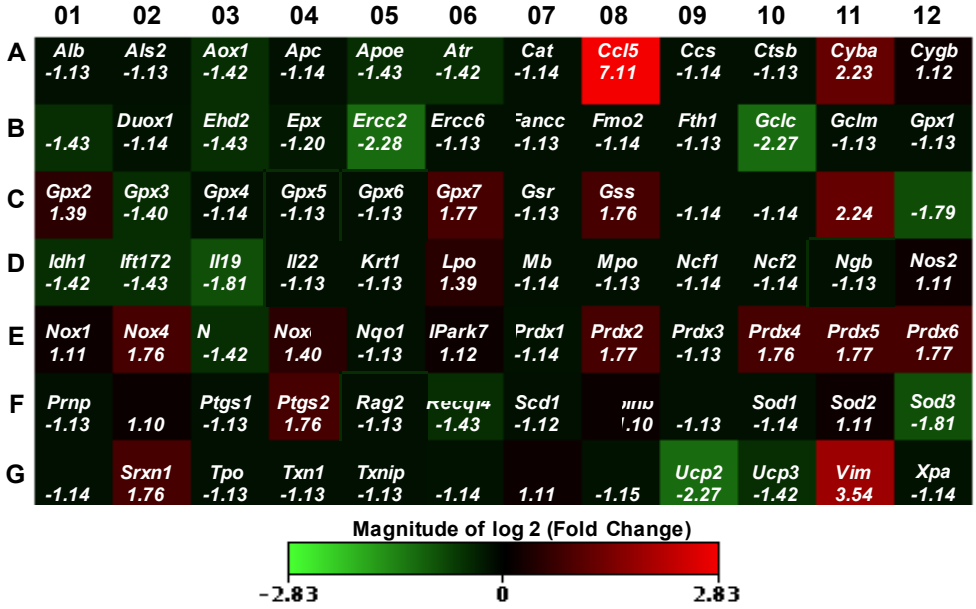

Effects of dietary grape on oxidative stress genes. Heat maps of control vs. 3% and 5% GP were generated to display gene fold changes. Upregulated genes are displayed in red and downregulated genes are shown in green, black boxes indicate no/negligible fold change in those particular genes.

Chapter 2: Supplementary Table S1

List of key altered genes in response to grape powder (GP) treatments. 18 genes were identified with ≥1.75-fold change and statistical significance (P<0.05) in mouse samples treated with 5% GP. The data from 3% GP group has also been shown for comparative analysis. Genes showing ≥1.75-fold change in 5% GP and ≥1.4-fold in 3% GP, resulting total 16 genes were used for subsequent RT-qPCR validation and IPA analysis.

			3% GP		5% GP	
Gene Symbol	Gene Name	Profiler Category	Fold Regulation	p-value	Fold Regulation	p-value
Ccl5	Chemokine (C-C motif) ligand 5	Oxidative Stress Responsive Gene	5.71	0.014645	7.11	0.000002
Cyba	Cytochrome b-245, alpha polypeptide	Superoxide Metabolism Gene	1.8	0.091247	2.23	0.0004
Ercc2	Excision repair cross-complementation group 2	Oxidative Stress Responsive Gene	-1.4	0.24914	-2.28	0.010589
Gclc	Glutamate-cysteine ligase, catalytic subunit	Oxidative Stress Responsive Gene	-1.4	0.247225	-2.27	0.009965
Gpx7	Glutathione peroxidase 7	Oxidative Stress Responsive Gene	1.79	0.003654	1.77	0.004132
Gss	Glutathione synthetase	Oxidative Stress Responsive Gene	1.42	0.215394	1.76	0.004271
Hmox1	Heme oxygenase (decycling) 1	Oxidative Stress Responsive Gene	2.27	0.000352	2.24	0.000424
Hspa1a	Heat shock protein 1A	Oxidative Stress Responsive Gene	-1.11	0.773925	-1.79	0.014468
Nox4	NADPH oxidase 4	Superoxide Metabolism Gene	1.42	0.221724	1.76	0.004844
Prdx2	Peroxiredoxin 2	Oxidative Stress Responsive Gene/ Peroxiredoxin	1.42	0.213154	1.77	0.004229
Prdx4	Peroxiredoxin 4	Peroxiredoxin (TPx)	1.42	0.215395	1.76	0.004488
Prdx5	Peroxiredoxin 5	Peroxiredoxin (TPx)	1.42	0.213666	1.77	0.004204
Prdx6	Peroxiredoxin 6	Peroxiredoxin (TPx)	1.43	0.210228	1.77	0.003882
Ptgs2	Prostaglandin-endoperoxide synthase 2	Peroxidase	1.43	0.210952	1.76	0.003908
Sod3	Superoxide dismutase 3, extracellular	Antioxidant	-1.12	0.7442	-1.81	0.010659
Srxn1	Sulfiredoxin 1 homolog	Antioxidant	1.41	0.225001	1.76	0.005224
Ucp2	Uncoupling protein 2	Superoxide Metabolism Gene	-2.24	0.011074	-2.27	0.01068
Vim	Vimentin	Oxygen Transporter	2.85	0.032417	3.54	0.000045

Chapter 2: Supplementary Table S2, page 1 of 3

Gene	Gene Description	Profiler Category	3% GP		5% GP	
			Fold Change	p-value	Fold Change	p-value
Alb	Albumin	Antioxidant	1.42	0.218858	-1.13	0.364246
Als2	Amyotrophic lateral sclerosis 2 (juvenile) homolog (human)	Oxidative Stress Responsive Gene	-1.42	0.236393	-1.13	0.360353
Aox1	Aldehyde oxidase 1	Involved in Reactive Oxygen Species (ROS) Metabolism	-1.13	0.751417	-1.42	0.592941
Apc	Adenomatosis polyposis coli	Antioxidant- Peroxidase	-1.41	0.251594	-1.14	0.363309
Apoe	Apolipoprotein E	Oxidative Stress Responsive Gene	1.14	0.654409	-1.43	0.172057
Atr	Ataxia telangiectasia and rad3 related	Oxygen Tansporter	-1.39	0.386002	-1.42	0.366689
Cat	Catalase	Antioxidant- Peroxidase, Oxidative Stress Responsive Gene	-1.41	0.240764	-1.14	0.339531
Ccl5	Chemokine (C-C motif) ligand 5	Oxidative Stress Responsive Gene	5.71	0.014645	7.11	0.000002
Ccs	Copper chaperone for superoxide dismutase	Involved in Superoxide Metabolism	1.42	0.215228	-1.14	0.345722
Ctsb	Cathepsin B	Antioxidant- Peroxidase, Oxidative Stress Responsive Gene	-1.41	0.240381	-1.13	0.354946
Cyba	Cytochrome b-245, alpha polypeptide	Involved in Superoxide Metabolism	1.8	0.091247	2.23	0.0004
Cygb	Cytoglobin	Oxygen Tansporter	1.8	0.08987	1.12	0.405717
Dnm2	Dynamin 2	Oxygen Tansporter	-1.4	0.242862	-1.43	0.220371
Duox1	Dual oxidase 1	Antioxidant- Peroxidase, Oxidative Stress Responsive Gene	-1.41	0.243269	-1.14	0.350213
Ehd2	EH-domain containing 2	Antioxidant- Peroxiredoxin	-1.41	0.203231	-1.43	0.190148
Epx	Eosinophil peroxidase	Antioxidant- Peroxidase, Oxidative Stress Responsive Gene	1.34	0.273282	-1.2	0.230678
Ercc2	Excision repair cross-complementing rodent repair deficiency, complementation group 2	Oxidative Stress Responsive Gene	-1.4	0.24914	-2.28	0.010589
Ercc6	Excision repair cross-complementing rodent repair deficiency, complementation group 6	Oxidative Stress Responsive Gene	1.42	0.213211	-1.13	0.360697
Fancc	Fanconi anemia, complementation group C	Oxygen Tansporter	1.43	0.21034	-1.13	0.355737
Fmo2	Flavin containing monooxygenase 2	Involved in ROS Metabolism	1.42	0.212799	-1.14	0.345907
Fth1	Ferritin heavy chain 1	Oxidative Stress Responsive Gene	1.43	0.210781	-1.13	0.353059
Gclc	Glutamate-cysteine ligase, catalytic subunit	Oxidative Stress Responsive Gene	-1.4	0.247225	-2.27	0.009965
Gclm	Glutamate-cysteine ligase, modifier subunit	Oxidative Stress Responsive Gene	1.43	0.205741	-1.13	0.345013
Gpx1	Glutathione peroxidase 1	Antioxidant- Glutathione Peroxidase, Oxidative Stress Responsive Gene	1.11	0.634835	-1.13	0.336807
Gpx2	Glutathione peroxidase 2	Antioxidant- Glutathione Peroxidase, Oxidative Stress Responsive Gene	1.14	0.88457	1.39	0.469283

Chapter 2: Supplementary Table S2, page 2 of 3

Gpx3	Glutathione peroxidase 3	Antioxidant- Glutathione Peroxidase, Oxidative Stress Responsive Gene	-1.11	0.380624	-1.4	0.225606
Gpx4	Glutathione peroxidase 4	Antioxidant- Glutathione Peroxidase, Oxidative Stress Responsive Gene	1.43	0.212575	-1.14	0.352836
Gpx5	Glutathione peroxidase 5	Antioxidant- Glutathione Peroxidase, Oxidative Stress Responsive Gene	1.43	0.213375	-1.13	0.356473
Gpx6	Glutathione peroxidase 6	Antioxidant- Glutathione Peroxidase, Oxidative Stress Responsive Gene	1.43	0.213375	-1.13	0.356473
Gpx7	Glutathione peroxidase 7	Antioxidant- Glutathione Peroxidase, Oxidative Stress Responsive Gene	1.79	0.003654	1.77	0.004132
Gsr	Glutathione reductase	Oxidative Stress Responsive Gene	-1.12	0.397303	-1.13	0.360304
Gss	Glutathione synthetase	Oxidative Stress Responsive Gene	1.42	0.215394	1.76	0.004271
Gstk1	Glutathione S-transferase kappa 1	Antioxidant- Glutathione Peroxidase	1.43	0.212967	-1.14	0.354319
Gstp1	Glutathione S-transferase, pi 1	Antioxidant- Glutathione Peroxidase	-1.12	0.389275	-1.14	0.349131
Hmox1	Heme oxygenase (decycling) 1	Oxidative Stress Responsive Gene	2.27	0.000352	2.24	0.000424
Hspa1a	Heat shock protein 1A	Oxidative Stress Responsive Gene	-1.11	0.773925	-1.79	0.014468
Idh1	Isocitrate dehydrogenase 1 (NADP+), soluble	Oxidative Stress Responsive Gene	-1.11	0.807066	-1.42	0.18914
Ift172	Intraflagellar transport 172 homolog (Chlamydomonas)	Oxygen Tansporter	-1.41	0.2433	-1.43	0.21774
Il19	Interleukin 19	Involved in ROS Metabolism	-1.41	0.248498	-1.81	0.083693
Il22	Interleukin 22	Involved in ROS Metabolism	1.43	0.213375	-1.13	0.356473
Krt1	Keratin 1	Oxidative Stress Responsive Gene	1.43	0.211246	-1.13	0.358458
Lpo	Lactoperoxidase	Antioxidant- Peroxidase	1.43	0.210268	1.39	0.231326
Mb	Myoglobin	Oxygen Tansporter	-1.4	0.259115	-1.14	0.359846
Mpo	Myeloperoxidase	Antioxidant- Peroxidase, Oxidative Stress Responsive Gene	1.42	0.215271	-1.13	0.356085
Ncf1	Neutrophil cytosolic factor 1	Involved in Superoxide Metabolism	1.43	0.212503	-1.14	0.350568
Ncf2	Neutrophil cytosolic factor 2	Involved in Superoxide Metabolism	1.42	0.216312	-1.14	0.351757
Ngb	Neuroglobin	Oxygen Tansporter	1.43	0.213375	-1.13	0.356473
Nos2	Nitric oxide synthase 2, inducible	Involved in Superoxide Metabolism	1.43	0.275414	1.11	0.406513
Nox1	NADPH oxidase 1	Involved in Superoxide Metabolism	-1.12	0.944014	1.11	0.633415
Nox4	NADPH oxidase 4	Involved in Superoxide Metabolism	1.42	0.221724	1.76	0.004844
Noxa1	NADPH oxidase activator 1	Involved in Superoxide Metabolism	-1.78	0.132915	-1.42	0.177651
Noxo1	NADPH oxidase organizer 1	Involved in Superoxide Metabolism	1.13	0.67067	1.4	0.159773
Nqo1	NAD(P)H dehydrogenase, quinone 1	Oxidative Stress Responsive Gene	1.43	0.213773	-1.13	0.372423
Park7	Parkinson disease (autosomal recessive, early onset) 7	Oxidative Stress Responsive Gene	-1.11	0.783525	1.12	0.399985

Chapter 2: Supplementary Table S2, page 3 of 3

Prdx1	Peroxiredoxin 1	Antioxidant- Peroxiredoxin, Oxidative Stress Responsive Gene	1.42	0.220131	-1.14	0.33925
Prdx2	Peroxiredoxin 2	Antioxidant- Peroxiredoxin, Oxidative Stress Responsive Gene	1.42	0.213154	1.77	0.004229
Prdx3	Peroxiredoxin 3	Antioxidant- Peroxiredoxin	1.42	0.213458	-1.13	0.354926
Prdx4	Peroxiredoxin 4	Antioxidant- Peroxiredoxin	1.42	0.215395	1.76	0.004488
Prdx5	Peroxiredoxin 5	Antioxidant- Peroxiredoxin	1.42	0.213666	1.77	0.004204
Prdx6	Peroxiredoxin 6	Antioxidant- Peroxiredoxin, Oxidative Stress Responsive Gene	1.43	0.210228	1.77	0.003882
Prnp	Prion protein	Oxidative Stress Responsive Gene	-1.12	0.39609	-1.13	0.370135
Psmb5	Proteasome (prosome, macropain) subunit, beta type 5	Oxidative Stress Responsive Gene	1.42	0.219841	1.1	0.663179
Ptgs1	Prostaglandin-endoperoxide synthase 1	Antioxidant- Peroxidase	1.45	0.19953	-1.13	0.363977
Ptgs2	Prostaglandin-endoperoxide synthase 2	Antioxidant- Peroxidase	1.43	0.210952	1.76	0.003908
Rag2	Recombination activating gene 2	Antioxidant- Peroxidase	1.43	0.213375	-1.13	0.356473
Recql4	RecQ protein-like 4	Involved in Superoxide Metabolism	-1.11	0.771828	-1.43	0.250213
Scd1	Stearoyl-Coenzyme A desaturase 1	Involved in Superoxide Metabolism	1.44	0.203015	-1.12	0.378903
Serpinb 1b	Serine (or cysteine) peptidase inhibitor, clade B, member 1b	Antioxidant- Peroxidase	1.78	0.087398	1.1	0.433564
Slc38a1	Solute carrier family 38, member 1	Oxygen Tansporter	1.42	0.213153	-1.13	0.353599
Sod1	Superoxide dismutase 1, soluble	Involved in ROS Metabolism, Oxidative Stress Responsive Gene	-1.12	0.390945	-1.14	0.348373
Sod2	Superoxide dismutase 2, mitochondrial	Involved in ROS Metabolism	1.13	0.335295	1.11	0.402898
Sod3	Superoxide dismutase 3, extracellular	Involved in ROS Metabolism	-1.12	0.7442	-1.81	0.010659
Sqstm1	Sequestosome 1	Oxidative Stress Responsive Gene	1.43	0.210373	-1.14	0.337401
Srxn1	Sulfiredoxin 1 homolog (S. cerevisiae)	Antioxidant	1.41	0.225001	1.76	0.005224
Tpo	Thyroid peroxidase	Antioxidant- Peroxidase, Oxidative Stress Responsive Gene	-1.11	0.797561	-1.13	0.722938
Txn1	Thioredoxin 1	Oxidative Stress Responsive Gene	-1.41	0.242038	-1.13	0.333495
Txnip	Thioredoxin interacting protein	Oxidative Stress Responsive Gene	1.43	0.211889	-1.13	0.353944
Txnrd1	Thioredoxin reductase 1	Antioxidant, Oxidative Stress Responsive Gene	1.43	0.2146	-1.14	0.34279
Txnrd2	Thioredoxin reductase 2	Antioxidant, Oxidative Stress Responsive Gene	1.42	0.211071	1.11	0.646497
Txnrd3	Thioredoxin reductase 3	Antioxidant	1.43	0.213614	-1.15	0.338762
Ucp2	Uncoupling protein 2 (mitochondrial, proton carrier)	Involved in Superoxide Metabolism	-2.24	0.011074	-2.27	0.01068
Ucp3	Uncoupling protein 3 (mitochondrial, proton carrier)	Oxidative Stress Responsive Gene	1.14	0.657215	-1.42	0.179396
Vim	Vimentin	Oxygen Tansporter	2.85	0.032417	3.54	0.000045
Xpa	Xeroderma pigmentosum, complementation group A	Oxidative Stress Responsive Gene	1.42	0.216064	-1.14	0.349442

Chapter 2: Supplementary Table S3

Antibodies used for western blotting (WB), immunohistochemistry (IHC), and/or slot blot (SB).

Gene Name	Supplier	Catalog Number	WB Dilution	IHC Dilution	SB Dilution	Molecular Weight (kDa)
PARP	Cell Signaling	9542	1:1000			116, 89
Caspase-7	Cell Signaling	12827	1:1000			35, 20
NRF2	Cell Signaling	12721	1:1000			97-100
B-Actin	Cell Signaling	4970, 3700	1:1000			45
PCNA	Santa Cruz	Sc-56	1:500			36
BCL-2	Santa Cruz	Sc-7382	1:500			26
4- Hydroxynonenal	Abcam	Ab46545	1:2000	1:50		n/a
Ki-67	Cell Signaling	12202		1:400		n/a
NRF2	Invitrogen	PA5-27882		1:100		n/a
CPD	Cosmo Bio	NM-DND-001			1:5000	n/a
(6-4) PP	Cosmo Bio	NM-DND-002			1:3000	n/a

Chapter 2: Supplementary Table S4

Primer sequences used for RT-qPCR validation.

Gene	Amplicon size (bp)	Orientation	Sequence (5'-3')	Length (bp)	Tm (°C)	Primer Bank ID
Ccl5	104	F	GCTGCTTTGCCTACCTCTCC	20	62.6	7305461a1
		R	TCGAGTGACAAACACGACTGC	21	62.8	
Cyba	127	F	TCACCAGGAATTACTACGTCCG	22	61.2	22094077a1
		R	GCTGCCAGCAGATAGATCACA	21	61.9	
Ercc2	152	F	ACCCGGAGCAGTTCTCCTAC	20	62.8	31542614a1
		R	GGTCACCTCCAGCGGATAAG	20	61.7	
Gclc	125	F	GGGGTGACGAGGTGGAGTA	19	62.3	33468897a1
		R	GTTGGGGTTTGTCCTCTCCC	20	62.1	
Gpx7	238	F	TCCGAGCAGGACTTCTACGAC	21	63	13195626a1
		R	TCTCCCTGTTGGTGTCTGGTT	21	62.8	
Gss	103	F	CAAAGCAGGCCATAGACAGGG	21	62.8	6680117a1
		R	AAAAGCGTGAATGGGGCATAC	21	61.3	
Hmox1	100	F	AAGCCGAGAATGCTGAGTTCA	21	61.7	6754212a1
		R	GCCGTGTAGATATGGTACAAGGA	23	61.2	
Nox4	145	F	GAAGGGGTTAAACACCTCTGC	21	60.6	7657389a1
		R	ATGCTCTGCTTAAACACAATCCT	23	60.2	
Prdx2	139	F	CACCTGGCGTGGATCAATACC	21	62.8	166235200c2
		R	GACCCCTGTAAGCAATGCCC	20	62.9	
Prdx4	101	F	CTCAAACTGACTGACTATCGTGG	23	60.4	7948999a1
		R	CGATCCCCAAAAGCGATGATTTC	23	62.1	
Prdx5	154	F	GGCTGTTCTAAGACCCACCTG	21	62.1	6755114a1
		R	GGAGCCGAACCTTGCCTTC	19	63	
Prdx6	115	F	CGCCAGAGTTTGCCAAGAG	19	61	6671549a1
		R	TCCGTGGGTGTTTCACCATTG	21	62.8	
Ptgs2	74	F	TGAGCAACTATTCCAAACCAGC	22	60.8	31981525a1
		R	GCACGTAGTCTTCGATCACTATC	23	60.3	
Srxn1	113	F	ATCGTGGTGCTGGATTGATTC	21	60.4	467583a1
		R	CACCCCAGAGATAAGATTACCCA	23	60.6	
Ucp2	109	F	ATGGTTGGTTTCAAGGCCACA	21	62.5	31543920a1
		R	CGGTATCCAGAGGGAAAGTGAT	22	61	
Vim	124	F	CGGCTGCGAGAGAAATTGC	19	61.8	31982755a1
		R	CCACTTTCCGTTCAAGGTCAAG	22	61.3	
Ki-67	104	F	ATCATTGACCGCTCCTTTAGGT	22	61.2	1177528a1
		R	GCTCGCCTTGATGGTTCCT	19	62	
Pcna	135	F	TTTGAGGCACGCCTGATCC	19	62.3	7242171a1
		R	GGAGACGTGAGACGAGTCCAT	21	63	
Gapdh	95	F	AGGTCGGTGTGAACGGATTTG	21	62.6	126012538c1
		R	GGGGTCGTTGATGGCAACA	19	62.6	
Actb	154	F	GGCTGTATTCCCCTCCATCG	20	61.8	6671509a1
		R	CCAGTTGGTAACAATGCCATGT	22	61.1	

Chapter 3a: Supplementary Figure S1

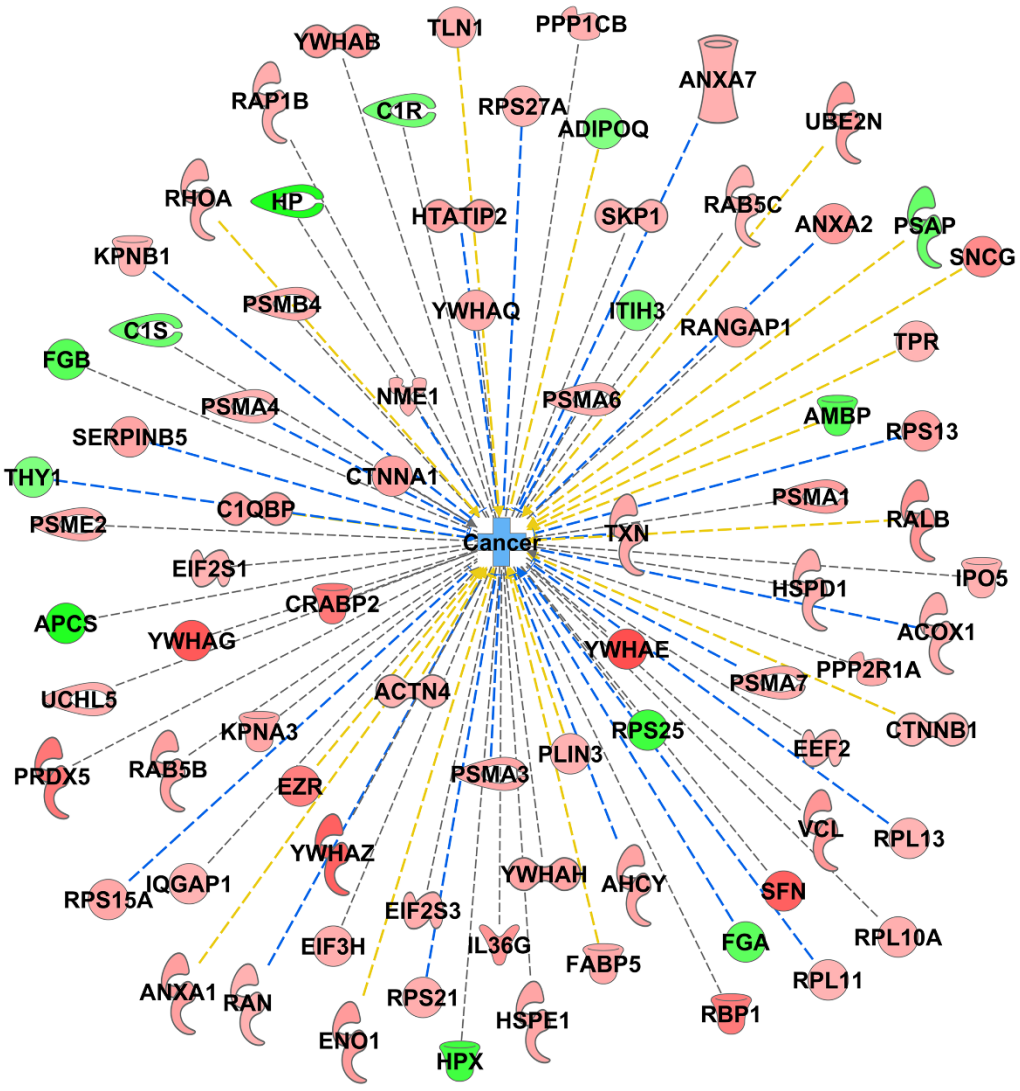

Functional analysis of the secondary cut-off analysis utilizing IPA (5% GP / Ctl) show interactions of proteins which act to inhibit cancer. Indirect interactions are denoted by dashed lines. Blue lines suggest inhibition: orange suggest activation; yellow suggest inconsistent findings; grey indicates that an effect is not predicted. Fold change of protein expression 5% GP / Ctl is indicated by green=downregulated, red=upregulated. IPA, Ingenuity Pathway Analysis. GP, grape powder. Ctl, control diet.

Chapter 3a: Supplementary Table S1: Antibodies used for immunoblotting

Gene Name	Supplier	Catalog Number	Dilution	Molecular Weight (kDa)
PSMA3	Proteintech	11887	1:500	28
PSMA6	Proteintech	11573	1:1000	28
PSMB7	Abclonal	A14771	1:1000	30
UCHL5	Proteintech	11527	1:500	38
APCS	Abclonal	A1996	1:500	30
Haptoglobin	Proteintech	16665	1:500	42
Fibrinogen alpha chain	Proteintech	20645	1:1000	60
Fibrinogen beta chain	Proteintech	16747	1:1000	50
AMBP	Abclonal	A1846	1:500	46
pERK1/2	Cell Signaling	9101	1:1000	42, 44
ERK1/2	Cell Signaling	9102	1:1000	42, 45
NF-κB	Invitrogen	510500	1:500	65
IkBα	Cell Signaling	9242	1:1000	39
B-Tubulin	Proteintech	10094	1:1000	55
β-Actin	Cell Signaling	4970, 3700	1:1000	45

Chapter 3a: Supplementary Table S2

Protein cut-off. A primary dataset (marked with X in 'FDR cut-off' section) was created by subjecting the 2,629 proteins to cut-off criteria: ≥3 unique peptides, fold change (5% GP / Control) ≥1.2, p-value ≤0.05, and q-value of ≤0.1, indicated by an X in the FDR cut-off column. A secondary dataset that includes all the proteins presented in this table was created excluding the FDR-calculated q-value.

UniProt ID	Gene names	Protein names	Unique peptides	Ratio	Fold Change	FDR cut-off
Ubiquitin Proteasome						
Q9R1P4	PSMA1	Proteasome subunit alpha type-1	10	1.58	1.58	X
O70435	PSMA3	Proteasome subunit alpha type-3	14	1.43	1.43	X
Q9R1P0	PSMA4	Proteasome subunit alpha type-4	10	1.23	1.23	X
Q9QUM9	PSMA6	Proteasome subunit alpha type-6	13	1.29	1.29	X
Q9Z2U0	PSMA7	Proteasome subunit alpha type-7	9	1.35	1.35	
P99026	PSMB4	Proteasome subunit beta type-4	6	1.36	1.36	X
P70195	PSMB7	Proteasome subunit beta type-7	5	1.28	1.28	X
Q9WUP7	UCHL5	Ubiquitin carboxyl-terminal hydrolase isozyme L5	4	1.31	1.31	X
P97372	PSME2	Proteasome activator complex subunit 2	3	1.39	1.39	
P62983	RPS27A	Ubiquitin-40S ribosomal protein S27a	8	1.21	1.21	
P63038	HSPD1	60 kDa heat shock protein, mitochondrial	30	1.35	1.35	
Q64433	HSPE1	10 kDa heat shock protein, mitochondrial	7	1.44	1.44	
Q9WTX5	SKP1	S-phase kinase-associated protein 1	7	1.24	1.24	
P61089	UBE2N	Ubiquitin-conjugating enzyme E2 N	6	1.58	1.58	
Acute Phase Response						
Q07456	AMBP	Alpha-1-microglobulin	9	0.61	-1.65	
P12246	APCS	Serum amyloid P-component	8	0.30	-3.37	
Q8CG16	C1RA	Complement C1r-A subcomponent	4	0.73	-1.38	
Q8CG14	C1S1	Complement C1s-A subcomponent	4	0.70	-1.43	
E9PV24	FGA	Fibrinogen alpha chain	27	0.63	-1.58	
Q8K0E8	FGB	Fibrinogen beta chain	37	0.62	-1.63	
Q61646	HP	Haptoglobin	20	0.46	-2.17	
Q91X72	HPX	Hemopexin	33	0.54	-1.85	
Q3U0P4	IL36G	Interleukin-36 gamma	3	1.72	1.72	
Q61704	ITIH3	Inter-alpha-trypsin inhibitor heavy chain H3	15	0.80	-1.25	
Q9JIW9	RALB	Ras-related protein Ral-B	4	1.76	1.76	X
Q99JI6	RAP1B	Ras-related protein Rap-1b	5	1.32	1.32	
Q00915	RBP1	Retinol-binding protein 1	4	2.14	2.14	X
Other Proteins						
O70456	SFN	14-3-3 protein sigma	17	2.56	2.56	
Q9CQV8	YWHAB	14-3-3 protein beta/alpha	5	1.64	1.64	
P62259	YWHAE	14-3-3 protein epsilon	13	2.83	2.83	
P61982	YWHAG	14-3-3 protein gamma;14-3-3 protein gamma, N-terminally processed	4	2.68	2.68	
P68510	YWHAH	14-3-3 protein eta	5	1.46	1.46	
P68254	YWHAQ	14-3-3 protein theta	7	1.32	1.32	
P63101	YWHAZ	14-3-3 protein zeta/delta	10	2.54	2.54	
Q9D2R0	AACS	Acetoacetyl-CoA synthetase	11	1.20	1.20	

Q6P542	ABCF1	ATP-binding cassette sub-family F member 1	6	1.23	1.23	
Q91V12	ACOT7	Cytosolic acyl coenzyme A thioester hydrolase	6	1.27	1.27	
Q9R0H0	ACOX1	Peroxisomal acyl-coenzyme A oxidase 1	5	1.35	1.35	
Q9Z2N8	ACTL6A	Actin-like protein 6A	7	1.29	1.29	
P57780	ACTN4	Alpha-actinin-4	21	1.23	1.23	
P03958	ADA	Adenosine deaminase	3	1.43	1.43	
Q60994	ADIPOQ	Adiponectin	4	0.83	-1.21	
P46664	ADSS	Adenylosuccinate synthetase isozyme 2	10	1.25	1.25	
P50247	AHCY	Adenosylhomocysteinase	19	1.47	1.47	X
A2AS37	AI182371		3	0.71	-1.40	
Q9JII6	AKR1A1	Alcohol dehydrogenase [NADP(+)]	13	1.32	1.32	
P45376	AKR1B1	Aldose reductase	13	1.46	1.46	
P45377	AKR1B8	Aldose reductase-related protein 2	4	1.33	1.33	
P10518	ALAD	Delta-aminolevulinic acid dehydratase	4	1.28	1.28	
P10107	ANXA1	Annexin A1	26	1.54	1.54	
P07356	ANXA2	Annexin A2	24	1.60	1.60	
Q3TET3	ANXA3	Annexin A3	11	1.40	1.40	
P48036	ANXA5	Annexin A5	15	3.05	3.05	
Q07076	ANXA7	Annexin A7	13	1.27	1.27	
Q921D0	ANXA8	Annexin A8	18	1.64	1.64	X
P51910	APOD	Apolipoprotein D	4	0.72	-1.38	
Q99PT1	ARHGDIA	Rho GDP-dissociation inhibitor 1	10	1.38	1.38	
Q61599	ARHGDIB	Rho GDP-dissociation inhibitor 2	7	1.62	1.62	
Q9CQW2	ARL8B	ADP-ribosylation factor-like protein 8B	3	1.30	1.30	
Q61024	ASNS	Asparagine synthetase [glutamine-hydrolyzing]	15	1.24	1.24	
Q09PK2	ASPRV1	Retroviral-like aspartic protease 1	4	2.10	2.10	
Q9CY64	BLVRA	Biliverdin reductase A	6	1.24	1.24	
Q9CQC6	BZW1	Basic leucine zipper and W2 domain-containing protein 1	4	1.51	1.51	X
Q8R5L1	C1QBP	Complement component 1 Q subcomponent-binding protein, mitochondrial	5	1.53	1.53	
Q8K182	C8A	Complement component C8 alpha chain	6	0.75	-1.33	
Q9D6N1	CA13	Carbonic anhydrase 13	5	1.38	1.38	
P62204	CALM1	Calmodulin	5	2.57	2.57	
Q9JM83	CALM4	Calmodulin-4	7	2.15	2.15	
P35564	CANX	Calnexin	25	1.43	1.43	
O88456	CAPNS1	Calpain small subunit 1	5	1.32	1.32	
Q5RKN9	CAPZA1	F-actin-capping protein subunit alpha-1	7	1.27	1.27	X
P47757	CAPZB	F-actin-capping protein subunit beta	15	1.31	1.31	X
Q9ER72	CARS	Cysteine--tRNA ligase, cytoplasmic	8	1.38	1.38	
O89094	CASP14	Caspase-14	5	1.70	1.70	
Q8K354	CBR3	Carbonyl reductase [NADPH] 3	12	1.21	1.21	
P06909	CFH	Complement factor H	37	0.63	-1.59	
P18760	CFL1	Cofilin-1	13	1.23	1.23	
Q61362	CHI3L1	Chitinase-3-like protein 1	3	1.54	1.54	
P30275	CKMT1	Creatine kinase U-type, mitochondrial	5	1.36	1.36	
Q9Z1Q5	CLIC1	Chloride intracellular channel protein 1	11	1.26	1.26	X
Q9DBP5	CMPK1	UMP-CMP kinase	4	1.25	1.25	
P61924	COPZ1	Coatomer subunit zeta-1	4	1.24	1.24	
Q9CQI6	COTL1	Coactosin-like protein	11	1.28	1.28	
P52825	CPT2	Carnitine O-palmitoyltransferase 2, mitochondrial	9	1.35	1.35	
P22935	CRABP2	Cellular retinoic acid-binding protein 2	3	2.16	2.16	
P56567	CSTA	Cystatin-A;Cystatin-A, N-terminally processed	8	1.73	1.73	

Q62426	CSTB	Cystatin-B	3	1.56	1.56	
P26231	CTNNA1	Catenin alpha-1	10	1.50	1.50	
Q02248	CTNNB1	Catenin beta-1	11	1.20	1.20	
Q91YL7	CWH43	PGAP2-interacting protein	3	1.30	1.30	
P56395	CYB5A	Cytochrome b5	3	1.45	1.45	
Q9DAR7	DCPS	m7GpppX diphosphatase	4	1.34	1.34	
A2ADY9	DDI2	Protein DDI1 homolog 2	6	1.36	1.36	
P54823	DDX6	Probable ATP-dependent RNA helicase DDX6	8	1.37	1.37	
O35290	EAR3	Eosinophil cationic-type ribonuclease 3	5	0.69	-1.46	
O70251	EEF1B	Elongation factor 1-beta	8	1.65	1.65	
Q80T06	EEF1D	Elongation factor 1-delta	10	1.62	1.62	
P58252	EEF2	Elongation factor 2	55	1.20	1.20	
Q6ZWX6	EIF2S1	Eukaryotic translation initiation factor 2 subunit 1	10	1.21	1.21	
Q9Z0N1	EIF2S3X	Eukaryotic translation initiation factor 2 subunit 3, X-linked	11	1.34	1.34	
Q91WK2	EIF3H	Eukaryotic translation initiation factor 3 subunit H	5	1.30	1.30	
O55135	EIF6	Eukaryotic translation initiation factor 6	6	1.40	1.40	
P17182	ENO1	Alpha-enolase	17	1.61	1.61	
Q8BGB7	ENOPH1	Enolase-phosphatase E1	3	1.24	1.24	
P57759	ERP29	Endoplasmic reticulum resident protein 29	5	2.57	2.57	
Q9D1Q6	ERP44	Endoplasmic reticulum resident protein 44	11	1.21	1.21	
Q9D952	EVPL	Envoplakin	10	1.21	1.21	
P26040	EZR	Ezrin	19	2.05	2.05	
P04117	FABP4	Fatty acid-binding protein, adipocyte	14	1.86	1.86	
Q05816	FABP5	Fatty acid-binding protein, epidermal	15	1.40	1.40	
Q61554	FBN1	Fibrillin-1	12	0.78	-1.28	
Q920E5	FDPS	Farnesyl pyrophosphate synthase	9	1.37	1.37	
Q9QXC1	FETUB	Fetuin-B	10	0.63	-1.58	
P30416	FKBP4	Peptidyl-prolyl cis-trans isomerase FKBP4	10	1.54	1.54	X
Q9JJ28	FLII	Protein flightless-1 homolog	11	1.30	1.30	
Q61598	GDI2	Rab GDP dissociation inhibitor beta	25	1.30	1.30	X
Q9CPU0	GLO1	Lactoylglutathione lyase	6	1.33	1.33	
Q9CPV4	GLOD4	Glyoxalase domain-containing protein 4	11	1.34	1.34	X
Q64521	GPD2	Glycerol-3-phosphate dehydrogenase	18	1.24	1.24	
P19157	GSTP1	Glutathione S-transferase P 1	5	2.02	2.02	
Q9D3B1	HACD2	Very-long-chain (3R)-3-hydroxyacyl-CoA dehydratase 2	3	1.36	1.36	
Q8CBB6	HIST1H2BQ	Histone H2B	7	0.56	-1.78	
P00493	HPRT1	Hypoxanthine-guanine phosphoribosyltransferase	7	1.45	1.45	X
Q3U816	HTATIP2	Oxidoreductase HTATIP2	3	1.51	1.51	
P58044	IDI1	Isopentenyl-diphosphate Delta-isomerase 1	5	2.43	2.43	
A0A0B4J1H9	IGKV1-132	Immunoglobulin kappa variable 1-132	3	0.50	-2.00	
Q8BKC5	IPO5	Importin-5	18	1.26	1.26	
Q9JKF1	IQGAP1	Ras GTPase-activating-like protein IQGAP1	57	1.22	1.22	
O35344	KPNA3	Importin subunit alpha-4	4	1.42	1.42	
P70168	KPNB1	Importin subunit beta-1	22	1.21	1.21	
Q91XL1	LRG1	Leucine-rich HEV glycoprotein	6	0.60	-1.65	
Q9DB27	MCTS1	Malignant T-cell-amplified sequence 1	3	1.31	1.31	X
Q6ZQI3	MLEC	Malectin	9	1.37	1.37	
P62774	MTPN	Myotrophin	4	2.00	2.00	
Q99JF5	MVD	Diphosphomevalonate decarboxylase	3	1.47	1.47	X
Q9R008	MVK	Mevalonate kinase	7	1.31	1.31	

Q6ZWQ9	MYL12A	Myosin regulatory light chain 12B	9	1.37	1.37	
Q9CZ42	NAXD	ATP-dependent (S)-NAD(P)H-hydrate dehydratase	7	0.78	-1.28	
P15532	NME1	Nucleoside diphosphate kinase A	3	1.22	1.22	
Q01768	NME2	Nucleoside diphosphate kinase	6	1.70	1.70	
Q9R1J0	NSDHL	Sterol-4-alpha-carboxylate 3-dehydrogenase, decarboxylating	6	1.25	1.25	
E9Q7G0	NUMA1	Nuclear mitotic apparatus protein 1	19	1.31	1.31	
P29758	OAT	Ornithine aminotransferase, mitochondrial	7	1.35	1.35	
Q9CZ30	OLA1	Obg-like ATPase 1	13	1.23	1.23	X
Q62422	OSTF1	Osteoclast-stimulating factor 1	3	1.87	1.87	
P09103	P4HB	Protein disulfide-isomerase	33	1.57	1.57	
P50580	PA2G4	Proliferation-associated protein 2G4	21	1.30	1.30	
Q6PHQ9	PABPC4	Polyadenylate-binding protein	8	1.25	1.25	
Q9DBJ1	PGAM1	Phosphoglycerate mutase 1	6	2.36	2.36	
P53810	PITPNA	Phosphatidylinositol transfer protein alpha isoform	7	1.56	1.56	
Q60963	PLA2G7	Platelet-activating factor acetylhydrolase	6	0.71	-1.40	
P43883	PLIN2	Perilipin-2	5	1.58	1.58	
Q9DBG5	PLIN3	Perilipin-3	11	1.23	1.23	
Q9R0E2	PLOD1	Procollagen-lysine,2-oxoglutarate 5-dioxygenase 1	6	0.69	-1.44	
Q99K51	PLS3	Plastin-3	20	1.65	1.65	
Q9D819	PPA1	Inorganic pyrophosphatase	14	1.34	1.34	
Q9R269	PPL	Periplakin	10	1.47	1.47	X
P62141	PPP1CB	Serine/threonine-protein phosphatase PP1-beta catalytic subunit	3	1.28	1.28	X
Q76MZ3	PPP2R1A	Serine/threonine-protein phosphatase 2A 65 kDa regulatory subunit A alpha isoform	10	1.38	1.38	
P63328	PPP3CA	Serine/threonine-protein phosphatase 2B catalytic subunit alpha isoform	4	1.74	1.74	
P99029	PRDX5	Peroxiredoxin-5, mitochondrial	11	2.19	2.19	
Q6GT24	PRDX6	Peroxiredoxin-6	14	1.39	1.39	
Q8BFQ1	PSAP	Prosaposin	6	0.68	-1.47	
Q99LS3	PSPH	Phosphoserine phosphatase	3	1.92	1.92	X
Q9EPB4	PYCARD	Apoptosis-associated speck-like protein containing a CARD	6	3.29	3.29	
Q8BVI4	QDPR	Dihydropteridine reductase	4	1.39	1.39	X
P61027	RAB10	Ras-related protein Rab-10	6	1.57	1.57	
P46638	RAB11B	Ras-related protein Rab-11B;Ras-related protein Rab-11A	9	1.65	1.65	X
Q91V41	RAB14	Ras-related protein Rab-14	9	1.21	1.21	
P53994	RAB2A	Ras-related protein Rab-2A	8	1.23	1.23	X
Q3TXV4	RAB31	Ras-related protein Rab-31	3	1.84	1.84	X
Q6PHN9	RAB35	Ras-related protein Rab-35	4	1.35	1.35	
P35276	RAB3D	Ras-related protein Rab-3D	3	1.55	1.55	
P61021	RAB5B	Ras-related protein Rab-5B	3	1.52	1.52	
Q8C266	RAB5C	Ras-related protein Rab-5C	6	1.25	1.25	
P35279	RAB6A	Ras-related protein Rab-6A;Ras-related protein Rab-6B	8	1.29	1.29	
P51150	RAB7A	Ras-related protein Rab-7a	12	1.32	1.32	
P55258	RAB8A	Ras-related protein Rab-8A	5	1.38	1.38	
Q91WG2	RABEP2	Rab GTPase-binding effector protein 2	5	1.23	1.23	
P62827	RAN	GTP-binding nuclear protein Ran	12	1.25	1.25	
P46061	RANGAP1	Ran GTPase-activating protein 1	11	1.30	1.30	
Q8BK67	RCC2	Protein RCC2	14	1.27	1.27	
Q9QUI0	RHOA	Transforming protein RhoA	6	1.38	1.38	
O35292	RNASE2B	Ribonuclease 2B	4	0.46	-2.18	

P53026	RPL10A	60S ribosomal protein L10a	7	1.28	1.28	
Q9CXW4	RPL11	60S ribosomal protein L11	8	1.21	1.21	
P47963	RPL13	60S ribosomal protein L13	9	1.21	1.21	
Q5M8M8	RPL29	60S ribosomal protein L29	7	0.80	-1.25	
Q921R2	RPS13	40S ribosomal protein S13	7	1.53	1.53	
P62245	RPS15A	40S ribosomal protein S15a	8	1.42	1.42	
Q9CQR2	RPS21	40S ribosomal protein S21	5	1.30	1.30	
P62852	RPS25	40S ribosomal protein S25	4	0.54	-1.86	
P50543	S100A11	Protein S100-A11	3	1.32	1.32	
Q99JZ4	SAR1A	GTP-binding protein SAR1a	8	1.54	1.54	
Q8BH69	SEPHS1	Selenide, water dikinase 1	3	1.24	1.24	
Q8R121	SERPINA 10	Protein Z-dependent protease inhibitor	6	0.69	-1.44	
P70124	SERPINB 5	Serpin B5	21	1.45	1.45	X
Q6P6K7	SERPINB 6C	Serpinb6c protein	7	1.50	1.50	
O08800	SERPINB 8	Serpin B8	6	1.23	1.23	
Q91VW3	SH3BGRL 3	SH3 domain-binding glutamic acid-rich-like protein3	4	3.38	3.38	
P50431	SHMT1	Serine hydroxymethyltransferase, cytosolic	12	1.36	1.36	
P57787	SLC16A3	Monocarboxylate transporter 4	3	1.28	1.28	
Q8VEM8	SLC25A3	Phosphate carrier protein, mitochondrial	13	1.31	1.31	
Q9Z0F7	SNCG	Gamma-synuclein	3	1.86	1.86	
Q6NZD2	SNX1	Sorting nexin-1	6	1.22	1.22	
Q9CWK8	SNX2	Sorting nexin-2	15	1.26	1.26	
Q9D8U8	SNX5	Sorting nexin-5	4	1.47	1.47	
Q6P8X1	SNX6	Sorting nexin-6	5	1.30	1.30	
P16546	SPTAN1	Spectrin alpha chain, non-erythrocytic 1	20	1.29	1.29	
Q6P069	SRI	Sorcin	6	1.33	1.33	
Q64674	SRM	Spermidine synthase	7	1.20	1.20	
Q8BL97	SRSF7	Serine/arginine-rich splicing factor 7	4	0.73	-1.37	
Q497J0	STFA1	Stefin-1	7	1.37	1.37	
P35173	STFA3	Stefin-3	7	1.69	1.69	
Q80X82	SYMPK	Symplekin	3	1.35	1.35	
Q9WVA4	TAGLN2	Transgelin-2	9	1.42	1.42	
Q93092	TALDO1	Transaldolase	15	1.52	1.52	
Q9D1E6	TBCB	Tubulin-folding cofactor B	7	1.23	1.23	
Q9JHF5	TCIRG1	V-type proton ATPase subunit a	5	0.77	-1.31	
P01831	THY1	Thy-1 membrane glycoprotein	3	0.81	-1.24	
Q8BH58	TIPRL	TIP41-like protein	3	1.40	1.40	X
P40142	TKT	Transketolase	27	1.22	1.22	
P26039	TLN1	Talin-1	88	1.27	1.27	
Q9D1D4	TMED10	Transmembrane emp24 domain-containing protein10	5	1.67	1.67	
Q8BXN9	TMEM87A	Transmembrane protein 87A	6	1.20	1.20	
Q8BFY9	TNPO1	Transportin-1	10	1.29	1.29	
P17751	TPI1	Triosephosphate isomerase	19	1.40	1.40	
Q7M739	TPR	Nucleoprotein TPR	6	1.21	1.21	X
P63028	TPT1	Translationally-controlled tumor protein	9	1.31	1.31	
E9PY51	TRAPPC8	Trafficking protein particle complex 8	3	1.40	1.40	
P10639	TXN	Thioredoxin	7	1.41	1.41	
Q3KQM4	U2AF2	Splicing factor U2AF 65 kDa subunit	5	1.37	1.37	
Q9CRB3	URAH	5-hydroxyisourate hydrolase	5	1.28	1.28	
E9Q6R7	UTRN	Utrophin	4	0.72	-1.39	
Q64727	VCL	Vinculin	40	1.68	1.68	

Q9QZ88	VPS29	Vacuolar protein sorting-associated protein 29	4	1.49	1.49	X
Q00519	XDH	Xanthine dehydrogenase/oxidase	40	1.21	1.21	
Q3UE92	XPNPEP1	Xaa-Pro aminopeptidase 1	18	1.23	1.23	
Q9CQW1	YKT6	Synaptobrevin homolog YKT6	7	1.62	1.62	X

Chapter 5: Supplementary Figure S1

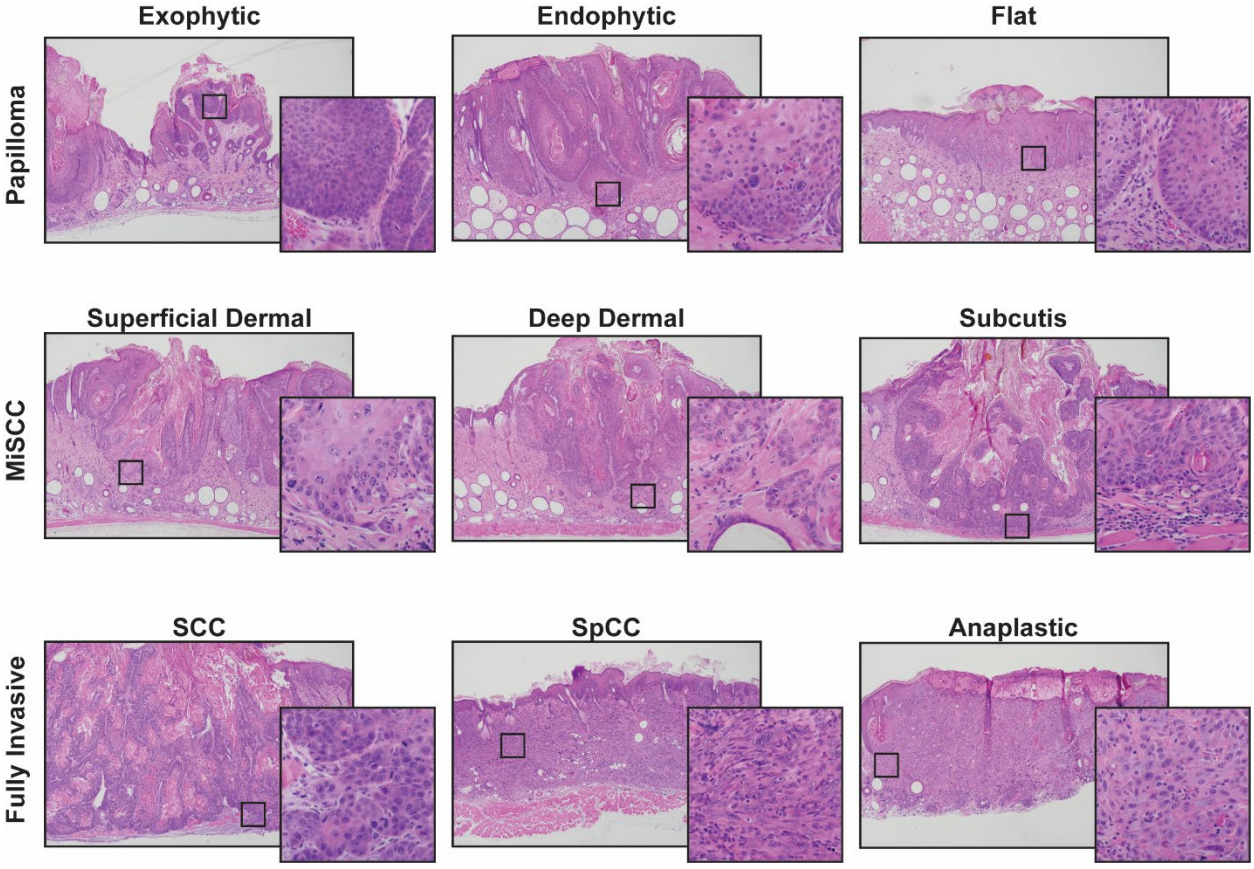

Chapter 5: Supplementary Table S1

Primer sequences used for RT-qPCR validation.

Refseq	*Gene*	Amplicon size (bp)	Orientation	Sequence (5'-3')	Length (bp)	Tm (°C)	Primer Bank ID
NM_009627	Adm	101	F	CACCCTGATGTTATTGGGTTCA	22	60	6752988a1
			R	TTAGCGCCCACTTATTCCACT	21	61.2	
NM_007464	Birc3	262	F	GCTGTGGCCTAATGCTAGACA	21	61.9	15030166a1
			R	GGACAATCTTGATTTGCTCGGAA	23	61.1	
NM_007552	Bmi1	116	F	ATCCCCACTTAATGTGTGTCCT	22	60.8	192203a1
			R	CTTGCTGGTCTCCAAGTAACG	21	60.6	
NM_009829	Ccnd2	154	F	GAGTGGGAACTGGTAGTGTTG	21	60	6753310a1
			R	CGCACAGAGCGATGAAGGT	19	62.4	
NM_133658	Ercc3	141	F	ATGGGCAAAAGAGATCGAGTG	21	60.1	19526800a1
			R	GTCCACCTGTTTCCCAGCG	19	62.9	
NM_011729	Ercc5	108	F	TGCTGGCCGTGGATATTAGC	20	62.1	26332843a1
			R	GCCGGTGGAATAATGTGAGAAGA	23	62.2	
NM_011809	Ets2	110	F	CCTGTCGCCAACAGTTTTCG	20	61.8	31542619a1
			R	TGGAGTGTCTGATCTTCACTGA	22	60.2	
NM_010274	Gpd2	197	F	GAAGGGGACTATTCTTGTGGGT	22	61.1	31981769a1
			R	GGATGTCAAATTCGGGTGTGT	21	60.6	
NM_010442	Hmox1	100	F	AAGCCGAGAATGCTGAGTTCA	21	61.7	6754212a1
			R	GCCGTGTAGATATGGTACAAGGA	23	61.2	
NM_011919	Ing1	100	F	CAGAGGAACGTCTCGCTGATG	21	62.5	29336057a1
			R	CGTCTGTCTCCCGTTTGAACTT	22	62.4	
NM_010699	Ldha	155	F	TGTCTCCAGCAAAGACTACTGT	22	60.7	6754524a1
			R	GACTGTACTTGACAATGTTGGGA	23	60.2	
NM_013914	Snai3	130	F	GGTCCCCAACTACGGGAAAC	20	62.2	7305643a1
			R	CTGTAGGGGGTCACTGGGATT	21	62.7	
NM_020584	Terf2ip	200	F	TGCCTTGTGGAAAGCGATG	19	60.7	15618999a1
			R	TGTTCTGTGGCTCTCCGCTAT	21	63	
NM_145705	Tinf2	200	F	TGCCTTGTGGAAAGCGATG	19	60.7	15618999a1
			R	TGTTCTGTGGCTCTCCGCTAT	21	63	
NM_001163635	Tnks2	115	F	CGCCCGAGAAGGTGAACAG	19	62.7	26338578a1
			R	TTTGCACCGTTCTGAAGAAGAT	22	60.2	
	ActB						

Chapter 5: Supplementary Table S2

Antibodies used for Immunhistochemistry and immunoblotting.

Protein Name	Supplier	Catalog Number	WB Dilution	Molecular Weight (kDa)	IHC dilution
PCNA	Invitrogen	PA5-27214			1:500
Ki67	Cell Signaling	12202			1:500
P63	Proteintech	12143			1:250
p-p38	Cell Signaling	4511	1:1000	40	
P38	Cell Signaling	9212	1:1000	40	
p-STAT3	Cell Signaling	9145	1:1000	79, 86	
STAT3	Cell Signaling	4904	1:2000	79, 86	
pErk1/2	Cell Signaling	9101	1:1000	42, 44	
ERK1/2	Cell Signaling	9102	1:1000	42, 45	
Vinculin	Cell Signaling	4650	1:1000	124	

Appendix 2: Effects and mechanism of nicotinamide against UVA- and/or UVB-mediated DNA damages in normal melanocytes

Originally published in *Photochemistry and Photobiology*

Photochem Photobiol, 2019 Jan, Volume 95, Issue 1, 331 - 337

Abstract

Melanoma incidences are increasing rapidly, and ultraviolet (UV) radiation from the sun is believed to be its major contributing factor. UV exposure causes DNA damage in skin which may initiate cutaneous skin cancers including melanoma. Melanoma arises from melanocytes, the melanin-producing skin cells, following genetic dysregulations resulting into hyperproliferative phenotype and neoplastic transformation. Both UVA and UVB exposure to the skin are believed to trigger melanocytic hyperplasia and melanomagenesis. Melanocytes by themselves are deficient in repair of oxidative DNA damage and UV-induced photoproducts. Nicotinamide, an active form of Vitamin B3 and a critical component of the human body's defense system has been shown to prevent certain cancers including nonmelanoma skin cancers. However, the mechanism of nicotinamide's protective effects is not well understood. Here, we investigated potential protective effects and mechanism of nicotinamide against UVA- and/or UVB- induced damage in normal human epidermal melanocytes. Our data demonstrated an appreciable protective effect of nicotinamide against UVA- and/or UVB- induced DNA damage in melanocytes by decreasing both cyclobutane pyrimidine dimers and 8-hydroxy-2′-deoxyguanine levels. We found that the photoprotective response of nicotinamide was associated with activation of nucleotide excision repair and NRF2. Further studies are needed to validate our findings in *in vivo* models.

Introduction

Ultraviolet (UV) radiation is a predominant environmental carcinogen and a major risk factor for skin cancers including melanoma (1). Solar UV radiation is the primary initiator of skin cancer by causing cutaneous DNA damage. Solar UV radiation that infiltrates the atmosphere and reaches the surface of the Earth is a mixture of UVA (320–400 nm) and UVB (280–320 nm) (2), and each UV component is capable of exerting a variety of effects on the skin cells, including DNA damage and oxidative stress (1). Although 95% of UVB radiation is absorbed in the protective ozone layer in our outer environment, the remaining 5% inbound UVB is a potent genotoxic agent to impart considerable response in skin cells, including melanocytes. UVB penetrates as deep as the epidermal basal cell layer of the skin and induces DNA damage (2), particularly in the form of cyclobutane pyrimidine dimers (CPDs), which are an important source of mutations in UV-induced melanoma (3). On the other hand, UVA is a potent driver of oxidative DNA damage in skin cells and can cause mutations by generating reactive oxygen species (ROS) (4) that oxidize guanine at the 8th position to produce 8-hydroxy-2′-deoxyguanine (8oxoG) (1). Interestingly, UVB also has been shown to produce 8oxoG in Chinese hamster cells (5) and primary human skin fibroblasts (6). Moreover, it has been shown that both UVA and UVB exposure to the skin can trigger melanocytic hyperplasia and melanomagenesis (7, 8). Melanocytes are melanin-producing skin cells that are primarily responsible for melanoma initiation. Wang et al. have shown that melanocytes by themselves are deficient in repair of oxidative DNA damage and UV-induced photoproducts (4). Thus, agents that can modulate DNA repair and prevent UV-induced DNA damage in melanocytes may reduce the risk of melanoma initiation and progression.

Nicotinamide is an amide form of Vitamin B3 or niacin and a critical component of the defense system of the human body which has been shown to enhance repair of genetic damage from various sources including UV radiation (9). Several studies have shown that nicotinamide

protects against non-melanoma skin cancer (10, 9). However, there is limited literature available on the protective effects of nicotinamide against UV-induced damages in melanocytes. Additionally, the exact mechanism of DNA damage repair by nicotinamide is not fully understood.

In this study, we determined the potential protective effects of nicotinamide against UVA-, and/or UVB- mediated damages in human melanocytes. Further, the mechanisms of nicotinamide- mediated protection against UV-induced DNA damage was explored at both gene and protein levels.

Materials and Methods

Melanocyte culture: Primary melanocytes isolated from neonatal human skin were obtained from the University of Wisconsin Skin Disease Research Center (UWSDRC) core facility. Melanocytes were cultured in Medium 254 (Gibco, Invitrogen, Carlsbad, CA, USA) supplemented with 1% human melanocyte growth supplement (HMGS) (Gibco, Invitrogen, Carlsbad, CA, USA).

UV exposure and nicotinamide treatment: Melanocytes were grown on either 60 mm dishes or chambered slides and at a confluency of 70-80% were washed twice with HBSS prior to UV exposure. Cells were pre-treated with 50 μM nicotinamide (3-Pyridinecarboxamide), obtained from Sigma-Aldrich (St Louis, MO, USA) for 24 h followed by exposure to a radiation dose of 3 J/cm^2 of UVA or 30 mJ/ cm^2 of UVB light or a combination of both 3 J/ cm^2 UVA and 30 mJ/ cm^2 UVB (UVAB) with a custom designed 120V Spectra UV instrument (Daavlin, Bryan, OH). The UV doses used in our study were selected based on the published studies on UVA- and UVB- mediated cutaneous responses (11, 12). Immediately after UV exposure, HBSS was replaced with fresh growth medium. Following UV exposure, cells were treated with 50 μM

nicotinamide for various time points and incubated at 37°C and 5% CO2 incubator. Cell pellets were stored at -80°C for protein or RNA isolation.

Immunostaining of 8oxoG and CPD: Melanocytes (5×10^4/chamber) were seeded and grown in 8-well glass chambered slides and pre-treated with 50 μM nicotinamide in culture medium for 24 h followed by UV exposure as described earlier. Post-UV-exposure, cells were maintained with or without 50 μM nicotinamide for up to 6 h at 37°C and 5% CO2. Immunostaining of 8oxoG and CPD was performed as described by Thompson et al. (13) using anti-thymine dimer (CPD) antibody or anti-8oxoG antibody (Supplementary Table 1). The staining was visualized by incubating the slides in the dark with Alexa Fluor 594 diluted 1:100 (red fluorescence) for 30 minutes at 37°C. Counterstaining was performed using 4', 6-diamidino-2-phenylindole (DAPI) (blue fluorescence) containing mounting media (Vector laboratories, Burlingame, CA, ISA). The images were visualized and captured using EVOS FL Auto Imaging System (Life Technologies, CA, USA).

Western blot analysis: For Western blot analysis, melanocytes (5×10^5 cells/2mL media) were seeded and grown for 24 h in 60 mm dishes. Cells were pre-treated with 50 μM nicotinamide for 24 h before exposing them to UVA and/or UVB. After UV exposure, cells were washed again and treated with 50 μm nicotinamide for 24 h. Cell lysates were prepared in ice-cold RIPA lysis buffer and subjected to SDS-PAGE. Proteins were transferred to a 0.2 μm nitrocellulose membrane (Bio-Rad, Hercules, CA), then blocked with 5% non-fat dry milk in TBS-T. Membranes were probed with appropriate primary antibody and secondary horseradish peroxidase (HRP) conjugated antibody (Cell Signaling Technology, Danvers, MA). Proteins were detected by chemiluminescence using Pierce ECL Western Blotting Substrate, or SuperSignal West Femto Chemiluminescent Substrates (Pierce, Rockford, IL). The quantification of the Western blot bands was performed using ImageJ (US National Institutes of

Health, Bethesda, MD, USA). The list of primary antibodies used in this study is provided in Supplementary Table S1.

Reverse transcription-quantitative real-time PCR (RT-qPCR) analysis: RT-qPCR analysis was done as previously described (14). Briefly, RNA isolation was performed using Qiagen RNA isolation kit. RT-qPCR analysis was performed for genes associated with nucleotide excision repair (NER) and base excision repair (BER) pathways. RNA was transcribed using first strand cDNA synthesis with random primers, dNTPs and M-MLV reverse transcriptase (Promega, WI). RT-qPCR was run using QuantStudio 3 (Thermo Fisher Scientific) with SYBR Premix Ex Taq II (TaKaRa), first strand cDNA, forward and reverse primers. Primer pairs for human SIRT1, P53, DDB1, DDB2, OGG1, ERCC1, ERCC2, CDK7 and GAPDH retrieved from PrimerBank (15) and ACTB (Origene, #HP204660) are detailed in Supplementary Table S2. RT-qPCR data were analyzed using QuantStudio™ design & analysis software (Thermo Fisher Scientific) and relative mRNA expression levels were calculated using the ΔΔCT comparative method. ACTB and GAPDH were used as endogenous controls.

Statistical analysis: The experiments were performed in multiple replicates and data are expressed as the mean±SEM. The statistical test used in data analysis to calculate statistical significance are indicated in respective figure legends.

Results

Effects of nicotinamide on UVA- and/or UVB- mediated modulations in 8oxoG in melanocytes

The level of 8oxoG in nucleus is widely used as a valuable biomarker for endogenous oxidative damage to DNA (16). The immunostaining of 8oxoG in primary human melanocytes showed that both UVA and/or UVB radiations significantly increased the levels of nuclear 8oxoG

when compared to no UV, as non-irradiated cells incubated with or without nicotinamide showed limited 8oxoG staining. The UVA- and/or UVB- mediated increase in 8oxoG levels were markedly reduced by nicotinamide in primary human melanocytes as observed from reduced 8oxoG staining compared to without nicotinamide-supplemented cells (Fig. 1). Thus, the results suggest that nicotinamide increased repair of oxidative DNA damage in the form of 8oxoG resulting from the UVA and/or UVB (Fig. 1).

Effects of nicotinamide on UVA- and/or UVB- mediated modulations in CPDs in melanocytes

CPDs are highly mutagenic and formed by exposure of skin cells to UVB radiation. CPDs are a measure of direct DNA damage responsible for mutations associated with skin cancer (17). The immunostaining of CPDs in the primary human melanocytes showed that the levels of nuclear CPD were noticeably increased following UVB exposure when compared to no UV or only UVA exposure. Further, the UVB-induced CPD levels were markedly reduced by nicotinamide in primary human melanocytes after UVB or a combination of UVA and UVB (Fig. 2). Thus, our data suggested that nicotinamide enhances repair of DNA damage in terms of CPD formation resulting from the UVB exposure.

Effects of nicotinamide on NER and/or BER pathways

To further determine the mechanism of nicotinamide- mediated protection against DNA damage caused by UVA and/or UVB at the gene level, we performed RT-qPCR analysis of important genes involved in DNA damage repair pathways (NER and BER) (Fig. 3). Sirtuin1 (SIRT1), a founding member of a family of nicotinamide adenine dinucleotide (NAD)-dependent histone deacetylases (18), and known to facilitates the NER pathway in UV-induced DNA damage repair (19), was significantly upregulated in response to nicotinamide in both UVB and UVAB groups. Interestingly, UVAB itself increased SIRT1 level, possibly to act as the first

responder against DNA damage. Tumor suppressor protein P53, which plays a major role as an architect of DNA damage repair by pausing the cell cycle to allow time for the repair (20), was upregulated in response to UVB and UVAB in melanocytes with relatively greater levels in nicotinamide treated cells after UVB-irradiation. Damage-specific DNA binding protein 1 (DDB1) recognizes UV-induced DNA lesions and initiates the NER process by binding to DDB2 to form the UV-damaged DNA-binding protein complex (21). Though DDB1 and DDB2 were upregulated in response to UVB and UVAB, nicotinamide treatment further enhanced their levels in these two groups. Additionally, 8-Oxoguanine glycosylase (OGG1), involved in both NER and BER pathways, was one of the DNA repair genes found to be markedly upregulated in all the treatment groups compared to no UV control. OGG1's primary role is the excision of 8-oxo-2'-deoxyguanosine (8oxo-dG), which is a form of oxidative DNA damage related to cause mutations and cancer (22). Our study further identified the upregulation of excision repair cross-complementation group 1 and 2 (ERCC1 and ERCC2) genes in UVB and UVAB as well as in response to nicotinamide in UVB and UVAB groups. Interestingly, the upregulation of ERCC2 was significantly higher in UVB with nicotinamide treated group compared to UVB alone, suggesting that ERCC2 play significant roles in nicotinamide mediated NER pathway to effectively repair DNA damages. ERCC2 also work as DNA helicase subunit of transcription factor TFIIH that unwinds the DNA in the 5′ to 3′ direction at the damaged location (23). Cyclin-dependent kinase 7 (CDK7) is an important component of the TFIIH, which play a major role in transcription initiation and DNA repair (24). CDK7 was found to be significantly upregulated in UVAB and in the UVB and UVAB groups treated with nicotinamide. Importantly, CDK7 was markedly higher in UVB and UVAB groups treated with nicotinamide than UVB and UVAB alone groups, elucidating the role of nicotinamide in the protection of UVB-induced DNA damages. Interestingly, for all these genes, compared to no UV group, no significant changes were observed in nicotinamide alone, and UVA group with or without nicotinamide treatment.

Next, we uploaded these significantly altered genes of the DNA damage repair pathway into Ingenuity Pathway Analysis (IPA, Qiagen) and identified an interaction network of nicotinamide-modulated genes. The network indicated links to other genes with potential involvement in DNA damage repair function. In addition, the potential participation of other key targets such as Histone H1, H3 and H4, RNA polymerase II, transcription factor CREB and growth arrest and DNA damage (GADD45) gene was found in the nicotinamide modulated gene network (Fig. 4). Overall, we found that nicotinamide mediated protection against DNA damage was mostly associated with nucleotide excision repair, as all the modulated genes were of NER pathway.

Effects of nicotinamide on NRF2-KEAP1 pathway in melanocytes after UVA- and/or UVB-treatment

NRF2–KEAP1 pathway has been shown to play a key role in the protection of the skin cells against UV induced oxidative DNA damage (25). To determine the potential mechanism of nicotinamide in protection from oxidative DNA damage caused by UVA and/or UVB, we used western blot analysis for NRF2 and KEAP1 proteins using cell lysates of UVA- and/or UVB-treated primary human melanocytes supplemented with or without nicotinamide. As shown in figure 5, UVA- and/or UVB- treatment decreased NRF2 expression in melanocytes when compared to no UV treatment. Whereas, nicotinamide supplementation significantly increased NRF2 expression in UVA- and/or UVB- treated melanocytes (Fig. 5A). Further, KEAP1, that inhibits NRF2 signaling, was decreased by nicotinamide in no UV, UVB- and UVAB- and increased in UVA- treated melanocytes, however, the modulations in KEAP1 were not statistically significant (Fig. 5B).

Discussion

This study was undertaken to determine the efficacy of nicotinamide against UVA- and/or UVB- mediated damaging responses in melanocytes as well as the mechanisms involved. Nicotinamide has been shown to prevent certain cancers including skin cancer (specifically non-melanoma skin cancers) possibly by facilitating DNA damage repair. In a recent phase III clinical trial, oral nicotinamide was found to be safe and effective in reducing the rates of new non-melanoma skin cancers and actinic keratoses in high-risk patients (10). However, there are limited studies on the efficacy of nicotinamide against melanoma. In this regard, a study by Thompson et al. showed that 50 μM nicotinamide protected melanocytes against UV-induced DNA damage in which melanocytes were irradiated with 2 J/cm^2 solar-simulated UV which was delivered from a 1000-W xenon arc lamp (13). We were interested in determining the distinct effects of UVA and UVB radiations and their combination in melanocytes to determine the protective effects and mechanisms of nicotinamide.

For this purpose, we used a custom-designed 120V Spectra UV instrument (Daavlin, Bryan, OH) that allows exposing cells to each UV region of the terrestrial solar spectrum (UVA and UVB) and provides precise control of UV wavelength and dose delivery. Using this unit, we determined the protective effects of nicotinamide on primary human neonatal melanocytes against UVA- and/or UVB- mediated DNA damages. In accordance to the study by Thompson et al. (13), we also observed that nicotinamide reduced CPD and 8oxoG levels in melanocytes, which were exposed to UVA and/or UVB radiations. However, the reduction in CPD and 8oxoG levels were greater in the case of UVB treated melanocytes compared to UVA or combined UVAB treatments. This trend was also observed in our further mechanistic investigations of nicotinamide mediated protection of photodamage in melanocytes.

Further, our study explored the involvement of several key genes associated with DNA damage signaling pathways in the facilitation of nicotinamide-mediated protection from UV-induced DNA damage. NER is an important DNA damage repair process, which detects and repairs lesions that cause both chemical and structural alterations of the DNA helix such as CPDs. Whereas, the BER is the main process by which cells repair free radical damage in DNA to avoid oxidative mutagenesis (26). We found significant upregulation in SIRT1, P53, DDB1, DDB2, OGG1, ERCC1, ERCC2 and CDK7 in response to UVB and UVAB irradiation possibly to cope with DNA damages, which was further enhanced by nicotinamide treatment conceivably for better protection. Interestingly, as shown in figure 4, SIRT1 and P53 appeared to be the main modulators of DNA damage repair pathway as they show direct and indirect interactions with most of DNA damage repair genes. Recent studies suggest that SIRT1 has important functions in DNA damage repair (reviewed in (18)). SIRT1 facilitates the NER pathway in UV-induced DNA damage repair and overexpression of SIRT1 protects from UV-induced damage (reviewed in (19)). Although nicotinamide was previously known as a SIRT1 inhibitor, recent studies suggest that it can also act as SIRT1 stimulator depending on context (reviewed in (27)). Whereas, p53 regulates the NER pathway by functioning as a transcription factor for various genes involved in NER or via direct response to DNA damage (28). In our study, we observed that nicotinamide enhanced expression of many NER pathway genes including SIRT1 and p53 after UVB and UVAB exposure, however, we did not observe any change in UVA-exposed groups. UVB radiation is the most mutagenic component of the UV spectrum causing DNA damage. Our data suggest that nicotinamide treatment significantly modulated DNA damage repair genes mostly related to NER pathway largely in response to UVB-induced DNA damages as well as in repair of DNA damages, which could be a major contributing factor in melanomagenesis, if left unrepaired.

Additionally, UVA and UVB radiation are also known to generate oxidative stress in human skin cells via increased cellular levels of reactive oxygen species (ROS) leading to DNA damages (25). The NRF2 signaling pathway is known to reduce oxidative DNA damage by transcriptional modulation of various antioxidant enzymes. Our data demonstrated that melanocytes exposed to UVA and/or UVB showed a reduction in NRF2 levels, which is in accordance with previously published studies (29, 30). Whereas, NRF2 upregulation has been shown to reduce UVB-induced damage in melanocytes (31). In our study, nicotinamide upregulated NRF2 expression after UVA- and/or UVB- treatments in primary human melanocytes. Thus, NRF2 signaling appears to be associated with nicotinamide's repair capabilities against UV-induced damages. Further, KEAP1 is a negative regulator of NRF2 and NRF2–KEAP1 is known to play an important role in the protection of the skin cells against UVB induced DNA damage (32, 25). Interestingly, we observed that there was a decreasing trend in KEAP1 levels after nicotinamide treatment in melanocytes in no UV, UVB- and UVAB- irradiated groups. Moreover, a non-significant increase in KEAP1 after nicotinamide treatment in UVA-irradiated cells suggest that the effects of nicotinamide may not be same as in UVB and UVAB treated groups.

Overall, understanding of the molecular mechanisms by which nicotinamide aid in repair of DNA damages caused by UVA and/or UVB may provide new insights and novel means towards protection against cutaneous damages, including melanoma. Further studies are required to validate these findings in in vivo models.

References

1 D'Orazio J, Jarrett S, Amaro-Ortiz A, Scott T: UV radiation and the skin. Int J Mol Sci 2013;14:12222-12248.

2 Chhabra G, Ndiaye MA, Garcia-Peterson LM, Ahmad N: Melanoma Chemoprevention: Current Status and Future Prospects. Photochem Photobiol 2017;93:975-989.

3 Brash DE: UV-induced Melanin Chemiexcitation: A New Mode of Melanoma Pathogenesis. Toxicol Pathol 2016;44:552-554.

4 Wang HT, Choi B, Tang MS: Melanocytes are deficient in repair of oxidative DNA damage and UV-induced photoproducts. Proc Natl Acad Sci U S A 2010;107:12180-12185.

5 Kielbassa C, Roza L, Epe B: Wavelength dependence of oxidative DNA damage induced by UV and visible light. Carcinogenesis 1997;18:811-816.

6 Kappes UP, Luo D, Potter M, Schulmeister K, Runger TM: Short- and long-wave UV light (UVB and UVA) induce similar mutations in human skin cells. J Invest Dermatol 2006;126:667-675.

7 Noonan FP, Dudek J, Merlino G, De Fabo EC: Animal models of melanoma: an HGF/SF transgenic mouse model may facilitate experimental access to UV initiating events. Pigment Cell Res 2003;16:16-25.

8 von Thaler AK, Kamenisch Y, Berneburg M: The role of ultraviolet radiation in melanomagenesis. Exp Dermatol 2010;19:81-88.

9 Nazarali S, Kuzel P: Vitamin B Derivative (Nicotinamide)Appears to Reduce Skin Cancer Risk. Skin Therapy Lett 2017;22:1-4.

10 Chen AC, Martin AJ, Choy B, Fernandez-Penas P, Dalziell RA, McKenzie CA, Scolyer RA, Dhillon HM, Vardy JL, Kricker A, St George G, Chinniah N, Halliday GM, Damian DL: A Phase 3 Randomized Trial of Nicotinamide for Skin-Cancer Chemoprevention. N Engl J Med 2015;373:1618-1626.

11 Syed DN, Afaq F, Mukhtar H: Differential activation of signaling pathways by UVA and UVB radiation in normal human epidermal keratinocytes. Photochem Photobiol 2012;88:1184-1190.

12 Hu QM, Yi WJ, Su MY, Jiang S, Xu SZ, Lei TC: Induction of retinal-dependent calcium influx in human melanocytes by UVA or UVB radiation contributes to the stimulation of melanosome transfer. Cell Prolif 2017;50

13 Thompson BC, Surjana D, Halliday GM, Damian DL: Nicotinamide enhances repair of ultraviolet radiation-induced DNA damage in primary melanocytes. Exp Dermatol 2014;23:509-511.

14 Garcia-Peterson LM, Ndiaye MA, Singh CK, Chhabra G, Huang W, Ahmad N: SIRT6 histone deacetylase functions as a potential oncogene in human melanoma. Genes Cancer 2017;8:701-712.

15 Wang X, Spandidos A, Wang H, Seed B: PrimerBank: a PCR primer database for quantitative gene expression analysis, 2012 update. Nucleic Acids Res 2012;40:D1144-1149.

16 Fortini P, Pascucci B, Parlanti E, D'Errico M, Simonelli V, Dogliotti E: 8-Oxoguanine DNA damage: at the crossroad of alternative repair pathways. Mutat Res 2003;531:127-139.

17 Berube R, Drigeard Desgarnier MC, Douki T, Lechasseur A, Rochette PJ: Persistence and Tolerance of DNA Damage Induced by Chronic UVB Irradiation of the Human Genome. J Invest Dermatol 2018;138:405-412.

18 Singh CK, Chhabra G, Ndiaye MA, Garcia-Peterson LM, Mack NJ, Ahmad N: The Role of Sirtuins in Antioxidant and Redox Signaling. Antioxid Redox Signal 2018;28:643-661.

19 Fan W, Luo J: SIRT1 regulates UV-induced DNA repair through deacetylating XPA. Mol Cell 2010;39:247-258.

20 Williams AB, Schumacher B: p53 in the DNA-Damage-Repair Process. Cold Spring Harb Perspect Med 2016;6

21 Iovine B, Iannella ML, Bevilacqua MA: Damage-specific DNA binding protein 1 (DDB1) is involved in ubiquitin-mediated proteolysis of p27Kip1 in response to UV irradiation. Biochimie 2011;93:867-875.

22 Yasui M, Kanemaru Y, Kamoshita N, Suzuki T, Arakawa T, Honma M: Tracing the fates of site-specifically introduced DNA adducts in the human genome. DNA Repair (Amst) 2014;15:11-20.

23 Oksenych V, Coin F: The long unwinding road: XPB and XPD helicases in damaged DNA opening. Cell Cycle 2010;9:90-96.

24 Rimel JK, Taatjes DJ: The essential and multifunctional TFIIH complex. Protein Sci 2018;27:1018-1037.

25 Kawachi Y, Xu X, Taguchi S, Sakurai H, Nakamura Y, Ishii Y, Fujisawa Y, Furuta J, Takahashi T, Itoh K, Yamamoto M, Yamazaki F, Otsuka F: Attenuation of UVB-induced sunburn reaction and oxidative DNA damage with no alterations in UVB-induced skin carcinogenesis in Nrf2 gene-deficient mice. J Invest Dermatol 2008;128:1773-1779.

26 Rastogi RP, Richa, Kumar A, Tyagi MB, Sinha RP: Molecular mechanisms of ultraviolet radiation-induced DNA damage and repair. J Nucleic Acids 2010;2010:592980.

27 Hwang ES, Song SB: Nicotinamide is an inhibitor of SIRT1 in vitro, but can be a stimulator in cells. Cell Mol Life Sci 2017;74:3347-3362.

28 Fitch ME, Cross IV, Ford JM: p53 responsive nucleotide excision repair gene products p48 and XPC, but not p53, localize to sites of UV-irradiation-induced DNA damage, in vivo. Carcinogenesis 2003;24:843-850.

29 Marrot L, Jones C, Perez P, Meunier JR: The significance of Nrf2 pathway in (photo)-oxidative stress response in melanocytes and keratinocytes of the human epidermis. Pigment Cell Melanoma Res 2008;21:79-88.

30 Kokot A, Metze D, Mouchet N, Galibert MD, Schiller M, Luger TA, Bohm M: Alpha-melanocyte-stimulating hormone counteracts the suppressive effect of UVB on Nrf2 and Nrf-dependent gene expression in human skin. Endocrinology 2009;150:3197-3206.

31 Janjetovic Z, Jarrett SG, Lee EF, Duprey C, Reiter RJ, Slominski AT: Melatonin and its metabolites protect human melanocytes against UVB-induced damage: Involvement of NRF2-mediated pathways. Sci Rep 2017;7:1274.

32 McMahon M, Itoh K, Yamamoto M, Hayes JD: Keap1-dependent proteasomal degradation of transcription factor Nrf2 contributes to the negative regulation of antioxidant response element-driven gene expression. J Biol Chem 2003;278:21592-21600.

Figure Legends

Figure 1: Effects of nicotinamide on UVA- and/or UVB- mediated modulations in 8oxoG in melanocytes.

Immunostaining of 8oxoG in melanocytes was performed 1 h post-UV-exposures with or without nicotinamide (50 μM) treatments. Representative images (20x magnification) of DAPI (blue color), 8oxoG staining (red color), and merged are shown for each group of cells. Scale bar = 200 μm. The data shown here represent the experiments done twice in duplicates.

Figure 2: Effects of nicotinamide on UVA- and/or UVB- mediated modulations in CPD in melanocytes.

Immunostaining of CPDs in melanocytes was performed 3 h post-UV-exposures with or without nicotinamide (50 μM) treatments. Representative merged images (20x magnification) of DAPI (blue color), CPD staining (red color) and merged are shown for each group of cells. Scale bar = 200 μm.

Figure 3: Effects of nicotinamide on nucleotide excision repair (NER) and/or base excision repair (BER) pathways.

RT-qPCR analysis of genes involved in DNA damage repair. Nicotinamide enhances repair of UV-induced DNA damage in melanocytes by modulating genes associated with the NER process. Statistical analyses were performed using one-way ANOVA with Tukey's multiple comparison test (GraphPad PRISM 5.0 software). The results are expressed as mean±SEM with statistical significance (* $P<0.05$, ** $P<0.01$, *** $P<0.001$, **** $P<0.001$) compared to no UV control. A star(s) above the lines (*) represents the statistical significance compared in respective treatment groups. The data shown here represent the experiments done thrice in duplicates.

Figure 4: Ingenuity Pathway Analysis (IPA, Qiagen) analysis of significantly modulated genes involved in DNA damage repair.

The predicted gene-gene interaction network was generated and analyzed using inputs of significantly modulated genes involved in DNA damage repair. Upregulated genes are displayed in red. The solid lines denote a robust correlation with partner genes, and dashed lines indicate statistically significant but less frequent correlations.

Figure 5: Effects of nicotinamide on NRF2-KEAP1 pathway in melanocytes after UVA- and/or UVB- induced DNA damages.

Western blot analysis for NRF2 and KEAP1 proteins involved in oxidative DNA damage repair 24 h post-UVA- and/or UVB- exposures in cell lysates (40 µg) of melanocytes supplemented with or without nicotinamide (50 µM). β-Actin was used as a loading control. Representative blots are shown here for the experiments performed in triplicates. Bar diagram shows the quantitative analysis of the bands using ImageJ. Statistical analyses were performed using one-way ANOVA (GraphPad PRISM 5.0 software) with Fisher's LSD test. The results are expressed as mean±SEM with statistical significance (* $P<0.05$, ** $P<0.01$, *** $P<0.001$). A star above the lines (*) represents the statistical significance compared in respective treatment groups.

Figures

Figure 1

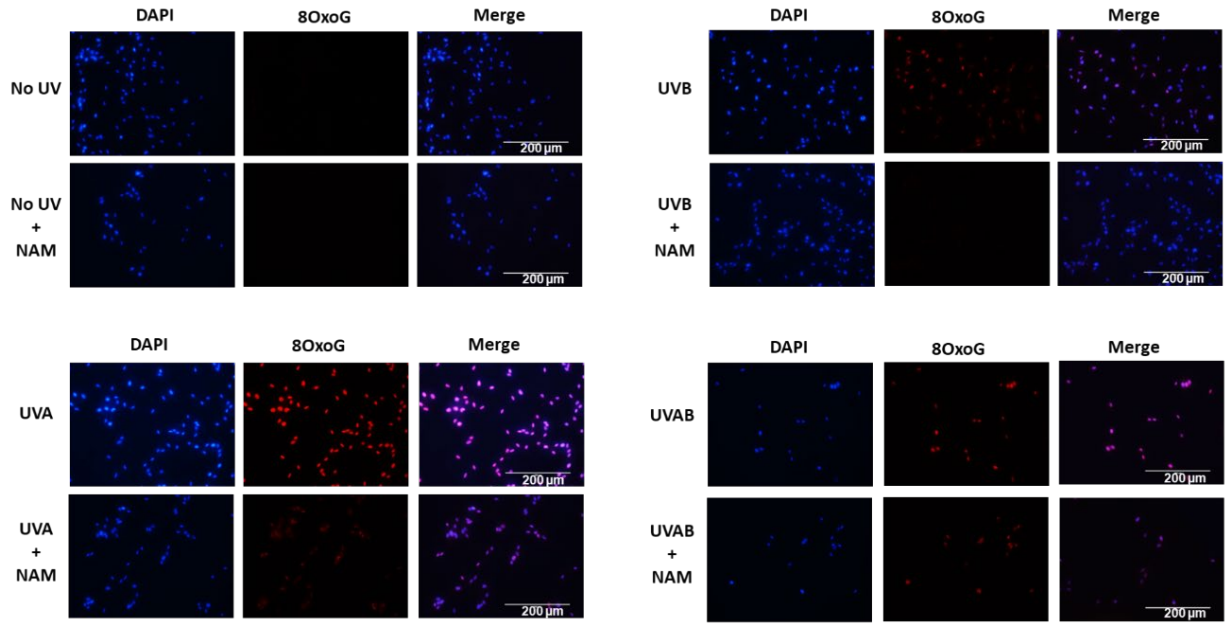

Figure 2

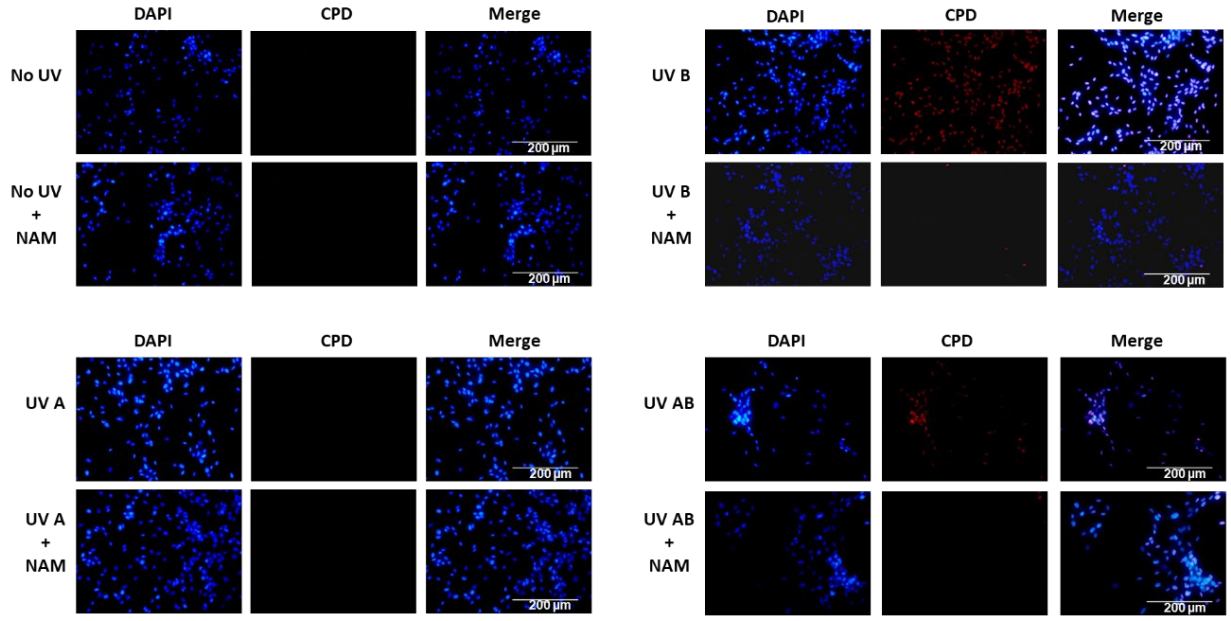
DAPI
CPD
Merge
No UV
No UV + NAM
UV B
UV B + NAM
UV A
UV A + NAM
UV AB
UV AB + NAM
200 µm

Figure 3

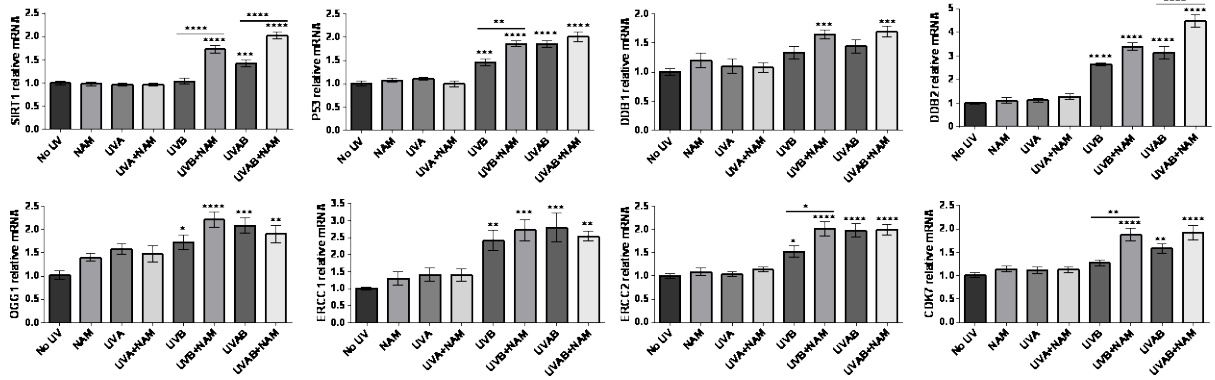
SIRT1 relative mRNA
P53 relative mRNA
DDB1 relative mRNA
DDB2 relative mRNA
OGG1 relative mRNA
ERCC1 relative mRNA
ERCC2 relative mRNA
CDK7 relative mRNA
No UV
NAM
UVA
UVA+NAM
UVB
UVB+NAM
UVAB
UVAB+NAM

Figure 4

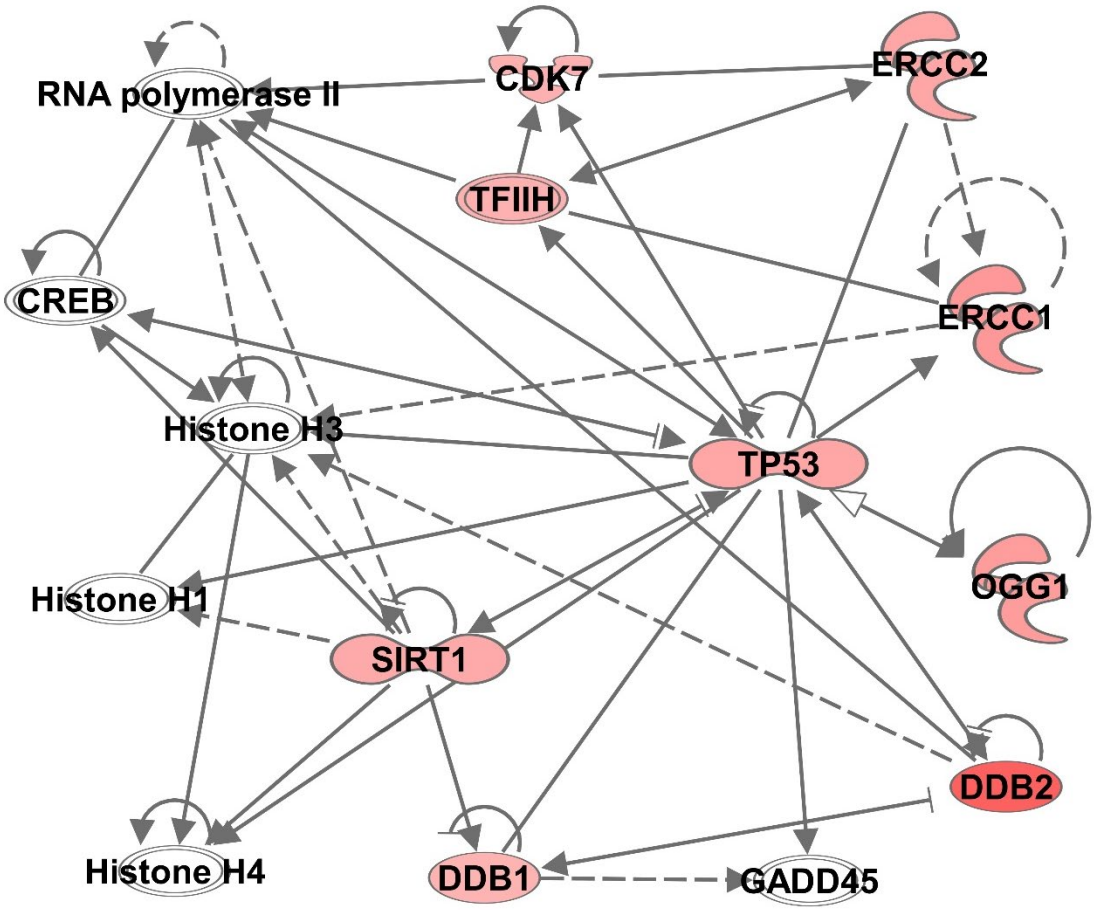
RNA polymerase II
CDK7
ERCC2
TFIIH
CREB
ERCC1
Histone H3
TP53
Histone H1
OGG1
SIRT1
DDB2
Histone H4
DDB1
GADD45

Figure 5

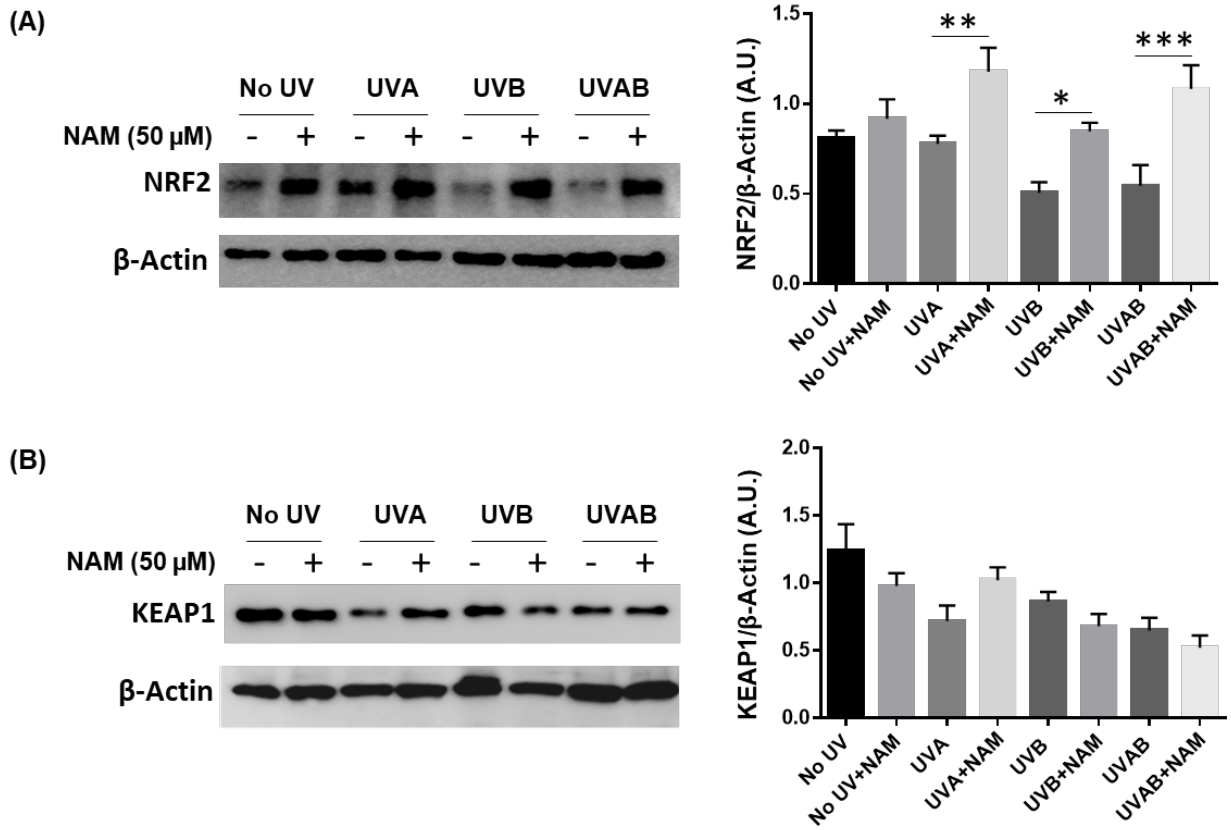
(A)
No UV
UVA
UVB
UVAB
NAM (50 μM)
- + - + - + - +
NRF2
β-Actin
NRF2/β-Actin (A.U.)
1.5
1.0
0.5
0.0
**
*
***
No UV
No UV+NAM
UVA
UVA+NAM
UVB
UVB+NAM
UVAB
UVAB+NAM
(B)
No UV
UVA
UVB
UVAB
NAM (50 μM)
- + - + - + - +
KEAP1
β-Actin
KEAP1/β-Actin (A.U.)
2.0
1.5
1.0
0.5
0.0
No UV
No UV+NAM
UVA
UVA+NAM
UVB
UVB+NAM
UVAB
UVAB+NAM